~~CONFIDENTIAL~~

MARSHALL SPACE FLIGHT CENTER HUNTSVILLE, ALABAMA

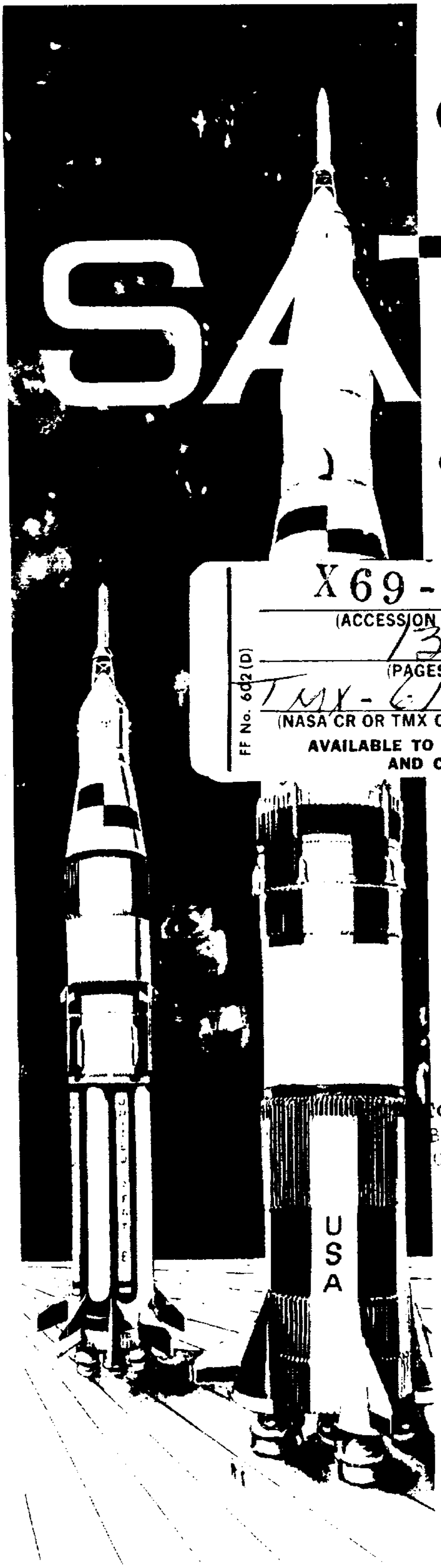

SATURN

MPR-SAT-FE-66-11
(Supersedes MPR-SAT-65-14)

July 14, 1966

X69-75421 (ACCESSION NUMBER)
None (THRU)
139 (PAGES)
(CODE)
TMX-61644 (NASA CR OR TMX OR AD NUMBER)
(CATEGORY)
FF No. 602(D)
AVAILABLE TO U.S. GOVERNMENT AGENCIES AND CONTRACTORS ONLY

RESULTS OF THE TENTH SATURN I LAUNCH VEHICLE TEST FLIGHT SA-10

[U]

CLASSIFICATION CHANGE
To UNCLASSIFIED
By authority of GDS-GP-4 Date 12/75
Changed by L. Shirk
Classified Document Master Control Station, NASA
Scientific and Technical Information Facility

SATURN FLIGHT EVALUATION WORKING GROUP

~~GROUP-4~~
~~Downgraded at 3 year intervals;~~
~~Declassified after 12 years.~~

~~CONFIDENTIAL~~

NATIONAL AERONAUTICS AND SPACE ADMINISTRATION

MSFC - Form 774 (Rev May 1966)

SECURITY NOTE

This document contains information affecting the national defense of the United States within the meaning of the Espionage Law, Title 18, U. S. C., Sections 793 and 794 as amended. The revelation of its contents in any manner to an unauthorized person is prohibited by law.

MPR-SAT-FE-66-11

RESULTS OF THE TENTH SATURN I LAUNCH VEHICLE TEST FLIGHT SA-10

By Saturn Flight Evaluation Working Group

George C. Marshall Space Flight Center

ABSTRACT

This report presents the results of the early engineering evaluation of the SA-10 test flight. Sixth of the Block II series, SA-10 was the fifth Saturn vehicle to carry an Apollo boilerplate (BP-9) payload and the third in a series to carry a Pegasus payload (Pegasus C). The performance of each major vehicle system is discussed with special emphasis on malfunctions and deviations.

This test flight of SA-10 was the tenth consecutive success for the Saturn I vehicles and marks the end of the Saturn I program. This was the third flight test of the Pegasus meteoroid technology satellite, the third flight test to utilize the iterative guidance mode, the fourth flight test utilizing the ST-124 guidance system for both stages, and the fifth flight test to demonstrate the closed loop performance of the path guidance during S-IV burn. The performance of the guidance system was successful and the insertion velocity was very near the expected value. This was also the third flight test of the unpressurized prototype production Instrument Unit and passive thermal control system which will be used on Saturn IB and V vehicles. All missions of the flight were successfully accomplished.

Any questions or comments pertaining to the information contained in this report are invited and should be directed to:

Director, George C. Marshall Space Flight Center
Huntsville, Alabama
Attention: Chairman, Saturn Flight Evaluation Working Group R-AERO-F (Phone 876-4575)

[redacted]

C67-357

GEORGE C. MARSHALL SPACE FLIGHT CENTER

MPR-SAT-FE-66-11

July 14, 1966

(Supersedes MPR-SAT-65-14)

RESULTS OF THE TENTH SATURN I LAUNCH VEHICLE TEST FLIGHT SA-10 [U]

~~GROUP 4~~
~~Downgraded at 3 year~~
~~intervals; declassified~~
~~after 12 years.~~

~~NOTICE — THIS DOCUMENT CONTAINS INFORMATION AFFECTING THE NATIONAL DEFENSE OF THE UNITED STATES WITHIN THE MEANING OF THE ESPIONAGE LAWS, TITLE 18, U.S.C., SECTIONS 793 AND 794. ITS TRANSMISSION OR THE REVELATION OF ITS CONTENTS IN ANY MANNER TO AN UNAUTHORIZED PERSON IS PROHIBITED BY LAW.~~

SATURN FLIGHT EVALUATION
WORKING GROUP

[redacted]

ACKNOWLEDGEMENT

Contributions to this report were made by various elements of MSFC, John F. Kennedy Space Center, Douglas Aircraft Company, Chrysler Corporation, IBM Corporation, Rocketdyne, and Pratt & Whitney. Without the joint efforts and assistance of these elements, this integrated report would not have been possible. The Saturn Flight Evaluation Working Group is especially indebted to the following for their major contributions:

John F. Kennedy Space Center
Douglas Aircraft Company
Chrysler Corporation Space Division
International Business Machines Corporation
Pratt & Whitney
Rocketdyne

George C. Marshall Space Flight Center

Research and Development Operations

Aero-Astrodynamics Laboratory

Aero-Space Environment Office
Aerodynamics Division
Flight Evaluation and Operations Studies Division

Astrionics Laboratory

Electrical Systems Integration Division
Flight Dynamics Branch
Guidance and Control Division
Instrumentation and Communications Division

Computation Laboratory

R& D Application Division

Propulsion and Vehicle Engineering Laboratory

Propulsion Division
Structures Division
Vehicle Systems Division

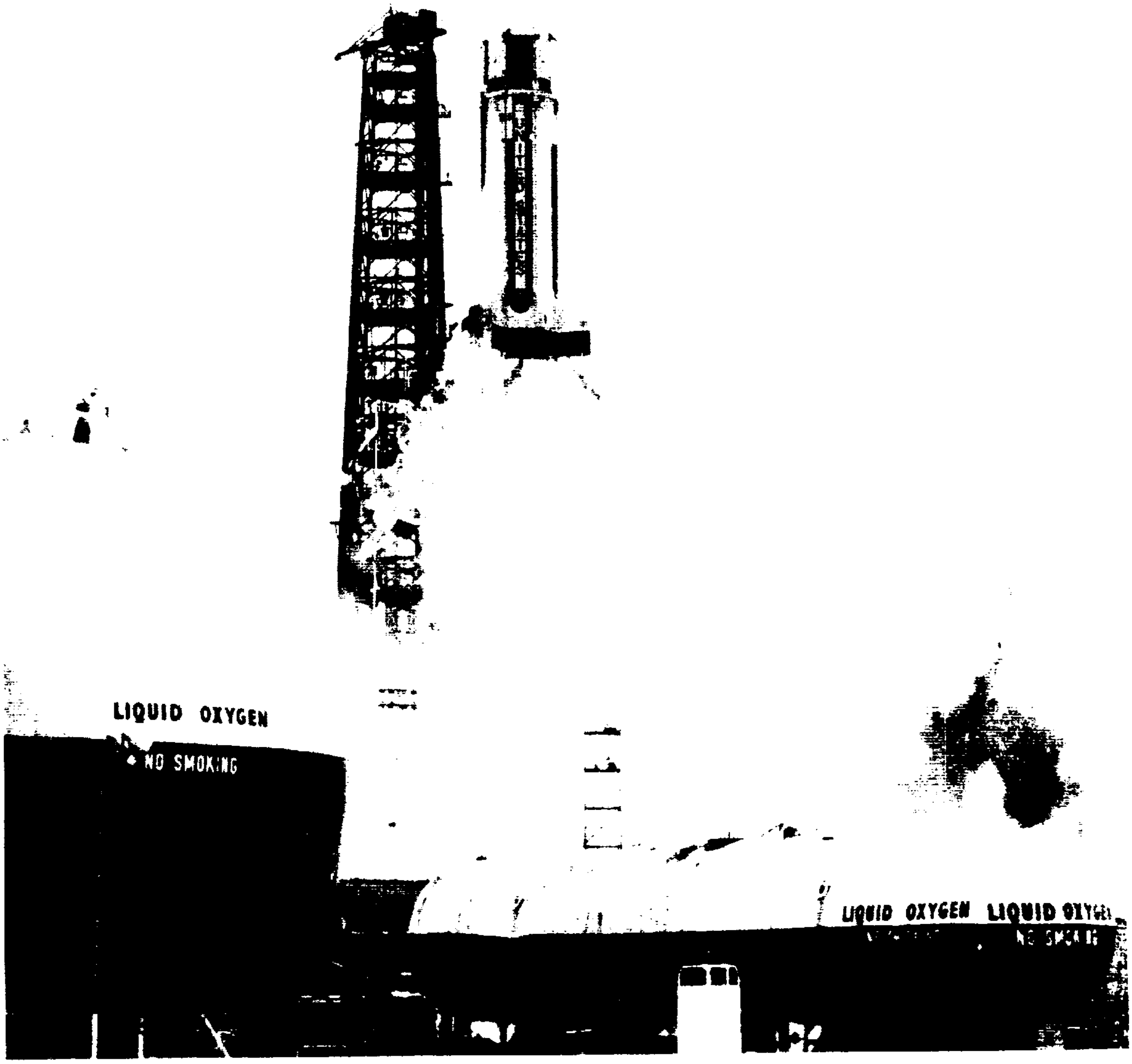
LIQUID OXYGEN
NO SMOKING
LIQUID OXYGEN
LIQUID OXYGEN
NO SMOKING

TABLE OF CONTENTS

Page

SECTION I. FLIGHT TEST SUMMARY 1
1.1 Flight Test Results 1
1.2 Test Objectives 2
1.3 Times of Events 2

SECTION II. INTRODUCTION 4

SECTION III. LAUNCH OPERATIONS 5
3.1 Summary 5
3.2 Prelaunch Milestones 5
3.3 Atmospheric Conditions 5
3.4 Countdown 5
3.5 Propellant Loading 5
3.5.1 S-I Stage 5
3.5.2 S-IV Stage 7
3.5.2.1 LOX 7
3.5.2.2 LH_2 8
3.5.2.3 Cold Helium 8
3.6 Holddown 9
3.7 Ground Support Equipment 9
3.7.1 Mechanical Ground Support Equipment 9
3.7.2 Electrical Support Equipment 9
3.8 Blockhouse Redline Values 9

SECTION IV. MASS CHARACTERISTICS 10
4.1 Vehicle Mass 10
4.2 Vehicle Center of Gravity and Moment of Inertia 10

SECTION V. TRAJECTORY 14
5.1 Summary 14
5.2 Trajectory Comparison with Nominal 14
5.3 Insertion Conditions (S-IV Cutoff + 10 Seconds) 17

SECTION VI. PROPULSION 18
6.1 Summary 18
6.2 S-I Stage Performance 18
6.2.1 Overall Stage Propulsion Performance 18
6.2.2 Flight Simulation of Cluster Performance 20
6.2.3 Individual Engine Performance 21
6.3 S-I Pressurization Systems 21
6.3.1 Fuel Pressurization System 21
6.3.2 LOX Tank Pressurization System 22
6.3.3 Control Pressure System 22
6.3.4 LOX-SOX Disposal System 22
6.3.5 Hydrogen Vent Duct Purge 23
6.4 S-I Stage Propellant Utilization 23
6.5 S-I Stage Hydraulic Systems 24
6.6 Retro Rocket Performance 25
6.7 S-IV Stage Propulsion 25
6.7.1 Overall S-IV Stage Propulsion Performance 25

Page

6.7.2 Stage Performance 25
6.7.2.1 Engine Analysis 25
6.7.2.2 Flight Simulation 26
6.7.3 Individual Engine Performance 28
6.7.3.1 Engine Cooldown 28
6.7.3.2 Start Transients 28
6.7.3.3 Steady State Operation 28
6.7.3.4 Cutoff Transients 29
6.8 S-IV Pressurization System 29
6.8.1 LH_2 Tank Pressurization 29
6.8.1.1 LH_2 Pump Inlet Conditions 30
6.8.2 LOX Tank Pressurization 31
6.8.2.1 Helium Heater Operation 32
6.8.2.2 LOX Pump Inlet Conditions 32
6.8.3 Cold Helium Supply 33
6.8.4 Control Helium System 33
6.9 Propellant Utilization 33
6.9.1 Propellant Mass History 34
6.9.2 System Response 34
6.9.3 PU System Command 34
6.10 S-IV Hydraulic System 35
6.11 Ullage Rockets 35

SECTION VII. GUIDANCE AND CONTROL 36
7.1 Summary 36
7.2 System Description 36
7.3 Control Analysis 38
7.3.1 S-I Stage Flight Control 38
7.3.1.1 Pitch Plane 38
7.3.1.2 Yaw Plane 38
7.3.1.3 Control Design Parameters 40
7.3.1.4 Roll Plane 40
7.3.2 S-IV Stage Flight Control 41
7.4 Functional Analysis 42
7.4.1 Control Sensors 42
7.4.1.1 Control Accelerometers 42
7.4.1.2 Angle-of-Attack Sensors 42
7.4.1.3 Rate Gyros 43
7.4.1.4 Control Acceleration Switch 43
7.4.1.5 Resolver Chain Error Comparison 43
7.4.1.6 Flight Control Computer and Actuator Analysis 43
7.5 Propellant Sloshing 44
7.5.1 S-I Powered Flight Sloshing 44
7.5.2 S-IV Powered Flight Sloshing 44
7.6 Guidance System Performance 45
7.6.1 Guidance Intelligence Errors 45
7.6.2 Guidance System Performance Comparisons 48
7.7 Guidance System Hardware 50
7.7.1 Guidance Signal Processor and Digital Computer Analysis 50
7.7.2 ST-124 Stabilized Platform System Hardware Analysis 50
7.8 ST-124 Gas Bearing GN_2 Supply System 51

TABLE OF CONTENTS (Cont'd)

Page

SECTION VIII. SEPARATION 53
8.1 Summary 53
8.2 S-I/S-IV Separation Dynamics 53
8.2.1 Translational Motion 53
8.2.2 Angular Motion 53
8.3 Apollo Shroud Separation 55

SECTION IX. STRUCTURES 56
9.1 Summary 56
9.2 Results During S-I Powered Flight 56
9.2.1 Moments and Normal Load Factors 56
9.2.2 Longitudinal Loads 56
9.2.3 Bending Oscillations 57
9.2.4 S-I Vibrations 58
9.2.4.1 Structural Measurements 58
9.2.4.2 Engine Measurements 58
9.2.4.3 Component Measurements 60
9.2.5 S-IV Vibrations 60
9.2.5.1 Structural Measurements 60
9.2.5.2 Engine Measurements 60
9.2.5.3 Component Measurements 60
9.2.6 Instrument Unit Vibrations 61
9.2.6.1 Structural Measurements 61
9.2.6.2 Component Measurements 61
9.2.7 Apollo (Pegasus) Vibrations 61
9.2.8 Structural Acoustics 61
9.2.8.1 S-I Stage 61
9.2.8.2 S-IV Stage 62
9.2.8.3 Instrument Unit 62
9.2.8.4 Apollo 62
9.3 Observed Structural Deviations 62
9.4 S-I/S-IV Interstage 62
9.5 Results During S-IV Powered Flight 64
9.5.1 Bending 64
9.5.2 S-IV Vibrations During S-IV Powered Flight 64
9.5.2.1 Structural Measurements 64
9.5.2.2 Engine Measurements 64
9.5.2.3 Component Measurements 64
9.5.3 Instrument Unit Vibrations 65
9.5.4 Apollo (Pegasus) Vibration 65
9.5.5 Apollo (Pegasus) Acoustics 65

SECTION X. ENVIRONMENTAL TEMPERATURES AND PRESSURES 66
10.1 Summary 66
10.2 S-I Stage Environment 66
10.2.1 Surface Pressures 66
10.2.2 S-I Stage Skin Temperatures and Heating Rates 66
10.2.3 Base Pressures and Tail Compartment Pressures 66

TABLE OF CONTENTS (Cont'd)

Page

10.2.4 Base Thermal Environment ... 66
10.2.4.1 Base Temperatures ... 67
10.2.4.2 Base Heating Rates ... 67
10.2.4.3 Engine Compartment Temperatures ... 67
10.2.5 S-I/S-IV Interstage Environment ... 6
10.2.5.1 S-I/S-IV Interstage Temperatures and Pressures ... 69
10.2.5.2 Detonation Pressures ... 69
10.3 S-IV Stage Environment ... 70
10.3.1 Environmental Pressures ... 70
10.3.1.1 Common Bulkhead Pressure ... 70
10.3.1.2 Base Heat Shield Pressure ... 70
10.3.2 Surface Temperatures and Heat Fluxes ... 70
10.3.2.1 Hydrogen Tank Temperatures ... 70
10.3.2.2 Aft Skirt Temperatures ... 70
10.3.2.3 Hydrogen Vent Line Temperature ... 70
10.3.2.4 Aft Skirt Heat Flux ... 70
10.3.2.5 Aft Interstage Heat Flux ... 71
10.3.3 Base Temperatures and Heat Fluxes ... 71
10.3.3.1 Base Thrust Structure Temperature ... 71
10.3.3.2 Base Heat Shield Temperatures ... 71
10.3.3.3 Base Heat Flux ... 71
10.4 Equipment Temperature and Pressure Environment ... 71
10.4.1 S-I Stage Instrument Compartment Environment ... 71
10.4.2 Instrument Unit Environment ... 71

SECTION XI. VEHICLE ELECTRICAL SYSTEMS ... 75
11.1 Summary ... 75
11.2 S-I Stage Electrical System ... 75
11.3 S-IV Stage Electrical System ... 75
11.4 IU Stage Electrical System ... 76

SECTION XII. AERODYNAMICS ... 77
12.1 Summary ... 77
12.2 Drag ... 77

SECTION XIII. INSTRUMENTATION ... 78
13.1 Summary ... 78
13.2 S-I Stage Measuring Analysis ... 78
13.2.1 S-I Measurement Malfunctions ... 78
13.2.2 S-I Measuring Reliability ... 78
13.3 S-IV Measuring Analysis ... 78
13.3.1 S-IV Measurement Malfunction ... 78
13.3.2 S-IV Measuring Reliability ... 78
13.4 IU Stage Measuring Analysis ... 78
13.4.1 IU Measurement Malfunctions ... 78
13.4.2 IU Measuring Reliability ... 78
13.5 Airborne Telemetry Systems ... 80
13.5.1 Telemetry Links ... 80
13.5.2 Data Acquisition ... 80
13.5.3 Calibration ... 80

TABLE OF CONTENTS (Concluded)

Page

13.6 Airborne Tape Recorders 80
  13.6.1 S-I Recorder 80
  13.6.2 S-IV Recorder 80
  13.6.3 IU Recorder 81
13.7 RF Systems Analysis 81
  13.7.1 Telemetry 81
  13.7.2 Tracking 82
  13.7.3 Television 83
13.8 Optical Instrumentation 83
  13.8.1 Engineering Sequential Cameras 83
  13.8.2 Tracking Cameras 84
13.9 Orbital Tracking and Telemetry Summary 84
  13.9.1 Tracking Summary 84
  13.9.2 Telemetry Summary 84

SECTION XIV. PEGASUS C 85
14.1 Summary 85
14.2 Pegasus C Performance 85
14.3 Orbital Attitude 85
  14.3.1 Nonpropulsive Vent System Performance 85
  14.3.2 Vehicle Attitude in Orbit 86
14.4 Pegasus Operation 87

SECTION XV. SUMMARY OF MALFUNCTIONS AND DEVIATIONS 88

APPENDIX. VEHICLE DESCRIPTION 89
A.1 Summary 89
A.2 S-I Stage 89
A.3 S-IV Stage 89
A.4 Instrument Unit 93
A.5 Payload 93
A.6 Pegasus C Satellite 93

INDEX 96

LIST OF ILLUSTRATIONS

Figure	Title	Page
3-1	Effect of Wind Speed on LOX Load	7
4-1	Vehicle Mass Center of Gravity and Mass Moment of Inertia for S-I Stage	10
4-2	Vehicle Mass Center of Gravity and Mass Moment of Inertia for S-IV Stage	10
5-1	S-I Trajectory	14
5-2	S-IV Trajectory	14
5-3	Earth Fixed Velocity	14
5-4	Total Inertial Acceleration	15
5-5	Mach Number and Dynamic Pressure	16
5-6	Booster Trajectory Ground Track	17
6-1	S-I Individual Engine and Stage Thrust Buildup	18
6-2	Vehicle Longitudinal Thrust and Specific Impulse	19
6-3	Vehicle Mixture Ratio and Total Flowrate	19
6-4	Inboard and Outboard Engine Thrust Decay	20
6-5	Flight Simulation Results	20
6-6	Deviation in Individual Engine Performance Parameters (S-I)	21
6-7	Gas Pressure in Fuel Tank and High Pressure Sphere	22
6-8	Prelaunch and Flight Center LOX Tank Pressure	22
6-9	LOX-SOX System Operation	23
6-10	Hydraulic Oil Pressure, Level, and Temperature	25
6-11	Total S-IV Stage Performance (Engine Analysis)	26
6-12	Propulsion Systems Performance Comparison (S-IV Stage)	27
6-13	Best Estimate of S-IV-10 Ignition and Cutoff Weight	28
6-14	Individual Engine Start Transients	28
6-15	S-IV Engine Cutoff Transients	29
6-16	S-IV Stage Fuel Tank Ullage Pressure	29
6-17	LH_2 Pump Inlet Conditions	30

LIST OF ILLUSTRATIONS (Cont'd)

Figure	Title	Page
6-18	S-IV Stage LOX Tank Ullage Pressure	31
6-19	S-IV Helium Heater Performance	32
6-20	LOX Pump Inlet Conditions	32
6-21	LOX Pump Inlet Temperatures	33
6-22	Typical Propellant Utilization Valve Position	34
6-23	Ullage Rocket Chamber Pressure	35
7-1	Guidance and Control System	37
7-2	S-I Stage Command Angles	39
7-3	Pitch Attitude Error, Angular Rate, and Average Actuator Position	39
7-4	Pitch Plane Wind Velocity	39
7-5	Yaw Attitude Error, Angular Rate, and Average Actuator Position	39
7-6	Yaw Plane Wind Velocity and Free Stream Angle of Attack	40
7-7	Comparison of Vehicle Control Parameters with Design Criteria	40
7-8	Roll Attitude Error, Angular Rate, and Average Actuator Position	40
7-9	S-IV Stage Attitude Errors	41
7-10	Vehicle Response to Pitch Plane Guidance Initiation	41
7-11	Pitch and Yaw Control Accelerometers	42
7-12	Calculated and Predicted Pitch Axis Resolver Chain Error	44
7-13	Slosh During S-I Powered Flight	44
7-14	ST-124 Stabilized Platform System Error Sources	45
7-15	Inertial Velocity Component Difference (Accelerometer-Tracking)	47
7-16	Residual Inertial Velocity Component Differences (Trajectory Analysis-Tracking)	48
7-17	Yaw Plane Delta-Minimum Guidance Parameters	50
7-18	ST-124 Gas Bearing System	51
8-1	Separation Sequence	53
8-2	Separation Distance and Incremental Velocities	53

LIST OF ILLUSTRATIONS (Cont'd)

Figure	Title	Page
8-3	SA-10 Angular Velocities During Booster Separation	54
8-4	S-IV Attitude Error During Separation	54
8-5	Pegasus Separation Comparisons	55
9-1	Pitch Bending Moment and Normal Load Factor	56
9-2	SA-10 Thrust Buildup Characteristics	57
9-3	Upper Pegasus Support Response to S-I Ignition	57
9-4	Vehicle Bending Frequencies and Amplitudes, Yaw	57
9-5	S-I Stage Vibrations	58
9-6	Component Vibration During S-I Stage Powered Flight	60
9-7	Instrument Unit Vibrations During S-I Powered Flight	61
9-8	Pegasus Vibrations	62
9-9	Apollo and Instrument Unit Acoustics	62
9-10	S-IV Aft Interstage View Looking Outboard with Interstage Folded Flat	63
9-11	S-I/S-IV Interstage Strain	64
9-12	Engine and Structural Component Vibrations During S-IV Stage Powered Flight	65
10-1	Temperature History of Upper and Lower Tail Shrouds and Engine Shroud	66
10-2	Heat Shield and Access Chute Gas Temperatures	67
10-3	Heat Fluxes for Heat Shield Inner Region and Access Chute	68
10-4	Total Heat Fluxes to Engine Bell and Aspirator	68
10-5	Heat Shield Forward Face Structural Temperatures	68
10-6	S-IV Aft Interstage	69
10-7	S-IV Stage Surface Temperature Environment	70
10-8	S-IV Stage Base Temperature Environment	72
10-9	IU Ambient and Component Temperatures and Pressures During Powered Flight	73
10-10	IU Ambient and Component Temperatures and Pressures During Orbit	74

LIST OF ILLUSTRATIONS (Concluded)

Figure	Title	Page
11-1	S-I Stage Current and Voltage	75
11-2	S-IV Stage Current and Voltage	76
11-3	IU Stage Battery Temperature, Voltage, Current, and Inverter Voltage	76
12-1	Axial Force Coefficient and Base Drag	77
14-1	SA-10 Roll Rate Analysis	87
14-2	SA-10 Orbital Roll Rates	87
A-1	SA-10 Vehicle Configuration	90
A-2	S-I Stage	91
A-3	S-IV Stage	92
A-4	Instrument Unit	94
A-5	Payload	95

LIST OF TABLES

Table	Title	Page
1-I	Times of Events	3
3-I	SA-10 Prelaunch Milestones	6
3-II	S-I-10 Propellant Weights at Ignition Command	8
4-I	Vehicle Masses	11
4-II	SA-10 Flight Sequence Mass Summary	12
4-III	Mass Characteristics Comparison	13
5-I	Cutoff Conditions	15
5-II	Significant Events	16
5-III	Booster Impact	17
5-IV	Insertion Elements Comparison	17
6-I	Average Stage Propulsion Parameters, SA-10	19
6-II	S-IV Stage Engine Analysis Performance	26
6-III	S-IV-10 Propulsion System	27
6-IV	Propellant Mass History	34
7-I	Guidance Intelligence Errors	46
7-II	Comparison of Inertial Guidance Velocities (V_i, $\dot{X}_i$, $\dot{Y}_i$, $\dot{Z}_i$)	47
7-III	Comparison of Space Fixed Velocities at S-IV Guidance Cutoff (630.252 Seconds Range Time)	48
7-IV	Comparison of Guidance Parameters at Orbital Insertion (640.252 Seconds Range Time)	49
9-I	Vibration Summary	59
13-I	Measurement Malfunctions	79
14-I	Nonpropulsive Vent Performance	86

ABBREVIATIONS AND SYMBOLS

Abbreviation	Definition
AGC	Automatic Gain Control
CDR	Command Destruct Receiver
CM	Command Module
CO	Cutoff
CSM	Combustion Stability Monitor
DDAS	Digital Data Acquisition System
DOD	Department of Defense
E. F.	Earth Fixed
EMF	Electro Motive Force
ESE	Electrical Support Equipment
EMR	Engine Mixture Ratio
ETR	Eastern Test Range
GLOTRAC	Global Tracking System
GSE	Ground Support Equipment
IECO	Inboard Engine Cutoff
IETD	Inboard Engine Thrust Decay
IGM	Iterative Guidance Mode
IP	Impact Position
LCC	Launch Control Center
LES	Launch Escape System
LOS	Loss of Signal
MILA	Merritt Island Launch Area
MISTRAM	Missile Trajectory Measurement System
MMC	Micrometeoroid Capsule
MOTS	Minitrack Optical Tracking Station
ms	Milliseconds
MSFN	Manned Space Flight Network
NORAD	North American Air Defense Command
NPSP	Net Positive Suction Pressure
NPV	Nonpropulsive Vent
OECO	Outboard Engine Cutoff
OETD	Outboard Engine Thrust Decay
PAFB	Patrick Air Force Base
PAM	Pulse Amplitude Modulated
PCM	Pulse Code Modulated
PDM	Pulse Duration Modulated
PRA	Patrick Air Force Base, 1963 Reference Atmosphere
PU	Propellant Utilization
RCS	Reaction Control System
RSS	Range Safety Signal
SAO	Smithsonian Astrophysical Observatory
SCM	Standard Cubic Meter
SM	Service Module
SOX	Solid Oxygen
STADAN	Space Tracking and Data Acquisition Network
U. T.	Universal Time
VCO	Voltage Controlled Oscillator

CONVERSION FACTORS TO INTERNATIONAL SYSTEM OF UNITS OF 1960

Parameter	Multiply	By	To Obtain
acceleration	ft/s^2	3.048×10^{-1} (exact)	m/s^2
area	in^2	6.4516×10^{-4} (exact)	m^2
barometer pressure	mbs	1.00×10^{-2} (exact)	N/cm^2
density	$slugs/ft^3$	5.153788185×10^2	kg/m^3
energy	Btu	1.0543503×10^3 (thermal chemical)	watt-s
mass flow rate	lb s/ft	4.5359237×10^{-1} (exact)	kg/s
force	lb	4.448221615	N (Newton)
heating rate	Btu/ft^2-s	1.1348931 (thermal chemical)	$watt/cm^2$
impulse	lb-s	4.448221615	N-s
length	ft	3.048×10^{-1} (exact)	m
	in	2.54×10^{-2} (exact)	m
mass	$lb\ s^2/ft$	4.5359237×10^{-1} (exact)	kg
moment	lb-ft	1.355817948	N-m
	lb-in	$1.12984829 \times 10^{-1}$	N-m
moment of inertia	$lb\text{-}ft\text{-}s^2$	1.355817948	$kg\text{-}m^2$
power	Btu/hr	2.9287508×10^{-4}	kw
pressure	lb/in^2	$6.894757293 \times 10^{-1}$	N/cm^2
	lb/ft^2	$4.788025898 \times 10^{-3}$	N/cm^2
specific weight	lb/ft^3	1.57087468×10^2	N/m^3
temperature	° F+459.67	$5.555555556 \times 10^{-1}$	°K
velocity	ft/s	3.048×10^{-1} (exact)	m/s
	knot*	$5.144444444 \times 10^{-1}$	m/s
volume	ft^3	$2.8316846592 \times 10^{-2}$ (exact)	m^3
	gallon**	$3.785411784 \times 10^{-3}$ (exact)	m^3

Note: $g_o = 9.80665\ m/s^2$ (exact)

* knot (International)
** gallon (U. S. Liquid)

MPR-SAT-FE-66-11

RESULTS OF THE TENTH SATURN I LAUNCH VEHICLE TEST FLIGHT SA-10

SECTION I. FLIGHT TEST SUMMARY

1.1 FLIGHT TEST RESULTS

Saturn launch vehicle SA-10, sixth of the Block II series vehicles and the third operational vehicle, was launched at 08:00 AM EST, July 30, 1965. This flight test was the tenth and last in a series of Saturn I vehicles to be flight tested. The flight test was the third in a series to launch a Pegasus satellite (Pegasus C) and was a complete success with all mission objectives achieved.

SA-10 was the sixth vehicle launched from complex 37B at Cape Kennedy, Florida, and represents the fifth launch of the Saturn/Apollo configuration. This was the second Saturn vehicle launch that required no technical holds. All operations were normal and the only hold was the 30-minute build-in-hold, used to make launch time coincident with the beginning of the launch window. The major anomaly associated with countdown operations was high surface winds; 8.7 m/s (16.9 knots) were prevalent during the hour preceding launch. The high surface winds resulted in an S-I stage LOX short load of approximately 725 kg (1600 lbm).

The actual trajectory of SA-10 was very close to nominal. The total velocity was 9.8 m/s higher than nominal at OECO and 1.06 m/s lower than nominal at S-IV cutoff. At S-IV cutoff the actual altitude was 0.04 km lower than nominal and the range was 1.33 km less than nominal. The cross range velocity deviated 0.62 m/s to the left of nominal at S-IV cutoff.

The S-IV stage and payload at orbital insertion (S-IV cutoff plus 10 seconds) had a space fixed velocity 0.7 m/s less than nominal, yielding a perigee altitude of 528.8 km and an apogee altitude of 531.9 km. Estimated orbital lifetime was 720 days, 5 days less than nominal.

The performance of both the S-I and S-IV propulsion systems was satisfactory for the SA-10 flight. The vehicle sea level longitudinal thrust of the S-I stage averaged between 0.82 percent (engine analysis) and 0.86 percent (flight simulation) higher than predicted. Vehicle specific impulse averaged between 0.15 percent (engine analysis) and 0.39 percent (flight simulation) lower than predicted. Inboard and outboard engine cutoff occurred 1.79 seconds and 1.69 seconds earlier than predicted, respectively. Outboard engine cutoff was initiated by the backup timer 6.1 seconds after inboard engine cutoff. The S-IV stage average vehicle longitudinal thrust deviation was between 0.29 percent (engine analysis) and 0.17 percent (flight simulation) higher than predicted. The specific impulse deviation was between 0.01 percent (engine analysis) and 0.21 percent (flight simulation) lower than predicted. The performance of all subsystems was as expected with the exception of the S-IV stage fuel pressurization system. The pressurization control solenoid valve did not open when required during a portion of the flight.

The overall performance of the SA-10 guidance and control systems was satisfactory. Vehicle response to all signals was properly executed including roll maneuver, pitch program, and path guidance (utilizing the iterative guidance scheme) during the S-IV stage flight.

Path guidance was initiated at 18.13 seconds after separation. Performance of the iterative guidance mode in the pitch plane and delta minimum in yaw was satisfactory in achieving insertion conditions very near those desired. The total space fixed velocity at S-IV cutoff measured by the ST-124 guidance system was 7592.02 m/s (7591.96 m/s was programmed for velocity cutoff), compared to a velocity of 7591.50 m/s determined from tracking. The difference between tracking and guidance was well within required tolerances.

Separation was executed smoothly with small control deviations. Separation transients were relatively small and well within design requirements.

Separation of the Apollo shroud occurred at 812.10 seconds, functioning as planned.

The SA-10 vehicle experienced maximum bending in the pitch plane at 74.2 seconds. A maximum static moment of 655,901 N-m was experienced at station 23.8 m (936 in). The structural flight loads on SA-10 were generally as expected and no Pogo effects were apparent. The vibrations observed on SA-10 were generally within the expected levels and compared well with SA-8. There was no evidence of S-I/S-IV interstage structural degradation during separation.

The measured pressure and temperature environment on the S-I and S-IV stage of SA-10 were generally similar to those measured on SA-8. Calorimeters were flown for the second time on the engine bell and aspirator surface of engines 3 and 7. The heating rates from these calorimeters were higher on SA-10 than on SA-9 and more nearly represent the actual environment.

The electrical system of SA-10 vehicle operated satisfactorily during boost and orbital phases of flight and all mission requirements were met. The long life battery in the Instrument Unit (IU) provided power to the P1 and F6 telemetry links for 140 minutes, which well exceeds the one orbit requirement.

Overall reliability of the SA-10 measuring system was 98.8 percent, considering only those measurements active at liftoff. There were 1018 measurements active at liftoff of which 12 failed during flight. All airborne tape recorders operated satisfactorily. The onboard TV system for SA-10 was cancelled prior to flight. The altimeter system and associated return-pulse-shape experiment failed to operate. The MISTRAM transponder failed at 63 seconds of flight and provided no usable data.

The photo/optical coverage for SA-10 was good. However, downrange cloud conditions prevented all of the 10.2 m (400 in) and 12.7 m (500 in) focal length cameras from recording usable data.

The Pegasus C spacecraft performance was satisfactory. At approximately 640.252 seconds, the S-IV stage, Instrument Unit, Apollo shroud and Pegasus were inserted into orbit with no appreciable pitch, yaw, or roll rate. The Pegasus wing deployment and all spacecraft systems worked properly and all measurements were initially within their predicted limits. A roll rate started to build up after wing deployment, as expected, and reached a maximum of 6.3 deg/s, as compared to 6.5 deg/s for SA-8 and 9.8 deg/s for SA-9.

1.2 TEST OBJECTIVES

Primary objectives

1. Collection and evaluation of meteoroid data in near earth orbit - Achieved:

    a. Determination of meteoroid penetration of satellite panels for three thicknesses of aluminum.

    b. Measurement of satellite's radiation environment and panel temperature to evaluate the validity of hit data.

    c. Determination of satellite's position and orientation relative to time of hit occurrence.

2. Continued demonstration of launch vehicle iterative guidance mode and evaluation of system accuracy - Achieved

Secondary objectives

1. Evaluation of the functional operation of the Pegasus meteoroid technology satellite's mechanical, structural, and electronics subsystems - Achieved

2. Evaluation of S-IV/IU/Service Module adapter (SMA) exterior thermal control coating - Achieved

3. Evaluation of boilerplate Command Module (CM)/SM separation from the S-IV/IU/SMA - Achieved

4. Evaluation of the S-IV stage nonpropulsive venting system - Achieved.

1.3 TIMES OF EVENTS

The times of events for SA-10 are contained in Table 1-I.

TABLE 1-I. TIMES OF EVENTS

Event	Range Time (sec)			Predicted Time Bases			
	Actual	Predicted	Act-Pred	Time from 1st Motion	Time from Guid. Zero (Ti)	Time from OECO (TB 3)	Time from S-IV Cutoff (TB 4)
First Motion	0.49	-	-	0			
LO Signal (Umb Disc)	0.711	-	-	-			
Guidance Detects LO	0.716	-	-	-			
Guidance Computes Zero Time (Ti)	0.737	-	-	-	0		
Brakes Released	8.97	8.97	-	-	8.23		
Pitch Command	9.28	9.28	0	-	8.54		
Roll Command	9.29	9.29	0	-	8.55		
Roll Completed	14.49	14.49	0	-	13.75		
Lock Modules	138.99	138.99	0	-	138.25		
Level Sense (TB 2)*	140.42	142.21	-1.79	141.72	-	-7.80	
IECO	142.22	144.01	-1.79	143.52	-	-6.00	
OECO	148.32	150.01	-1.69	149.52	-	0	
Computer Detects OECO (TB 3)	148.32	150.01	-1.69	-	-	0	
Ullage Rockets Ignite	149.03	150.72	-1.69	-	-	0.71	
Separation/Retro Ignition Signal	149.13	150.82	-1.69	-	-	0.81	
Open S-IV Accumulators	149.93	151.62	-1.69	-	-	1.61	
S-IV Start Command	150.83	152.52	-1.69	-	-	2.51	
Signal to Jettison Ullage/LES	161.13	162.82	-1.69	-	-	12.81	
Introduce Guidance	167.26	(168.15 169.05)	(-0.89 -1.79)	-	-	18.14-19.04	
S-IV Guidance Cutoff Signal	630.25	632.57	-2.32	632.08	-	-	-0.69
Computer Sense S-IV CO (TB 4)	630.94	633.26	-2.32	-	-	-	0
Insertion	640.25	642.57	-2.32	642.08	-	-	
Close Auxiliary NPV Ports	811.00	813.17	-2.17	-	-	-	179.91
Initial Pegasus Forward Restraint Sep.	812.00	814.17	-2.17	-	-	-	180.91
Initiate Apollo Shroud Sep.	812.10	814.27	-2.17	-	-	-	181.01
Initiate Pegasus Wing Restraint and Energize Wind Deployment Motors	872.00	874.27	-2.27	-	-		241.01
End Wing Deployment (motors stop)	911.40	914.27	-2.87	-	-	-	281.01

Note: Range zero occurred at 13:00:00 ZULU time.

* Time Base 2 (Low Level Sense)

SECTION II. INTRODUCTION

This report presents the results of the early engineering evaluation of the SA-10 test flight. Performance of each major vehicle system is discussed with special emphasis on malfunctions and deviations.

The report is published by the Saturn Flight Evaluation Working Group, comprised of representatives from all Marshall Space Flight Center laboratories, John F. Kennedy Space Center, MSFC's prime contractors for the S-I stage (Chrysler), the S-IV stage (Douglas), and the IU stage (IBM), and engine contractors (Rocketdyne and Pratt & Whitney). Therefore, the report represents the official MSFC position at this time. This report will not be followed by a similarly integrated report unless continued analysis or new evidence should prove the conclusions presented here partially or entirely wrong. Final evaluation reports may, however, be published by the MSFC laboratories and the stage contractors covering some of the major systems or special subjects as required.

SECTION III. LAUNCH OPERATIONS

3.1 SUMMARY

SA-10 was the second Saturn launch that required no technical holds. All operations were normal and the only hold was the 30-minute built-in hold. This was not needed but was used to make launch time coincident with the beginning of the launch window at 8:00 AM EST.

Two minor anomalies were detected during the countdown operation. A leak developed in the flex connection between the fixed LOX overland line from the storage facility and the S-I fill mast, and a separation of the environmental control system duct to the Pegasus occurred at the umbilical tower. Both problems were corrected without impact on the countdown.

Surface wind conditions were much higher than normal. The wind speed prevalent in the hour preceding launch was 9.3 m/s (18 knots) at a height of 24 m. This high surface wind condition resulted in a LOX short load of approximately 725 kg (1600 lbm).

The ground support equipment sustained considerably more damage than on any previous launch.

3.2 PRELAUNCH MILESTONES

A chronological summary of events and preparations leading to the launch of SA-10 is shown in Table 3-I.

3.3 ATMOSPHERIC CONDITIONS

Launch day weather conditions were satisfactory. High surface winds were prevalent in the hour preceding launch but were not above the design wind limitations. Some specific atmospheric observations at launch were:

1. Surface winds - mean wind speed for one minute was 6.2 m/s with gusts up to 9.8 m/s from 210-degree azimuth

2. Cloud coverage - 0.5 cirrus at unknown altitude, 0.2 alto-cumulus at a base height of 3050 m, and 0.1 cumulo-nimbus at a base height of 460 m

3. Ambient pressure - 10.163 N/cm^2

4. Ambient temperature - 299.9°K

5. Relative humidity - 71 percent

6. Visibility - 16 km.

3.4 COUNTDOWN

The launch countdown for SA-10 began Wednesday, July 28, at 11:20 hours at T-1005 minutes. No difficulties were encountered and the count was held at T-605 minutes at 18:00 hours as planned. Countdown was resumed July 29 at 21:25 hours. There were no interruptions in the count until the planned 30-minute hold at T-30. However, a problem did exist in the S-I stage LOX fill line on the launcher. A leak developed in the flex connection between the fixed LOX overland line from the storage facility and the S-I fill mast. Minor countdown work-arounds were made to allow for replacement of the flex connection. A separation of the environmental control system duct to the Pegasus payload occurred on the umbilical tower. Reconnection of this line was made without the impact on the count.

At the time of launch all mandatory range and field instrumentation was classified at "Go" with the exception of one S-I hydraulic temperature measurement which failed earlier in the count. Since this was considered a red line measurement, a waiver for deletion of this measurement was required and granted by MSFC.

3.5 PROPELLANT LOADING

3.5.1 S-I STAGE

The function of the S-I stage propellant loading system is to tank accurately the LOX and fuel required to achieve flight mission objectives. The propellants required are based on propulsion performance obtained from simulated flight predictions.

The weight of LOX tanked by the loading system for a given pressure value is primarily dependent upon wind speed during loading. Forced air currents around the LOX tanks cause temperature stratification within the LOX columns and increased boiloff at the surface. Also, a higher ullage pressure is present in the outer tanks because vaporized LOX flows through the interconnect to the center tank before being vented to the atmosphere. This ullage pressure differential results in the outer LOX levels being lower than the level in the center tank. Since the LOX loading system is connected only to the center tank, a difference exists between the actual LOX weight and the apparent weight based on the density and height of the LOX column in the center tank. This weight decrement, or short load, is shown with respect to wind speed in Figure 3-1.

TABLE 3-I. SA-10 PRELAUNCH MILESTONES

Date	Event
May 31, 1965	S-I-10 arrived via barge (S-IV-10 arrived 5/10/65).
June 1, 1965	IU arrived.
June 2, 1965	S-I erection complete.
June 8, 1965	S-IV erected.
June 9, 1965	IU erected. All umbilical connections complete.
June 21, 1965	SM and SM adapter arrived.
June 22, 1965	Pegasus C arrived.
June 25, 1965	Pegasus C deployment test completed.
June 29, 1965	CM and LES arrived.
June 30, 1965	S-I and S-IV full tank pressure tests completed.
July 6, 1965	Pegasus C, SM, CM, and adapter erected.
July 8, 1965	LES erected.
July 9, 1965	Swing arm, plug drop OAT systems tests completed with satisfactory quick-look results.
July 12, 1965	Q-ball installation complete. All ordnance installation complete.
July 13, 1965	Simulated LOX and LH_2 loading tests completed with satisfactory results.
July 15, 1965	Launch vehicle cryogenic tanking test completed.
July 20, 1965	Flight readiness test completed.
July 23, 1965	RP-1 loading completed.
July 26, 1965	Countdown Demonstration Test, Precount.
July 27, 1965	Countdown Demonstration Test, Count.
July 28, 1965	Countdown Precount start 1120 and 1800.
July 29, 1965	Begin Launch Count 2125.
July 30, 1965	Liftoff scheduled for 0800.

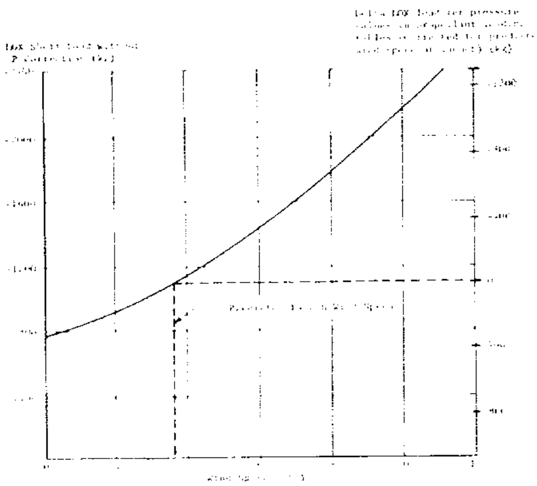

FIGURE 3-1. EFFECT OF WIND SPEED ON LOX LOAD

Environmental conditions for the time of SA-10 launch were forecast from meteorological data. These were used to establish propellant loading criteria that would permit a constant S-I stage weight to be maintained for the allowable range of fuel temperature. The S-I-10 propellant loading tables were generated to provide the differential pressure values necessary for the loading computers to tank the LOX and fuel required for the actual fuel density at launch. The differential pressure values given in the loading tables compensate for the LOX short load at the predicted launch wind speed of 3.6 m/s (7 knots) based on the mean surface winds for the month of July. The right scale of Figure 3-1 shows that as wind speed varies from the predicted value, the actual LOX weight is either more or less than the weight indicated by the LOX loading system.

The total S-I propellant weights are listed in Table 3-II. Predicted propellant weights used to determine S-I stage performance were based on nominal LOX and fuel densities established from environmental conditions expected at launch. The propellant weight requirements at ignition are based on the nominal LOX density and the actual fuel density at S-I stage ignition. Average fuel density at ignition, determined from fuel temperature in tanks F1 and F3 together with the density manometer reading in tank F4, was as predicted.

Propellant loading system weights listed in the table were determined from the manometer readings immediately prior to propellant system pressurization. The fuel manometer value indicated the fuel weight to be only 68 kg (149 lbm) more than required for the fuel density at ignition. The LOX manometer value indicated the LOX weight to be only 69 kg (151 lbm) less than required for a 3.6 m/s (7 knot) wind condition at ignition. However, the wind speed prevalent in the hour preceding launch was approximately 8.7 m/s (16.9 knots). Figure 3-1 reveals that for this wind speed the actual LOX weight should be approximately 816 kg (1800 lbm) less than indicated by the loading system.

Reconstructed weights shown in the table were determined from telemetered probe data in conjunction with the Mark IV computer program reconstruction of propellant consumption during holddown. The reconstructed fuel weight is within 136 kg (300 lbm) of the weight required at ignition. The reconstructed LOX weight is 725 kg (approximately 1600 lbm) less than required at ignition due to the high winds.

3.5.2 S-IV STAGE

3.5.2.1 LOX

The LOX system was successfully loaded with LOX by cooling down and filling in two phases: main fill and replenish. The automatic LOX loading system, in conjunction with the LOX main fill pump, was successfully utilized for loading the LOX tank. S-IV stage LOX system precool was initiated by starting the LOX system precool timer 4 hours and 9 minutes prior to liftoff. The LOX vent valves remained open throughout the loading operation. The LOX transfer line was precooled for approximately 8 minutes prior to the initiation of LOX main fill, which occurred when approximately 318 kg (700 lbm) of LOX had been filled into the tank. The LOX main fill line pressure reached a maximum of 147 N/cm^2 (213 psi) and stabilized at 141 N/cm^2 (204 psi). At approximately the 4-percent level, a stabilized loading rate of 0.0454 m^3/s (720 gpm) was achieved. This loading rate was maintained until the 99-percent mass level was attained at approximately 21 minutes after the initiation of LOX transfer line precool. At this level, the loading system secured the main fill pump and closed the main LOX fill valve as scheduled.

After countdown of the S-I and S-IV LOX replenish system was completed, the LOX replenishing operation was initiated 2 hours and 25 minutes prior to liftoff. During this operation, the LOX in the tank was allowed to boil off to the 99.5-percent level. It was replenished to the 99.75-percent level at a rate of approximately 0.0126 m^3/s (200 gpm). This replenishing cycle continued until the start of the 150-second automatic count. At this time, the tank was pressurized, and final LOX replenishment was completed. The fill valve was closed manually when the loading panel observer noted that the fill valve had not been

TABLE 3-II. S-I-10 PROPELLANT WEIGHTS AT IGNITION COMMAND

Propellant	Weight Requirements		Weight Indications		Weight Deviations (5)			
	Pred. Prior to Launch (1)	Ignition (2)	ΔP Loading System (3)	Reconstructed (4)	ΔP Loading	(%)	Reconstructed	(%)
LOX (kg)	279,795	279,795	279,726	279,070	-68	-0.02	-725	-0.26
(lbm)	616,842	616,842	616,691	615,244	-151	-0.02	-1598	-0.26
Fuel (kg)	125,248	125,248	125,316	125,376	67	0.05	128	0.10
(lbm)	276,124	276,124	276,273	276,407	149	0.05	283	0.10
Total (kg)	405,043	405,043	405,042	404,446	-1	0.00	-597	-0.15
(lbm)	892,966	892,966	892,964	891,651	-2	0.00	-1315	-0.15

(1) Predicted propellant weights were based on a LOX density of 1129.78 kg/m^3 (70.53 lbm/ft^3) and a fuel density of 804.77 kg/m^3 (50.24 lbm/ft^3).

(2) Propellant weights required at ignition are based on a LOX density of 1129.78 kg/m^3 (70.53 lbm/ft^3) and a fuel density of 804.77 kg/m^3 (50.24 lbm/ft^3) determined immediately prior to launch.

(3) Propellant weights indicated by the loading system are based on pressure readings immediately prior to propellant system pressurization.

(4) Reconstructed propellant weights are based on discrete probe data in conjunction with the Mark IV reconstruction.

(5) Weight deviations are referenced to weight requirements at ignition.

automatically commanded to close at the 100-percent LOX level. The manual closing of the valve resulted in a LOX overload of 143 kg (316 lbm). The LOX load indicated by the PU system at liftoff was 38,339 kg (84,524 lbm).

3.5.2.2 LH_2

The fuel system was satisfactorily loaded with LH_2 by cooling down and filling in four stages: initial fill, main fill, replenish, and reduced replenish. The automatic fuel loading system was successfully utilized for loading the LH_2 tank. Loading of LH_2 into the S-IV stage was initiated 1 hour and 48 minutes prior to liftoff.

The LH_2 transfer line had been precooled for approximately 10 minutes prior to the initiation of LH_2 initial fill. Cooldown of the LH_2 transfer line was accomplished through the helium precool heat exchanger and the stage LH_2 tank. Initial fill was accomplished with an LH_2 replenish line pressure of 16 to 19 N/cm^2 (23 to 28 psi), and with the LH_2 tank vents open. The initial fill rate was 0.0295 m^3/s (467 gpm). Monitoring of the LH_2 tank ullage pressure during this initial fill operation revealed that the tank pressure did not decrease below the prefill ambient pressure. At the 16-percent mass level, main fill was initiated, and the rate increased to 0.121 m^3/s (1915 gpm). When the 96-percent level was reached 33 minutes after the initiation of LH_2 precool, the main fill valve was closed manually. LH_2 replenish was then initiated manually, and the LH_2 loading system was placed in the automatic mode. The LH_2 level then cycled between the 99.25-percent (reduced replenish position) and the 99.5-percent mass level (replenish closed position). This replenishing cycle continued until the start of the 150-second automatic count. The fuel load indicated by the PU system at liftoff was 7790 kg (17,174 lbm).

3.5.2.3 COLD HELIUM

Prior to the initiation of LH_2 loading, the cold helium spheres were prepressurized to 621 N/cm^2 (900 psi) to prevent the spheres from collapsing as they cooled down during the initial part of LH_2 loading.

Cold helium loading was initiated approximately 87 minutes before launch. After the spheres were submerged at approximately the 75-percent LH_2 mass level, the pressure was increased to, and maintained at, 2068 to 2103 N/cm^2 (3000 to 3050 psi). The design load temperature of 33.3°K at a pressure of 2068 N/cm^2 (3000 psi) was attained approximately 55 minutes following the initiation of LH_2 loading. At liftoff, the spheres were charged to 2146 N/cm^2 (3112 psi) at 22.7°K.

3.6 HOLDDOWN

All combustion stability monitor (CSM) systems performed satisfactorily during launch of SA-10. The maximum and average vibration levels are recorded below.

Eng. No.	Meas. No.	Max G's (RMS)	Average G's (RMS)
1	XE-57-1	25	15
2	XE-57-2	20	12
3	XE-57-3	22	13
4	XE-57-4	30	16
5	XE-57-5	45	14
6	XE-57-6	13	10
7	XE-57-7	40	13
8	XE-57-8	25	14

3.7 GROUND SUPPORT EQUIPMENT

3.7.1 MECHANICAL GROUND SUPPORT EQUIPMENT

The postlaunch evaluation of the operational ground support equipment systems revealed that considerably more damage was incurred than on any previous launch. Damage to the launcher, engine service platform, holddown arms, environmental control system, pneumatic distribution system, and firing accessories was considered normal, with more damage to that equipment located north of the launcher center line.

The cable trays on the north side of the umbilical tower at the 10.7 m (35 feet) level were damaged extensively and many of the cables badly burned. There was considerably more damage to the swing arms than has occurred previously, particularly flex hoses, electrical cables, and ECS ducts. The greater damage sustained by the swing arms was due to a steady 9.3 to 11.3 m/s (18 to 22 knot) wind blowing from the south/southwest. Scheduled refurbishment of launch complex 37B minimizes the impact of the damage.

3.7.2 ELECTRICAL SUPPORT EQUIPMENT

The electrical support equipment responded and performed normally during the SA-10 countdown and automatic sequence.

No damage was sustained by any functioning hardware other than the tower cabling, which was burned excessively during liftoff.

3.8 BLOCKHOUSE REDLINE VALUES

Blockhouse redline values are limits placed on critical engine and vehicle parameters to indicate safe conditions for ignition and launch. These measurements are monitored in the blockhouse during countdown. When a redline value is exceeded and a condition detrimental to the mission is indicated, the countdown is halted and disposition is made. If the problem is not considered detrimental to mission success, the countdown is continued. If the problem is of a more serious nature and cannot be corrected in time to continue the countdown after a short hold, the launch is aborted and rescheduled.

All values are within the redline limits and necessitated no holds for the Saturn SA-10 countdown. An S-I hydraulic temperature measurement failed early in the countdown and was waived by MSFC through the launch information exchange facility (LIEF).

Review of the SA-10 launch films revealed that the GH_2 vent disconnects on swing arm 3 operated properly at liftoff. Therefore, it has been concluded that the malfunction which occurred on SA-8 was properly corrected. The correction was made by increasing the pneumatic actuator pressure, which in turn increased the force available to achieve separation of the GH_2 vent disconnects.

SECTION IV. MASS CHARACTERISTICS

4.1 VEHICLE MASS

The total vehicle mass was 511,159 kg (1,126,913 lbm) at first motion; 62,583 kg (137,972 lbm) at S-IV ignition and approximately 10,324 kg (22,761 lbm) in orbit (dry weight after Apollo separation). Table 4-I is a vehicle mass breakdown at significant flight events. A flight sequence summary is given in Table 4-II. The predicted mass data presented in this section are derived from Reference 1. The propellant masses presented in the tables refer to total amount down to and including the propellant masses in the engines. The S-IV stage masses are based on a composite of engine analysis and PU system analysis, and are considered the best estimate from the composite standpoint. The best estimate of the total second flight stage as determined from the flight simulation analysis is presented in Section VI and is considered the best estimate from the consumption standpoint.

4.2 VEHICLE CENTER OF GRAVITY AND MOMENT OF INERTIA

Longitudinal and radial center of gravity, and roll, pitch, and yaw moments of inertia are given in Table 4-III. The parameters and mass are plotted versus burning time in Figures 4-1 and 4-2.

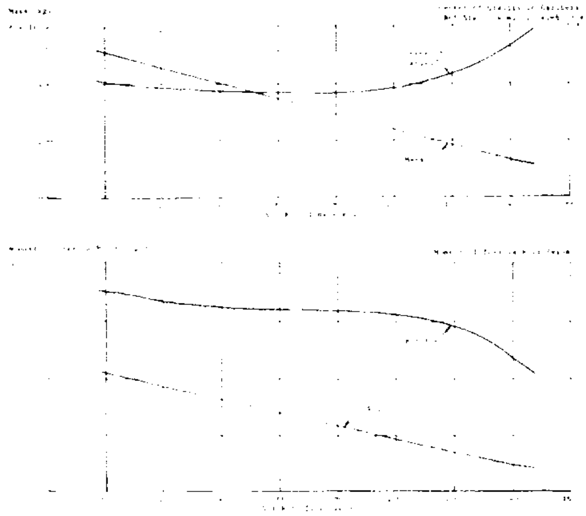

FIGURE 4-1. VEHICLE MASS CENTER OF GRAVITY AND MASS MOMENT OF INERTIA FOR S-I STAGE

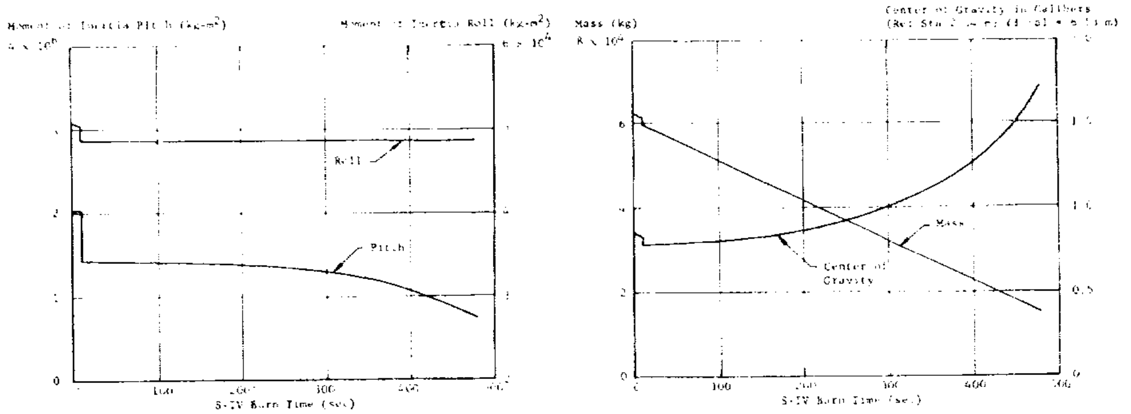

FIGURE 4-2. VEHICLE MASS CENTER OF GRAVITY AND MASS MOMENT OF INERTIA FOR S-IV STAGE

~~CONFIDENTIAL~~

TABLE 4-I. VEHICLE MASSES

EVENT	IGNITION COMMAND		FIRST MOTION		OUTBOARD ENGINE CUTOFF		SEPARATION		S-IV STAGE IGNITION COMMAND		S-IV STAGE CUTOFF		S-IV STAGE END OF THRUST DECAY	
	Pred*	Actual	Pred*	Actual	Pred*	Actual	Pred*	Actual	Pred*	Actual	Pred*	Actual	Pred*	Actual
RANGE TIME (sec.)	[illegible]	[illegible]	0	[illegible]	[illegible]	[illegible]	[illegible]	[illegible]	[illegible]	[illegible]	[illegible]	[illegible]	[illegible]	[illegible]
MASS (kg)														
S-I Stage, Dry	47,189	47,165	47,189	47,165	47,189	47,165	47,189	47,165						
LOX in Container	[illegible]	[illegible]	[illegible]	[illegible]	[illegible]	[illegible]	[illegible]	0						
RP-1 in Container	[illegible]	124,234	[illegible]	[illegible]	[illegible]	[illegible]	[illegible]	[illegible]						
LOX Below Container	[illegible]	3,443	3,638	[illegible]	[illegible]	[illegible]	1,150	1,158						
RP-1 Below Container	[illegible]	2,092	[illegible]	[illegible]	[illegible]	[illegible]	2,302	2,302						
LOX Ullage Gas (GOX & He)	46	[illegible]	[illegible]	[illegible]	[illegible]	[illegible]	1,246	[illegible]						
RP-1 Ullage Gas (N_2)	17	18	13	24	[illegible]	132	125	131						
S-I Retro Rocket Prop	613	613	613	613	613	613	613	613						
N_2 RP-1 Press S-IV Purge	[illegible]	[illegible]	121	[illegible]	[illegible]	[illegible]	114	114						
Other N_2	16	16	16	[illegible]	15	12	16	12						
Helium N_2 Vent Purge	3	3	3	[illegible]	3	3	3	3						
Hydraulic Oil	13	13	13	[illegible]	13	13	13	13						
Oronite	14	14	14	[illegible]	4	4	4	4						
Frost	454	454	[illegible]	[illegible]										
Environmental Gas	172	172	172	[illegible]										
TV Camera Purge N_2		[illegible]		[illegible]		[illegible]		[illegible]						
Total S-I Stage	[illegible]	[illegible]	[illegible]	[illegible]	[illegible]	53,616	[illegible]	[illegible]						
S-I/S-IV Interstage Dry	[illegible]	[illegible]	977	972	[illegible]	972	[illegible]	[illegible]						
Environmental Gas	124	124	124	124										
Total S-I/S-IV Interstage	1,100	1,095	[illegible]	1,095	[illegible]	[illegible]	[illegible]	[illegible]						
S-IV Stage Dry & MSFC Inst	[illegible]	[illegible]	[illegible]	[illegible]	[illegible]	[illegible]	[illegible]	[illegible]	[illegible]	[illegible]	[illegible]	[illegible]	[illegible]	[illegible]
LOX in Container	38,152	[illegible]	[illegible]	38,372	38,092	38,319	[illegible]	38,313	[illegible]	[illegible]	[illegible]	155	[illegible]	[illegible]
LH_2 in Container	[illegible]	[illegible]	[illegible]	[illegible]	[illegible]	[illegible]	[illegible]	7,653	[illegible]	[illegible]	[illegible]	[illegible]	[illegible]	[illegible]
LOX Below Container	[illegible]	[illegible]	[illegible]	[illegible]	[illegible]	[illegible]	[illegible]	[illegible]	[illegible]	[illegible]	[illegible]	[illegible]	[illegible]	[illegible]
LH_2 Below Container	[illegible]	7	[illegible]	[illegible]	[illegible]	[illegible]	[illegible]	[illegible]	[illegible]	[illegible]	[illegible]	[illegible]		
LOX Ullage Gas (He & GOX)	[illegible]	13	15	[illegible]	16	13	[illegible]	[illegible]	[illegible]	13	[illegible]	96	[illegible]	[illegible]
LH_2 Ullage Gas (He & GH_2)	[illegible]	[illegible]	[illegible]	[illegible]	[illegible]	[illegible]	[illegible]	[illegible]	[illegible]	[illegible]	70	[illegible]	[illegible]	[illegible]
Ullage Rocket Grain	[illegible]	[illegible]	[illegible]	[illegible]	[illegible]	[illegible]	[illegible]	[illegible]	[illegible]	[illegible]				
Ullage Rocket Cases	[illegible]	126	[illegible]	126	130	126	[illegible]	[illegible]	[illegible]	[illegible]				
Helium Pneumatic	3	3	[illegible]	[illegible]	3	3	[illegible]	3	[illegible]	[illegible]	3	[illegible]	[illegible]	[illegible]
Helium LOX Press Supply	[illegible]	58	[illegible]	[illegible]	[illegible]	[illegible]	58	58	[illegible]	[illegible]	[illegible]	[illegible]	[illegible]	[illegible]
Helium Makeup Supply	[illegible]	[illegible]	[illegible]	1	1	1	1	1	1	[illegible]	[illegible]	[illegible]	[illegible]	[illegible]
Frost	[illegible]	[illegible]	[illegible]	5										
LOX in Engines					[illegible]	[illegible]	[illegible]	15	15	15	15	[illegible]		
LH_2 in Engines					[illegible]	[illegible]	[illegible]	4	[illegible]	[illegible]	[illegible]	[illegible]		
Total S-IV Stage	[illegible]	53,002	[illegible]	53,002	[illegible]	52,832	[illegible]	[illegible]	[illegible]	[illegible]	[illegible]	[illegible]	6,994	[illegible]
Vehicle Instr Unit Dry	1,190	1,197	1,190	1,197	1,190	1,197	1,190	1,197	1,190	[illegible]	1,190	[illegible]	1,190	[illegible]
Vehicle Instr Unit-N_2	18	18	18	18	18	18	18	18	18	18	18	[illegible]	18	[illegible]
Total Vehicle Instr Unit	1,208	[illegible]	1,208	[illegible]	1,208	[illegible]	[illegible]	[illegible]	1,208	[illegible]	[illegible]	[illegible]	[illegible]	[illegible]
Payload	8,739	[illegible]	[illegible]	[illegible]	[illegible]	[illegible]	[illegible]	[illegible]	[illegible]	[illegible]	[illegible]	[illegible]	[illegible]	[illegible]
First Flight Stage Total	[illegible]	[illegible]	[illegible]	511,159	117,035	117,239	[illegible]	116,531						
Second Flight Stage Total							[illegible]	62,643	[illegible]	[illegible]	15,526	15,651	[illegible]	[illegible]
MASS (lbm)														
S-I Stage, Dry	[illegible]	[illegible]	[illegible]	[illegible]	104,033	[illegible]	104,033	[illegible]						
LOX in Container	[illegible]	[illegible]	[illegible]	[illegible]		6		0						
RP-1 in Container	[illegible]	[illegible]	[illegible]	[illegible]	[illegible]	[illegible]	[illegible]	[illegible]						
LOX Below Container	[illegible]	[illegible]	8,026	[illegible]	[illegible]	[illegible]	2,536	2,554						
RP-1 Below Container	[illegible]	[illegible]	[illegible]	[illegible]	[illegible]	[illegible]	[illegible]	5,075						
LOX Ullage Gas (GOX & He)	[illegible]	[illegible]	[illegible]	[illegible]	[illegible]	[illegible]	[illegible]	[illegible]						
RP-1 Ullage Gas (N_2)	38	[illegible]	[illegible]	[illegible]	[illegible]	[illegible]	274	[illegible]						
S-I Retro Rocket Prop	[illegible]	[illegible]	1,352	[illegible]	[illegible]	[illegible]	[illegible]	1,352						
N_2 RP-1 Press S-IV Purge	[illegible]	[illegible]	[illegible]	[illegible]	[illegible]	[illegible]	[illegible]	[illegible]						
Other N_2	36	[illegible]	[illegible]	[illegible]	[illegible]	[illegible]	26	[illegible]						
Helium N_2 Vent Purge	6	6	6	6	6	6	6	6						
Hydraulic Oil	28	28	[illegible]	[illegible]	[illegible]	[illegible]	28	[illegible]						
Oronite	32	32	[illegible]	32	8	[illegible]	8	8						
Frost	1,000	1,000	[illegible]	1,000										
Environmental Gas	379	[illegible]	[illegible]	379										
TV Camera Purge N_2		15		[illegible]		[illegible]		15						
Total S-I Stage	1,066,663	[illegible]	[illegible]	[illegible]	[illegible]	[illegible]	[illegible]	[illegible]						
S-I/S-IV Interstage Dry	2,153	[illegible]	[illegible]	2,142	[illegible]	[illegible]	[illegible]	2,142						
Environmental Gas	273	273	273	273										
Total S-I/S-IV Interstage	[illegible]	[illegible]	2,626	2,615	2,153	[illegible]	[illegible]	2,142						
S-IV Stage Dry & MSFC Inst	[illegible]	[illegible]	14,197	14,207	[illegible]	14,207	[illegible]	14,207	[illegible]	[illegible]	14,197	14,207	[illegible]	[illegible]
LOX in Container	[illegible]	[illegible]	84,111	[illegible]	83,956	[illegible]	83,952	84,465	[illegible]	84,440	530	[illegible]	[illegible]	[illegible]
LH_2 in Container	17,168	17,177	17,168	17,177	[illegible]	16,876	[illegible]	[illegible]	[illegible]	16,855	[illegible]	[illegible]	[illegible]	[illegible]
LOX below Container	152	[illegible]	[illegible]	152	152	152	[illegible]	152	[illegible]	[illegible]	[illegible]	152	[illegible]	[illegible]
LH_2 below Container	[illegible]	[illegible]	[illegible]	15	[illegible]	[illegible]	[illegible]	[illegible]	[illegible]	[illegible]	15	15	[illegible]	[illegible]
LOX Ullage Gas (He & GOX)	[illegible]	28	[illegible]	28	[illegible]	28	[illegible]	28	[illegible]	29	[illegible]	211	[illegible]	211
LH_2 Ullage Gas (He & GH_2)	[illegible]	19	[illegible]	19	36	19	36	19	36	19	[illegible]	106	[illegible]	106
Ullage Rocket Grain	243	[illegible]	[illegible]	[illegible]	[illegible]	[illegible]	235	[illegible]	[illegible]	[illegible]				
Ullage Rocket Cases	286	277	286	277	286	277	286	277	286	277				
Helium Pneumatic	[illegible]	[illegible]	[illegible]	[illegible]	[illegible]	[illegible]	7	7	[illegible]	[illegible]	[illegible]	6	[illegible]	6
Helium LOX Press Supply	[illegible]	[illegible]	[illegible]	[illegible]	[illegible]	128	125	128	[illegible]	[illegible]	[illegible]	42	[illegible]	[illegible]
Helium Makeup Supply	3	2	3	2	3	2	3	2	[illegible]	[illegible]	3	1	[illegible]	1
Frost	90	10	90	10										
LOX in Engines					25	28	27	33	33	33	33	33		
LH_2 in Engines					4	9	4	9	[illegible]	4	4	9		
Total S-IV Stage	[illegible]	116,866	[illegible]	116,866	116,309	116,472	[illegible]	116,452	[illegible]	[illegible]	15,497	[illegible]	[illegible]	[illegible]
Vehicle Instr Unit Dry	2,623	2,638	2,623	2,638	2,623	2,638	2,623	2,638	2,623	2,638	2,623	2,638	2,623	[illegible]
Vehicle Instr Unit-N_2	40	40	40	40	40	40	40	40	40	40	40	40	40	40
Total Vehicle Instr Unit	2,663	2,678	2,663	2,678	2,663	2,678	2,663	2,678	2,663	2,678	2,663	2,678	2,663	2,678
Payload	19,267	19,276	19,267	19,276	18,965	18,972	18,965	18,972	18,965	18,972	16,070	16,019	16,070	16,019
First Flight Stage Total	1,141,476	1,140,556	1,128,124	1,126,913	258,018	258,468	256,903	256,907						
Second Flight Stage Total							137,611	136,102	137,435	137,972	34,230	[illegible]	[illegible]	34,435

*Predicted weights are those reported in R-P&VE-VAW-65-102

~~CONFIDENTIAL~~

TABLE 4-II. SA-10 FLIGHT SEQUENCE MASS SUMMARY

MASS HISTORY	ACTUAL		PREDICTED	
	kg	(lbm)	kg	(lbm)
S-I Stage @ Ground Ignition	453,288	999,329	453,893	1,000,663
S-I/S-IV Interstage @ Ground Ignition	1,095	2,415	1,100	2,426
S-IV Stage @ Ground Ignition	53,007	116,860	52,824	116,457
Vehicle Instrument Unit @ Ground Ignition	1,215	2,678	1,208	2,663
Payload @ Ground Ignition	8,743	19,274	8,739	19,267
1st Flight Stage @ Ground Ignition	517,348	1,140,556	517,764	1,141,476
S-I Thrust Buildup Propellants	-6,189	-13,643	-6,056	-13,352
1st Flight Stage @ First Motion	511,159	1,126,913	511,708	1,128,124
S-I Mainstage Propellants	-391,545	-863,209	-392,331	-864,943
S-I Frost	-454	-1,000	-454	-1,000
S-I Fuel Additive	-254	-560	-256	-566
S-I Lube Oil (Oronite)	-11	-24	-11	-24
S-I N_2 for S-IV Tail Purge	-83	-183	-41	-90
S-I Environmental Control	-172	-379	-172	-379
S-I IETD Propellants	-960	-2,116	-945	-2,081
Seal Purge	-4	-10		
S-I/S-IV Interstage Environmental Control	-123	-273	-123	-273
S-IV Chilldown LOX	-40	-88	-55	-121
S-IV Chilldown LH_2	-132	-291	-107	-237
S-IV Frost	-5	-10	-41	-90
Payload Environmental Control	-137	-302	-137	-302
1st Flight Stage @ Cutoff Signal	117,239	258,468	117,035	258,018
S-I N_2 for S-IV Tail Purge	-9	-20	-4	-10
S-I OETD Propellants (To Separation)	-691	-1,523	-671	-1,479
S-IV Chilldown LOX	-3	-7	-6	-13
S-IV Chilldown LH_2	-3	-6	-2	-5
S-IV Ullage Rocket Propellants	-2	-5	-4	-8
1st Flight Stage @ Separation	116,531	256,907	116,348	256,503
S-I Stage @ Separation	-52,917	-116,663	-52,952	-116,739
S-I/S-IV Interstage @ Separation	-972	-2,142	-977	-2,153
S-IV Chilldown LOX	-12	-26	-13	-28
S-IV Chilldown LH_2	-7	-16	-4	-10
S-IV Ullage Rocket Propellants	-40	-88	-63	-138
2nd Flight Stage @ Ignition	62,583	137,972	62,339	137,435
S-IV Mainstage Propellants*	-45,388	-100,064	-45,315	-99,903
S-IV Helium Heater Propellants	-11	-24	-11	-24
S-IV Ullage Rocket Propellants	-68	-150	-44	-97
S-IV Ullage Rocket Cases	-126	-277	-130	-286
Launch Escape System	-1,339	-2,953	-1,313	-2,895
2nd Flight Stage @ Cutoff Signal**	15,651	34,504	15,526	34,230
S-IV Thrust Decay Propellants	-11	-24	-11	-24
S-IV Propellants Below Pump Inlets	-19	-42	-19	-42
2nd Flight Stage @ End of Thrust Decay**	15,621	34,438	15,496	34,164
Orbital Flight Stage (After Apollo Sep)	10,324	22,761	10,323	22,758

* Includes Thrust Buildup Propellants (to 90% thrust)
** Predicted Values are for a Depletion Cutoff

Note: IETD - Inboard Engine Thrust Decay
OETD - Outboard Engine Thrust Decay

TABLE 4-III. MASS CHARACTERISTICS COMPARISON

EVENT		MASS		LONGITUDINAL C.G. (X STA.)		RADIAL C.G.		ROLL MOMENT OF INERTIA		PITCH MOMENT OF INERTIA		YAW MOMENT OF INERTIA	
		[illegible]	[illegible]	[illegible]	[illegible]	[illegible] inches	[illegible]	[illegible]	[illegible]	[illegible]	[illegible]	[illegible]	[illegible]
[illegible]	Pred*	[illegible]		[illegible]		[illegible]		[illegible]		[illegible]		[illegible]	
	Actual	[illegible]	[illegible]	[illegible]	[illegible]	[illegible]	[illegible]	[illegible]	[illegible]	[illegible]	[illegible]	[illegible]	[illegible]
[illegible]	Pred*	[illegible]		[illegible]		[illegible]		[illegible]		[illegible]		[illegible]	
	Actual	[illegible]	[illegible]	[illegible]	[illegible]	[illegible]	[illegible]	[illegible]	[illegible]	[illegible]	[illegible]	[illegible]	[illegible]
[illegible]	Pred*	[illegible]		[illegible]		[illegible]		[illegible]		[illegible]		[illegible]	
	Actual	[illegible]	[illegible]	[illegible]	[illegible]	[illegible]	[illegible]	[illegible]	[illegible]	[illegible]	[illegible]	[illegible]	[illegible]
[illegible]	Pred*	[illegible]		[illegible]		[illegible]		[illegible]		[illegible]		[illegible]	
	Actual	[illegible]	[illegible]	[illegible]	[illegible]	[illegible]	[illegible]	[illegible]	[illegible]	[illegible]	[illegible]	[illegible]	[illegible]
[illegible]	Pred*	[illegible]		[illegible]		[illegible]		[illegible]		[illegible]			
	Actual	[illegible]	[illegible]	[illegible]	[illegible]	[illegible]	[illegible]	[illegible]	[illegible]	[illegible]	[illegible]		
1st Flight Stage [illegible]	Pred*	[illegible]		[illegible]		[illegible]		[illegible]		[illegible]			
	Actual	[illegible]	[illegible]	[illegible]	[illegible]	[illegible]	[illegible]	[illegible]	[illegible]	[illegible]	[illegible]		
[illegible]	Pred*	[illegible]		[illegible]		[illegible]		[illegible]		[illegible]			
	Actual	[illegible]	[illegible]	[illegible]	[illegible]	[illegible]		[illegible]	[illegible]	[illegible]	[illegible]		
1st Flight Stage [illegible]	Pred*	[illegible]		[illegible]		[illegible]		[illegible]		[illegible]			
	Actual	[illegible]	[illegible]	[illegible]	[illegible]	[illegible]	[illegible]	412,683	[illegible]	[illegible]	[illegible]		
1st Flight Stage [illegible]	Pred*	[illegible]		[illegible]		[illegible]		[illegible]		[illegible]			
	Actual	[illegible]	[illegible]	[illegible]	[illegible]	[illegible]		[illegible]	[illegible]	[illegible]	[illegible]		
[illegible] Flight Stage [illegible]	Pred*	[illegible]		[illegible]		[illegible]		[illegible]		[illegible]		[illegible]	
	Actual	[illegible]	[illegible]	[illegible]	[illegible]	[illegible]	[illegible]	[illegible]	[illegible]	[illegible]	[illegible]	[illegible]	[illegible]
2nd Flight Stage [illegible]	Pred**	[illegible]		[illegible]		[illegible]		[illegible]		[illegible]		[illegible]	
	Actual	[illegible]	[illegible]	[illegible]	[illegible]	[illegible]	[illegible]	[illegible]	[illegible]	[illegible]	[illegible]	[illegible]	[illegible]
2nd Flight Stage [illegible]	Pred*	[illegible]		[illegible]		[illegible]		[illegible]		[illegible]		[illegible]	
	Actual	[illegible]	[illegible]	[illegible]	[illegible]	[illegible]	[illegible]	[illegible]	[illegible]	[illegible]	[illegible]	[illegible]	[illegible]
[illegible] S-IVB-IV [illegible] at Separation	Pred*	[illegible]		[illegible]		[illegible]		[illegible]		[illegible]			
	Actual	[illegible]	[illegible]	[illegible]	[illegible]	[illegible]	[illegible]	[illegible]	[illegible]	[illegible]	[illegible]		
[illegible]	Pred*	[illegible]		[illegible]		[illegible]		[illegible]		[illegible]		[illegible]	
	Actual	[illegible]	[illegible]	[illegible]	[illegible]	[illegible]	[illegible]	[illegible]	0.55	[illegible]	[illegible]	[illegible]	[illegible]

Note: Percent Deviation = (Deviation ÷ Actual) x 100. [illegible]

* [illegible]

** [illegible]

5.1 SUMMARY

The actual trajectory of SA-10 was very close to nominal. The total velocity was 9.8 m/s higher than nominal at OECO and 1.06 m/s lower than nominal at S-IV cutoff. At S-IV cutoff the actual altitude was 0.04 km lower than nominal and the range was 1.33 km less than nominal. The cross range velocity deviated 0.62 m/s to the left of nominal at S-IV cutoff.

A theoretical free flight trajectory of the separated S-I booster indicates that the impact ground range was 8.0 km longer than nominal. Impact, assuming the tumbling booster remained intact, occurred at 725.8 seconds.

The S-IV payload at orbital insertion (S-IV cutoff + 10 seconds) had a space fixed velocity 0.7 m/s less than nominal, yielding a perigee altitude of 528.8 km and an apogee altitude of 531.9 km. Estimated orbital lifetime was 720 days, 5 days less than nominal.

5.2 TRAJECTORY COMPARISON WITH NOMINAL

Actual and nominal altitude, range and cross range (Z_e) are compared graphically in Figure 5-1 for the S-I phase of flight and in Figure 5-2 for the S-IV phase. Actual and nominal total earth fixed velocities are shown graphically in Figure 5-3. Comparisons of the actual and nominal parameters at the three cutoff events are shown in Table 5-I. The nominal trajectory is presented in Reference 2.

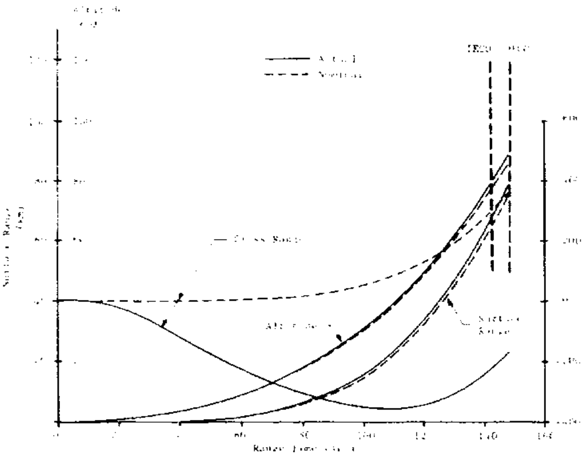

FIGURE 5-1. S-I TRAJECTORY

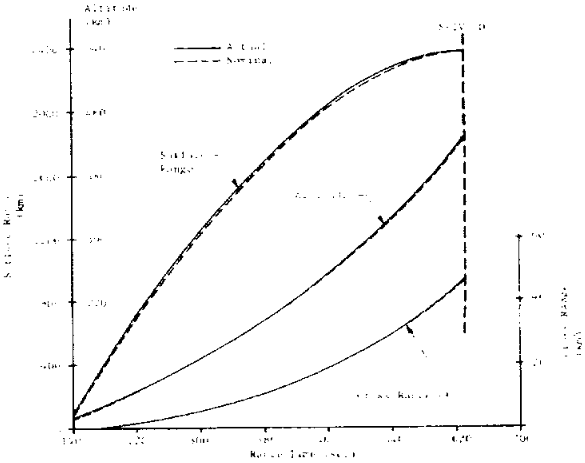

FIGURE 5-2. S-IV TRAJECTORY

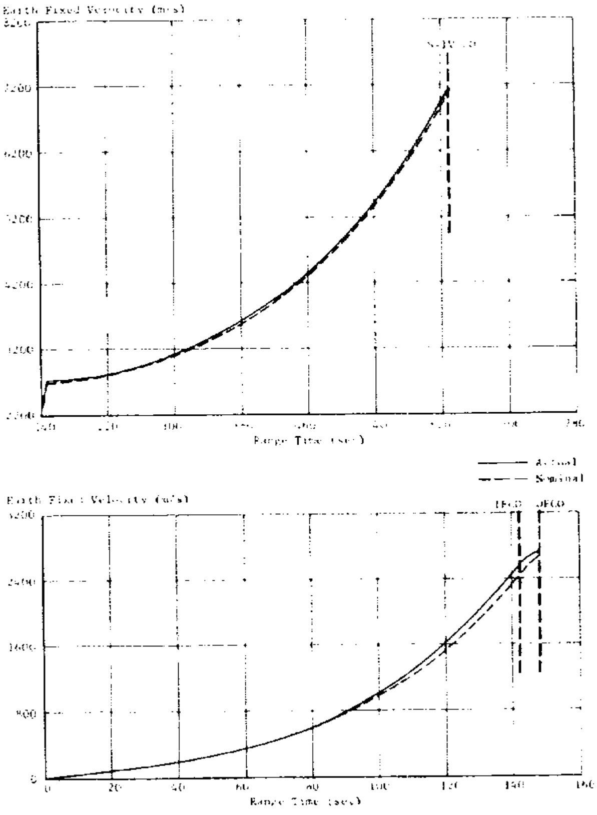

FIGURE 5-3. EARTH FIXED VELOCITY

TABLE 5-I. CUTOFF CONDITIONS

Parameter	IECO			OECO			S-IV CO (Guidance Signal)		
	Actual	Nominal	Act-Nom	Actual	Nominal	Act-Nom	Actual	Nominal	Act-Nom
Range Time (sec)	142.22	144.01*	-1.79	148.32	150.01*	-1.69	630.252	632.575	-2.323
Altitude (km)	79.32	79.12	0.20	89.50	88.94	0.56	535.71	535.75	-0.04
Range (km)	67.01	67.44	-0.43	79.38	79.70	-0.32	1842.88	1844.21	-1.33
Cross Range, Z_e (km)	-0.22	0.31	-0.53	-0.16	0.37	-0.53	46.05	46.40	0.35
Cross Range Velocity, $\dot{Z}_e$ (m/s)	8.47	10.38	-1.91	10.22	11.97	-1.75	221.66	222.28	-0.62
Earth Fixed Velocity (m/s)	2564.49	2556.97	7.52	2724.63	2714.87	9.76	7150.60	7151.66	-1.06
Earth Fixed Velocity Vector Elevation (deg)	39.516	38.757	0.759	38.693	37.968	0.725	0.014	0.006	0.008
Earth Fixed Velocity Vector Azimuth (deg)	95.642	95.696	-0.054	95.735	95.781	-0.046	105.374	105.384	-0.010
Space Fixed Velocity (m/s)	2894.69	2890.23	4.46	3058.05	3051.17	6.88	7591.41	7591.96	-0.55
Total Inertial Acceleration (m/s²)	60.28	59.95	0.33	31.38	31.13	0.25	25.23	25.53	-0.30

*Based on First Motion Time of 0.49 Second.

Earth Fixed Velocity Accuracy
OECO ± 0.3 m/s
S-IV CO ± 0.5 m/s

Altitude Accuracy
OECO ± 30 m
S-IV CO ± 100 m

Altitude and range were greater than nominal during S-I and S-IV burn. The actual earth fixed velocity was 9.8 m/s greater than nominal at OECO. The longitudinal acceleration was slightly higher than nominal for the S-I and S-IV stage operations (Fig. 5-4).

The S-IV stage cut off 2.32 seconds earlier than nominal; considering a 1.69-second early S-I stage cutoff, the S-IV stage had a 0.63-second shorter burning time. The actual space fixed velocity at the S-IV cutoff signal, given by the guidance computer (630.252), was 0.5 m/s less than nominal. Slightly higher than nominal S-IV stage thrust and flowrate, along with the excess S-I cutoff velocity, account for the early S-IV cutoff.

Mach number and dynamic pressure are shown in Figure 5-5. These parameters were calculated using measured meteorological data to an altitude of 55 km. Above this altitude the U.S. Standard Reference Atmosphere was used.

Comparisons of actual and nominal parameters at significant event times are given in Table 5-II. Apex, loss of telemetry, and impact apply only to the discarded S-I stage.

The S-IV cutoff signal was given by the guidance computer at 630.252 seconds; however, the solenoids for the propellant valves on the S-IV stage did not receive the signal until 0.022 second later. The velocity increments imparted to the vehicle subsequent

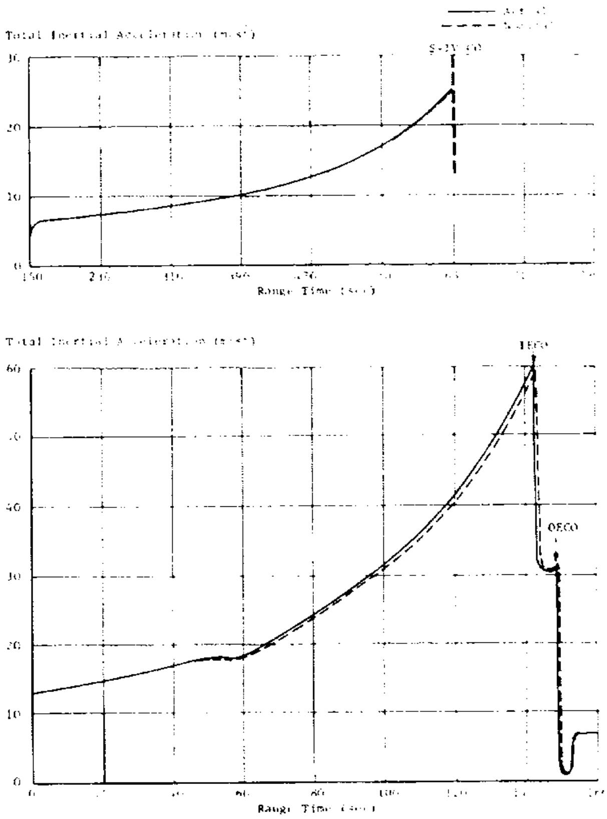

FIGURE 5-4. TOTAL INERTIAL ACCELERATION

TABLE 5-II. SIGNIFICANT EVENTS

Event	Parameter	Actual	Nominal	Act-Nom
First Motion	Range Time (sec) Total Inertial Acceleration (m/s^2)	0.49 12.95	0.49 12.82	0.00 0.13
Mach 1	Range Time (sec) Altitude (km)	54.805 7.22	54.766 7.27	0.039 -0.05
Maximum Dynamic Pressure	Range Time (sec) Dynamic Pressure (N/cm^2) Altitude (km)	68.75 3.418 12.23	67.49 3.267 11.54	1.26 0.151 0.69
Maximum Total Inertial Acceleration (S-I Stage)	Range Time (sec) Acceleration (m/s^2)	142.32 60.40	144.11 60.07	-1.79 0.33
Maximum Earth Fixed Velocity (S-I Stage)	Range Time (sec) Velocity (m/s)	148.55 2730.70	150.31 2724.17	-1.76 6.53
Apex (S-I Stage)	Range Time (sec) Altitude (km) Range (km) Earth Fixed Velocity (m/s)	353.0 261.80 489.32 2041.7	350.9 254.56 485.35 2058.0	2.1 7.24 3.97 -16.3
Loss of Telemetry (S-I Stage)	Range Time (sec) Altitude (km) Range (km) Total Inertial Acceleration (m/s^2) Elevation Angle from Pad (deg)	572.0 65.0 929.2 -4.18 -0.32	572.0 52.4 934.8 -4.25 -1.07	0.0 12.6 -5.6 0.07 0.75
Impact (S-I Stage)	Range Time (sec) Range (km) Cross Range (km) Geodetic Latitude (deg) Longitude (deg)	725.8 985.4 18.8 27.1958 70.6699	720.3 977.4 19.6 27.2019 70.7510	5.5 8.0 -0.8 -0.0061 -0.0811
Maximum Total Inertial Acceleration (S-IV Stage)	Range Time (sec) Acceleration (m/s^2)	630.35 25.25	632.68 25.55	-2.33 -0.30
Maximum Earth Fixed Velocity (S-IV Stage)	Range Time (sec) Velocity (m/s)	630.55 7153.85	632.88 7154.48	-2.33 -0.63

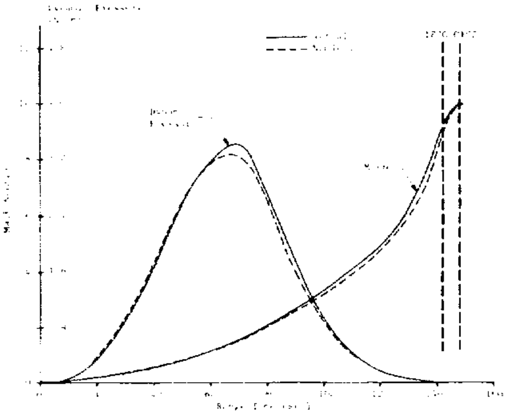

FIGURE 5-5. MACH NUMBER AND DYNAMIC PRESSURE

to the guidance cutoff signal are given below for the S-I and S-IV stage at OECO and S-IV guidance cutoff, respectively.

VELOCITY GAIN (m/s)

Event	Actual	Nominal
OECO	5.3	5.3
S-IV CO	2.9	3.1

A theoretical free flight trajectory was computed for the discarded S-I stage using initial conditions from the reference trajectory at separation. There was no tracking coverage of the discarded S-I stage on SA-10. A nominal tumbling drag coefficient was assumed for the reentry phase. The calculated impact location relative to the launch site is shown in Figure 5-6. Table 5-III presents the booster impact location from the actual and nominal free flight trajectory.

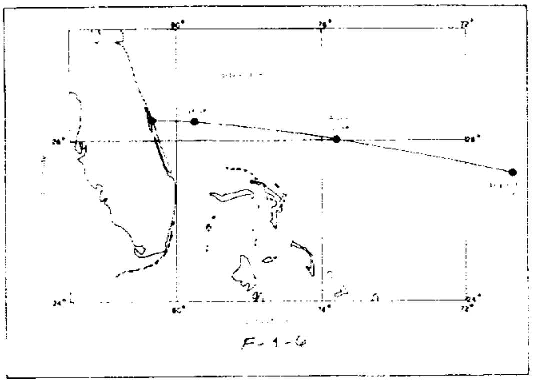

FIGURE 5-6. BOOSTER TRAJECTORY GROUND TRACK

TABLE 5-III. BOOSTER IMPACT

Parameter	Actual (Calc)	Nominal	Act-Nom
Surface Range* (km)	985.4	977.4	8.0
Cross Range (km)	18.8	19.6	-0.8
Geodetic Latitude (deg)	27.1958	27.2019	-0.0061
Longitude (deg)	70.6699	70.7510	-0.0811
Range Time (sec)	725.8	720.3	5.5

* Surface range is measured from launch site.

5.3 INSERTION CONDITIONS (S-IV CUTOFF + 10 SECONDS)

Insertion condition solutions were made using the Antigua and Grand Turk data at insertion, the Carnarvon downrange tracking, and the Merritt Island and Ascension tracking on the return pass over the Cape area. The data were used in various combinations and solutions solving and not solving for effective drag. In addition the orbital ephemeris, which was used to generate the predicted tracking, had a velocity impulse of approximately -0.3 m/s applied at the separation time of the Apollo shroud from the S-IV/ Pegasus C (812 seconds range time). The magnitude and direction of this impulse were determined from the telemetered output of the guidance system.

The maximum variations, considering all solutions made, in position and velocity components from the insertion parameters quoted were 200 m in positions and 0.5 m/s in velocities.

Table 5-IV shows a comparison between the actual and nominal orbital insertion elements. The tracking residuals which represent the differences between the actual tracking observations and the observations calculated for the orbit defined by the insertion elements given in the tabulation were of the magnitudes experienced on previous Saturn flights. The average residual errors of the range measurements were approximately 12 m and of the azimuth and elevation measurements approximately 0.02 degree.

TABLE 5-IV. INSERTION ELEMENTS COMPARISON

Event	Actual	Nominal	Act-Nom
Time of Orbital Insertion (Range Time sec)	640.252	642.575	-2.323
Space Fixed Velocity (m/s)	7594.3	7595.0	-0.7
Flight Path Angle (deg)	0.0052	-0.0008	0.0060
Altitude (km)	535.7	535.7	0.0
Ground Range (km)	1908.9	1910.2	-1.3
Cross Range (km)	48.3	48.6	-0.3
Cross Range Velocity (m/s)	225.7	226.3	-0.6
Apogee Altitude (km)*	531.9	531.9	0.0
Perigee Altitude (km)*	528.8	531.6	-2.8
Period (min)	95.2	95.3	-0.1
Inclination (deg)	28.88	28.88	0.00
Excess Circular Velocity (m/s)	-0.8	-0.1	-0.7
Lifetime (days)	720	725	-5

* The apogee and perigee altitudes are referenced to a spherical earth radius 6378.165 km.

SECTION VI. PROPULSION

6.1 SUMMARY

The performance of both the S-I and S-IV propulsion systems was satisfactory for the SA-10 flight. SA-10 was the sixth Saturn vehicle to employ H-1 engines at a thrust level of 836,000 N (188,000 lbf) to power the S-I stage. SA-10 also represents the sixth flight of the RL10A-3 engines to power the S-IV stage.

The vehicle sea level longitudinal thrust of the S-I stage averaged 0.82 percent higher than predicted from the engine analysis and 0.86 higher than predicted from the flight simulation analysis. Vehicle specific impulse averaged 0.15 percent lower than predicted for the engine analysis and 0.39 percent lower than predicted for the flight simulation analysis. Inboard and outboard engine cutoff occurred 1.79 seconds and 1.69 seconds earlier than predicted, respectively. Outboard engine cutoff was initiated by the backup timer 6.1 seconds after inboard engine cutoff. The performance of all pressurization systems, purge systems, hydraulic systems, and other associated systems was satisfactory.

The propulsion performance of the S-IV stage was within design limits throughout the stage powered flight. The average vehicle longitudinal thrust deviation was 0.29 percent higher than predicted from the engine analysis and 0.17 percent higher than predicted from the flight simulation. The longitudinal specific impulse deviation was 0.01 percent lower than predicted from the engine analysis and 0.21 percent lower than predicted from the flight simulation analysis. Satisfactory performance was obtained from the individual engines, the LOX tank pressurization systems, the helium heater, the hydraulic systems, the PU systems, and the nonpropulsive vent system. The fuel pressurization system functioned properly with the exception that the pressurization control solenoid valve did not open when required during a portion of the flight.

6.2 S-I STAGE PERFORMANCE

6.2.1 OVERALL STAGE PROPULSION PERFORMANCE

The propulsion system of the S-I stage performed satisfactorily. The eight engines ignited satisfactorily, with no indication of any abnormal chamber pressure transients on any engine. The ignition command was initiated -2.64 seconds before liftoff signal. The engine starting sequence was within the expected tolerances of the prescribed 100 ms delay between starting pairs. The largest deviation in the thrust buildup times in the engines that received ignition signal at the same time was 58 ms between engines 6 and 8. Figure 6-1 illustrates the individual engine thrust buildup and S-I stage thrust buildup.

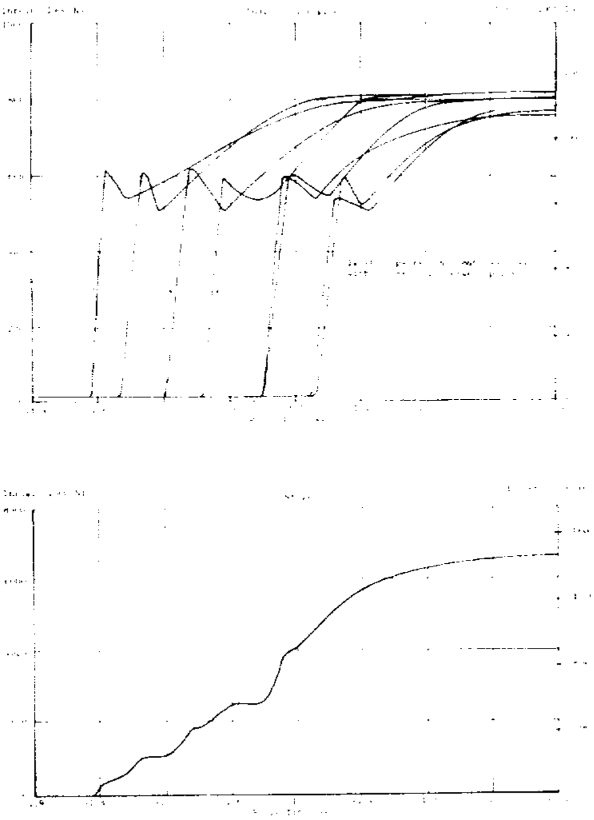

FIGURE 6-1. S-I INDIVIDUAL ENGINE AND STAGE THRUST BUILDUP

The vehicle longitudinal altitude thrust shown in Figure 6-2 averaged approximately 0.9 percent higher than predicted. The vehicle specific impulse (lower portion of Fig. 6-2) averaged approximately 0.1 percent lower than predicted.

Vehicle total propellant flowrate and mixture ratio are shown in Figure 6-3. The flight mixture ratio averaged approximately 0.5 percent lower than predicted. The lower than predicted mixture ratio can be attributed primarily to a lower than predicted LOX density.

Average S-I propulsion parameters from the engine analysis method corrected to sea level are summarized in Table 6-I.

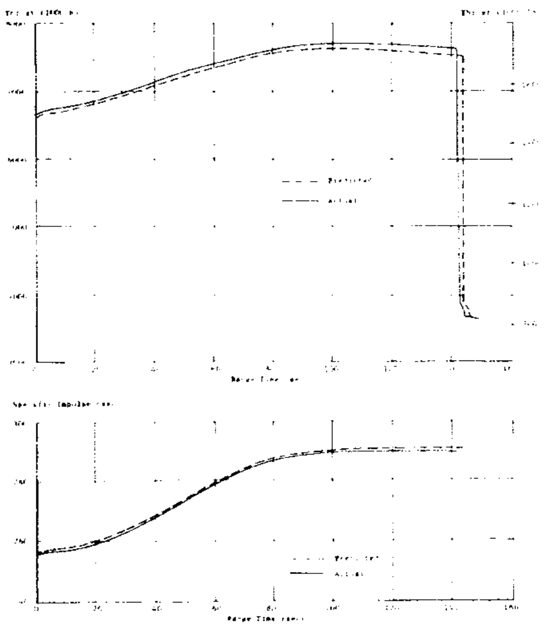

FIGURE 6-2. VEHICLE LONGITUDINAL THRUST AND SPECIFIC IMPULSE

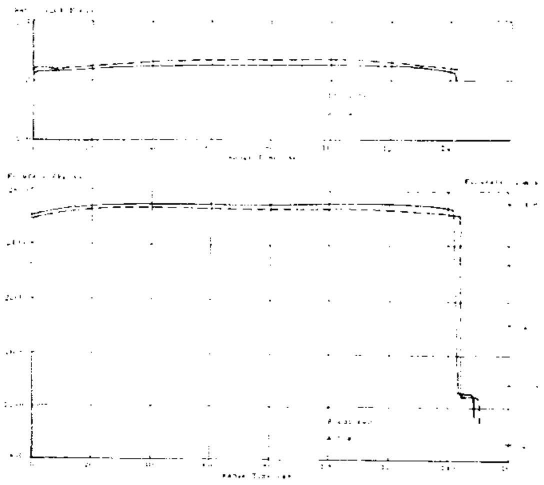

FIGURE 6-3. VEHICLE MIXTURE RATIO AND TOTAL FLOWRATE

TABLE 6-I. AVERAGE STAGE PROPULSION PARAMETERS, SA-10

Parameter	Predicted	Engine Analysis	Percentage Dev. Fm. Predicted	Flight Simulation	Percentage Dev. Fm. Predicted
Liftoff Weight (kg) (lbm)	511,707 1,128,121	511,132 1,126,853	-0.11	511,132 1,126,853	-0.11
Sea Level Thrust (N) (lbf)	6,790,517 1,526,569	6,846,414 1,539,135	0.82	6,849,180 1,539,757	0.86
Flow Rate (kg/s) (lbm/s)	2,682.3 5,913.5	2,709.1 5,972.6	1.00	2,715.2 5,986.1	1.23
Sea Level Specific Impulse (sec)	258.2	257.70	-0.15	257.2	-0.39
Vehicle Weight (kg) (142.22 sec Range Time) (lbm)	130,585.68 287,892.15	126,159 278,134	-3.5	125,282 276,200	-4.2

The engine cutoff sequence was normal for all engines. Inboard engine cutoff (IECO) occurred 1.79 seconds earlier than predicted. Approximately 0.4 second of the difference can be attributed to the 725.7 kg (1600 lbm) less than predicted LOX load. The increased power levels account for 1.2 seconds. The LOX level in tank 04 which initiated the cutoff sequence was about 2.54 cm (1 in) lower than the average outboard tank level and accounts for 0.1 second of the difference. The low levels also account for time differential between IECO and OECO being 6.1 seconds with a backup timer cutoff instead of the predicted 6.0

seconds. Figure 6-4 shows the chamber pressure decays of the inboard and outboard engines.

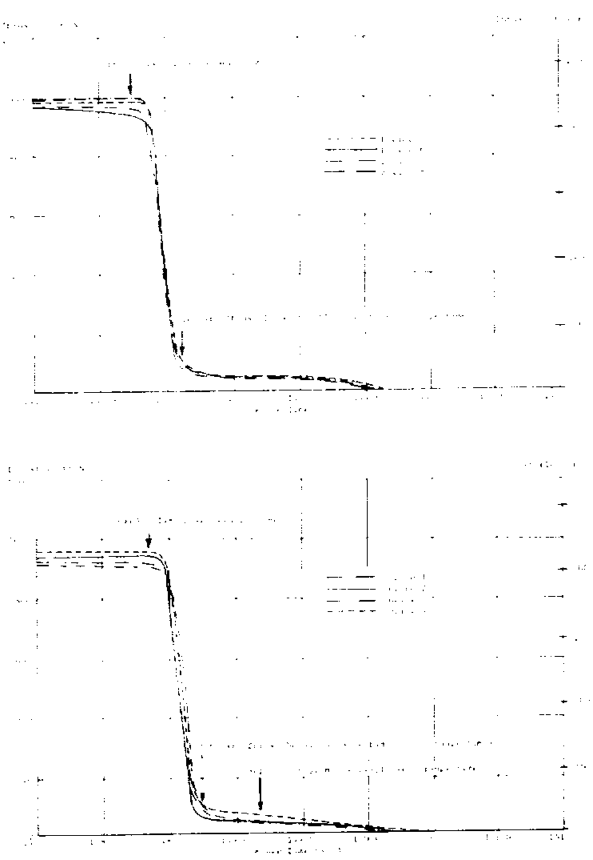

FIGURE 6-4. INBOARD AND OUTBOARD ENGINE THRUST DECAY

6.2.2 FLIGHT SIMULATION OF CLUSTER PERFORMANCE

The vehicle longitudinal sea level specific impulse, vehicle longitudinal sea level thrust, and total weight loss rate were derived from the telemetered propulsion system measurements in a simulation of the tracked trajectory. The simulation of the tracked trajectory was accomplished through the use of a six-degree-of-freedom trajectory calculation incorporating a differential correction procedure. This program determined corrections to the level of the vehicle longitudinal sea level thrust, total weight loss rate and vehicle drag correction that would yield the best fit to the velocity and acceleration from the observed trajectory. The liftoff weight as given by the MSFC weight group was considered known.

Previous analyses of all Saturn I Block II flights have indicated that the variation of the vehicle thrust as a function of time using telemetered engine measurements was consistent with the observed trajectory. It is theorized that this is a result of the clustered engines and that the effect is somehow a function of the flow from the inboard engines choking after approximately 65 seconds of flight. The cluster effect that was derived from SA-7 (lower part of Fig. 6-5) was assumed to be common to all Block II vehicles and produced reasonable solutions.

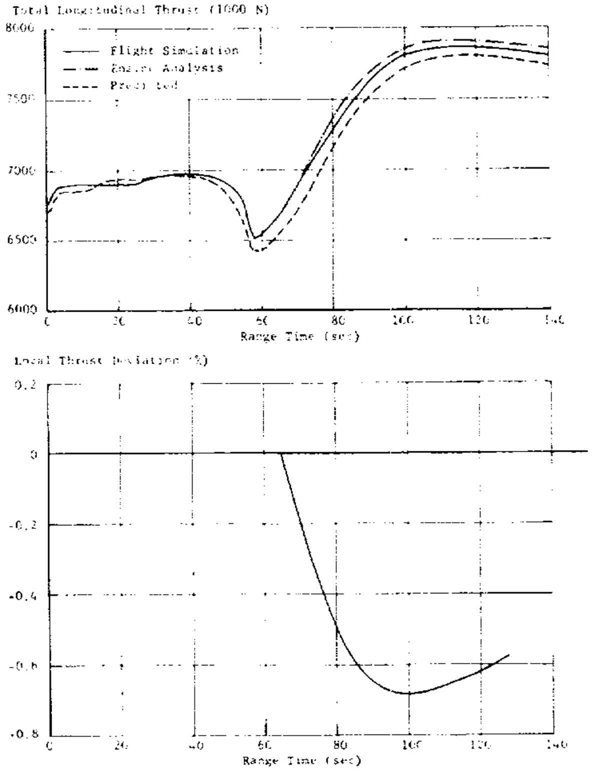

FIGURE 6-5. FLIGHT SIMULATION RESULTS

Although the cluster effect shown in Figure 6-5 was used to alter the local thrust shape in the flight simulation program, it is possible that this effect could be some force other than a thrust shape deviation. A change where this effect would act on the effective force of the vehicle in the trajectory computation program would not affect the propulsion system evaluation results since the average sea level thrust is used as a reference.

The solid line in upper portion of Figure 6-5 shows the total longitudinal force necessary to match the observed trajectory (assuming the mass history from the flight simulation analysis is correct). This represents the sum of all forces acting on the vehicle along the longitudinal axis, which includes engine thrust, turbine exhaust, drag, cluster effects, etc. The dashed line in this figure is the predicted total longitudinal force for SA-10.

Table 6-I presents a summary of the average values and deviations of liftoff weight, sea level thrust, flowrate, sea level specific impulse and vehicle weight near inboard engine cutoff signal from the flight simulation method compared with the postflight engine analysis and predicted values. The axial force coefficient resulting from this solution along with the predicted axial force coefficient for SA-10 is presented in Section XII.

The maximum deviations of the simulated trajectory from the tracked trajectory were 0.5 m/s in velocity and 0.1 m/s^2 in acceleration. This is indicative of the goodness of fit of the simulation.

6.2.3 INDIVIDUAL ENGINE PERFORMANCE

The performance of all eight engines was satisfactory. Reconstructed thrust levels for all engines were slightly higher than predicted except for engine position one. The thrust levels for engine position two were estimated solely from the telemetered chamber pressure since the turbopump speed data for this engine were not valid. Therefore, the deviations from predicted may be slightly inaccurate for this engine. Significant discrepancies exist between reconstructed and telemetered chamber pressures for engine positions 4, 6, 7, and 8. Reconstructed engine specific impulses for all engines were below the predicted values. Figure 6-6 presents the percent deviation from predicted for the reconstructed thrust and specific impulse.

Higher than predicted thrust levels have occurred during the past four flights, including SA-10. The higher than predicted thrust levels on SA-10 cannot be attributed to flight conditions. LOX pump inlet and fuel pump inlet pressures averaged within 0.7 N/cm^2 (1 psi) of predicted values. Fuel density was as predicted. The LOX pump inlet temperatures averaged 0.7°K higher than predicted because of the high wind velocities at launch. This deviation represents an average decrease from the predicted LOX pump inlet density of 3.8 kg/m^3 (0.24 lbm/ft^3). A lower than predicted LOX pump inlet density of this magnitude should have decreased thrust by approximately 0.5 percent.

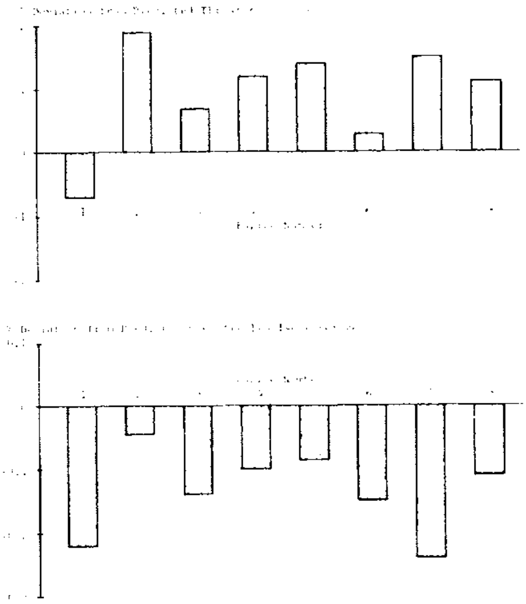

FIGURE 6-6. DEVIATION IN INDIVIDUAL ENGINE PERFORMANCE PARAMETERS (S-I)

6.3 S-I PRESSURIZATION SYSTEMS

6.3.1 FUEL PRESSURIZATION SYSTEM

Fuel tank pressurization provides increased tank structural rigidity as well as adequate engine fuel pump inlet pressure.

Fuel tank pressurization to 11.72 N/cm^2 gauge (17 psig) of a 3.7-percent ullage was accomplished in 7.6 seconds. The pressure in the fuel tanks (Fig. 6-7) agreed closely with the pressure seen on past flights and predicted values. The fuel container pressure was 6.9 N/cm^2 gauge (10 psig) at OECO.

The number of fuel tank pressurization valves that were operational during SA-10 flight were:

Time Interval (Range Time sec)	Number of Scheduled Pressurization Valves
0 to 39.5	3
39.5 to 54.5	2
54.5 to 70.5	1
70.5 to OECO	0

Pressurization valve number 2 was changed from normally closed on SA-8 to normally open on SA-10 to increase system reliability.

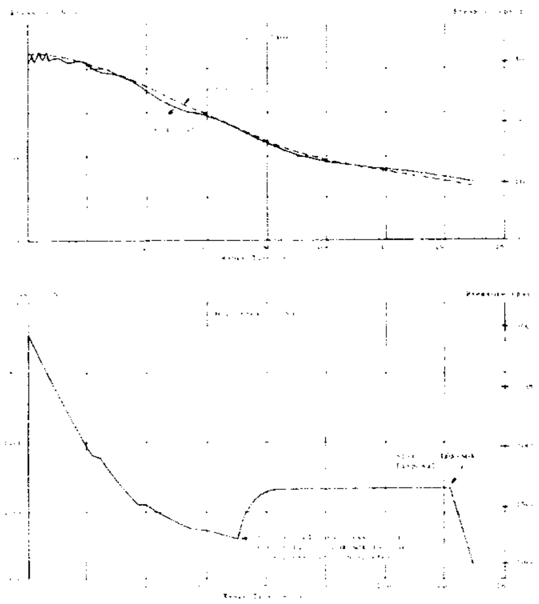

FIGURE 6-7. GAS PRESSURE IN FUEL TANK AND HIGH PRESSURE SPHERE

6.3.2 LOX TANK PRESSURIZATION SYSTEM

Prepressurization of the 3.7-percent LOX tank ullage to approximately 41.4 N/cm^2 (60 psi) was accomplished in 75.6 seconds. The LOX tank vent and relief valves were closed at T-163 seconds range time. Helium bubbling started at -153 seconds. The center LOX tank pressure (Fig. 6-7) rose to 13.6 N/cm^2 (19.7 psi) at -103 seconds when helium bubbling was terminated and LOX tank prepressurization commenced. A 0.325-cm (0.128 in) diameter orifice was selected to accomplish prepressurization of the LOX tanks in the required 50 to 90 seconds. Relief valve number 2 took more than 2 minutes to indicate closed during the automatic sequence. The valve indicator was found to be faulty during the propellant loading test. No corrective action was taken because the closed signal was not required in the automatic sequence and it was confirmed that the valve was operating properly.

Pressure histories used for prediction and actual center LOX tank pressures are shown in Figure 6-8. The SA-10 LOX tank pressure compares within 1.17 N/cm^2 (1.7 psi) of that used for prediction. The maximum center LOX tank pressure was 36.9 N/cm^2 (53.5 psi) at 35 seconds range time. Although this is greater than the set point of the GOX flow control valve (GFCV), which is 34.5 ± 1.7 N/cm^2 (50 ± 2.5 psi), it represents expected system performance. When the GFCV is at its fully closed position (against stop), the GOX flowrate will be about 7.94 kg/s (17.5 lbm/s). This flow exceeds that necessary to maintain a nominal 34.5 N/cm^2 (50 psi) in the LOX tanks for a portion of the flight.

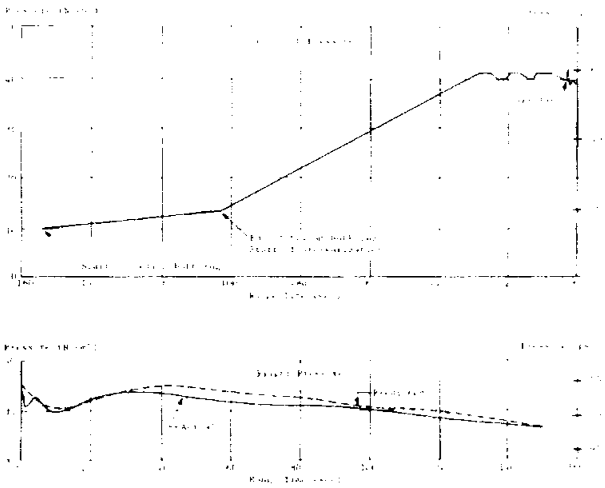

FIGURE 6-8. PRELAUNCH AND FLIGHT CENTER LOX TANK PRESSURE

The GFCV reached its full closed position at 5 seconds range time and left its full closed stop at 93 seconds when the center LOX tank pressure was 33.5 N/cm^2 (51.5 psi), indicating proper response of the GFCV.

6.3.3 CONTROL PRESSURE SYSTEM

The pneumatic control system supplies GN_2 at a regulated pressure of 517.1 ± 34.5 N/cm^2 gauge (750 ± 50 psig) for operation of the LOX system pressure relief valves 1 and 2, the LOX vent valve, the LOX replenishing control valve, suction line prevalve control valves, engine turbopump gear box pressurization, and calorimeter and LOX pump seal purging.

The control pressure system regulated pressure was between 506.8 and 510.9 N/cm^2 gauge (735 and 741 psig), well within the specified pressure band. The control equipment supply sphere pressure was 1999.5 N/cm^2 (2900 psi) at liftoff and 1644.4 N/cm^2 (2385 psi) at 150 seconds which is considerably higher than SA-9 and SA-8 because fewer calorimeters were purged.

6.3.4 LOX-SOX DISPOSAL SYSTEM

The LOX-SOX disposal system purges the S-I/S-IV interstage area of any LOX or SOX which falls from the S-IV stage engine thrust chamber during the chilldown cycle prior to S-I/S-IV stage separation. Gaseous nitrogen is supplied to the dispersal ring manifolds located under each of the S-IV stage engines to keep the area inert so that the engines ignite in a noncombustible atmosphere.

All measurements indicated successful operation of the LOX-SOX disposal system. Pressure equalization between the 0.57 m^3 (20 ft^3) nitrogen spheres of the fuel tank pressurization system and the four triplex spheres occurred at 70.5 seconds. Equalization was indicated by an increase in pressure in the fuel pressurization systems 0.57 m^3 (20 ft^3) spheres from 844.7 N/cm^2 (1225 psi) to 1123.8 N/cm^2 (1630 psi), just 6.9 N/cm^2 (10 psi) higher than on SA-8 flight (Fig. 6-7).

The S-I/S-IV vent ports were blown at 140.72 seconds by exploding bridgewire (EBW) charges. A sudden drop in S-I/S-IV interstage temperature at approximately 141 seconds indicated the initiation of S-IV LOX chilldown. The plenum chamber pressure shown in Figure 6-9 increased rapidly at 141.9 seconds indicating the opening of LOX-SOX valves 2, 3, 5, and 6 with the start of LOX-SOX disposal. A pressure surge at 144.12 seconds showed that valve number 4 opened and at 145.62 seconds another rise in pressure showed that valves 1 and 7 opened, completing the sequenced operations. These events occurred 1.79 seconds earlier than predicted because of the early start of time base 2 (propellant level sensor actuation). Maximum pressure in the plenum chamber was 210.3 N/cm^2 gauge (305 psig) which compared favorably with that of SA-8 and SA-9.

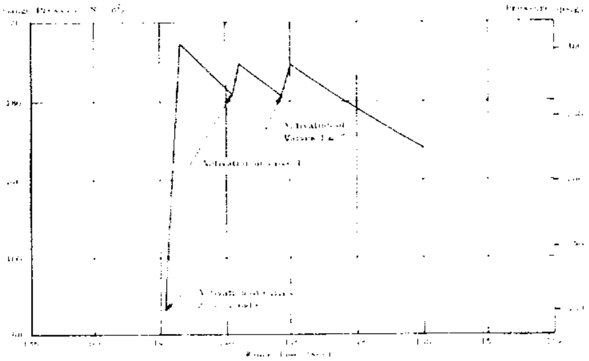

FIGURE 6-9. LOX-SOX SYSTEM OPERATION

6.3.5 HYDROGEN VENT DUCT PURGE

The hydrogen vent duct purge system removes the chilldown hydrogen flowing through the S-IV stage plumbing at approximately 35 seconds prior to S-I/S-IV stage separation. The hydrogen is removed from the S-IV stage through three 0.3 m (12 in) diameter ducts that lead down the sides of the S-I/S-IV interstage and the S-I stage in the line with stub fins II, III, and IV. Prior to launch, low pressure helium from a ground source is used to purge the three ducts. A helium triplex sphere assembly onboard the S-I stage supplies helium for purging after liftoff. The purge continues through the chilldown operation and S-I stage powered flight.

The hydrogen vent duct purge system operated satisfactorily. The hydrogen vent duct purge supply pressure was 1954.7 N/cm^2 (2835 psi) at liftoff. A steady decay of sphere pressure to 450.2 N/cm^2 (653 psi) at 148 seconds indicated expected operation of the system.

6.4 S-I STAGE PROPELLANT UTILIZATION

Propellant utilization, the ratio of propellant consumed to propellant loaded, is an indication of the propulsion system performance and the capability of the propellant loading system to tank the proper propellant loads. Propellant utilization for the S-I-10 stage was satisfactory and within 0.2 percent of predicted. The predicted and actual (reconstructed) percent of loaded propellants utilized during the flight are shown as follows:

	Prelaunch Day Predicted (%)	Flight (%)
Total	99.17	99.23
Fuel	98.24	98.42
LOX	99.58	99.59

The propellant loading criteria for S-I-10 were similar to those for S-I-9 and S-I-8, and called for simultaneous depletion of usable propellants for a fixed mainstage total propellant consumption. The ratio of LOX to fuel loaded was dependent on the fuel density at ignition command.

SA-10 was the fourth Block II flight on which a LOX starvation cutoff of the outboard engines was attempted. The LOX and fuel level cutoff probe heights and flight sequencer settings were determined for a 1.8-second time interval between any cutoff actuation and IECO, and an expected 6.0-second time interval between any IECO and OECO. OECO was to be initiated by the deactuation of the thrust OK pressure switch on any outboard engine when LOX starvation occurred. It was assumed, as for S-I-9 and S-I-8, that a total of approximately 321 kg (707 lbm) of LOX from the outboard suction lines was usable. This is equivalent to approximately 0.28 m^3 (75 gal). The backup timer (flight sequencer) was set to initiate OECO 6.1 seconds after IECO if LOX starvation cutoff had not occurred within that time. To insure against fuel starvation, fuel depletion cutoff probes were located in the F2 and F4 container sumps. The center LOX tank sump orifice diameter, which was 0.47 m (18.5 in), was the same as for S-I-9 and S-I-8. Based on S-I-9 and S-I-8 flight results, a liquid level height differential between the center LOX tank and the outboard LOX tanks of approximately 7.6 cm (3.0 in) at IECO was assumed for the prediction.

The cutoff sequence on the S-I-10 stage commenced with the signal from the LOX level cutoff probe in container 04 at 140.42 seconds. IECO signal was received 1.8 seconds later at 142.22 seconds. OECO was initiated by the backup timer 6.1 seconds after IECO, at 148.32 seconds. LOX starvation was not achieved. The average liquid level height differential between the center LOX tank and the outboard LOX tanks at IECO was approximately 7.1 cm (2.8 in). However, the level in tank 04 was approximately 2.54 cm (1 in) lower than the average level in the outboard LOX tanks when the cutoff probe actuated. Therefore, there was approximately 181 kg (400 lbm) more LOX onboard than predicted at IECO, which explains why LOX starvation was not achieved.

Inboard engine cutoff was 1.79 seconds earlier than predicted. The shorter than predicted S-I-10 stage burn time can be attributed to the LOX load being approximately 725.7 kg (1600 lbm) less than required for the fuel density at ignition command (see Section III), and the stage performance being higher than predicted (see Para. 6.2). The low LOX level in tank 04 also contributed approximately 0.1 second to the short burning time.

The propellant residuals indicated that the reconstructed LOX residual was only 16.3 kg (36 lbm) less than the prelaunch day prediction. Since the LOX residual was very close to predicted and LOX starvation was not achieved, it must be concluded that the usable LOX in the outboard engine suction lines is greater than the amount assumed for the prediction. This conclusion agrees with the flight results from S-I-9 and S-I-8.

A fuel bias of 839 kg (1850 lbm) was specified for SA-10. The fuel bias minimizes the total propellant residuals associated with the possible variation in the actual stage mixture ratio from the predicted stage mixture ratio. If the specified propellant weights had been loaded and the performance had been as predicted, the fuel bias would have remained as residual fuel after cutoff. The reconstructed fuel residual was 220.0 kg (485 lbm) less than the prelaunch day prediction. However, the reconstructed fuel load was approximately 136.1 kg (300 lbm) greater than required by the propellant loading tables for the fuel density at ignition command. The LOX load was approximately 725.7 kg (1600 lbm) less. Approximately 326.6 kg (720 lbm) more fuel would have been burned if an additional 725.7 kg (1600 lbm) of LOX had been loaded. It is concluded that if the proper propellant loads had been onboard, approximately 682.7 kg (1505 lbm) of the fuel bias would have been used.

Propellant utilization was analyzed from signals received from three types of probes located in the nine propellant containers.

A system of 15 discrete level probes was located in each container. An electrical signal was initiated by each probe as it was uncovered by the liquid level.

Propellant level cutoff probes were located in the LOX containers 02 and 04 and fuel containers F2 and F4. The cutoff probe signal times and setting heights from container bottoms were:

Container	Height (cm)	Height (in)	RT (sec)
02	69.7	27.45	141.04
04	69.7	27.45	140.42
F2	80.0	31.50	141.41
F4	80.0	31.50	141.42

The continuous level probe located near the bottom of each propellant container indicated the liquid level from 28.4 to 130.0 cm (11.2 to 51.2 in) of container bottom.

6.5 S-I STAGE HYDRAULIC SYSTEMS

The four outboard H-1 engines are gimbal mounted to the S-I stage thrust structure. Controlled positioning of these engines provides thrust vectoring for vehicle attitude control and steering. Hydraulic actuators allow positioning by gimbaling the four outboard engines in response to signals from the flight control computer. There are eight actuators, two for each outboard engine. Four independent, closed loop hydraulic systems provide the force required for each actuator movement. Each outboard engine is capable of a gimbal of ± 8 degrees.

Hydraulic system operation during the S-I-10 flight test was satisfactory. Sufficient source pressures were maintained by each of the independent, closed loop systems. The oil temperatures remained within assigned limits, and the hydraulic oil level trends were as expected. Figure 6-10 shows bands of the hydraulic oil pressure, level, and temperature as measured on the four independent closed loop hydraulic systems.

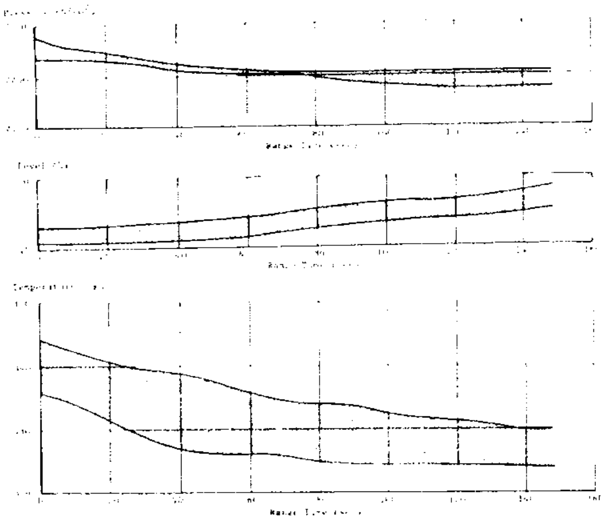

FIGURE 6-10. HYDRAULIC OIL PRESSURE, LEVEL, AND TEMPERATURE

6.6 RETRO ROCKET PERFORMANCE

Four solid propellant retro rockets are mounted on the S-I stage spider beam and arranged 90 degrees apart and midway between the main fin position. The purpose of the retro rockets is to decelerate the S-I stage after it separates from the S-IV stage to prevent a possible collision between the two stages.

The performance of the retro rockets on SA-10 was satisfactory. Ignition signal to the retro rockets occurred at 149.13 seconds and ignition of the individual rockets was further insured by the EBW voltage signals of each retro rocket. The retro rocket combustion chamber pressure measurements flown on previous flights were not installed on SA-10. Longitudinal acceleration measurements were used to evaluate the SA-10 retro rocket performance. By comparing the longitudinal acceleration measurements of S-I-8 and S-I-10 and the average retro rocket burning time on SA-8, the average burning time of the SA-10 retro rockets was determined to be approximately 2.2 seconds. Nominal burning time of the retro rockets is 2.15 seconds.

Chamber pressure buildup and decay transients for each rocket on SA-10 could not be determined due to the absence of the combustion chamber pressure measurements, but can be assumed normal due to the similarity of burning times and stage longitudinal acceleration curves during retro rocket burning on S-I-8 and S-I-10 stages.

6.7 S-IV STAGE PROPULSION

6.7.1 OVERALL S-IV STAGE PROPULSION PERFORMANCE

The S-IV propulsion system performed satisfactorily during the S-IV-10 flight. Except for a temporary malfunction in the fuel pressurization system, all subsystems operated within design limitations. The fuel tank pressurization system malfunction is explained in detail in paragraph 6.8.1. This malfunction did not affect the accomplishment of the mission.

6.7.2 STAGE PERFORMANCE

Two separate analyses were employed in reconstructing the S-IV stage six-engine performance.

The first method, an engine analysis, used the telemetered engine parameters to compute stage longitudinal thrust, stage longitudinal specific impulse, and stage mass flowrate. The effects of the 6-degree engine cant angle to the vehicle centerline, helium heater flowrates, helium heater thrust, 67 N (15 lbf), and chilldown vent thrust, 667 N (150 lbf), are included in the presentation of stage performance parameters. Due to the nature of the analysis, clustering effect on stage longitudinal thrust, 2785 N (626 lbf), is not included unless specifically adjusted to compare results with the flight simulation.

The second method, a postflight simulation, used the thrust and mass flow shapes obtained from the engine analysis, adjusting the levels to simulate the actual trajectory as closely as possible. The simulation was constrained to the cutoff weight determined from capacitance probe data, point level sensor data, and measured stage dry mass, and included the cluster effects as an inherent part of the simulation.

6.7.2.1 ENGINE ANALYSIS

The engine performance of the S-IV-10 flight was reconstructed from the start of LH_2 cooldown to engine cutoff. Statistical confidence in the reconstructed values was established by the relative agreement of three independent computer programs. The calculated performance values deviated from the predicted values by the amounts shown in Table 6-II.

Based on data obtained from the acceptance test of the S-IV-10 stage, propellant depletion time had been predicted as 483.13 seconds from engine start

TABLE 6-II. S-IV STAGE ENGINE ANALYSIS PERFORMANCE

Parameter	Predicted	Actual	% Deviation
Thrust (N) (lbf)	398,819 89,658	399,851 89,890	0.29
Specific Impulse (sec)	429.376	429.377	0.001
LH_2 Flowrate (kg/s) (lbm/s)	15.799 34.831	15.731 34.682	-0.43
LOX Flowrate (kg/s) (lbm/s)	78.916 173.981	79.261 174.741	0.44
Total Flowrate (kg/s) (lbm/s)	94.715 208.810	94.992 209.423	0.29
Mixture Ratio	4.995	5.039	0.88

command. The actual depletion time, determined by calculating the time to deplete the best estimate residuals (454 kg or 1001 lbm LOX and 87 kg or 191 lbm LH_2), using the average stage consumption rates, would have been 484.91 seconds burn time, or 1.78 seconds longer than predicted.

All performance values and excursions were within the predicted bands and shapes. Performance profiles comparing the prediction to the actual for thrust, flowrate, specific impulse, and mixture ratio are presented in Figure 6-11. The parameters shown are unbiased for clustering effects.

Thrust includes the summation of the six-engine individual thrusts corrected for the 6-degree cant angle, 6.67 N (15 lbf) helium heater thrust, 6.67 N (150 lbf) cooldown duct thrust, and 600 N (135 lbf) base pressure effects, but does not include the -2785 N (-626 lbf) clustering effect.

Total flow includes the summation of the six-engine individual total flowrates and the helium heater total flowrate, which is 0.022 kg/s (0.05 lbm/s).

Specific impulse is the result of dividing the indicated thrust by the indicated total flowrate.

6.7.2.2 FLIGHT SIMULATION

A six-degree-of-freedom trajectory simulation program was used to adjust the S-IV propulsion system parameters obtained by the engine analysis. Using a differential correction method, this simulation program determined adjustments to engine analysis stage longitudinal thrust and stage mass flowrate that yielded a simulation trajectory which closely matched the observed trajectory. The simulated trajectory, with adjusted propulsion system parameters incorporated into it, was compared to the observed trajectory, and the following average (root-sum-square) and maximum differences were found:

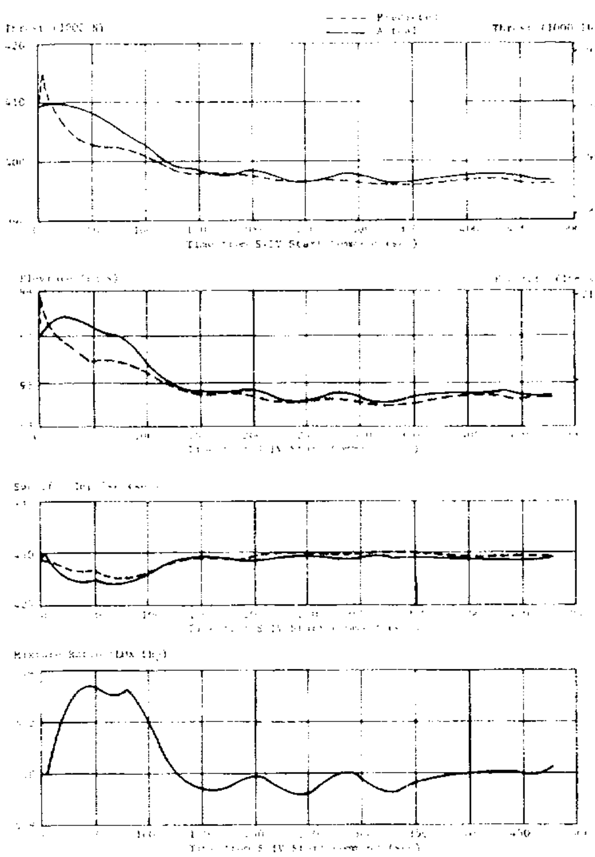

FIGURE 6-11. TOTAL S-IV STAGE PERFORMANCE (ENGINE ANALYSIS)

	Average Dev.	Maximum Dev.
Slant Range	25 m	47 m at 300 sec.
Earth Fixed Velocity	0.3 m/s	0.6 m/s at 240 sec.
Altitude	32 m	54 m at 310 sec.

The maximum inaccuracies in the simulated propulsion system parameters are estimated at 0.3 percent for specific impulse, and 0.2 percent for thrust and mass flowrate. These inaccuracies were caused by inaccuracies in the simulation technique and in observed trajectory data. An additional uncertainty is the accuracy of the best estimate of vehicle mass to which the simulation is constrained. Any inaccuracy in the best estimate of vehicle mass causes additional inaccuracies in thrust and mass flowrate, but not in specific impulse. By considering this additional uncertainty, the inaccuracies are estimated to be 0.3 percent for each of the propulsion system parameters.

Table 6-III compares the predicted engine analysis and simulated stage longitudinal thrust, stage mass flowrate, and stage longitudinal specific impulse. Figure 6-12 compares the predicted values to the postflight engine analysis, and trajectory simulation results for each S-IV stage flight tested.

TABLE 6-III. S-IV-10 PROPULSION SYSTEM

Parameter	* Predicted	Engine * Analysis	Flight * Simulation
Longitudinal (N)	395,433	396,466	396,127
Vehicle Thrust (lbf)	33,897	89,129	89,053
Vehicle Mass (kg/s)	94.71	95.00	95.06
(lbm/s)	208.8	209.42	209.58
Longitudinal Vehicle Specific Impulse (sec)	425.8	425.60	424.9

* Average values between 90 percent thrust and S-IV cutoff.

Definition of Propulsion Parameters

Longitudinal vehicle thrust accounts for engine cant angle and includes helium heater thrust, and thrust originating at the cooldown vents due to leakage of LH_2 through the engine cooldown valves during engine operation. Ullage rocket thrust and predicted aerodynamic base drag (600.5 N or 135 lbf thrust effect) are not included. The engine analysis thrust level is adjusted downward 2785 N (626 lbf) to account for average engine clustering effects derived from previous vehicles. The flight simulation includes the engine clustering effect as an inherent part of the simulation.

Vehicle mass loss rate includes all stage mass flowrates, such as the sum of individual engine propellant mass flowrates, leakage of LH_2 through the cooldown valves, and helium heater propellant mass flow.

Longitudinal vehicle specific impulse is vehicle longitudinal thrust divided by vehicle mass loss rate.

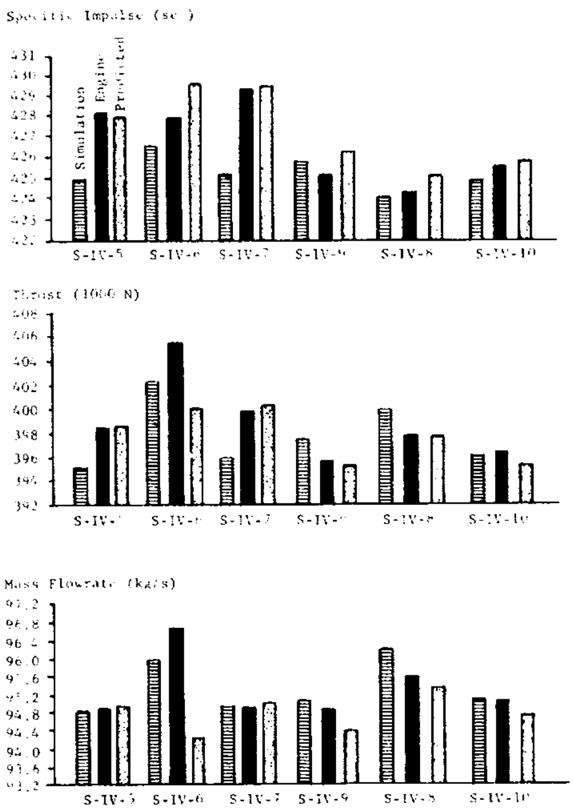

The correction factors applied to this bar chart are the same as those used in Table 6-II except for the predictions and engine analysis prior to S-IV-9 which do not include corrections due to clustering effects.

FIGURE 6-12. PROPULSION SYSTEMS PERFORMANCE COMPARISON (S-IV STAGE)

Each of the simulated propulsion system parameters was within 0.5 percent of predicted. Stage mass flowrate and stage longitudinal thrust were 0.38 and 0.17 percent higher than predicted, respectively, and the longitudinal specific impulse was 0.21 percent lower than predicted.

The trajectory simulation technique provides a method of determining vehicle mass history, if the vehicle mass at any point or points in time on the trajectory is accurately known. Figure 6-13 presents the approach used to determine the best estimate of ignition and cutoff weight to which the flight simulation was constrained. The "box" shown defines the region that the best estimate of ignition and cutoff weight must lie within in order to satisfy the analysis results from capacitance probe and point level sensor at cutoff and capacitance probe and engine analysis at ignition. The diagonal line represents the flight simulation results. Any point on the nominal flight simulation line provides the same "fit" to the observed trajectory; however, average values for the propulsion parameters vary directly with the magnitude of the ignition and cutoff weight selected for the flight simulation constraint point. A least square criterion was applied to the data presented, and the best estimate and tolerance of the ignition and cutoff weights were determined to be 62,551 ± 94 kg (137,902 ± 209 lbm) and 15,632 ± 24 kg (34,463 ± 54 lbm), respectively. This does not exactly agree with the masses presented in Section IV but is within the tolerances and is believed to be the best estimate from a consumption standpoint.

The nominal flight simulation solution which came nearest to achieving the best-estimate point is shown in Figure 6-13. It indicates that the ignition and cutoff weights were 62,572 kg (137,951 lbm) and 15,626 kg (34,451 lbm), respectively.

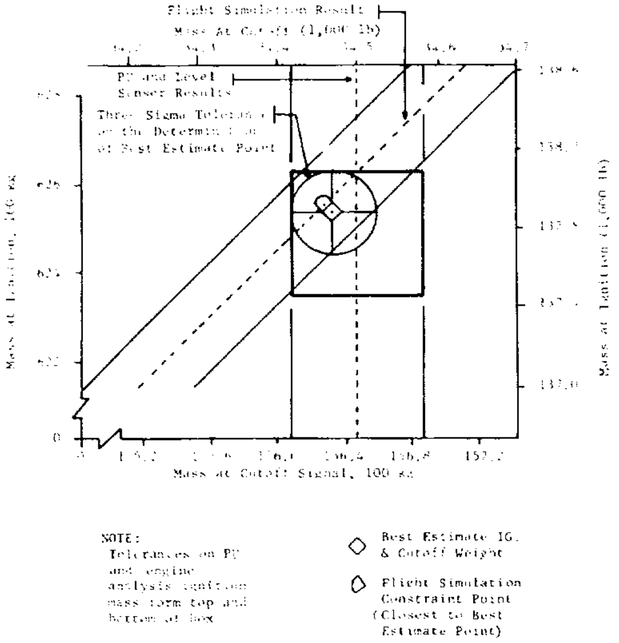

FIGURE 6-13. BEST ESTIMATE OF S-IV-10 IGNITION AND CUTOFF WEIGHT

6.7.3 INDIVIDUAL ENGINE PERFORMANCE

The six Pratt & Whitney RL10A-3 engines, which powered the S-IV stage, functioned satisfactorily during prestart, start, steady state, and cutoff. All engine events occurred as scheduled, and performance levels of all engines were consistent with performance levels established during acceptance testing.

6.7.3.1 ENGINE COOLDOWN

The engine cooldown period was 39.72 seconds for LH_2 and 10.1 seconds for LOX. The LH_2 cooldown period was 1.69 seconds shorter than predicted due to the early cutoff of the S-I stage. The LH_2 consumption during the chilldown period was 146 kg (322 lbm), or an average flowrate of 0.61 kg/s/eng (1.351 lbm/s/eng). The LOX consumption during the chilldown period was 84 kg (185 lbm), or an average flowrate of 1.40 kg/s/eng (3.05 lb/s/eng).

6.7.3.2 START TRANSIENTS

Normal start transients were noted for all engines. The engine thrust buildup to the 90 percent level was achieved by all engines between 1.791 and 2.028 seconds after engine start command. Figure 6-14 shows the six engine start transients. The thrust overshoot was less than 5 percent for all engines during the start transient. The total impulse to 95 percent thrust was 89,899 N-s (20,210 lbf-s), as compared to the predicted value of 81,136 ± 10,898 N-s (18,240 ± 2450 lbf-s).

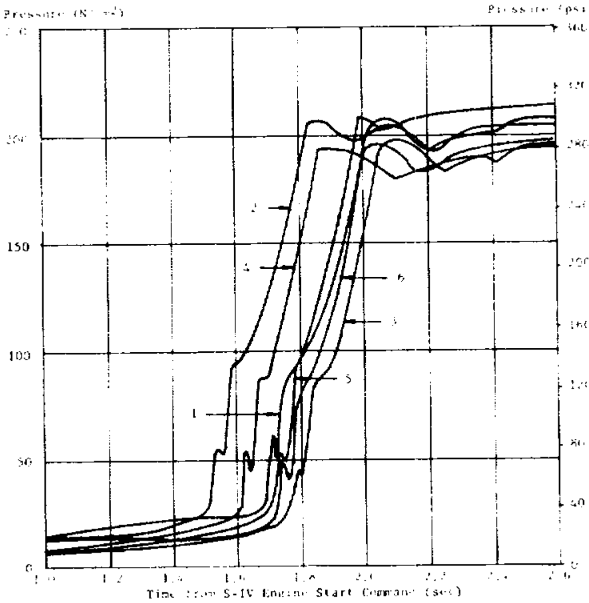

FIGURE 6-14. INDIVIDUAL ENGINE START TRANSIENTS

6.7.3.3 STEADY STATE OPERATION

Satisfactory performance of the engines was demonstrated throughout the flight. Average specific impulse for the engines was 430.26 seconds, with a mean total thrust level of 400,860 N (90,085 lbf). These values are not corrected for cant angle. Maximum and minimum mixture ratio levels during the flight were 5.34 and 4.95, respectively. The maximum mixture ratio occurred at a PU valve angle of minus 22 degrees (approximately 186 seconds range time, while the minimum occurred at an angle of plus 15 degrees (approximately 471 seconds range time).

6.7.3.4 CUTOFF TRANSIENTS

The S-IV-10 stage cutoff was initiated by a signal from the guidance computer at 630.252 seconds. At that time, the vehicle was 198,679 km (1234.14 miles) from the Tel 2 receiving station, and telemetry signals, with a velocity which was approximating that of light, required 6.64 milliseconds to reach the station from the vehicle. When this correction is made to the data, the total cutoff impulse after the generating signal to 0 percent thrust is 48,165 N-s (10,828 lb-s), as determined from engine analysis. This includes the delay due to relay action, and 2224 N-s (500 lb-s) for the chilldown duct impulse, but does not include engine cant angle. This value is within the predicted spread of 48,930 ± 400 N-s (11,000 ± 900 lb-s) and is consistent with the value determined from the velocity gains after cutoff which is 45,550 N-s (10,240 lb-s) ($\Delta V = 2.9$ m/s).

All engines experienced a smooth cutoff transient, as shown in Figure 6-15. All engines reached 10 percent thrust decay between 0.104 and 0.118 seconds after S-IV engine cutoff command.

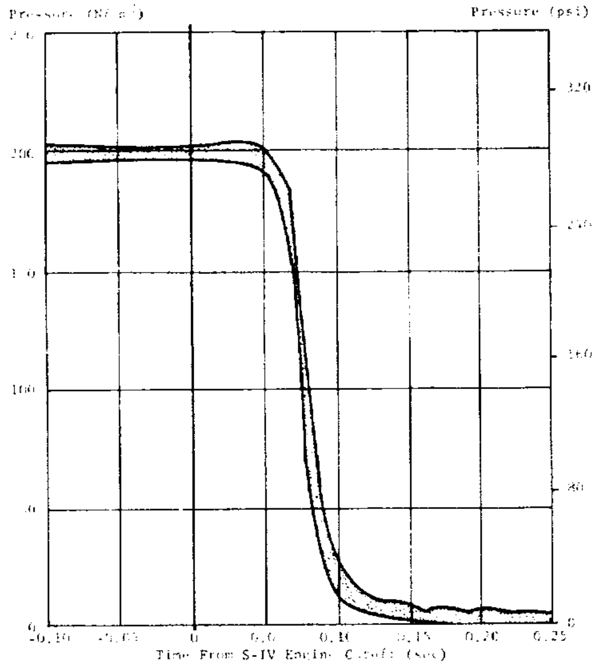

FIGURE 6-15. S-IV ENGINE CUTOFF TRANSIENTS

6.8 S-IV PRESSURIZATION SYSTEM

6.8.1 LH_2 TANK PRESSURIZATION

During the S-IV-10 flight, the LH_2 tank pressurization system performed satisfactorily, with the exception that the pressurization control solenoid valve did not open when required during a portion of the flight.

Figure 6-16 presents the LH_2 tank ullage pressures during prepressurization, S-I boost, and S-IV flight.

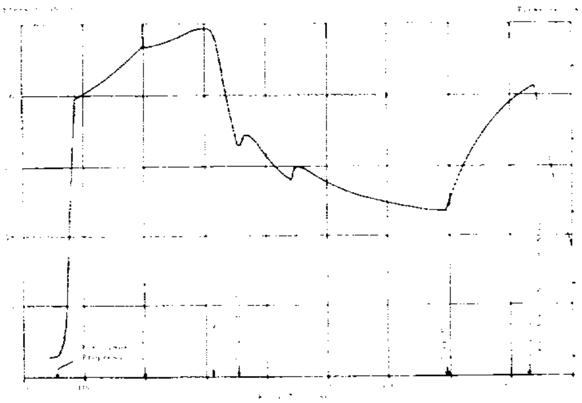

FIGURE 6-16. S-IV STAGE FUEL TANK ULLAGE PRESSURE

As shown in Figure 6-16, the control solenoid valve cycled properly at approximately 240 seconds. However, at approximately 291 seconds the control solenoid valve failed to open as required, as in the preceding control valve cycle. The pressurization orifice inlet pressure data indicated that the control solenoid valve was subsequently actuated at the time of the step pressurization command, and closed properly when the ullage pressure switch sensed an ullage pressure of 21.9 N/cm^2 (31.8 psi).

The failure of the control valve to actuate upon command can be attributed to a temporary contamination of the pilot poppet within the control valve or to a failure of the low limit ullage pressure switch which commands the valve to open. Inasmuch as the pressure switch was functioning at 231 seconds the former possibility appears to be more likely. Upon energizing the step solenoid valve, GH_2 pilot bleed, which is interconnected between the step and control valve, may have back flowed toward the control valve, causing any contamination present to be dislodged, thus enabling the pilot poppet, and subsequently the main poppet, to open.

The control valve malfunction did not affect vehicle performance. However, the LH_2 pump inlet conditions were not within the engine specification range for a major portion of the flight (340 seconds) because of the control valve malfunction. In addition, higher pump inlet temperatures (0.1 to 0.2°K higher than previous flights) were experienced as a result of environmental conditions and subsequent higher heat input.

The LH_2 tank was prepressurized with ground-supplied helium from 11.2 to 25.9 N/cm^2 (16.2 to 37.5 psi). During ground hold, the ullage pressure increased to 28.8 N/cm^2 (41.7 psi) at liftoff. The ullage pressure continued to increase to 29.7 N/cm^2 (43.1 psi) at initiation of engine cooldown. This rise in ullage pressure is attributed to normal heat and mass transfer to the ullage.

The ullage pressure decreased during cooldown and was approximately 23.2 N/cm^2 (33.7 psi) at S-IV-10 engine start command. Ambient helium makeup of the LH_2 tank was not required because of the high tank pressure at initiation of cooldown.

Fuel tank pressurization was accomplished during flight by tapping GH_2 off the engine supply aft of the main fuel shutoff valve, and routing in through the fuel tank pressurization system. Prior to the control solenoid valve malfunction and the initiation of step pressurization, the LH_2 tank ullage pressure cycled between 21.1 to 21.9 N/cm^2 (30.6 to 31.8 psi).

The initiation of step pressurization by the propellant utilization system at 482.61 seconds opened the step pressure solenoid valve, allowing the tank pressure to increase toward the vent setting. The ullage pressure increased from 19.3 N/cm^2 (28.0 psi) at initiation of step pressurization to 26.2 N/cm^2 (38.0 psi) at S-IV-10 stage cutoff.

The average GH_2 pressurant temperature was approximately 178°K. The average pressurant flowrates obtained during normal, control, and step pressurization were 0.054, 0.081, and 0.129 kg/s (0.118, 0.179, and 0.285 lbm/s), respectively. The average ullage temperature was approximately 157°K.

During flight, 36.7 kg (80.85 lbm) of GH_2 were used to pressurize the tank.

The performance of the nonpropulsive vent system was as expected. Section 14.3 contains details on system performance.

6.8.1.1 LH_2 PUMP INLET CONDITIONS

Based on engine performance data, the LH_2 pump inlet conditions were adequate, although minimum required conditions were not achieved for a major portion of the flight (Fig. 6-17). Minimum NPSP was 2.20 N/cm^2 (3.19 psi) at initiation of step pressurization. The combination of the control solenoid valve malfunction and the higher pump inlet temperature resulted in a lower NPSP than would normally have been expected. Assuming normal pressurization system operation (average ullage pressure of 21.4 N/cm^2 or 31 psi) the minimum NPSP would have been approximately 4.1 N/cm^2 (5.9 psi) at step pressurization. If the pump inlet temperature had been within the temperature range experienced on previous flights, the NPSP would have been 0.4 to 0.8 N/cm^2 (0.6 to 1.2 psi) higher. In considering both factors, the

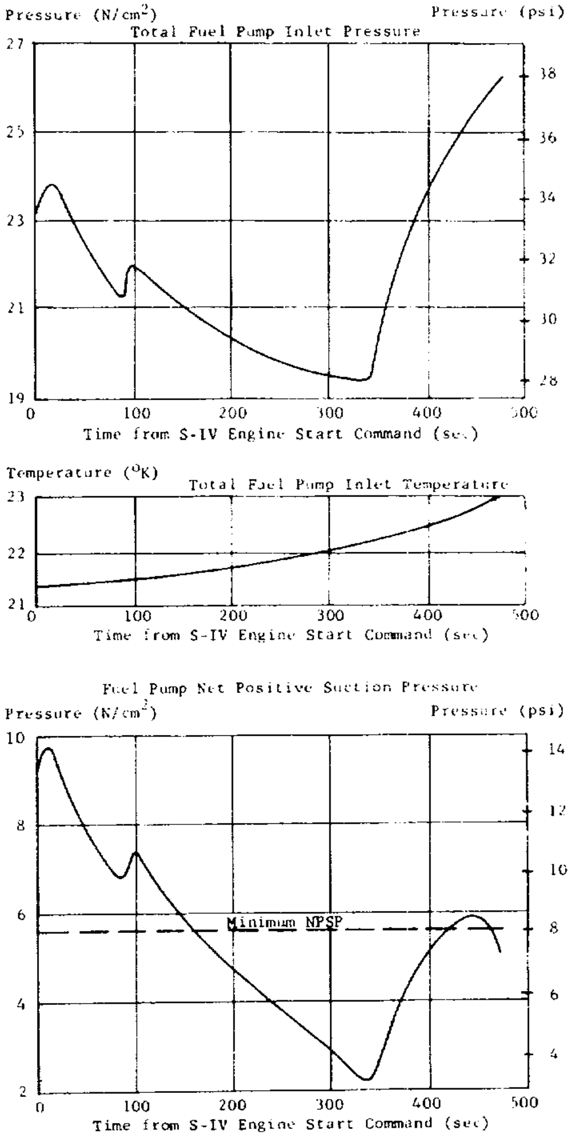

FIGURE 6-17. LH_2 PUMP INLET CONDITIONS

minimum NPSP would have been 4.5 and 4.9 N/cm^2 (6.5 and 7.1 psi).

6.8.2 LOX TANK PRESSURIZATION

During S-IV-10 stage flight, the operation of the LOX tank pressurization system was satisfactory. The LOX tank was pressurized with cold helium from a ground source 147 seconds prior to liftoff. During S-IV powered flight, pressure was provided to the LOX tank by the helium heater. Figure 6-18 shows the LOX tank ullage pressure during prepressurization, S-I boost, and S-IV flight.

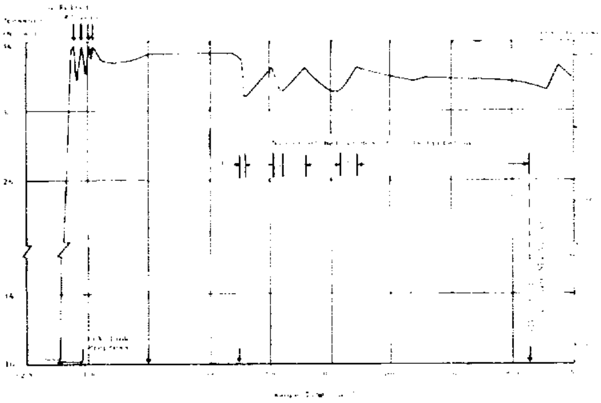

FIGURE 6-18. S-IV STAGE LOX TANK ULLAGE PRESSURE

Throughout flight, the total inlet pressures of the engines were above 32.9 N/cm^2 (47.8 psi), and the NPSP was well above the minimum required limit of 10.3 N/cm^2 (15 psi). The minimum NPSP was 22 N/cm^2 (32 psi), which occurred at cutoff. At the initiation of the automatic count 147 seconds prior to liftoff, the LOX tank was prepressurized to approximately 33.8 N/cm^2 (49 psi), with approximately 2 kg (4.5 lbm) of ground supplied helium.

Between 122 and 92 seconds prior to liftoff, LOX tank vent valve 2 cycled four times due to continued final LOX replenishing. The LOX tank ullage pressure then decayed to 32.8 N/cm^2 (47.5 psi) at approximately 60 seconds prior to liftoff, after which it rose steadily to 33.4 N/cm^2 (48.4 psi) at liftoff. The LOX tank ullage pressure remained constant during S-I boost until LOX prestart. At S-IV engine start command, the ullage pressure was approximately 33.1 N/cm^2 (48 psi). During S-IV stage powered flight, the LOX tank pressurization system performed satisfactorily, with the ullage pressure decreasing from 33.1 N/cm^2 (48 psi) to 30.9 N/cm^2 (44.9 psi) during the start transient, and then cycling three times in a band between 31.2 and 32.6 N/cm^2 (45.2 and 47.3 psi) during steady-state operation.

At approximately 345 seconds the helium heater secondary coil valve closed and the heater remained on single coil mode for the remainder of S-IV powered flight. After 345 seconds, the ullage pressure decreased at a slower rate than on the previous helium heater single coil operation, and finally stabilized at 31.9 N/cm^2 (46.2 psi) 100 seconds later. The ullage pressure then increased slightly and stabilized at 32.1 N/cm^2 (46.5 psi) between 461 and 492 seconds. The ullage pressure then gradually decreased to 31.7 N/cm^2 (46 psi) until engine cutoff at 630.25 seconds.

The LOX tank ullage pressure profile discussed above was effected primarily by a drifting cold helium regulator discharge pressure which caused the helium heater inlet pressure to increase from 165 N/cm^2 (240 psi) at S-IV engine start command (150.83 seconds) to 188 N/cm^2 (272 psi) at engine cutoff (630.25 seconds). After the initiation of heater single coil mode at 345 seconds, the helium heater inlet pressure remained above 179 N/cm^2 (260 psi) for the duration of heater operation. This high heater inlet pressure was reflected in a higher-than-normal pressurant flowrate during single coil mode. Beginning at 431 seconds, the helium heater inlet pressure shifted from 181 N/cm^2 (262 psi) to 184 N/cm^2 (267 psi) 5 seconds later. This shift resulted in a maximum single coil flowrate of 0.083 kg/s (0.183 lbm/s), which is the largest single coil flowrate experienced in any S-IV stage test (0.068 kg/s or 0.15 lbm/s is nominal). This 3.4 N/cm^2 (5 psi) shift in heater inlet pressure was reflected in a 0.2 N/cm^2 (0.3 psi) increase in ullage pressure during this period.

Although the single coil mode of operation was not designed to establish a stabilization of LOX tank ullage pressure, the ullage pressure stabilized at approximately 32.1 N/cm^2 (46.5 psi). This does not constitute an ullage pressure control problem. This fact is particularly true since the high pressurant flowrate was combined with an above average helium heater combustion temperature which maximized at 1322°K (Fig. 6-19). Thus, the unique combined effects of a cold helium regulator which drifted to the high side of its operating band and a high combustion temperature which was caused by an unusually low LH$_2$ tank ullage pressure were not sufficient to cause the LOX tank ullage pressure to increase to the level of the upper control switch pressure of 32.6 N/cm^2 (47.3 psi). If the regulator discharge pressure had continued to drift beyond the design limit of 190 N/cm^2 (275 psi), or if complete loss of regulation had occurred, the regulator backup pressure switch would have commanded the cold helium solenoid valve to close, thereby terminating helium pressurant flow. As the switch sensed the decrease in regulator discharge pressure, it would have commanded the control valve to open, and would have continued in a "bang-bang" mode of control.

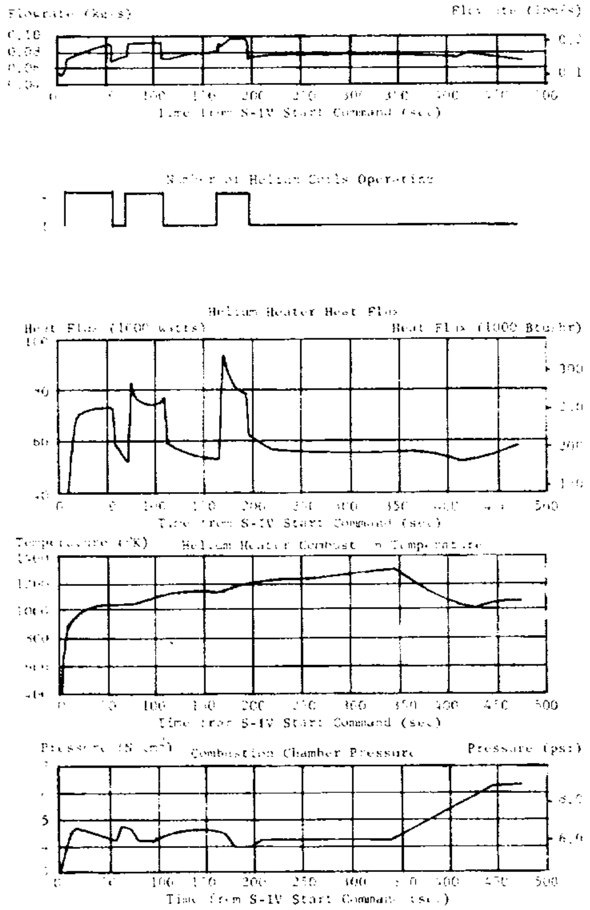

FIGURE 6-19. S-IV HELIUM HEATER PERFORMANCE

6.8.2.1 HELIUM HEATER OPERATION

As shown in Figure 6-19, the S-IV-10 flight demonstrated the operational capability of the helium heater as an integral component of the S-IV stage LOX tank pressurization system. Helium heater ignition was normal at S-IV engine start command, with the combustion temperature rising rapidly to above 556°K within three seconds. The combustion temperature continued to rise until it reached 1147°K at 105 seconds after S-IV ignition, and remained relatively constant for the next 62 seconds. The combustion temperature then began to rise again, and reached a maximum of 1322°K at 341 seconds after S-IV ignition. This rise in combustion temperature was due to a rise in the helium heater injector mixture ratio, which was in turn caused by a low LH_2 tank ullage pressure (see Section 6.8.1). The combustion temperature performed as expected for the existing conditions, and the maximum temperature of 1322°K was below the redline limit of 1367°K. The temperature decreased after the initiation of LH_2 tank step pressurization.

Helium heater heat flux was satisfactory for the full duration of S-IV powered flight, averaging approximately 56,565 watts (193,000 Btu/hr) during single coil operation and 76,788 watts (262,000 Btu/hr) during double coil operation. The helium heater secondary control valve cycled three times during S-IV powered flight, with single coil mode of operation occuring 76.7 percent of the time.

6.8.2.2 LOX PUMP INLET CONDITIONS

The LOX supply system delivered the necessary quantity of LOX to the engine pump inlets, while maintaining the required pressure and temperature conditions. The LOX pump inlet temperatures stabilized at the bulk temperature of 90.6°K within 5 seconds after engine start. The temperature then increased slowly, reaching an average of 91.7°K by S-IV stage engine cutoff. Throughout S-IV operation, the inlet conditions, shown in Figure 6-20, were within

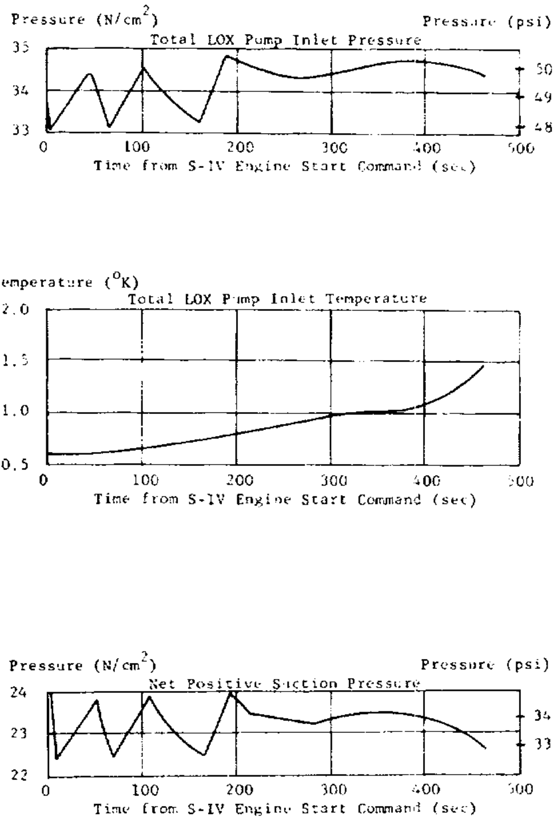

FIGURE 6-20. LOX PUMP INLET CONDITIONS

specified engine operating limits of temperature and pressure. Cold helium bubbling was initiated 489 seconds prior to liftoff and continued satisfactorily until termination 188 seconds prior to liftoff. The LOX pump inlet temperatures decreased normally, and at termination of cold helium bubbling, were within the range of 77.2°K to 79.4°K. This temperature range compared favorably to expected values. By prestart, the temperature range had increased (91.4 to 94.2°K) and was within the required limits (90 to 95.6°K). At engine start, the inlet temperatures were between 90.7 and 91.4°K. Figure 6-21 provides a time history covering LOX pump inlet temperatures during cold helium bubbling and LOX pump cooldown.

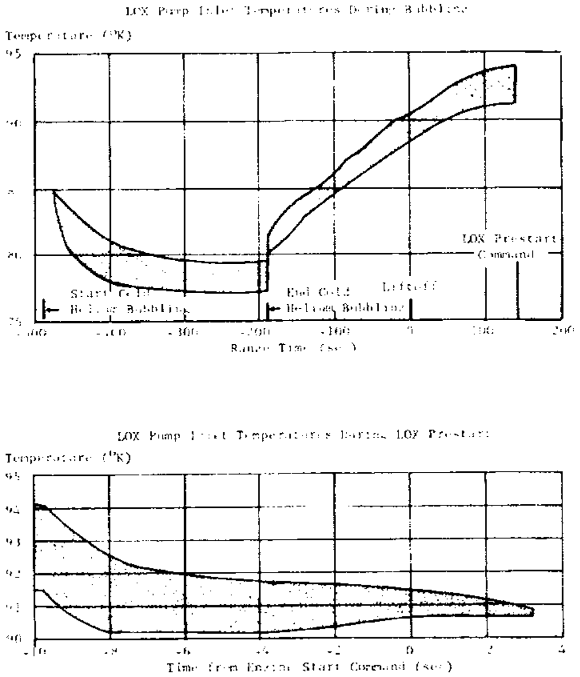

FIGURE 6-21. LOX PUMP INLET TEMPERATURES

6.8.3 COLD HELIUM SUPPLY

During S-IV stage flight, the cold helium supply was adequate. At SA-10 liftoff, the pressure and temperature in the cold helium spheres were 2146 N/cm^2 (3112 psi) and 22.7°K, respectively, indicating a helium mass of 58.2 kg (128.4 lbm). Based upon integration of the pressurant flowrate during S-IV powered flight, it was determined that 38.6 kg (85.2 lbm) of helium were expended for LOX tank pressurization from liftoff to S-IV stage engine cutoff. No makeup pressurization was required during S-I boost. The total amount of cold helium residuals in the bottles after S-IV engine cutoff was 18.9 kg (14.6 lbm) based on indicated bottle pressure and temperature. This would indicate that 39.4 kg (86.8 lbm) of helium were consumed, based on bottle conditions. This value is in good agreement with the integrated flowrate of 38.6 kg (85.2 lbm).

6.8.4 CONTROL HELIUM SYSTEM

The operation of the S-IV-10 pneumatic control system was satisfactory during preflight checkout and during flight. The control helium sphere was pressurized to approximately 2033 N/cm^2 (2950 psi); it decreased during powered flight to approximately 1844 N/cm^2 (2675 psi) at S-IV engine cutoff. The sphere temperature ranged from a maximum of 291°K at liftoff to a minimum of 273°K at approximately 350 seconds. By S-IV engine cutoff, the sphere temperature had increased to 276°K. The control helium regulator operated within the desired band of 324 N/cm^2, plus 31 and minus 17 N/cm^2 (470 psi, plus 45 and minus 25 psi). The outlet pressure of the regulator varied between 336 and 323 N/cm^2 (487 and 468 psi) during flight.

6.9 S-IV PROPELLANT UTILIZATION

The propellant utilization (PU) system performed satisfactorily except for the failure of the LOX fill valve to close automatically, causing a LOX overload before the valve was closed manually (see Section III). The desired propellant load was 38,196 kg (84,208 lbm) of LOX, and 7777 kg (17,145 lbm) of LH$_2$. According to the PU system fine mass strip charts, the S-IV propellant mass at liftoff was 38,339 kg (84,524 lbm) of LOX, and 7790 kg (17,174 lbm) of LH$_2$. The residuals above the pump inlets at command cutoff were 454 kg (1001 lbm) of LOX (including 5 kg, or 11 lbm, of LOX trapped in the tank) and 87 kg (191 lbm) of LH$_2$.

Based upon average rates of consumption, a LOX flowrate (including boiloff) of 79.4 kg/s (175.1 lbm/s) and an LH$_2$ flowrate (including boiloff and consumption due to pressurization) of 15.8 kg/s (34.8 lbm/s), when added to the best estimate residuals of 454 kg (1001 lbm) of LOX and 87 kg (191 lbm) of LH$_2$, would have caused S-IV depletion cutoff to occur 5.48 seconds later than the actual flight command cutoff time. Depletion cutoff would have occurred at 484.91 seconds burn time, as compared to the predicted cutoff time of 483.13 seconds burn time. If the S-IV-10 stage had been permitted to continue to propellant depletion (LH$_2$ depletion cutoff), there would have been a residual of 18.6 kg (41 lbm) of LOX, which is an equivalent PU efficiency of 99.96 percent.

As a comparison, if the flight had been conducted without the control of engine mixture ratio (EMR) by the PU system, a LOX depletion cutoff would have occurred with a residual of 113 kg (250 lbm) of LH_2. This is equivalent to an efficiency of 99.75 percent. This analysis is derived from comparing actual open loop EMR, based upon propellant supply conditions at the engine pump inlets, to nominal predicted open loop EMR.

6.9.1 PROPELLANT MASS HISTORY

The propellant mass history at various events, as determined by the composite best estimate, is presented in Table 6-IV below. The values are for total liquid propellant mass above the engine inlet. The actual propellants onboard at S-I liftoff, as determined by the weighted average technique (composite best estimate), were within 0.64 percent for LOX and 0.27 for LH_2 of the quantities desired.

TABLE 6-IV. PROPELLANT MASS HISTORY

Event	LOX		LH_2	
	kg	lbm	kg	lbm
S-I Liftoff	38,441	84,747	7,798	17,192
LH_2 Prestart	38,441	84,747	7,798	17,192
LOX Prestart	38,441	84,747	7,689	16,951
S-IV Ignition	38,357	84,562	7,652	16,870
PU Activation	38,100	83,996	7,599	16,754
Residual	454	1,001	87	191

These mass and accuracy values are determined by applying a weighted average technique to the mass accuracy values and to the flowrate integral, PU system, and flight simulation masses.

6.9.2 SYSTEM RESPONSE

The PU system responded properly during S-IV-10 flight, and provided the PU valve movement necessary to correct for mass errors inherent within the system. Figure 6-22 shows the typical movement of a PU valve during S-IV flight.

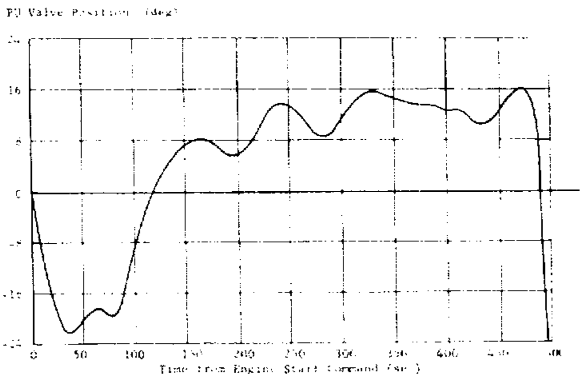

FIGURE 6-22. TYPICAL PROPELLANT UTILIZATION VALVE POSITION

At the time of PU system activation, the system sensed a positive equivalent LOX mass error, indicating an excess in LOX of 290 kg (639 lbm), and positioned the PU valve for a higher engine mixture ratio (EMR) to correct the error. The factors primarily responsible for this PU valve excursion were nonlinearities in the system, open loop flow variations, and the initial LOX mass error sensed in the system. This initial mass error on SA-10 was caused by loading errors and by nonnominal cooldown usage as detected by the PU system.

The average engine mixture ratio excursions during flight varied between 5.34 and 4.95; these excursions are well within engine operation capabilities.

6.9.3 PU SYSTEM COMMAND

The PU system is designed to originate three commands:

1. PU system gain change
2. LH_2 tank step pressure
3. Arm all engine cutoff.

All three commands occurred at the proper times; however, the third command was preceded by a signal from the IU.

The PU system gain change command was scheduled to occur when the PU system indicated that the LOX mass had decreased to 32,860 ± 544 kg (72,445 ± 1200 lbm). The command was observed to occur at 217.85 seconds. The LOX mass at this time was 32,842 kg (72,405 lbm), which was within the tolerance range.

The LH_2 tank step pressure command was scheduled to occur when the PU system indicated that the LOX mass had reached 11,255 ± 544 kg (24,813 ± 1200 lbm). This command was observed to occur at 491.38 seconds, at which time the LOX mass was 11,222 kg (24,785 lbm). This mass value was within tolerance.

The Arm-all-engine cutoff command was scheduled to occur when the PU system indicated that the LOX mass had reached 878 ± 227 kg (1936 ± 500 lbm), or upon command of the IU. The IU command, which preceded the PU system command, occurred at 589.4 seconds. The PU system command was observed to occur at 624.94 seconds, at which time the LOX mass was 847 kg (1867 lbm). This mass was within tolerance.

6.10 S-IV HYDRAULIC SYSTEM

The hydraulic systems of all six engines functioned properly during S-IV-10 powered flight. Telemetry data of pressure, temperature, and position were similar to the previous flights. No system malfunction or incipient performance degradation was evident in the data received.

Prior to engine start, the engines were satisfactorily positioned by the accumulator charge. At engine start, the pressurized fluid of the hydraulic pumps recharged the accumulators to the bottomed position and maintained operating pressures above the accumulator GN_2 pressures. All of these events were consistent with normal system operation.

6.11 ULLAGE ROCKETS

Ullage rocket performance was satisfactory, and all rockets jettisoned properly at 161.13 seconds. The ullage rocket ignition command was given at 149.03 seconds, with chamber pressure of each of the four rockets increasing at a rate of approximately 19,016 N/cm²/s (27,600 psi/s) as shown in Figure 6-23.

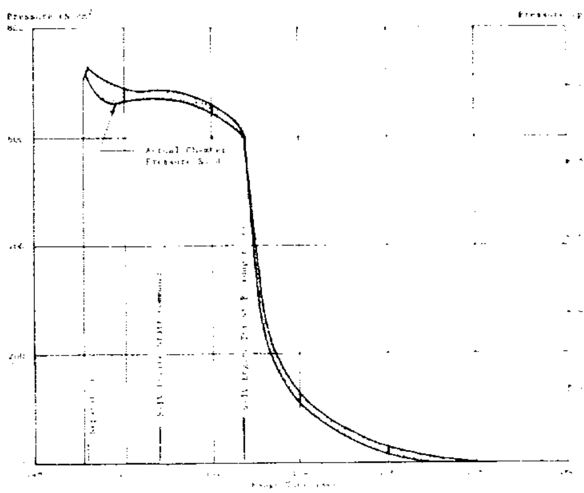

FIGURE 6-23. ULLAGE ROCKET CHAMBER PRESSURE

The pressure averaged approximately 675 N/cm² (980 psi) and was within the nominal predicted operating band of 689 ± 69 N/cm² (1000 ± 100 psi). The burn time at which the pressure was above 90 percent thrust or approximately 586 N/cm² (850 psi) was 3.7 seconds, as compared to the required minimum burn time of 3.0 seconds. A comparison of the flight data with the manufacturer's data reveals that the overall pressure profiles during burning were typical for a grain temperature of 294°K. At burnout, the chamber pressures of all four rockets decreased simultaneously.

Total stage ullage rocket impulse (parallel to the axis of the stage) was 183,711 N-s (41,300 lbf-s), and the total ullage rocket impulse (parallel to the axis of the rocket) was 225,649 N-s (50,728 lbf-s).

SECTION VII. GUIDANCE AND CONTROL

7.1 SUMMARY

The overall performance of the guidance and control system was as expected and very satisfactory. A maximum roll attitude error of -2.1 degrees occurred at 58 seconds due to the unbalanced aerodynamic forces caused by the S-I stage turbine exhaust duct fairings.

A vehicle roll deviation of -2.8 degrees developed during separation, mainly due to the 0.51-degree total misalignment of the S-IV ullage rockets, but was quickly reduced to zero when S-IV control became effective.

The overall performance of the guidance system was very satisfactory. The vehicle's total space fixed velocity from tracking at S-IV cutoff was 7591.50 m/s at an altitude of 535.706 km and a space fixed path angle of 90.007 degrees. In each case the differences between these values derived from precalculated minus computer, precalculated minus tracking, and computer minus tracking fell well within the 3σ band indicating excellent overall guidance system accuracy. The ST-124 velocity components are in agreement with those indicated by the ASC-15 computer throughout flight.

The measured velocity differences are the telemetered ST-124 accelerometer data minus tracking. The predicted differences are based upon the ST-124 laboratory calibration test results. These predicted differences were adjusted for the ST-124 stable element leveling and azimuth alignment errors determined at launch. In all cases, the measured velocity differences fall within the 3σ error bands. In addition, there is rather good agreement between the measured and predicted velocity differences in the range and cross range directions. However, the agreement between the measured and predicted altitude velocity difference is rather poor. The observed space fixed velocity was 0.5 m/s less than the computer presetting. If the ST-124 laboratory calibration data had been used to adjust the preset space fixed velocity the resulting error would have been about 0.4 m/s greater than the desired cutoff velocity. The increase in vehicle velocity due to S-IV thrust decay, determined from guidance, was 0.13 m/s less than the predicted value of 3.04 m/s. Tracking indicates a 2.8 m/s velocity increase due to thrust decay; however, this is due to round-off error since guidance was used to construct the trajectory during the cutoff periods.

7.2 SYSTEM DESCRIPTION

SA-10 was the fourth Saturn vehicle to employ a fully active ST-124 guidance system. The principal functions of this system were:

1. To generate attitude error signals for vehicle control and steering throughout flight.
2. To issue timed discretes to the spacecraft, Instrument Unit, S-IV, and S-I stages for sequencing vehicle events throughout the entire flight period including Pegasus wing deployment.
3. To compute and issue steering commands for active path guidance during S-IV stage burn.
4. To terminate path guidance and initiate S-IV engine shutdown at the preset space fixed velocity.

The ST-124 guidance system consisted of the ST-124 stabilized platform assembly and electronics box, the GSP-24 guidance signal processor, and the ASC-15 digital computer. Figure 7-1 shows the interrelationship between the components of this system and their integration with the elements of the vehicle's control system. The operational periods of these major guidance and control system components are also indicated.

The ST-124 guidance system generated attitude error signals ($\Delta\varphi$'s) by comparing the three command resolver signals (χ's) with the four ST-124 gimbal resolver position signals (θ's). The angular rate information required for damping vehicle disturbances was obtained from the three axis control rate gyro package located in the Instrument Unit. Vehicle lateral acceleration control was accomplished in both the pitch and yaw planes during S-I flight by means of two body fixed control accelerometers located in the Instrument Unit.

In order to supply the total vehicle system with the basic timing signals from a single source (ASC-15 computer), new time bases must be generated during flight. The first time base started when the Instrument Unit umbilical separated from the vehicle and ended at S-I propellant level sensor arming. The second time base began at activation of the first propellant level sensor and terminated when the S-I thrust OK switches were ganged for backup of the normal OECO mode. The third time base commenced with OECO and continued throughout the remainder of powered

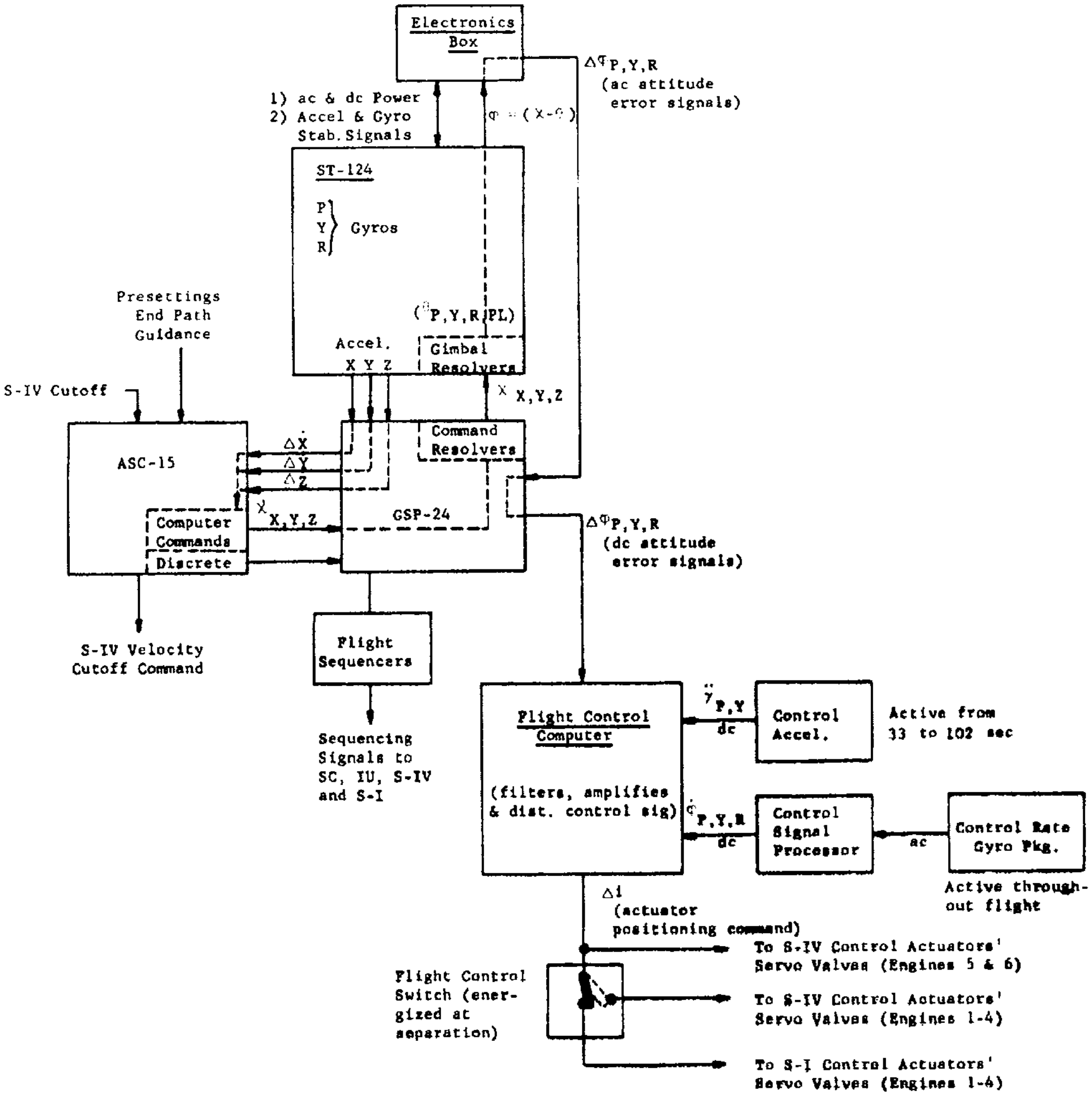
Electronics Box
$\Delta\varphi_{P,Y,R}$ (ac attitude error signals)
1) ac & dc Power
2) Accel & Gyro Stab. Signals
$\varphi = (\chi - \theta)$
ST-124
P Y R Gyros
($\theta_{P,Y,R,PL}$)
Accel. X Y Z
Gimbal Resolvers
$\chi_{X,Y,Z}$
Presettings End Path Guidance
S-IV Cutoff
ASC-15
$\Delta\dot{X}$
$\Delta\dot{Y}$
$\Delta\dot{Z}$
Computer Commands
Discrete
$\chi_{X,Y,Z}$
Command Resolvers
GSP-24
$\Delta\varphi_{P,Y,R}$ (dc attitude error signals)
S-IV Velocity Cutoff Command
Flight Sequencers
Sequencing Signals to SC, IU, S-IV and S-I
Flight Control Computer
(filters, amplifies & dist. control sig)
$\ddot{\gamma}_{P,Y}$
dc
Control Accel.
Active from 33 to 102 sec
$\dot{\varphi}_{P,Y,R}$
dc
Control Signal Processor
ac
Control Rate Gyro Pkg.
Active throughout flight
Δi (actuator positioning command)
Flight Control Switch (energized at separation)
To S-IV Control Actuators' Servo Valves (Engines 5 & 6)
To S-IV Control Actuators' Servo Valves (Engines 1-4)
To S-I Control Actuators' Servo Valves (Engines 1-4)

FIGURE 7-1. GUIDANCE AND CONTROL SYSTEM

flight (until S-IV guidance cutoff command). The final time base started when the computer sensed cutoff (0.688 second actual compared to 0.685 second predicted) after S-IV cutoff signal.

Pitch and yaw plane path guidance initiated at separation command plus 18.13 seconds. This was accomplished by unlocking the brakes on the three command resolvers in the guidance signal processor, loading the ladder networks in the digital computer according to the measured guidance values, and issuing the computed correction signals ($\dot{\chi}$) to the command resolvers in the guidance signal processor.

The iterative guidance mode (IGM) was employed for the pitch plane path guidance program to compute the required steering command ($\dot{\chi}_Z$) from the real time measured state variables each second. Tolerances in engines and stage alignment, resolver chain errors, computational time lags, and other inherent conditions result in the misalignment of the thrust vector with respect to the guidance plane. Pitch plane steering misalignment correction (SMC or χ_{ZC}) was introduced shortly after guidance initiation to correct for this condition.

Delta-minimum path guidance, where the vehicle is constrained to a predetermined reference, was employed in the yaw plane. Both the cross range velocity and displacement were utilized to steer the vehicle back into the reference plane. The range of possible initial conditions at the introduction of guidance necessitated limiting the cross range steering command (χ_{CR}) to 0.25 radian (14.3 degrees) to prevent saturation for too long a time.

When the computer's space fixed velocity vector reached the initial ASC-15 computer presetting (V_s = 7546.00 m/s), the signal was issued to lock command modules, the steering commands were arrested, and path guidance was terminated. The computer then shifted to a faster cycle in which it searched for the cutoff velocity of 7592.00 m/s, space fixed. When this value was attained, the computer issued the guidance cutoff command which initiated shutdown of the S-IV engines. The final space fixed velocity achieved by the vehicle at the end of S-IV thrust decay was predicted to be 3.04 m/s higher than the velocity at guidance cutoff command. The actual velocity gained due to thrust decay was 2.9 m/s.

7.3 CONTROL ANALYSIS

7.3.1 S-I STAGE FLIGHT CONTROL

7.3.1.1 PITCH PLANE

In the pitch plane, the performance of the control system was very good. The magnitudes of the control parameters were small throughout S-I stage flight. The maximum values observed near the Mach 1 and maximum dynamic pressure regions were:

Parameters	Units	Magnitude	Range Time (sec)
Attitude Error	(deg)	0.8	77.5
Angle of Attack (free-stream)	(deg)	-0.9	74.2
Angular Rate	(deg/s)	-1.0	72.5
Normal Acceleration	(m/s^2)	-0.5	74.5
Actuator Position	(deg)	-1.3	73.8
Angle-of-Attack Dynamic Pressure Product	($deg\text{-}N/cm^2$)	3.2	74.1

The vehicle pitch and roll programs were provided by the ASC-15 computer. The pitch program (χ_Z), which consists of a third order time dependent polynomial with three time segments, began at 9.28 seconds and was arrested at 138.99 seconds at 52.5 degrees from the launch vertical (Fig. 7-2). This program is identical to that of SA-8 and essentially provides a minimum angle of attack through the high dynamic pressure region, assuming a zero wind profile.

Significant first mode propellant slosh frequencies (0.9 to 1.3 Hz) were indicated by the pitch angular rate and engine actuator deflections (Fig. 7-3) between 70 and 120 seconds. This sloshing is similar to SA-9 and SA-8, but the peak to peak value in the angular rate of 0.2 deg/s was smaller on SA-10.

Figure 7-4 shows the comparison of the winds and angles of attack calculated from the onboard Q-ball measurements and a rawinsonde balloon release near launch time. The angle-of-attack wind (calculated from Q-ball angle of attack, attitude angle, and trajectory angle) is in fair agreement with the rawinsonde wind. The largest pitch wind component near max Q was 10.2 m/s.

7.3.1.2 YAW PLANE

Performance of the control system in the yaw plane was very satisfactory (Fig. 7-5). Maximum control values for S-I powered flight were:

Parameters	Units	Magnitude	Range Time (sec)
Attitude Error	(deg)	-0.6	78.5
Angle of Attack (free-stream)	(deg)	1.1	75.5
Angular Rate	(deg/s)	0.3	80.0
Normal Acceleration	(m/s^2)	0.6	75.5
Actuator Position	(deg)	-0.7	78.5
Angle-of-Attack Dynamic Pressure Product	($deg\text{-}N/cm^2$)	3.5	76.5

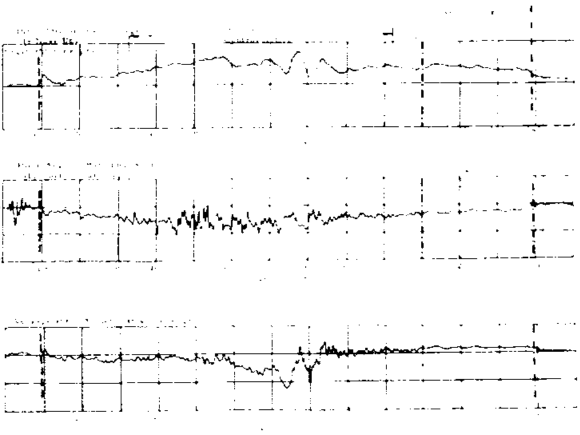

FIGURE 7-3. PITCH ATTITUDE ERROR, ANGULAR RATE, AND AVERAGE ACTUATOR POSITION

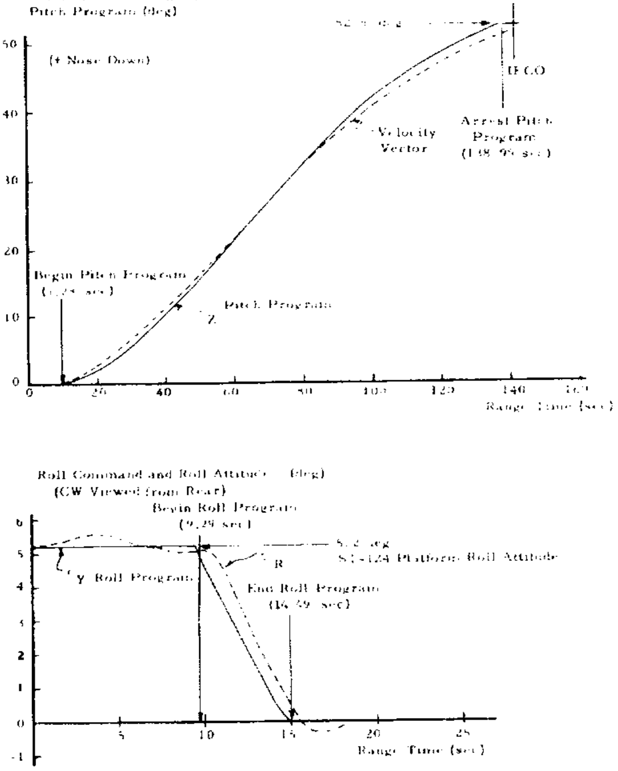

FIGURE 7-2. S-I STAGE COMMAND ANGLES

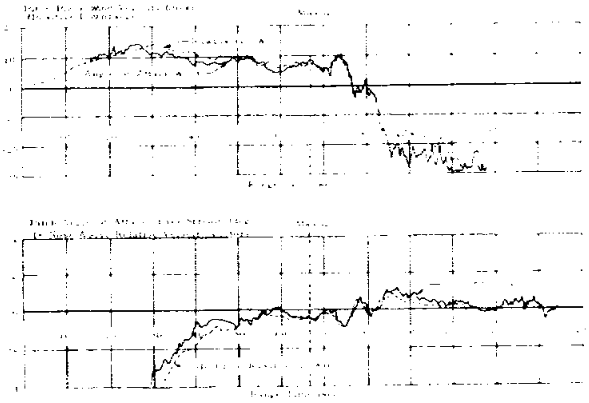

FIGURE 7-4. PITCH PLANE WIND VELOCITY

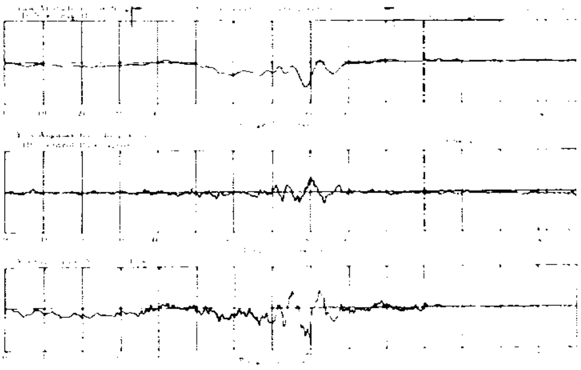

FIGURE 7-5. YAW ATTITUDE ERROR, ANGULAR RATE, AND AVERAGE ACTUATOR POSITION

The rawinsonde and angle-of-attack yaw plane winds are shown in Figure 7-6. A close comparison was obtained by assuming a 0.2-degree yaw misalignment of the Q-ball sensor. The maximum yaw wind component near max Q was 9.8 m/s computed from the onboard Q-ball and 12 m/s from the rawinsonde balloon release.

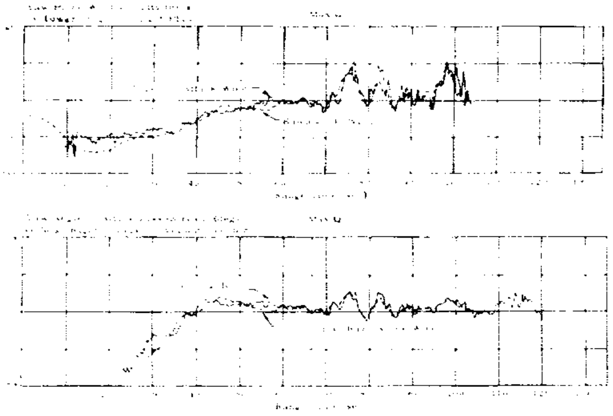

FIGURE 7-6. YAW PLANE WIND VELOCITY AND FREE STREAM ANGLE OF ATTACK

7.3.1.3 CONTROL DESIGN PARAMETERS

A comparison of the SA-10 flight results and Block II control system design criteria for total actuator deflection; angle of attack; and dynamic pressure, angle-of-attack product is shown in Figure 7-7. The design values are based on a 95 percent nondirectional wind velocity with 2 σ shears and 11 percent variation in aerodynamics. Two sigma variations in propulsion system performance and vehicle mass characteristics were also considered in arriving at the design values. The SA-10 data are well within the design values, falling either below or in the lower portion of the envelope observed on the previous Block II flights.

7.3.1.4 ROLL PLANE

SA-10 roll control functioned as expected. Roll parameters are shown in Figure 7-8. At 9.29 seconds the required launch-to-flight azimuth (90 to 95.2 degrees roll maneuver) program began, rotating the vehicle's pitch and yaw axes into coincidence with the stabilized axes. The required 5.2-degree maneuver, executed at a rate of 1 deg/s, was completed at 14.49 seconds (Fig. 7-2).

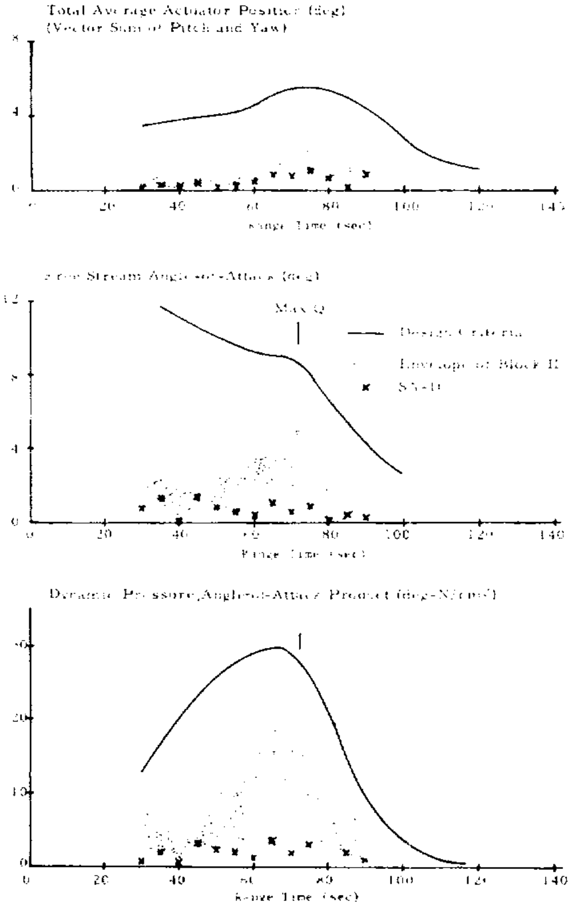

FIGURE 7-7. COMPARISON OF VEHICLE CONTROL PARAMETERS WITH DESIGN CRITERIA

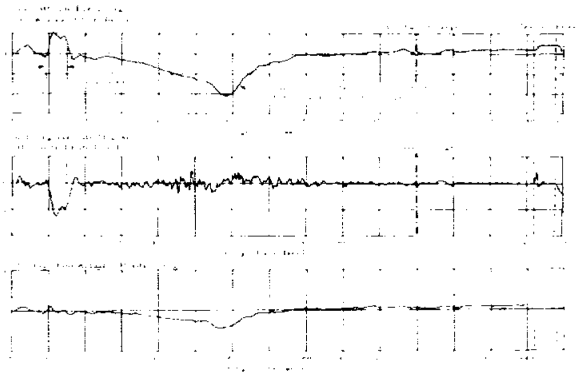

FIGURE 7-8. ROLL ATTITUDE ERROR, ANGULAR RATE, AND AVERAGE ACTUATOR POSITION

The roll axis maximum control values measured S-I stage propelled flight were:

Parameter	During Roll Maneuver		After Roll Maneuver	
	Magnitude	Range Time (sec)	Magnitude	Range Time (sec)
Attitude Error (deg)	1.0	11.2	-2.1	58.0
Angular Rate (deg/s)	-1.3	12.0	0.5	49.1
Engine Deflection Roll (deg)	0.1	10.5	-0.4	58.0

As on previous flights, a significant attitude error (-2.1 degrees) was observed near max Q. This roll attitude error is attributed to unsymmetrical flow about the turbine exhaust fairings (see Reference 3).

7.3.2 S-IV STAGE FLIGHT CONTROL

The performance of the vehicle control system was excellent throughout S-IV powered flight. The system responded properly to the transients during S-I stage separation and following path guidance initiation. The pitch, yaw, and roll attitude errors are presented in Figure 7-9.

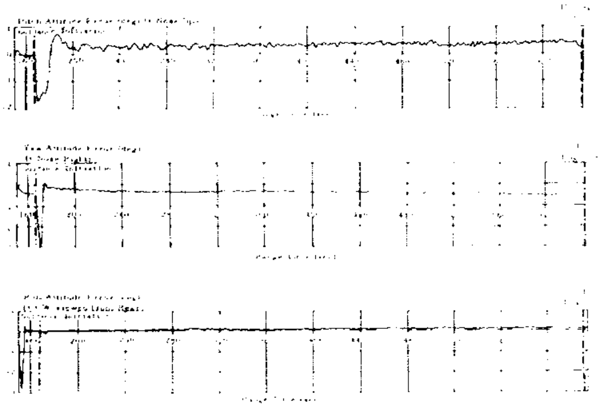

FIGURE 7-9. S-IV STAGE ATTITUDE ERRORS

At path guidance initiation (167.26 seconds), the vehicle's space fixed velocity was 0.16 percent higher than predicted and its altitude was about 1.9 km higher than predicted. This condition caused the guidance system to issue a nose up pitch steering command correction ($\Delta\chi_Z$) which peaked at 10.9 degrees from the previous value of 52.5 degrees, at 180 seconds. During this period (at 171 seconds), the ST-124 platform issued a maximum nose down pitch attitude error signal of 1.7 degrees to the vehicle flight control system. The vehicle pitch program (χ_Z) reached a minimum angle of 41.6 degrees at 180 seconds (Fig. 7-10).

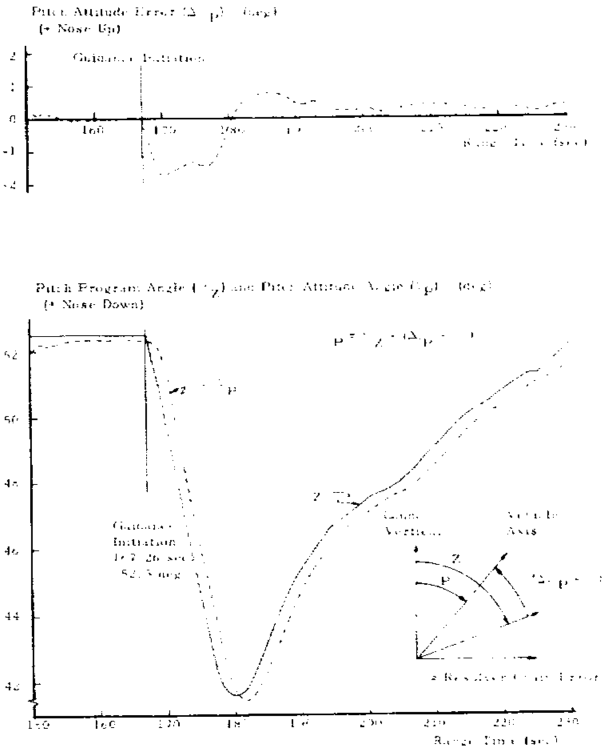

FIGURE 7-10. VEHICLE RESPONSE TO PITCH PLANE GUIDANCE INITIATION

In the yaw plane, the ASC-15 computer data showed that the vehicle was slightly to the left (7.2 m/s and 800 m) at guidance initiation. Consequently, the guidance system issued maximum steering command corrections of 4.2 degrees χ_X and 3.9 degrees χ_Y (nose right and CW viewed from the rear) at 172 seconds; i.e., χ_{CR} reached a maximum value of 5.7 degrees at 172 seconds. At this time the largest attitude error signals issued by the ST-124 to the vehicle flight control system were -3.0 degrees yaw (nose left) and 0.2 degrees CCW roll. The maximum yaw and roll attitudes resulting from the initiation of yaw plane guidance were 5.5 degrees (nose right) and 0.5 degree CW, both at 174 seconds.

The overall performance of the guidance system was excellent. At guidance initiation the computer indicated that the vehicle was slightly to the left. About 270 seconds later these initial values of 7.2 m/s and 800 m reached 0 m/s and 144 m to the left. A slight yaw steady state attitude error caused the cross range velocity and displacement (measured by the computer) to increase to -0.3 m/s and -180 m at S-IV cutoff; these values compare favorably with the precalculated trajectory values of -0.1 and -187 meters.

The pitch plane steering misalignment correction term (χ_{ZC}), introduced some 6 seconds after guidance initiation, increased from 0.9 degree shortly after guidance initiation to 1.5 degrees at the end of path guidance. This variation was well within the expected range.

The S-IV stage steady state attitude errors and engine deflections were near the predicted values. The mean pitch attitude error increased from 0.3 degree nose-up at 200 seconds to 0.4 degree at 625 seconds. The predicted steady state attitude error histories differed from flight values by 0.2 degree or less, in a nose-up direction. The minor discrepancy between the measured and predicted values can be accounted for by small thrust vector misalignments and a center of gravity offset different from predicted.

The mean yaw attitude error increased from 0.2 degree nose-left at 180 seconds to 0.5 degree nose-left at 625 seconds. The predicted steady state attitude error histories differed from flight values by 0.1 degree in a nose-left direction. This discrepancy is attributed to the same factors as the pitch attitude error discrepancy.

The mean roll attitude error was less than 0.1 degree throughout S-IV stage powered flight.

Vehicle steering commands were arrested when the space fixed velocity vector computed by the guidance system reached 7546.0 m/s. This occurred about 2.0 seconds before S-IV guidance cutoff command. The steering command angle χ_z was arrested at 124.05 degrees (630.25 seconds), just 0.13 degree less than predicted. Predicted cutoff time was 632.57 seconds.

The angular rates resulting from steering arrest and S-IV stage thrust decay were nearly zero. At the end of S-IV thrust decay the angular rates were -0.04 deg/s in pitch, -0.06 deg/s in yaw and 0.01 deg/s in roll.

7.4 FUNCTIONAL ANALYSIS

7.4.1 CONTROL SENSORS

7.4.1.1 CONTROL ACCELEROMETERS

The two body fixed control accelerometers which were located in the Instrument Unit to provide partial load relief in the pitch and yaw planes from 33 to 102 seconds, functioned properly. Figure 7-11 shows the measured lateral accelerations, translated to the vehicle CG. Peak lateral accelerations of -0.5 m/s^2 in pitch and 0.6 m/s^2 in yaw were measured near max Q. In general, these telemetered values agree with flight simulation results within 0.1 m/s^2. S-I and S-IV propellant sloshing and the first two vehicle bending modes were evident in these measurements during portions of the time that accelerometer control was active.

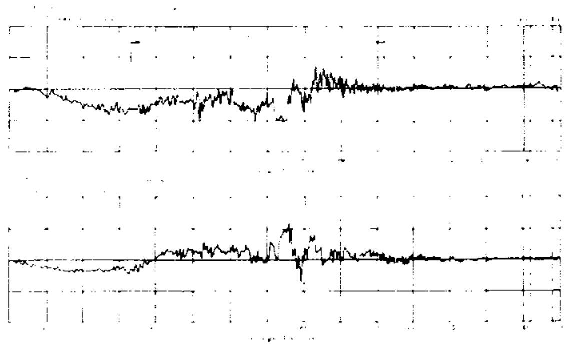

FIGURE 7-11. PITCH AND YAW CONTROL ACCELEROMETERS

7.4.1.2 ANGLE-OF-ATTACK SENSORS

Pitch and yaw angle-of-attack components were measured by a model F16 Q-ball angle-of-attack transducer mounted on the tip of the launch escape system (LES) and by Edcliff angle-of-attack meters mounted on booms at the tips of fins I and II. The Q-ball transducer functioned properly. When using a 0.2-degree yaw misalignment on the Q-ball, results compare well with the calculated angles of attack from measured wind data, trajectory parameters, and telemetered attitude angles. The Edcliff meters did not function properly during any portion of the flight. It was impossible to find any factors that could correlate these measurements with the calculated or Q-ball angles of attack. No explanation for the discrepancy was found since two previous flight tests of these measurements, in the same location, produced reliable data. Maximum angles of attack of -1.0 degree in pitch and 1.1 degrees in yaw were measured near the max Q region.

SA-10 was the second flight test of a network to determine the vector sum of the pitch and yaw angle-of-attack Q-ball measurements for possible use in the future emergency detection system (EDS). This measurement indicated probable satisfactory performance for EDS use. As on SA-8, the reduction of the telemetered signal is sensitive to the lower nonlinear portion of the calibration curve. However, this applies to small angles less than 1.0 degree and is not considered a problem for EDS use.

7.4.1.3 RATE GYROS

SA-10 carried only two rate gyro packages; both functioned properly. A ± 10 deg/s range, 3-axis control rate gyro package located in the Instrument Unit was used to provide pitch, yaw, and roll angular rate information for vehicle control throughout flight. The second rate gyro package, also a 3-axis of ± 10 deg/s range, was a control type unit being flown for development purposes and was located in the thrust structure area of the S-I stage.

7.4.1.4 CONTROL ACCELERATION SWITCH

The control acceleration switch on SA-10 appeared to close about 1.0 second later than predicted, which is longer than that observed on SA-9 and SA-8. Laboratory tests of this switch located in the Instrument Unit indicated a switch closure initiation value of 0.303 g with a time delay of 0.4 second (time from sensing of g value to switch closed signal). Following is a comparison of the operation of this switch on the last three flights. A note of caution must be made when evaluating this tabulation since the measurement F55-802 is on a commutated channel.

Parameters	SA-8	SA-9	SA-10
Switch Setting (g)	0.254	0.254	0.303
Predicted Time Delay (sec)	0.3	0.3	0.4
Actual Delay (sec)	0.7	0.9	1.4
Delay After Separation Command (sec)	0.7	1.0	0.9

7.4.1.5 RESOLVER CHAIN ERROR COMPARISON

The total resolver chain error in any axis is the angle difference between the output angle generated by the ST-124 and the input angle commanded by the ASC-15 computer.

A comparison between predicted and calculated pitch axis resolver chain error is shown as a function of the pitch command resolver angle (χ_z) in Figure 7-12. The calculated resolver error was obtained by subtracting the calculated pitch attitude error from the telemetered attitude error. The calculated attitude error was obtained from a vector balance using the guidance system measured space fixed acceleration, the body fixed pitch and longitudinal accelerations, and the telemetered pitch steering command (χ_z). Predicted and calculated values of pitch axis resolver error have the same general shape and indicate fair agreement except for the period during S-IV stage flight after guidance initiation. These pitch axis resolver chain errors had only an extremely minor effect on the vehicle latitude at S-IV cutoff.

Since the predicted resolver chain errors based on laboratory measurements in the yaw and roll axes were very small, no comparison was attempted between predicted and calculated values.

7.4.1.6 FLIGHT CONTROL COMPUTER AND ACTUATOR ANALYSIS

The commands issued by the control computer to position the actuators were correct throughout the entire controlled flight period of both stages. These engine positioning commands were well within the load, gimbal rate, and torque capabilities of the S-I and S-IV actuators. The performance of all eight S-I and all twelve S-IV stage actuators was satisfactory.

Parameter	Type of Data	Event		
		Liftoff	max Q	OECO
Gimbal Rate (deg/s)	Measured	1	2	1
	Design Limit	11	17	11
Torque (N-m)	Measured	6,700	10,780	14,150
	Design Limit	13,500	29,200	22,500

S-I Stage (maximum actuator deflection was -1.3 degrees; occurred near max Q)

Parameter	Type of Data	Event	
		Ignition	Cutoff
Gimbal Rate (deg/s)	Measured	3.3	0.4
	Design Limit	18.8	
Torque (N-m)	Measured	700	420
	Design Limit	1180	

S-IV Stage (maximum actuator deflection between S-IV ignition and S-IV cutoff was 1.7 degrees; measured at 151 seconds)

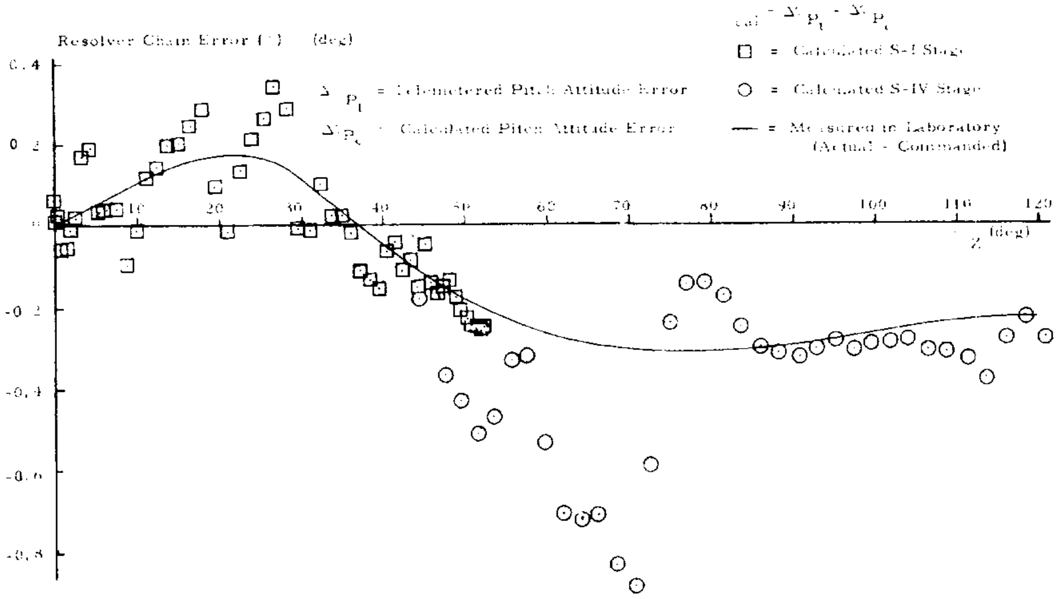

FIGURE 7-12. CALCULATED AND PREDICTED PITCH AXIS RESOLVER CHAIN ERROR

7.5 PROPELLANT SLOSHING

7.5.1 S-I POWERED FLIGHT SLOSHING

None of the S-I stage propellant tanks carried slosh monitoring instruments; however, both S-IV stage tanks were instrumented with a continuous level sensor for the S-IV propellant utilization system which also indicates S-IV slosh amplitudes.

The pitch and yaw engine actuator positions were bandpass filtered at the slosh frequency; the resulting predominant frequencies are shown in the top portion of Figure 7-13. The maximum peak-to-peak response of the engines to sloshing was 0.34 degree in pitch at 85 seconds and 0.26 degree in yaw at 77 seconds (middle portion of Figure 7-13). The S-IV LOX slosh amplitudes, calculated from onboard slosh monitoring and theoretical transfer functions using engine deflections, are compared with SA-8 at the bottom of Figure 7-13. As on SA-8 it appears that the actuator deflections result from the vehicle being driven by S-IV LOX tank sloshing from 75 to 110 seconds.

7.5.2 S-IV POWERED FLIGHT SLOSHING

The LOX and LH_2 slosh amplitudes and frequencies were very similar to those measured on the SA-8 flight. The slosh amplitude history agrees with the pattern seen on previous flights, and the frequencies agree well with those predicted.

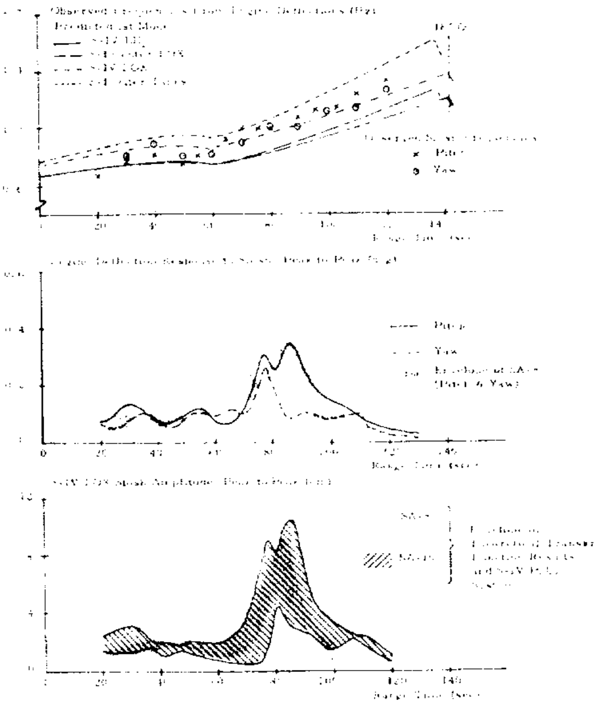

FIGURE 7-13. SLOSH DURING S-I POWERED FLIGHT

7.6 GUIDANCE SYSTEM PERFORMANCE

The overall performance of the ST-124 guidance system (ST-124 stabilized platform and electronic box, guidance signal processor and ASC-15 computer) was very satisfactory. Detailed analysis of the telemetered guidance system data is discussed in subsequent parts of this section.

7.6.1 GUIDANCE INTELLIGENCE ERRORS

Guidance intelligence errors are defined as the differences between the range, altitude, and cross range inertial velocity components measured by the ST-124 accelerometers and the corresponding parameters calculated from tracking data.

The sources of the guidance intelligence errors may be divided into two general categories; component errors and system errors. The component errors, scale factor and bias, are those which are attributed directly to the guidance accelerometers. The system errors, contributed by the stabilized element on which the accelerometers mount, are: gyro drift rates (constant and g-dependent), platform leveling errors, nonorthogonality of the accelerometer measuring directions, and misalignment of the platform flight azimuth. With the exception of the leveling and azimuth errors, information on expected errors was obtained by laboratory measurements several weeks prior to launch. The leveling and azimuth errors were determined from data which were available only immediately before liftoff.

The predicted ST-124 inertial velocity differences for the SA-10 flight test were based on laboratory calibration of the ST-124 stabilized platform system (Fig. 7-14 and Table 7-I). Additional velocity differences due to accelerometer leveling and azimuth alignment errors were determined from launch data. The ST-124 system 3 σ error band for each velocity component is used as the standard for comparison with the actual inertial velocity differences determined from the postflight trajectory analysis.

Examination of each inertial velocity component difference (accelerometer-tracking) displayed in Figure 7-14 indicates that some of the inflight velocity error sources do not agree with the laboratory and prelaunch error sources within the 3 σ limits. In fact, in several cases ($\delta\dot{Y}/\ddot{X}$, $\delta\dot{Y}/\ddot{Y}$, $\delta\dot{Z}/\ddot{X}$) the analysis errors were smaller and within the 3 σ limits whereas eight of the predicted errors were larger ($\delta\dot{X}$, $\delta\dot{Y}$, $\delta\dot{Z}$, $\delta\dot{X}/\ddot{X}$, $\delta\dot{X}/\ddot{Y}$, $\delta\dot{Y}/\ddot{X}$, $\delta\dot{Z}/\ddot{X}$, SF_Z) than 3 σ.

The magnitude of the predicted lateral velocity deviation was similar to that which was actually

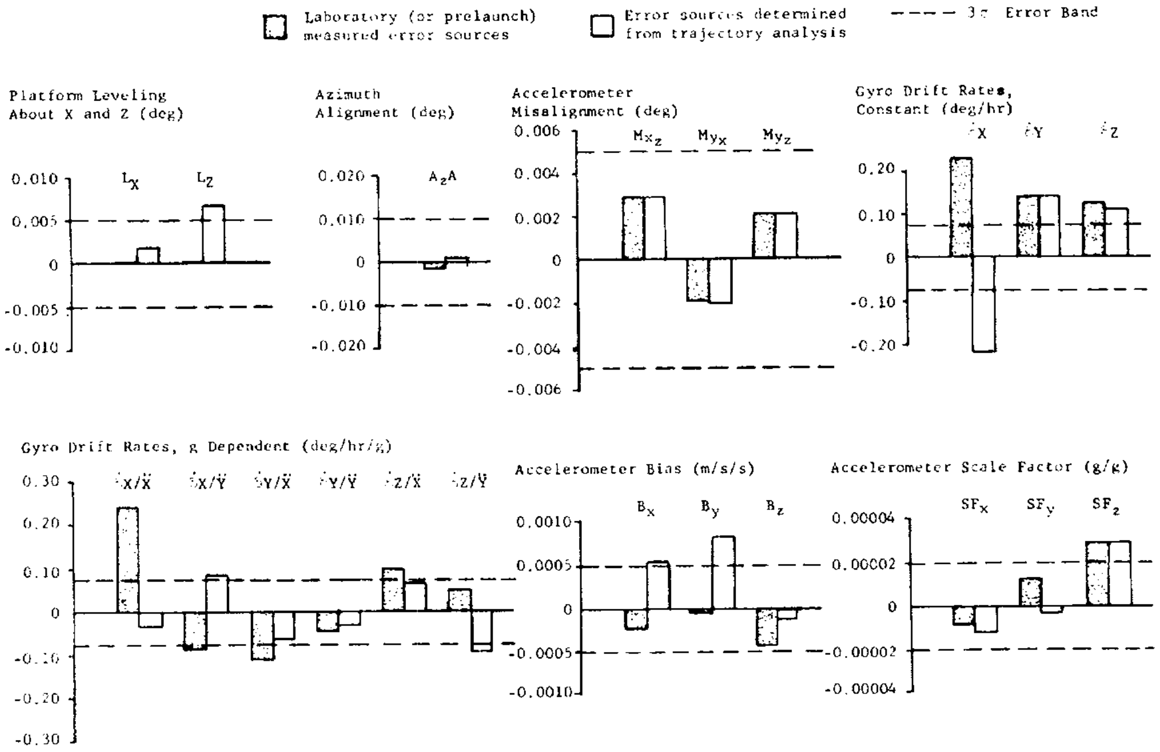

FIGURE 7-14. ST-124 STABILIZED PLATFORM SYSTEM ERROR SOURCES

~~CONFIDENTIAL~~

TABLE 7-I. GUIDANCE INTELLIGENCE ERRORS

Parameters	Symbol	Units	Laboratory and Pre-Launch Meas. Error Sources	Error Sources Established from Traj. Analysis	3 σ Error Band	Inertial Velocity Difference at S-IV Cutoff (m/s)					
						$\Delta\dot{X}_i$		$\Delta\dot{Y}_i$		$\Delta\dot{Z}_i$	
						Lab	Traj	Lab	Traj	Lab	Traj
1. System Errors											
a. Platform Leveling		deg			±0.005						
1) About X Axis	L_X		0	-0.169×10^{-2}		0	0	0	0	0	0.09
2) About Z Axis	L_Z		0	0.697×10^{-2}		0	0.38	0	-0.90	0	0
b. Azimuth Alignment	A_zA	deg	-1.39×10^{-3}	0.091×10^{-2}	±0.01	0		0		-0.17	0.12
c. Accelerometer Misalignments		deg			±0.005						
1) Range Accel Rotated Toward Z Axis	M_{X_Z}		0.2944×10^{-2}	0.2944×10^{-2}		0	0	0	0	0	0
2) Altitude Accel Rotated Toward X Axis	M_{Y_X}		-0.186×10^{-2}	-0.193×10^{-2}		0	0	0.24	0.25	0	0
3) Altitude Accel Rotated Toward Z Axis	M_{Y_Z}		0.2139×10^{-2}	0.2139×10^{-2}		0	0	0	0	0	0
d. Gyro Drift Rates, Constant		deg/hr			±0.075						
1) Yaw (X) Gyro (About X Axis)	$\dot{\delta}X$		0.230	-0.226		0	0	0	0	0.02	-0.02
2) Roll (Y) Gyro (About Y Axis)	$\dot{\delta}Y$		0.138	0.139		0	0	0	0	1.74	1.73
3) Pitch (Z) Gyro (About Z Axis)	$\dot{\delta}Z$		0.125	0.112		-0.01	-0.01	-1.57	-1.40	0	0
e. Gyro Drift Rates, g-Dependent		deg/hr/g			±0.075						
1) Yaw (X) Gyro (About X Axis Due to $\ddot{X}$)	$\dot{\delta}X/\ddot{X}$		0.241	-0.043		0	0	0	0	0.12	-0.02
2) Yaw (X) Gyro (About X Axis Due to $\ddot{Y}$)	$\dot{\delta}X/\ddot{Y}$		-0.086	0.086		0	0	0	0	0.22	-0.21
3) Roll (Y) Gyro (About Y Axis Due to $\ddot{X}$)	$\dot{\delta}Y/\ddot{X}$		-0.111	-0.096		0	0	0	0	-1.51	-1.30
4) Roll (Y) Gyro (About Y Axis Due to $\ddot{Y}$)	$\dot{\delta}Y/\ddot{Y}$		-0.045	-0.028		0	0	0	0	-0.55	-0.34
5) Pitch (Z) Gyro (About Z Axis Due to $\ddot{X}$)	$\dot{\delta}Z/\ddot{X}$		0.101	0.094		-0.05	-0.05	-1.38	-1.27	0	0
6) Pitch (Z) Gyro (About Z Axis Due to $\ddot{Y}$)	$\dot{\delta}Z/\ddot{Y}$		0.049	-0.120		0.12	-0.29	-0.59	1.44	0	0
2. Component Errors											
a. Accelerometer Bias		m/s/s			$\pm 5.0 \times 10^{-4}$						
1) Range Accelerometer	B_x		-2.3×10^{-4}	5.20×10^{-4}		-0.15	0.33	0	0	0	0
2) Altitude Accelerometer	B_y		-0.46×10^{-4}	7.40×10^{-4}		0	0	-0.03	0.47	0	0
3) Cross Range Accelerometer	B_z		-4.2×10^{-4}	-1.6×10^{-4}		0	0	0	0	-0.10	0
b. Accelerometer Scale Factor		g/g			$\pm 2.0 \times 10^{-5}$						
1) Range Accelerometer	SF_x		-0.84×10^{-5}	-1.26×10^{-5}		-0.06	-0.09	0	0	0	0
2) Altitude Accelerometer	SF_y		1.3×10^{-5}	-0.38×10^{-5}		0	0	0.04	-0.01	0	0
3) Cross Range Accelerometer	SF_z		2.9×10^{-5}	2.9×10^{-5}		0	0	0	0	0	0
				Total Error (m/s)		-0.15	0.27	-3.29	-1.42	-0.40	-0.05

~~CONFIDENTIAL~~

observed but was opposite in polarity (Fig. 7-15). The required change in drift rates to produce this condition is reflected in the drift rates ($\delta\dot{X}$, $\delta\dot{X}/\dot{X}$, $\delta\dot{Y}/\dot{Y}$), as shown in Figure 7-14 and Table 7-I.

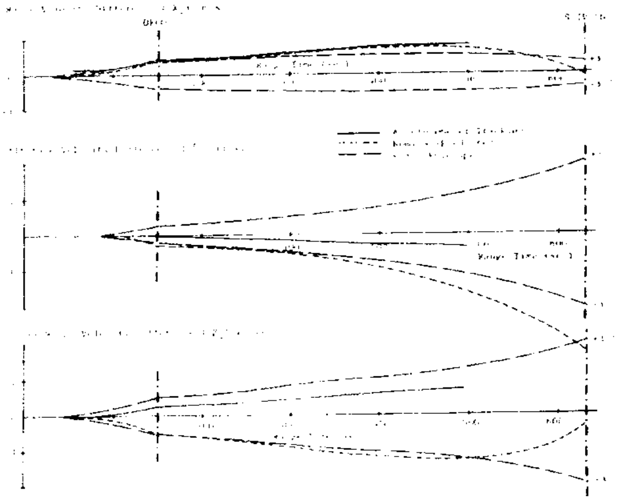

FIGURE 7-15. INERTIAL VELOCITY COMPONENT DIFFERENCE (ACCELEROMETER-TRACKING)

A comparison of the accelerometer, tracking, and precalculated trajectory inertial velocity components, and total velocities is presented in Table 7-II. The velocity differences between the accelerometers and the tracking data indicate satisfactory consistency at the various flight times and all of the inertial velocity differences (accelerometer-tracking) fall within the 3 σ band.

Figure 7-15 compares the inertial velocity component differences (accelerometer-tracking) with the 3 σ error bands. The indicated predicted velocity differences at S-IV cutoff are the laboratory total velocity differences from Table 7-I. Figure 7-16 shows the residual inertial velocity components (trajectory analysis-tracking) together with the velocity component differences (accelerometer-tracking and trajectory analysis results). The trajectory analysis is a simulation of the inertial velocity components using the guidance errors shown in Table 7-I. The residual velocity differences fall well within the tracking accuracies, indicating a satisfactory trajectory analysis solution to the measured velocity differences.

TABLE 7-II. COMPARISON OF INERTIAL GUIDANCE VELOCITIES (V_i, $\dot{X}_i$, $\dot{Y}_i$, $\dot{Z}_i$)

Event Range Time (sec)	Type of Data	Total Velocity (m/s)		Range Velocity (m/s)		Altitude Velocity (m/s)		Cross Range Velocity (m/s)	
		Actual	Vel. Diff.	Actual	Vel. Diff.	Actual	Vel. Diff.	Actual	Vel. Diff.
IECO 142.22	Accelerometer	3591.1		2024.6		2966.0		-5.9	
	Tracking	3591.2		2024.3		2966.2		-6.2	
	Precalculated	3588.0		2039.7		2951.8		-4.5	
	Accel - Track		-0.1		0.3		-0.2		0.3
	Precal - Track		-3.2		15.4		-14.4		1.7
OECO 148.32	Accelerometer	3778.9		2179.8		3086.9		-6.1	
	Tracking	3779.0		2179.6		3087.1		-6.4	
	Precalculated	3772.7		2193.0		3069.8		-4.8	
	Accel - Track		-0.1		0.2		-0.2		0.3
	Precal - Track		-6.3		13.4		-17.3		1.6
Guidance Initiation 167.26	Accelerometer	3886.2		2268.3		3155.5		-7.1	
	Tracking	3886.1		2268.1		3155.6		-7.5	
	Precalculated	3879.1		2280.8		3137.7		-5.7	
	Accel - Track		0.1		0.2		-0.1		0.4
	Precal - Track		-7.0		12.7		-17.9		1.8
S-IV Cutoff 630.252	Accelerometer	8039.8		7398.0		3147.7		-0.3	
	Tracking	8040.2		7397.9		3149.0		-0.3	
	Precalculated	8050.5		7400.0		3170.4		-0.1	
	Accel - Track		-0.4		0.1		-1.3		0.0
	Precal - Track		10.3		2.1		21.4		0.2
	3 σ Error Band		±0.7		±0.5		±1.5		±1.9
Orbital Insertion 640.252	Accelerometer	8041.4		7400.4		3146.1		-0.3	
	Tracking	8041.8		7400.3		3147.5		-0.3	
	Precalculated	8052.2		7402.5		3168.7		-0.1	
	Accel - Track		-0.4		0.1		-1.4		0.0
	Precal - Track		10.4		2.2		21.2		0.2

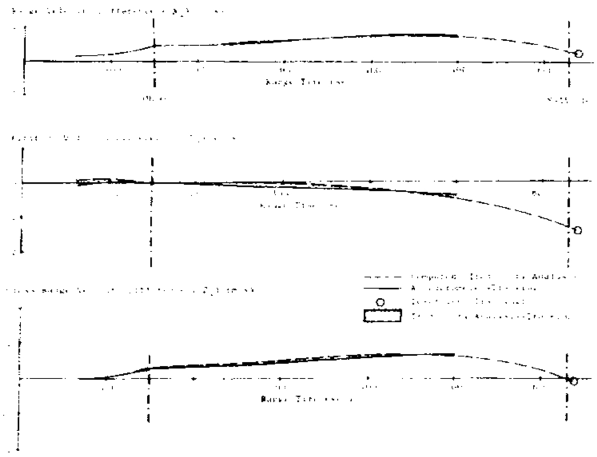

FIGURE 7-16. RESIDUAL INERTIAL VELOCITY COMPONENT DIFFERENCES (TRAJECTORY ANALYSIS-TRACKING)

7.6.2 GUIDANCE SYSTEM PERFORMANCE COMPARISONS

A comparison of the precalculated trajectory and ASC-15 computer space fixed velocity and velocity components at S-IV cutoff with the tracking data is presented in Table 7-III. The velocity differences (computer-tracking) fall within the specified 3 σ error bands. The total space fixed velocity differences of 0.5 m/s was the result of a 0.1 m/s error in $\dot{X}_S$, a 1.2 m/s error in $\dot{Y}_S$, and a 0.1 m/s error in $\dot{Z}_S$. The contribution of each of the component errors to the total velocity error was as follows: $\Delta\dot{X}_S$ (20 percent or 0.1 m/s), $\Delta\dot{Y}_S$ (80 percent or 0.4 m/s), and $\Delta\dot{Z}_S$ (0 percent or 0 m/s).

The space fixed range and altitude velocity differences (computer-tracking) indicate the excellent performance of the iterative guidance mode (IGM) scheme in the pitch plane; i.e. while $\Delta\dot{X}_S$ and $\Delta\dot{Y}_S$ differ from the precalculated trajectory values by approximately twice the 3 σ error values, the total space fixed velocity vector difference is only 0.5 m/s. This is the third flight test in which the predicted and actual space fixed cross range velocity differences fell within 3 σ (± 1.81 m/s) of each other at S-IV cutoff.

In Table 7-IV, the precalculated trajectory and ASC-15 computer parameters are compared with tracking at orbital insertion. As in the case of the comparison made at S-IV cutoff, the total measured errors (computer-tracking) at orbital insertion all fall within the 3 σ error band. The increase in vehicle total velocity between S-IV cutoff command and orbital insertion was 2.9 m/s, which agrees very well with the predicted increase of 3.04 m/s.

The satisfactory performance of the yaw plane (delta-minimum) guidance scheme is shown in Figure 7-17. The ASC-15 computer cross range velocity and displacement at guidance initiation (7.2 m/s and 800 m) were reduced to minimum values at about 270 seconds. The increase in all parameters (velocity, displacement, and steering command) after this time is due to the increasing vehicle lateral CG offset and/or increasing thrust vector misalignment. Due to these conditions, the cross range velocity and displacement increased to -0.3 m/s and -180 m at S-IV cutoff.

TABLE 7-III. COMPARISON OF SPACE FIXED VELOCITIES AT S-IV GUIDANCE CUTOFF (630.252 Seconds Range Time)

Data Source	V_S Total Velocity (m/s)	ΔV_S Total Velocity Difference (m/s)	$\dot{X}_S$ Range Velocity (m/s)	$\Delta\dot{X}_S$ Range Velocity Difference (m/s)	$\dot{Y}_S$ Altitude Velocity (m/s)	$\Delta\dot{Y}_S$ Altitude Velocity Difference (m/s)	$\dot{Z}_S$ Cross Range Velocity (m/s)	$\Delta\dot{Z}_S$ Cross Range Velocity Difference (m/s)
ASC-15 Computer	7592.0		7183.4		-2456.8		-35.5	
Tracking	7591.5		7183.3		-2455.6		-35.6	
Precal Trajectory	7592.0		7182.6		-2459.0		-35.6	
Computer-Tracking		0.5		0.1		1.2		0.1
3 σ Error Band		±0.80		±0.40		±1.63		±1.81
Precal Traj-Tracking		0.5		-0.7		-3.4		0.0

TABLE 7-IV. COMPARISON OF GUIDANCE PARAMETERS AT ORBITAL INSERTION (640.252 Seconds Range Time)

Parameter	Units	Symbol	Precalculated Trajectory	ASC-15 Computer	Tracking Trajectory	Error (Precal-Trk)	Total Meas Error (ASC-15-Trk) E	Estimated 3 σ Error Band*	Error** Factor $\frac{E}{3\sigma}$	Residual*** Error |E-3 σ
Total Velocity	m/s	V_S	7595.0	7594.9	7594.3	0.7	0.6	±0.85	0.71	
Total Radius Vector	m	R_T	6,910,007	6,910,005	6,909.964	43	41	+402 -313	0.10	
Path Angle	deg	θ_{PL}	90.000	90.002	90.013	-0.013	-0.011	+0.014 -0.012	0.92	
Altitude	m	h	535,708	535,710	535,667	41	43	+402 -313	0.11	
Range Velocity	m/s	$\dot{X}_S$	7157.7	7158.5	7158.2	-0.5	0.3	+0.55 -0.43	0.55	
Altitude Velocity	m/s	$\dot{Y}_S$	-2539.6	-2537.4	-2536.0	-3.6	-1.4	+1.98 -1.86	0.75	
Cross Range Velocity	m/s	$\dot{Z}_S$	-35.4	-35.0	-35.4	0.0	0.4	+1.79 -2.53	0.22	
Range Displacement	m	X_S	2,310,482	2,308,374	2,308,136	2,346	238	+250 -202	0.95	
Altitude Displacement	m	Y_S	6,512,283	6,513,028	6,513,067	-784	-39	+379 -323	0.12	
Cross Range Displacement	m	Z_S	-6,618	-6,374	-6,671	53	297	+381 -585	0.78	
Cross Range Velocity (Inertial)	m/s	$\dot{Z}_i$	-0.1	-0.3	-0.3	0.2	0.0	+1.92 -2.26	-	
Cross Range Displacement (Inertial)	m	Z_i	-188	-183	-397	209	214	+311 -701	0.69	

* Unsymmetrical 3 σ values are due to known biases in the ASC-15 computer or in the guidance system.

** Error factors greater than 1.00 indicate that the total measured error exceeds the applicable 3 σ error.

*** Residual errors exist only where the measured error exceeds the 3 σ error.

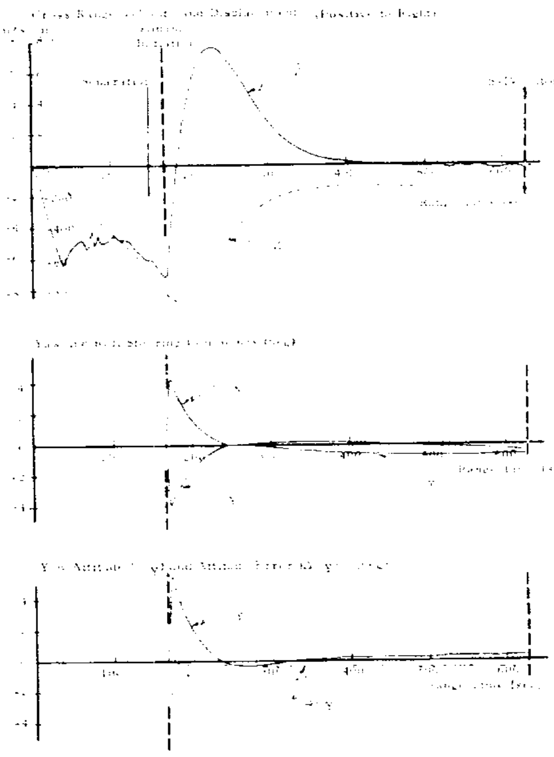

FIGURE 7-17. YAW PLANE DELTA-MINIMUM GUIDANCE PARAMETERS

7.7 GUIDANCE SYSTEM HARDWARE

7.7.1 GUIDANCE SIGNAL PROCESSOR AND DIGITAL COMPUTER ANALYSIS

The overall performance of the guidance system hardware was completely satisfactory. The countdown procedure introduced on SA-9, which forces a recycling of the digital computer back through guidance release 45 seconds before liftoff (rather than almost 2 minutes before), was continued on SA-10. This approach gives updated "C" resolver readings much closer to liftoff and minimizes the possible inertial velocity errors sensed by the computer at liftoff. This scheme eliminated all inertial velocity errors at SA-10 liftoff.

S-IV cutoff occurred 2.32 seconds earlier than predicted; this condition was attributed to a slightly higher than predicted performance of both stages.

The precalculated space fixed velocity at orbital insertion was 7595.0 m/s; the value determined by tracking was 7594.3 m/s. The difference of only 0.7 m/s verifies ability to achieve a desired orbital insertion velocity accurately.

The digital computer issued all its sequencing command functions satisfactorily. The bit-by-bit comparison program was used to evaluate the inflight operation of the ASC-15 computer equipment. This analysis was made to confirm the correct operation of both the physical equipment and the flight program. Due to the nature of the analysis program, not all of the guidance computer telemetry was examined on a bit-by-bit basis; only those quantities computed by the flight program were examined. All navigation and guidance quantities were examined with the exception of minor loop telemetry (accelerometer readings and mode codes).

The total number of computer telemetry words from liftoff to entry into the cutoff loop was 52,668. Of this number, 51,671 or 98.1 percent were available for examination by the bit-by-bit comparison program. The remainder was lost due to staging and restart of the bit-by-bit program after the staging dropouts. Sixty percent of the telemetry was examined by the bit-by-bit program; the remainder was minor loop telemetry. Thus, 57.4 percent of the total ASC-15 computer telemetry during the time interval considered was examined in this analysis. An estimated 2.6 percent of the telemetry were lost due to dropouts. This number includes the data lost in the RF blackout during staging.

From this analysis, it was concluded that the ASC-15 computer and flight program operated correctly during flight.

7.7.2 ST-124 STABILIZED PLATFORM SYSTEM HARDWARE ANALYSIS

The overall performance of the ST-124 system was satisfactory. Table 7-I shows the various error sources which contributed to the total predicted and measured inertial velocity components. The predicted velocity differences are based upon the hardware error sources determined by laboratory platform system calibration tests in addition to prelaunch measured ST-124 leveling and azimuth alignment errors, and agree with the inertial velocity deviations determined by tracking within the 3 σ band for the range and cross range values (± 0.7 m/s and ± 1.9 m/s, respectively). The predicted altitude velocity difference does not fall within the 3 σ band (± 1.5 m/s) although the measured altitude velocity deviation does. The range velocity component is unique in that both the predicted and measured differences fall well within the 3 σ band and also agree closely with each other.

The three gyro stabilizing servoloop error signals indicated maximum values less than ± 0.1 degree (pitch gyro) and ± 0.25 degree (yaw and roll gyros).

The redundant gimbal servoloop error signal measured a maximum angle of 0.1 degree. The three guidance accelerometer servoloop signals' peak values were 0.35 degree (altitude accelerometer transient during liftoff) and 0.3 and 0.15 degrees in the range and cross range accelerometer, respectively. All these measured values indicate normal servoloop operation. The range and cross range guidance accelerometer encoder outputs verified the satisfactory functional performance of these instruments.

The three-phase power supplied to the ST-124 system by inverter 2 had the following average voltages:

Phase AB	~ 115 volts ac
Phase BC	~ 116 volts ac
Phase CA	~ 114.75 volts ac

Phase voltages are specified to average 115 ± 1 volt ac under a balanced load and to differ from each other by not more than 1.5 volts ac. The three phases averaged 115.2 volts ac and the maximum difference was 1.25 volts ac between phases BC and CA. The 56-volt dc supply averaged an acceptable 56 volts.

7.8 ST-124 GAS BEARING GN_2 SUPPLY SYSTEM

The SA-10 gas bearing GN_2 supply system, located in the Instrument Unit with the ST-124 stabilized platform system, provided dry and highly filtered gaseous nitrogen at a regulated temperature, pressure, and flowrate to the ST-124 gas bearing components. This supply system consisted of one high pressure storage bottle, a heating and pressure regulating assembly, pressure limit switches, calibration and check valves, temperature and pressure gauges, and interconnecting tubing. The detailed arrangement of the system is presented in Figure 7-18.

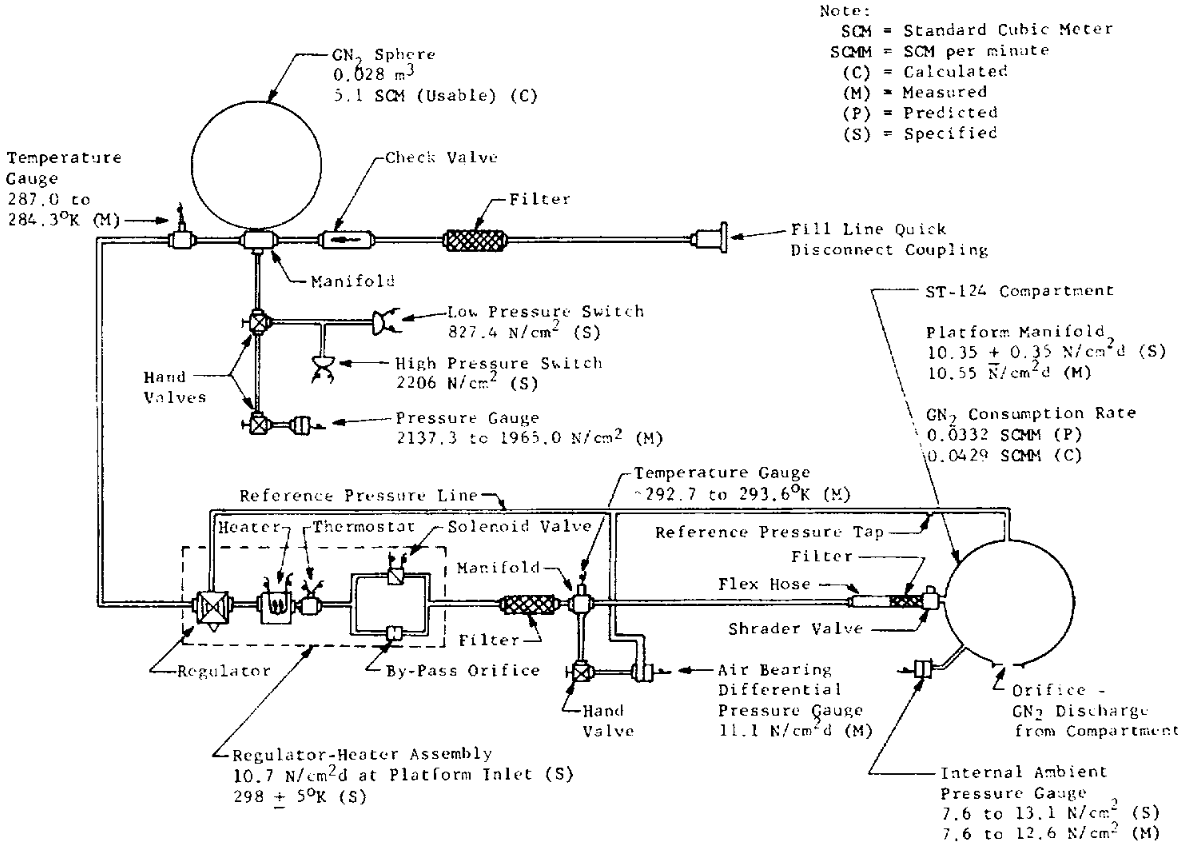
Note:
SCM = Standard Cubic Meter
SCMM = SCM per minute
(C) = Calculated
(M) = Measured
(P) = Predicted
(S) = Specified
GN₂ Sphere
0.028 m³
5.1 SCM (Usable) (C)
Temperature Gauge
287.0 to 284.3°K (M)
Check Valve
Filter
Fill Line Quick Disconnect Coupling
Manifold
Low Pressure Switch
827.4 N/cm² (S)
High Pressure Switch
2206 N/cm² (S)
Hand Valves
Pressure Gauge
2137.3 to 1965.0 N/cm² (M)
ST-124 Compartment
Platform Manifold
10.35 + 0.35 N/cm²d (S)
10.55 N/cm²d (M)
GN₂ Consumption Rate
0.0332 SCMM (P)
0.0429 SCMM (C)
Temperature Gauge
~292.7 to 293.6°K (M)
Reference Pressure Line
Heater
Thermostat
Solenoid Valve
Manifold
Reference Pressure Tap
Filter
Flex Hose
Shrader Valve
Filter
Regulator
By-Pass Orifice
Hand Valve
Air Bearing Differential Pressure Gauge
11.1 N/cm²d (M)
Orifice - GN₂ Discharge from Compartment
Regulator-Heater Assembly
10.7 N/cm²d at Platform Inlet (S)
298 ± 5°K (S)
Internal Ambient Pressure Gauge
7.6 to 13.1 N/cm² (S)
7.6 to 12.6 N/cm² (M)

FIGURE 7-18. ST-124 GAS BEARING SYSTEM

The SA-10, SA-9, and SA-8 supply systems were modified somewhat from those employed on previous Saturn Block II vehicles because of the change to the unpressurized Instrument Unit. The ST-124 enclosure pressure was used as a reference instead of the IU ambient pressure to maintain the gas bearing supply differential pressure. This was accomplished by routing a pneumatic line from the ST-124 enclosure back to the GN_2 pressure regulator.

The ST-124 stabilized platform enclosure ambient pressure was maintained within the desired pressure range of 13.1 N/cm^2 (19 psi) to 7.6 N/cm^2 (11 psi) throughout flight. The actual pressure varied from 12.6 N/cm^2 (18.2 psi) at liftoff to 7.6 N/cm^2 (11 psi) at S-IV cutoff.

The performance of the supply system was satisfactory. The GN_2 storage bottle (0.028 m^3) was pressurized to 2137 N/cm^2 (3100 psi) by the high pressure ground supply before liftoff. This value is well within the specified launch requirement of 1941 to 2217 N/cm^2 gauge (2815 to 3215 psig). From liftoff to S-IV cutoff, the ST-124 gas bearing consumed 0.450 SCM (8.8 percent of the total usable supply of 5.10 SCM (180 SCF). The average inflight consumption rate of the gas bearings was 0.0429 SCM/min, or 29 percent more than the predicted rate of 0.0332 SCM/min, based on the laboratory test of the ST-124. The gas consumption predicted for the SA-10 flight was approximately 22 percent lower than the actual consumption for the SA-10 flight. This is comparable to that observed on SA-9 and SA-8.

About two hours before liftoff, the average temperature of the GN_2 supplied to the ST-124 was 295°K (298 ± 5°K specified) and the measurement was displaying its characteristic thermostatic cycling. At -97 minutes S-IV LH_2 loading began and the temperature dropped rapidly, reaching the lower measuring range limit (293°K) at about -85 minutes. The measurement remained off scale for about 68 minutes, then gradually increased to about 293.4°K at liftoff. The measurement was again out of measuring limits from approximately 130 to 300 seconds of flight. The temperature of the GN_2 supplied to the inlet of the ST-124 is estimated to range from about 293°K at liftoff to around 290°K at 175 seconds and back to 293°K at S-IV cutoff. The GN_2 temperature probably averaged about 5 to 8°K below the specified value of 298°K. The ST-124 inertial gimbal temperature and the ST-124 mounting frame temperature averaged about 4°K lower than during laboratory tests.

This is the first of the unpressurized IU Saturn I vehicles (SA-9, 8, and 10) in which the pressure between the regulator discharge and the ST-124 compartment was measured as a differential pressure. Heretofore, this measurement has been a gauge pressure measurement at the measuring cross. In SA-10 the vent of the transducer at the measuring cross was teed into the reference line between platform and regulator giving a desired differential measurement across the platform. The approximately constant 11.1 N/cm^2 differential (16 psid) measured during flight must be reduced by approximately 0.48 N/cm^2 (0.7 psi) to obtain the platform manifold pressure value. The 0.48 N/cm^2 (0.7 psi) reduction is due to a 0.13 N/cm^2 (0.2 psi) pressure drop caused by the filter between the measuring cross and platform inlet and additionally a 0.35 N/cm^2 (0.5 psi) pressure drop from the platform inlet to the manifold. This gives a measured inlet manifold differential pressure of 10.55 N/cm^2 (15.3 psi), well within the specified value of 10.35 ± 0.35 N/cm^2 differential (15 ± 0.5 psid).

8.1 SUMMARY

Separation of the SA-10 vehicle was accomplished in the same manner as for previous Block II vehicles. The separation scheme was executed within the desired time frame.

First motion between stages was observed within 0.05 second of separation command. The S-IV-10 stage engines cleared the interstage within 0.87 second of separation command, which is just 0.01 second longer than for SA-8. Separation transients were relatively small and well within design requirements.

Separation of the Apollo shroud was initiated at 812.00 seconds, 2.17 seconds earlier than predicted. The velocity imparted to the S-IV/Pegasus due to separation was -0.3 m/s. The separation and ejection system functioned as planned.

8.2 S-I/S-IV SEPARATION DYNAMICS

8.2.1 TRANSLATIONAL MOTION

The actual separation sequence for the SA-10 vehicle is shown in Figure 8-1. First motion time and separation distance were determined from accelerometer data. This was the first Block II vehicle which did not have extensometers to measure the separation distance between stages. Separation was completed at 150.0 seconds.

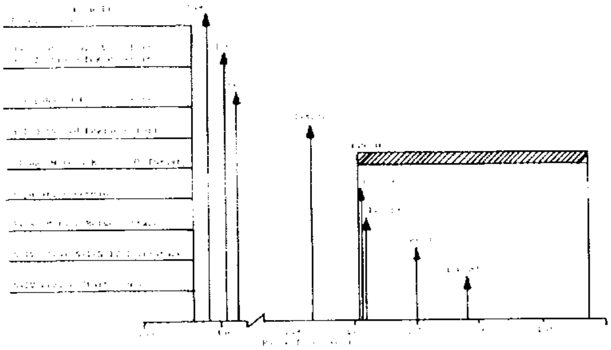

FIGURE 8-1. SEPARATION SEQUENCE

Figure 8-2 shows the SA-10 separation distance between stages compared to SA-8. The two stages had separated by 12.1 m at S-IV ignition, which is 9.1 m greater than the specified minimum distance but is in good agreement with predicted nominal separation distance. The SA-10 separation required 0.14 m (5.5 in) of the 0.74 m (29 in) lateral clearance available.

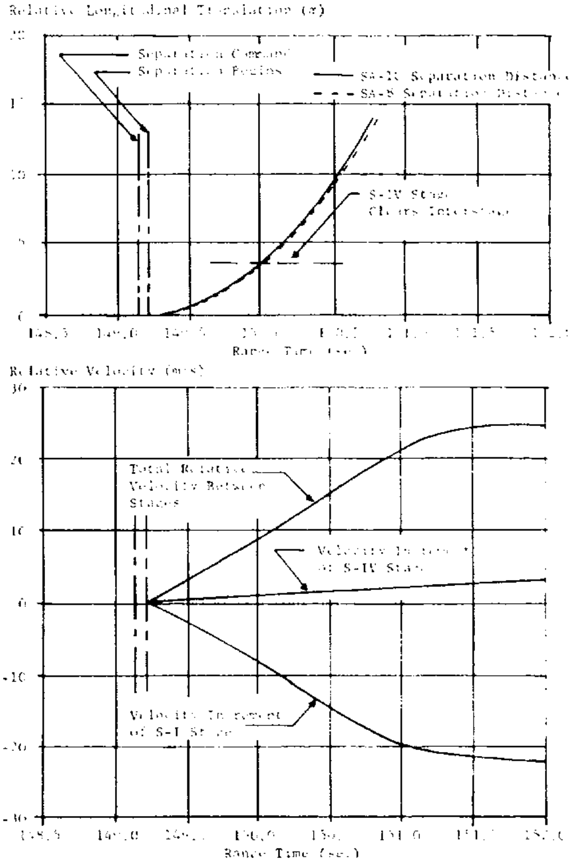

FIGURE 8-2. SEPARATION DISTANCE AND INCREMENTAL VELOCITIES

This required clearance corresponds to less than a one sigma variation from nominal. Figure 8-2 also shows the velocity increment imparted to each stage and the total relative velocity between stages.

8.2.2 ANGULAR MOTION

At separation command S-IV attitude errors and SA-10 angular rates were well below the design values of one degree and one deg/s, respectively (see Figs. 8-3 and 8-4). During and after the separation period (149.13 to 150.0 seconds), very small S-IV attitude errors and angular rates were observed in pitch and yaw direction (≤ 0.2 deg/s).

After separation the S-I pitch and yaw angular rates increased to a maximum of -2 deg/s (nose-down) and -0.8 deg/s (nose-left), respectively. These rates are approximately the same magnitude and direction observed on all Block II vehicles and could be attributed to a systematic misalignment of the retro rockets.

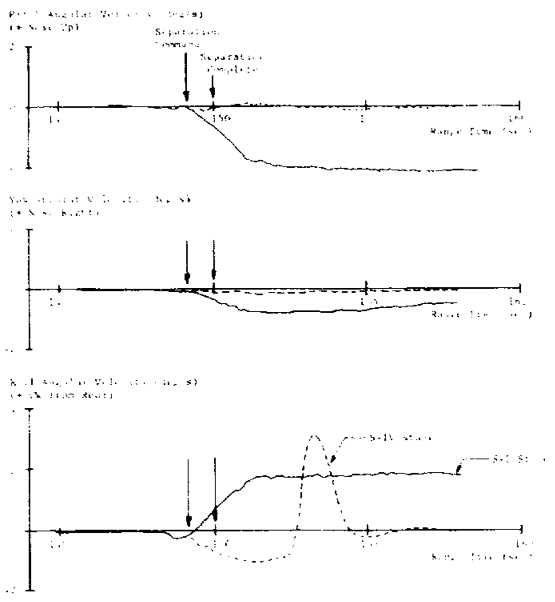

FIGURE 8-3. SA-10 ANGULAR VELOCITIES DURING BOOSTER SEPARATION

The S-IV-10 roll transient (CW looking forward) that occurred after separation has the same characteristic shape as that of S-IV-9, but is approximately 0.8 deg/s less than on S-IV-9. S-IV-8 had a much smaller roll transient and was in the opposite direction. The maximum S-IV roll rate was 3.1 deg/s, which resulted from the corrective action of the S-IV engines. The initial excursion can be attributed to a 0.51-degree total ullage rocket misalignment. This misalignment was well within expected three sigma variations. The average S-IV roll moment during ullage rocket burning was 397 N-m (293 ft-lb). No problems were experienced in controlling this roll excursion.

The maximum S-IV roll rate attitude error of 2.75 degrees occurred approximately 3.5 seconds after separation command (Fig. 8-4).

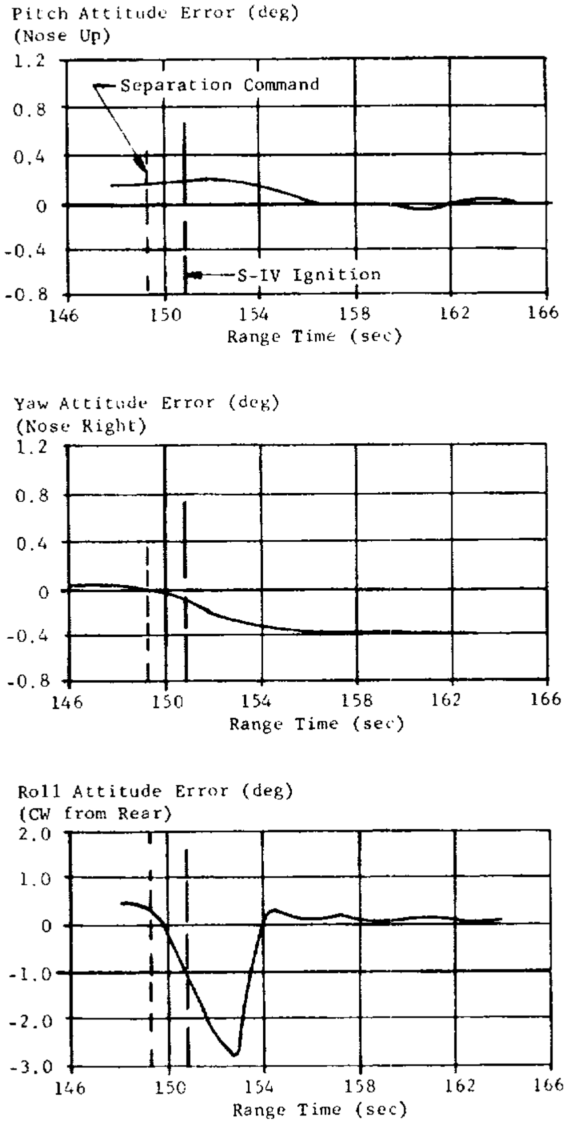

FIGURE 8-4. S-IV ATTITUDE ERROR DURING SEPARATION

8.3 APOLLO SHROUD SEPARATION

Apollo shroud separation occurred at 812.00 seconds, 2.17 seconds earlier than predicted. During the Apollo boilerplate spacecraft separation from the S-IV stage, the vehicle tumble rate was very low. The low tumble rate induced negligible loads into the Pegasus guide rails.

Predicted command and service module displacement and velocity relative to the S-IV stage were based on a 32-percent energy loss due to friction, determined from test results. The predicted velocity and displacement for zero tumble rates are presented in Reference 4. A comparison of the predicted and measured data, presented in Figure 8-5, indicates the 32-percent energy loss to be a fairly close estimate. The displacements and velocities were calculated using dimensions from an engineering drawing and do not reflect manufacturing tolerances or assembly misalignment. The scatter in the data from the guide rails is attributed to these inaccuracies. It is concluded from this evaluation that the Pegasus separation and ejection system functioned as planned. The velocity impulse imparted to the S-IV/Pegasus, determined from the guidance accelerometer, was -0.3 m/s due to the Apollo shroud separation.

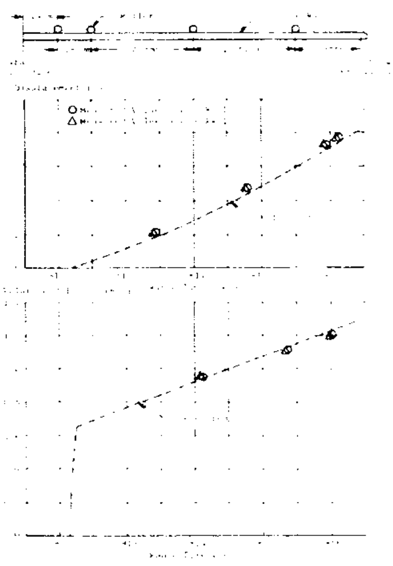

FIGURE 8-5. PEGASUS SEPARATION COMPARISONS

SECTION IX. STRUCTURES

9.1 SUMMARY

The SA-10 vehicle experienced maximum bending in the pitch plane at approximately 74.2 seconds. The maximum bending moment of 655,901 N-m was experienced at station 23.8 m (936 in).

The structural flight loads on SA-10 were generally as expected and no POGO effects were apparent.

The bending oscillations observed on SA-10 were not significantly different from SA-8.

The vibrations observed on SA-10 were generally within the expected levels and compared well with SA-8. Vibration data obtained on the thrust chamber domes were considered invalid except for the longitudinal axis measurement on engine 1. Data from this measurement appeared normal.

The S-IV stage vibrations were within the expected limits.

There was no evidence of S-I/S-IV interstage structural degradation during separation.

9.2 RESULTS DURING S-I POWERED FLIGHT

9.2.1 MOMENTS AND NORMAL LOAD FACTORS

The maximum bending moment experienced by the Saturn SA-10 vehicle during flight occurred at 74.2 seconds and was in the pitch plane. Figure 9-1 presents the distribution of this bending moment and the corresponding normal load factor distribution. The maximum bending moment on SA-10 was 655,901 N-m in the pitch plane at station 23.8 m (936 in). This maximum moment is 92 percent of the maximum moment experienced by the SA-8 vehicle.

The slope of the load factor distribution line indicates the rotational acceleration of the vehicle. The angle of attack (α) and gimbal angle (β) which produced the depicted normal load factor, when nominal aerodynamic and weight data were considered, were used in deriving the bending moment distribution. The gimbal angle agrees with the telemetered value while the angle of attack is 0.6 degree higher than the telemetered value. This discrepancy has consistently shown up on the last several flights and no explanation is presently available.

The strain gauge moment reading taken during flight is represented at its pickup station 23.9 m.

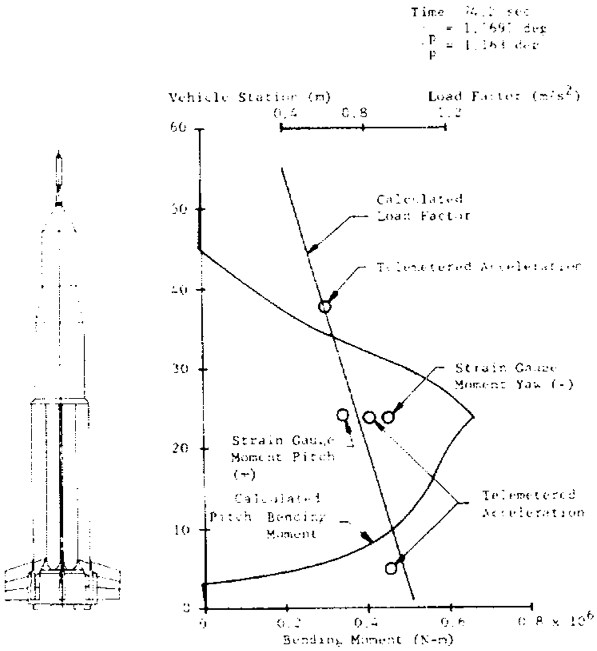

FIGURE 9-1. PITCH BENDING MOMENT AND NORMAL LOAD FACTOR

There is poor agreement between this strain gauge moment and the calculated moment distribution. The calculated maximum pitch moment was approximately twice as large as the corresponding strain gauge moment. Agreement between strain gauge moment and calculated moment has been very good on past flights. Therefore, it is suggested that further investigation be made in this area.

Ground winds are being investigated to determine their effects on the vehicle and will be presented later.

9.2.2 LONGITUDINAL LOADS

Measurements used to evaluate vehicle longitudinal response fall into the following categories:

a. Structural acceleration measurements

b. Engine combustion chamber pressure measurements

c. Engine LOX and fuel pump pressure measurements.

An investigation was made to compare the calculated response of the system for the observed applied forces during thrust buildup period. The buildup period is defined as the time interval from ignition of the first engine to vehicle liftoff. The engines were scheduled to ignite in pairs, with 100 ms delay between pairs to limit the vibratory force to 20 percent of the static thrust. Figure 9-2 shows the engine staggering times (ignition delay) to be less desirable than the ideal values of 100 ms. The resulting dynamic response was 13 percent of the maximum thrust, which is identical to previous Block II responses except for SA-8 (7 percent).

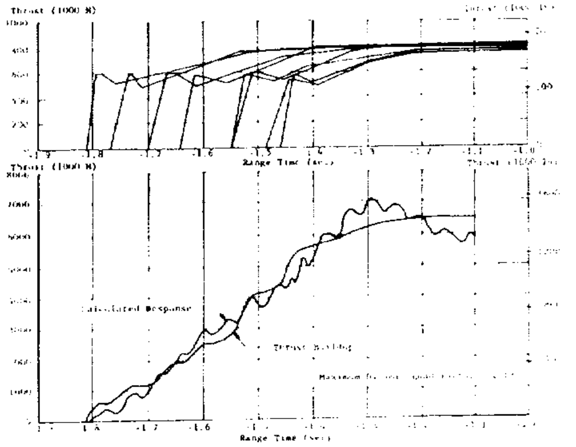

FIGURE 9-2. SA-10 THRUST BUILDUP CHARACTERISTICS

The response of the structure supporting the Pegasus mounting bracket was determined for SA-10 during the thrust buildup period. The measured response is compared with the calculated response in Figure 9-3.

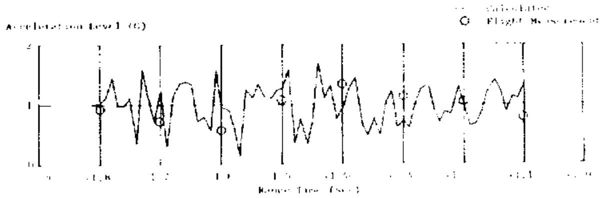

FIGURE 9-3. UPPER PEGASUS SUPPORT RESPONSE TO S-I IGNITION

A cross correlation analysis is being used to investigate the possibility of Pogo having occurred during the SA-10 flight. Preliminary results indicate no evidence of Pogo.

9.2.3 BENDING OSCILLATIONS

The SA-10 flight data indicated no significant difference in bending oscillations from SA-8. The response amplitudes for SA-10 were low, in the range of 0 to 10 Hz, with the highest value of 0.06 G_{rms} recorded in the IU yaw plane at max Q. A filter bandwidth of 0.66 Hz was used for data evaluation. Both pitch and yaw conditions were investigated.

Figure 9-4 (top half) represents the SA-10 flight bending frequencies at the S-IV, station 35.6 m (1400 in), and at IU, station 37.6 m (1479 in), compared to dynamic test frequencies for the yaw condition. Some of the data scatter can be attributed to the cluster modes interacting with the main bending modes. Flight bending frequencies in the pitch condition were similar to the yaw condition.

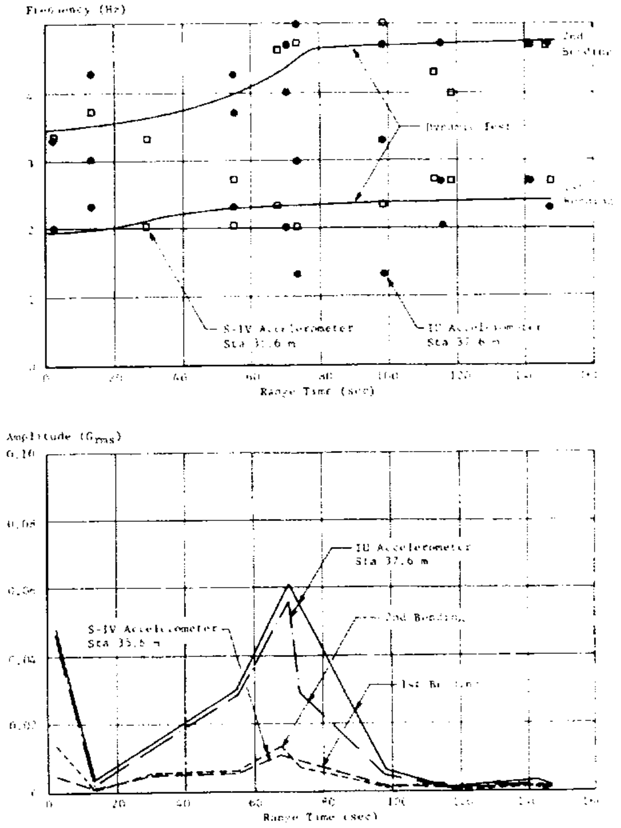

FIGURE 9-4. VEHICLE BENDING FREQUENCIES AND AMPLITUDES, YAW

Figure 9-4 (bottom half) shows the vehicle response at the same stations in the yaw plane. The response amplitude was low, in the range of 0 to 10

Hz, and was lower than the corresponding response amplitude for SA-8. The figure shows that the peak amplitude of 0.06 G_{rms} occurred at max Q. Vehicle response amplitudes at the S-IV station in the pitch plane were somewhat larger than in the corresponding yaw plane. Vehicle response amplitudes at the IU station in the pitch plane were larger than in the corresponding yaw plane from 0 to 40 seconds, but were smaller during the remainder of S-I powered flight. All accelerometers appeared to function normally and the telemetered data were as expected.

After separation of the S-I stage and jettisoning of the LES, the vehicle bending response was very low.

9.2.4 S-I VIBRATIONS

9.2.4.1 STRUCTURAL MEASUREMENTS

There were six accelerometers located on the S-I stage structure. All telemetered vibration data appeared valid. The measured response of the S-I structure was normal throughout powered flight and did not exceed expected levels. The maximum vibration was induced by the acoustic and aerodynamic noise environments present during launch and max Q. Table 9-I lists the maximum vibration levels encountered at various S-I stage and Instrument Unit locations. A time history of the S-I-10 structural, engine, and component vibration envelopes are compared to S-I-8 in Figure 9-5. The unusually high vibration levels measured on the shear panel located between fin lines III and IV on SA-8 were not experienced on SA-10.

9.2.4.2 ENGINE MEASUREMENTS

There were 16 accelerometers located on the H-1 engines and engine components. All telemetered vibration data appeared valid except that from thrust chamber dome measurements E11-2, E11-4, E11-6, E33-3, E33-5, and E33-7. Response characteristics of valid measurements were generally as expected. Maximum excitation was self induced by the operating characteristics of the engines and related components.

The longitudinal and lateral axis vibration data obtained on the thrust chamber domes were considered invalid except for the longitudinal axis measurement on engine 1 (E33-1). Response characteristics from this measurement were similar to those obtained from hardwire measurements made during static firing of Block II vehicles. Data from the E33-1 measurement also compared favorably with valid SA-6 data. The maximum SA-10 response amplitude was 10.3 G_{rms}, during launch.

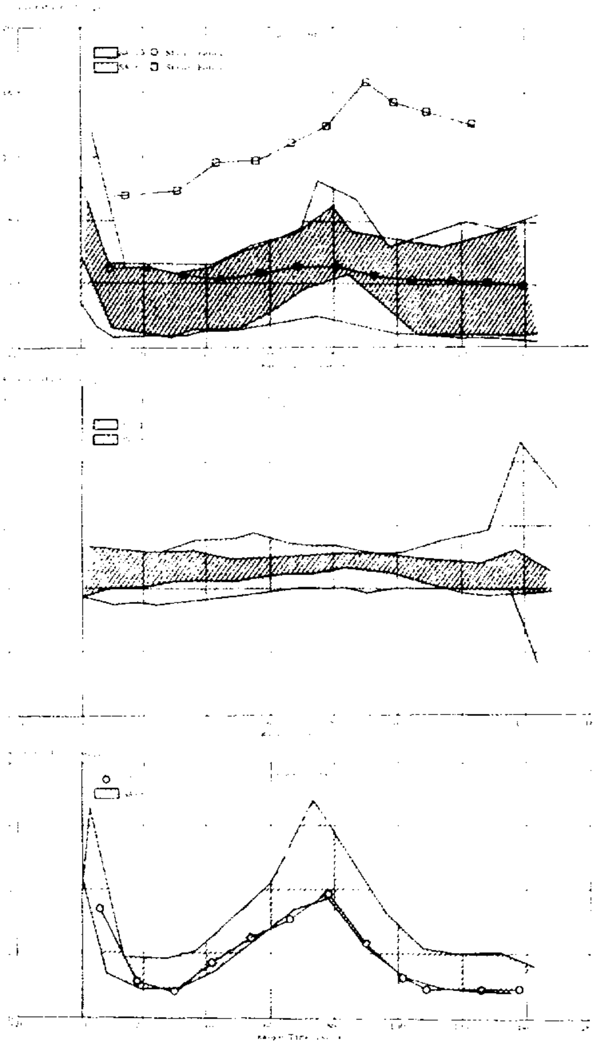

FIGURE 9-5. S-I STAGE VIBRATIONS

Acquisition of reliable telemetered data from thrust chamber dome measurements remains a problem. Comparisons between telemetered and hardwire data obtained from adjacent measurements on the engine domes have shown large discrepancies during recent static firings of Block II vehicles. An acceptable explanation as to why these telemetered data were distorted has not been found; however, investigation is continuing.

The vibration data obtained from turbine gear box measurements on all engines were considered valid. Gear box response on engines 4 and 8 appeared high near engine cutoff; however, similar increases in vibration have occurred during previous flights. The maximum vibration amplitude was 34.5 G_{rms} on the

TABLE 9-I. VIBRATION SUMMARY

Area Monitored	Max Level (G_{rms})	Flight Period	Remarks
S-I STAGE			
STRUCTURAL MEASUREMENTS			
Shear Beam/Shear Panels	13.7	LO	The maximum SA-10 response amplitudes were 2.8 G_{rms} higher during launch and 0.6 G_{rms} higher during max Q than the maximum SA-8 response amplitudes. The composite vibration levels measured on the shear panels between fin lines III and IV (E136-9) were equal to or lower than expected levels for this structure.
Spider Beam	9.9	75 sec	The response of the exterior spider beam spoke, measured along fin line I, was 9.3 G_{rms} higher during the critical flight periods than during the noncritical flight periods.
ENGINE MEASUREMENTS			
Thrust Chamber Domes	10.3	LO	Invalid data except for the longitudinal axis measurement on engine 1. This measurement compares favorably with hardwire measurements made during static firings of Block II vehicles.
Turbine Gear Box	34.5	138 sec	This level was 12 G_{rms} higher than the maximum vibration measured on SA-8.
COMPONENT MEASUREMENTS			
9A3 Distributor Mounting	3.9	75 sec	The maximum SA-8 response amplitude was 6.9 G_{rms} in the pitch axis during max Q.
INSTRUMENT UNIT			
STRUCTURAL MEASUREMENTS			
Lower Mounting Ring	7.8	LO	Measured between fin positions III and IV. 8.2 G_{rms} max on SA-8.
Upper Mounting Ring	5.1	65 sec	Measured between fin positions III and IV. 8.5 G_{rms} max on SA-8.
COMPONENT MEASUREMENTS			
ST-124 Inertial Gimbal	1.2	LO	0.7 G_{rms} at LO on SA-8. SA-8 max was 1.4 G_{rms} at 67 sec.
ST-124 Mtg Frame and Support	6.7	70 sec	2.4 G_{rms} lower than the level recorded for this measurement during SA-8 launch.
Air Bearing Supply	5.1	LO	3.5 G_{rms} max during max Q on SA-8.
RF Assembly Panel	2.3	LO	2.2 G_{rms} max during max Q on SA-8.
Guidance Computer	4.7	65 sec	Perpendicular to computer support. 6.4 G_{rms} max at LO on SA-8.

engine 4 gear box at 138 seconds. This level was 12 G_{rms} higher than the maximum vibration measured on the engine 2 gear box during the SA-8 flight. This was the first vehicle in the Saturn I, Block II series on which all eight turbine gear boxes were instrumented. The time history envelopes are shown in Figure 9-5.

9.2.4.3 COMPONENT MEASUREMENTS

There was one accelerometer located on a component of the S-I stage. The telemetered data appeared valid and the measured vibration was normal throughout powered flight.

The measurement was located on the ring frame in the lower skirt of fuel tank 1 at the attach point of the 9A3 distributor mounting bracket. The maximum level reached 3.9 G_{rms} in the longitudinal axis during max Q. This level compared with a maximum of 3.8 G_{rms} for the same measurement made during SA-8 max Q. The maximum SA-8 response amplitude was 6.9 G_{rms} in the pitch axis during max Q. The time history envelope is shown in Figure 9-5.

9.2.5 S-IV VIBRATIONS

9.2.5.1 STRUCTURAL MEASUREMENTS

Two measurements were made on the forward ring of the forward interstage. The vibration levels from these measurements compared favorably with the levels measured during the SA-8 flight (Fig. 9-6). There were no indications of structural weakening or failure throughout flight.

9.2.5.2 ENGINE MEASUREMENTS

Twelve measurements were made on the engines. The accelerometers were located on the gear case housing of each engine, the PU valve positioner of engine 4, and at the attach points of the LH_2 and LOX feedlines to engine 1. As established from previous flights, the vibration levels on the engines were low, and were considered negligible during S-I stage powered flight.

9.2.5.3 COMPONENT MEASUREMENTS

Sixteen measurements were monitored on the S-IV stage at the thrust structure, aft skirt, LH_2 tank dome, and aft LOX tank dome.

The thrust structure measurements were located at the cold helium regulator, PU computer, inverter, helium heater, and heat shield. No usable data were obtained from the measurements at the PU computer and inverter. The vibration levels at the remaining components were comparable to the levels measured during the SA-8 flight, except for those measured during launch (Fig. 9-6). The SA-10 flight indicated a higher level during launch because the data used to define the upper envelope were not the same as those taken during the SA-8 flight. The data used to define the upper envelope of SA-10 were obtained from the cold helium regulator.

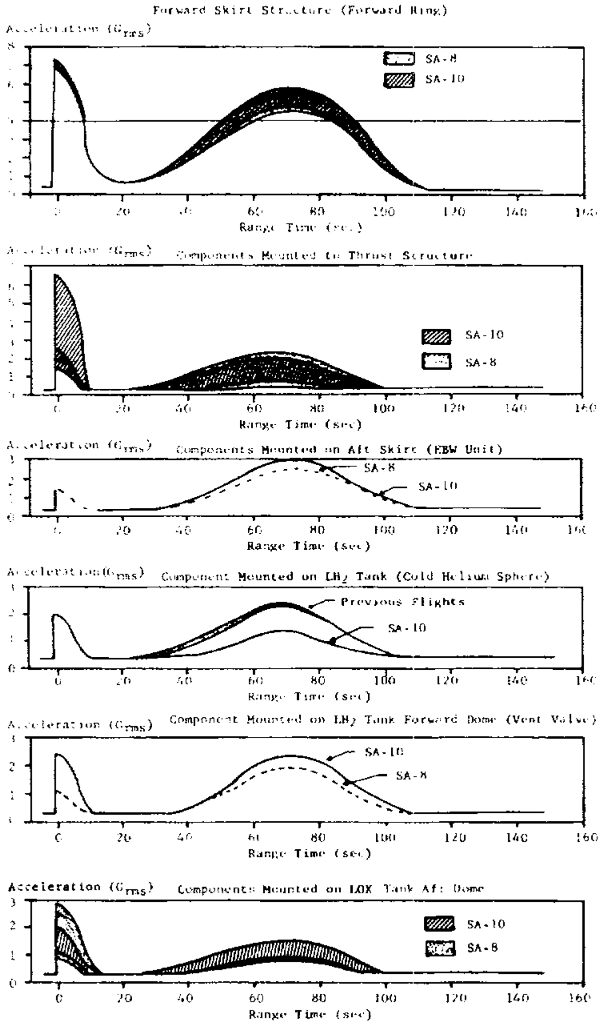

FIGURE 9-6. COMPONENT VIBRATION DURING S-I STAGE POWERED FLIGHT

The aft skirt measurement was located at the EBW unit. The vibration levels compared favorably with the levels measured during the SA-8 flight (Fig. 9-6).

The LH_2 tank measurements were located at the point where the cold helium sphere attaches to the tank skin. The measurement in the thrust direction did not provide usable data. The vibration levels normal to the tank skin were lower than the levels on previous flights (Fig. 9-6).

The forward LH_2 tank dome measurements were located at the LH_2 tank vent valve. The vibration levels were slightly higher than the SA-8 flight levels but were well within the design limits of the vent valve (Fig. 9-6).

The aft LOX tank dome measurements were made at the LOX PU probe, the LOX tank vent valve and the LOX feedline. The vibration levels compared favorably with the levels measured during the SA-8 flight (Fig. 9-6). The vibration levels at the various components were well within the expected limits during S-I stage powered flight.

9.2.6 INSTRUMENT UNIT VIBRATIONS

The Saturn SA-10 vehicle was the third of the Block II series to fly a prototype model of the production Instrument Unit (IU). Components were mounted to panels attached directly to the 3.05 m (120 in) diameter wall instead of in pressurized tubes as before. The SA-10 vibration levels correlated closely with the levels measured during SA-8 and SA-9 flights.

9.2.6.1 STRUCTURAL MEASUREMENTS

There were eight accelerometers located on the upper (Apollo) and lower IU mounting rings. All telemetered data were valid. The vibration measured on the mounting rings was normal throughout powered flight. Maximum vibration occurred during the critical flight periods when the structure was excited by the acoustic and aerodynamic noise (Fig. 9-7).

9.2.6.2 COMPONENT MEASUREMENTS

There were 16 accelerometers located on various IU components. All telemetered vibration data appeared valid. The vibration measured on the guidance system was normal throughout powered flight. The vibration environment of the air bearing supply, RF assembly, and guidance computer was measured for the third time during the SA-10 flight. Maximum levels occurred during the critical flight periods when the IU skin to which the component mounting panels were attached was excited by acoustic and aerodynamic noise environments (Fig. 9-7).

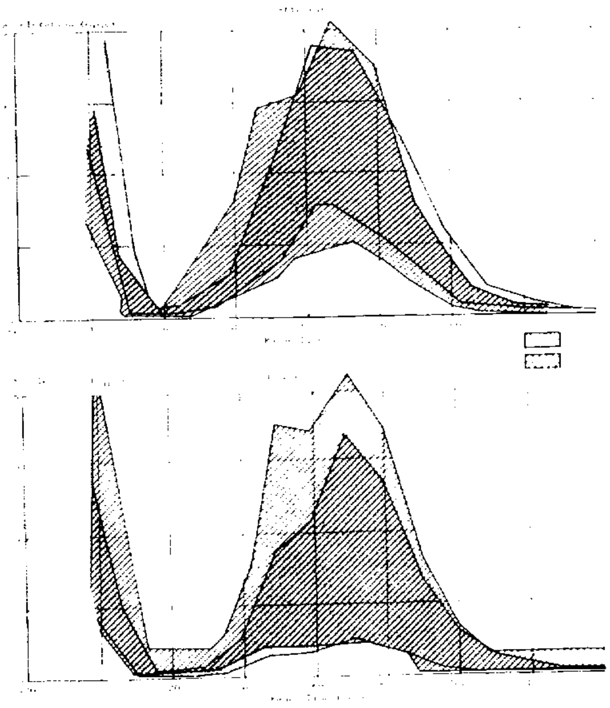

FIGURE 9-7. INSTRUMENT UNIT VIBRATIONS DURING S-I POWERED FLIGHT

9.2.7 APOLLO (PEGASUS) VIBRATIONS

There were four accelerometers located on the micrometeoroid capsule (MMC) mounting rings. All the telemetered data were valid. These measurements were also made on the SA-8 and SA-9 flights.

The vibration of the upper MMC mounting ring was measured at longeron 6. The maximum level reached 2.6 G_{rms} during launch. The maximum SA-8 level was 3.0 G_{rms} during max Q, and the maximum SA-9 level was 4.2 G_{rms} during launch. The time history envelopes are shown in Figure 9-8.

The vibration in the lower MMC mounting ring was also measured at longeron 6. The maximum level reached 3.1 G_{rms} during launch. The maximum SA-8 level was 3.0 G_{rms} during max Q, and the maximum SA-9 level was 2.7 G_{rms} shortly after launch. The time history envelopes are shown in Figure 9-8.

9.2.8 STRUCTURAL ACOUSTICS

9.2.8.1 S-I STAGE

The internal acoustic environment was measured in the lower S-I stage thrust structure. This measurement was considered invalid. It was also invalid during SA-8 but was considered reliable during SA-9. Analysis of the raw data indicated an apparent malfunction of the instrumentation system.

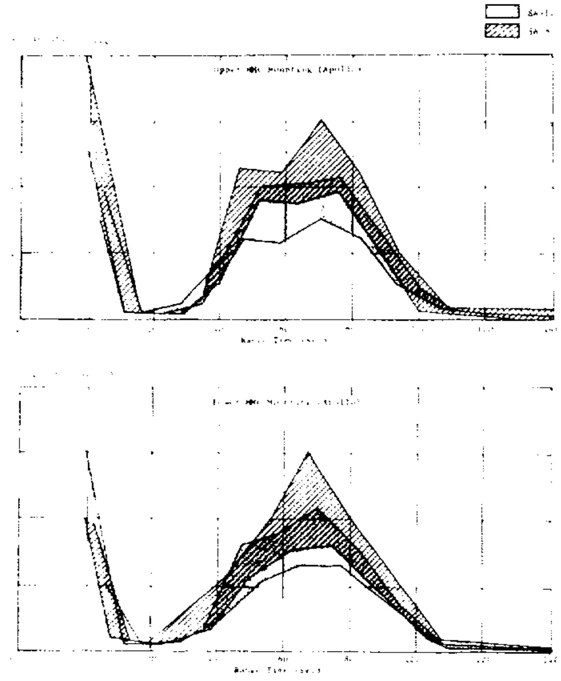

FIGURE 9-8. PEGASUS VIBRATIONS

9.2.8.2 S-IV STAGE

Two microphones were flush mounted internally and externally to the forward interstage. Due to an instrumentation malfunction, neither measurement provided usable data during the flight.

9.2.8.3 INSTRUMENT UNIT

The internal acoustic environment adjacent to the guidance system at station 37.6 m (1480 in) was measured with one microphone. The telemetered data were considered valid. The maximum level measured was 138.5 db during launch and 128.5 db during max Q. The predicted levels were 140 db and 130.5 db, respectively. The SA-8 levels were 138.0 db and 128.5 db, respectively. The time history envelope is shown in Figure 9-9.

9.2.8.4 APOLLO

The internal acoustic environment of the Apollo stage was measured with one microphone located near the external skin at station 38.0 m (1495 in). The maximum sound pressure level (139.5 db) was measured during launch. The Mach 1/max Q environment was 5 db higher than predicted and 3 to 5 db higher than measured during SA-9. The environment was comparable to that of SA-8 through Mach 1; however, the 5 db decrease in the environment measured during SA-8 was not present during SA-10. The variations in the environment were due to the installation of a control motor upstream of this measurement location on vehicles SA-8 and SA-10, and the difference in the angles of attack during these flights.

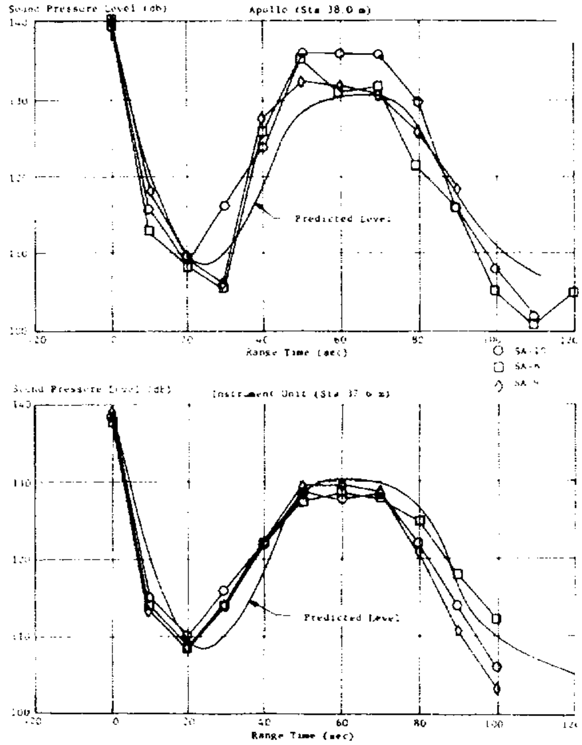

FIGURE 9-9. APOLLO AND INSTRUMENT UNIT ACOUSTICS

The flow field over the external skin in the vicinity of this measurement greatly influenced the local acoustic environment. The installation of the control motor caused the flow to increase in turbulence and induced shocks. This increased excitation extended through max Q during SA-10 due to the positive angle of attack in pitch. The SA-10 predicted levels were 140 db during launch and 130.5 db during Mach 1/max Q. The time history envelopes are shown in Figure 9-9.

9.3 OBSERVED STRUCTURAL DEVIATIONS

There was no evidence of structural degradation or component malfunction during the SA-10 flight.

9.4 S-I/S-IV INTERSTAGE

Sixteen channels of instrumentation were utilized on the SA-10 vehicle to monitor any panel debonding anomaly such as that observed on SA-5 and SA-7. Six channels were used to establish the interstage temperature and pressure environment (see Section 10.2.5.1). The remaining ten channels (strain, breakwires, acoustic, and shock acceleration) were used to study the structural behavior before, during, and after separation. Location of the special aft interstage panel debonding instrumentation is shown in Figure 9-10.

Biaxial strain gauges were installed on the inner skin adjacent to the external engine GH_2 chilldown duct brackets, between fin planes I and IV, and fin planes II and III at station 29.1 m (1145.7 in). The strain gauges appeared to function normally, and the strain histories followed the trends of the SA-8 data. The deviations noted between predicted and actual strains after 80 seconds of flight can be attributed to lower than predicted skin temperatures. The circumferential leg of the biaxial strain gauge shows an increase after launch to a peak tensile strength at the maximum skin temperature. Subsequently, a gradual reduction in strain was recorded, with a compressive dip at IECO and OECO, corresponding to the Poisson effect. These dips resulted from the loss of axial acceleration. There was also a sharp dip at separation resulting from the loss of loop restraint. Uniaxial strain gauges were located on the bracket supporting the disconnect assembly at the following locations: between fin planes I and IV (area of previous debonding), and between fin planes II and III. The primary purpose of the gauges was to measure any abrupt change in strain levels. A malfunction of a disconnect assembly would have been reflected by a large compressive stress in the instrumented leg of the bracket. Since no behavior of this nature was indicated, it has been concluded that no malfunction occurred. The strain data recorded at separation was very erratic, although it appears that some tensile load was induced into the brackets. However, normal disconnect operation would be expected to produce tensile loading.

An abrupt change in strain on both brackets occurred at 140.8 seconds after liftoff, being more severe between fin planes II and III. The abrupt strain changes are considered a result of shock from activation of the blowout panels.

A shock accelerometer was installed on the inside skin of the interstage, adjacent to the disconnect support bracket, between fin planes I and IV. As was the case with the SA-8 data, the accelerometer data exhibited full scale transients which were damped by low frequency oscillations. These transients occurred at approximately 15 seconds and at 153 seconds (4 seconds after separation); they are attributed to the accelerometer being overdriven. All other transients can be explained by expected shock influences. The body bending accelerometer that apparently became loose and picked up a longitudinal component of thrust

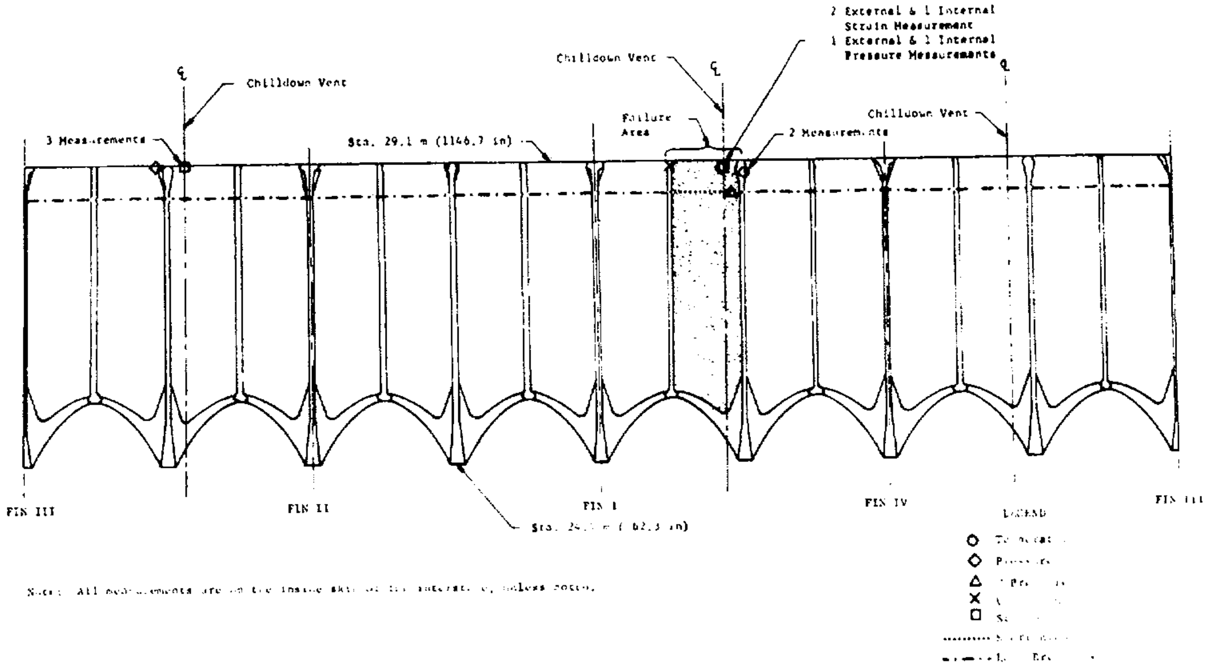

FIGURE 9-10. S-IV AFT INTERSTAGE VIEW LOOKING OUTBOARD WITH INTERSTAGE FOLDED FLAT

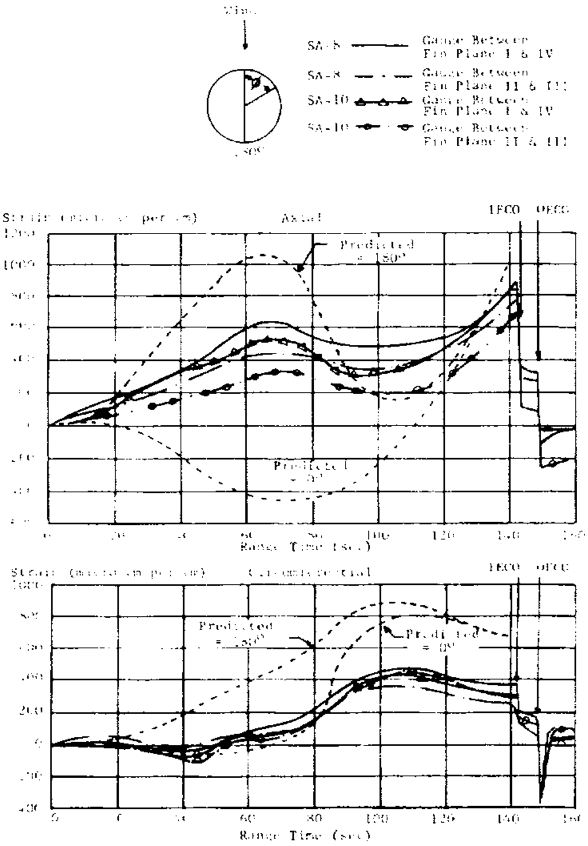

FIGURE 9-11. S-I/S-IV INTERSTAGE STRAIN

on SA-8 did not exhibit the same characteristics on SA-10.

Two breakwires were installed around the inside circumference of the interstage. Breakwire number 1 spanned only the panel in the area of previous debonding, with minimum overlap onto the adjacent panels. Breakwire number 2 covered the remaining seven panels making up the interstage. Breakwire number 1 indicated no breakage before, during, or after separation. Breakwire number 2 shorted electrically at 140.8 seconds as a result of the blowout panel shock. This event was correlated with the strain data to verify that the integrity of the interstage had not been damaged. A similar occurrence happened on SA-8 also. Steps had been taken to prevent this from happening again, but these were apparently inadequate.

In summary, the results of the evaluation of data, which were obtained from instrumentation installed to determine structural behavior, have established a high degree of certainty that no panel debonding occurred. From the flight data obtained on SA-8 and SA-10 it appears highly unlikely that the natural environment during separation could have caused the panel debonding on SA-5 and SA-7. However, no data were obtained from the acoustic measurements.

9.5 RESULTS DURING S-IV POWERED FLIGHT

9.5.1 BENDING

No significant body bending motion was recorded on the S-IV-10.

9.5.2 S-IV VIBRATIONS DURING S-IV POWERED FLIGHT

9.5.2.1 STRUCTURAL MEASUREMENTS

The two measurements on the forward ring of the forward interstage indicated very low vibration levels, similar to S-IV-8, and were considered negligible during S-IV stage powered flight.

9.5.2.2 ENGINE MEASUREMENTS

Engine measurements were made in the gear case housing of each engine. The vibration levels compared favorably with the levels measured during S-IV-8 stage powered flight (Fig. 9-12). There were no indications of abnormal turbopump operation.

Two measurements were made on the PU valve positioner of engine 4. The vibrations showed slightly different trends when compared to the SA-8 flight levels. The levels were lower in the thrust direction and higher in the lateral direction than SA-8 (Fig. 9-12). The data from the lateral direction measurement were invalid after 360 seconds. Although the levels were higher in the lateral direction, comparable levels were measured on the positioner during battleship tests, with no detrimental effect to the PU valve.

Accelerometers were located at the attach points of the LH_2 and LOX feedlines to engine 1. The data from the LH_2 feedline measurement in the thrust direction were invalid. The vibration levels on the feedlines compared favorably with the levels measured during the SA-8 flight (Fig. 9-12).

The engine vibration environment was considered normal throughout S-IV stage powered flight.

9.5.2.3 COMPONENT MEASUREMENTS

Component vibration measurements were taken at the thrust structure, aft skirt, LH_2 tank,

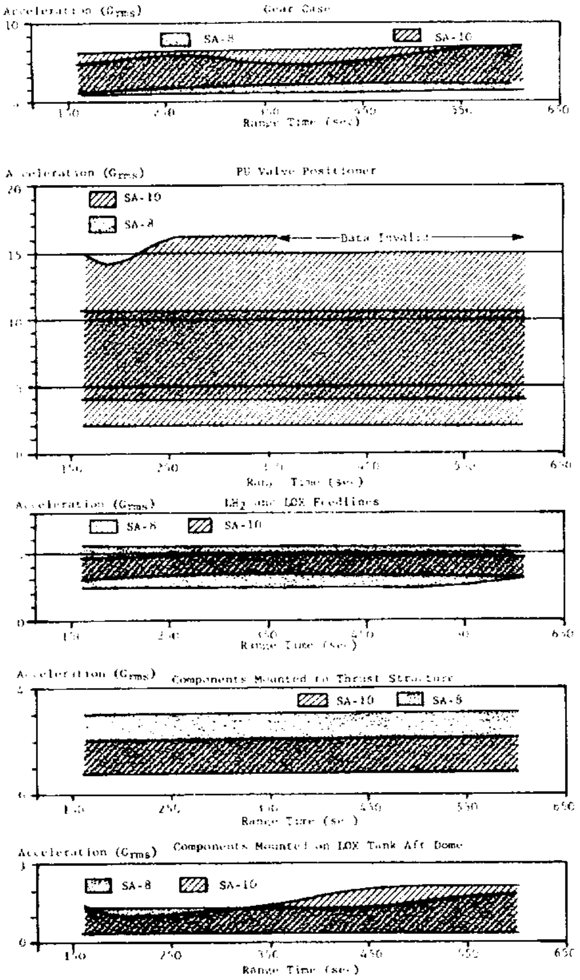

FIGURE 9-12. ENGINE AND STRUCTURAL COMPONENT VIBRATIONS DURING S-IV STAGE POWERED FLIGHT

forward LH_2 tank dome, and aft LOX tank dome. As established from previous flights, the vibration levels at the components mounted on the aft skirt (EBW unit), LH_2 tank (cold helium sphere), and forward LH_2 tank dome (vent valve) were low, and were considered negligible during S-IV stage powered flight.

The vibration levels at the components mounted to the thrust structure (cold helium regulator, PU computer, inverter, helium heater, and heat shield) and aft LOX tank dome (vent valve, PU probe, and feedline) were comparable to levels measured during S-IV-8 stage powered flight (Fig. 9-12).

The vibration levels at the various components were low during S-IV stage powered flight.

9.5.3 INSTRUMENT UNIT VIBRATIONS

There were no significant vibrations in the IU during S-IV powered flight. The vibration levels measured during this period were the same order of magnitude as the levels measured during the S-I mainstage period.

9.5.4 APOLLO (PEGASUS) VIBRATION

The Apollo vibration levels were negligible during S-IV powered flight.

9.5.5 APOLLO (PEGASUS) ACOUSTICS

The Apollo acoustics levels were negligible during S-IV powered flight.

10.1 SUMMARY

Measured pressure and temperature environments on the S-I and S-IV stages of the SA-10 flight vehicle were generally similar to those measured on SA-8 flight. Thermal instrumentation on the S-I-10 stage was drastically reduced over that flown on previous Saturn I, Block II vehicles. Structural temperatures on the forward side of the heat shield showed no evidence of water being present in this area for S-I-10, as opposed to results of previous flights. Calorimeters were flown for the second time on the engine bell and aspirator surfaces of engines 3 and 7. Analysis of data from these calorimeters shows heating rates which are higher and more representative of the expected environment than those measured on SA-9. This is attributed to an improvement in the installation of the calorimeters for SA-10.

10.2 S-I STAGE ENVIRONMENT

10.2.1 SURFACE PRESSURES

Surface pressure instrumentation on S-I-10 was basically similar to that flown on previous flight vehicles. Differential pressures measured across the spider beam fairing and across the tail shroud were in good agreement with previous flight results. Fin surface pressures indicated very little aerodynamic loading as a consequence of the relatively small angles of attack flown by SA-10.

10.2.2 S-I STAGE SKIN TEMPERATURES AND HEATING RATES

Aerodynamic heating data from thermocouple measurements flown on the tail shroud and the engine shroud agreed well with analytical predictions and with previous flight results (Fig. 10-1). There were no other aerodynamic heating measurements flown on S-I-10.

10.2.3 BASE PRESSURES AND TAIL COMPARTMENT PRESSURES

Measured pressures on the S-I-10 base and inside the tail compartments agreed well with previous flight data. Pressure environments in the thrust frame compartment above the firewall and in the engine compartment below the firewall were nearly uniform throughout flight, as expected. Pressure loading across the heat shield was nominal with a maximum downward pressure differential of approximately 0.96 N/cm² occurring at 58 seconds.

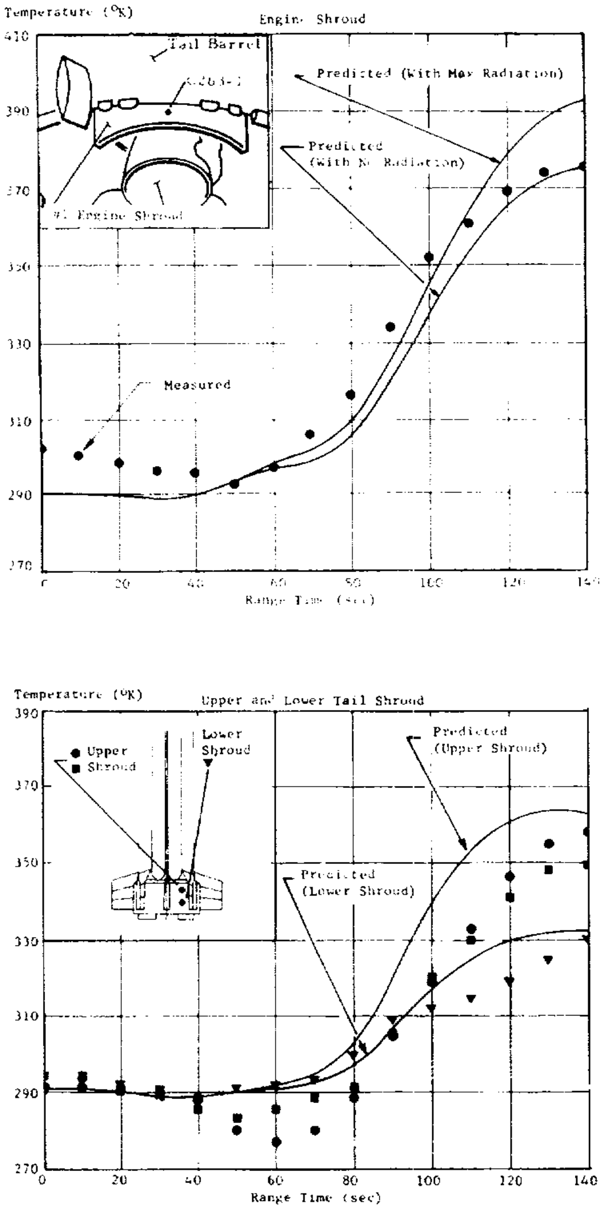

FIGURE 10-1. TEMPERATURE HISTORY OF UPPER AND LOWER TAIL SHROUDS AND ENGINE SHROUD

10.2.4 BASE THERMAL ENVIRONMENT

Base thermal instrumentation for SA-10 was considerably reduced in number over that flown on previous Saturn I Block II vehicles. Of the five major regions assumed to have uniform heating (heat shield inner and outer regions, flame shield, fin trailing edge, and engine shroud), only the inner region was instrumented with heating rate sensors. This consisted of only one total and one radiation calorimeter. As on S-I-9, 15 total calorimeters were mounted on the engine bells and aspirator surfaces of engines 3 and 7.

10.2.4.1 BASE TEMPERATURES

Gas temperatures measured on the heat shield outer region were in excellent agreement with the Block II data band. Maximum gas temperatures recorded in the heat shield outer region were slightly over 1200°K at an altitude of 12 km (Fig. 10-2).

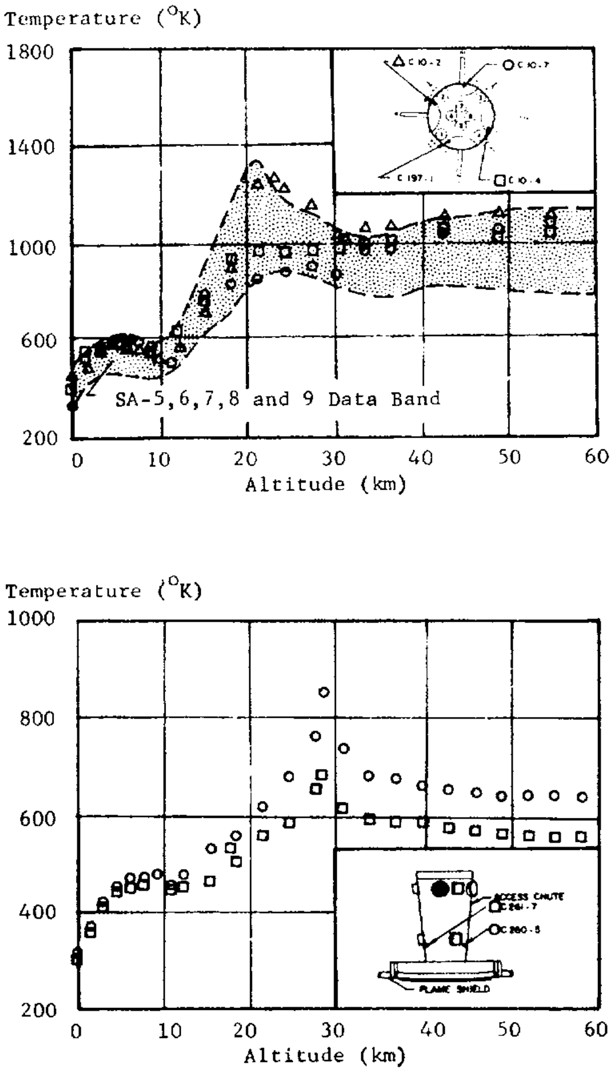

FIGURE 10-2. HEAT SHIELD AND ACCESS CHUTE GAS TEMPERATURES

There were no other gas thermocouples flown on the heat shield or on any of the other major base areas normally instrumented.

Two gas thermocopules were mounted on the access chute on the forward side of the flame shield (Fig. 10-2). Temperatures recorded by these instruments were generally lower than on the data from inner or outer region thermocouples flown on SA-10 or on previous Block II flights. Maximum temperatures between 700 and 850°K were recorded at 28 km altitude.

10.2.4.2 BASE HEATING RATES

Only two calorimeters, one total and one radiation, were mounted in the inner region of the S-I-10 base. Measured heat fluxes generally show good agreement with previous Saturn I, Block II data (Fig. 10-3). The total heating rate indicated very little heating at altitudes between 8 and 15 km. This low response had been noted on the SA-7 and SA-9 flights and may be attributed to physical blockage of radiant heat energy to the gauge (Ref. 5). The radiation heat rate measured on S-I-10 was consistent with the results from previous Block II flights.

Two total heat flux calorimeters, one slug and one membrane, were mounted on the access chute for this flight (Fig. 10-3). These instruments were located 90 degrees apart and one 25.4 cm aft of the other. A maximum heat flux of approximately 5 watts/cm^2 occurred at liftoff. The excellent agreement between the heating rates from these calorimeters gives a high degree of confidence in the thermal environment for this region.

Fifteen slug-type total calorimeters were mounted on the engine bells and aspirator surfaces of engines 3 and 7. These measurements were first flown on S-I-9, but the installation was improved on S-I-10 to give the calorimeters better exposure to both radiant and convective environments. Heat flux data from some of the measurements are shown in Figure 10-4. As expected, higher heating rates were indicated by data from the S-I-10 flight with the maximum heating generally occurring at liftoff. These data are considered much better than those obtained from S-I-9, although 11 of the 15 calorimeters did not respond properly during the entire S-I-10 powered flight.

10.2.4.3 ENGINE COMPARTMENT TEMPERATURES

Gas temperatures in the engine compartment remained normal throughout flight, indicating that no excessive temperatures or fires occurred on S-I-10.

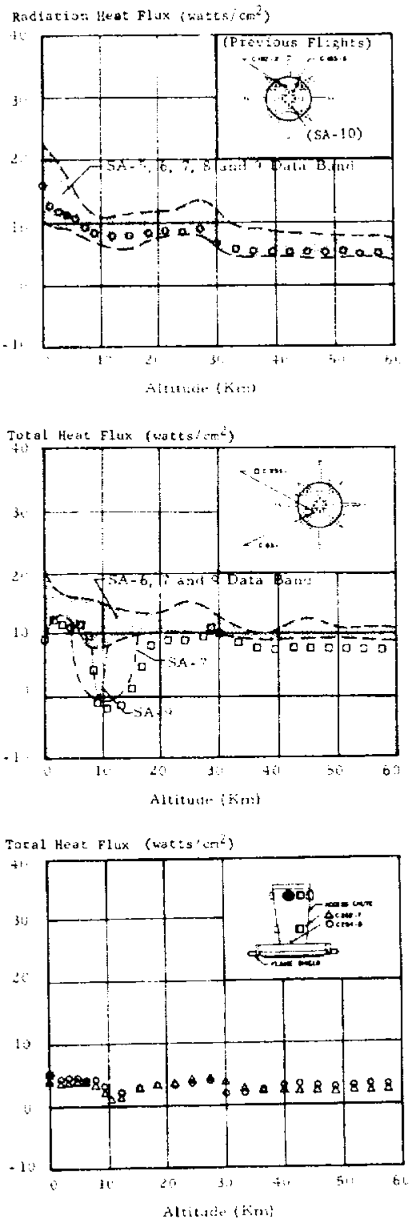

FIGURE 10-3. HEAT FLUXES FOR HEAT SHIELD INNER REGION AND ACCESS CHUTE

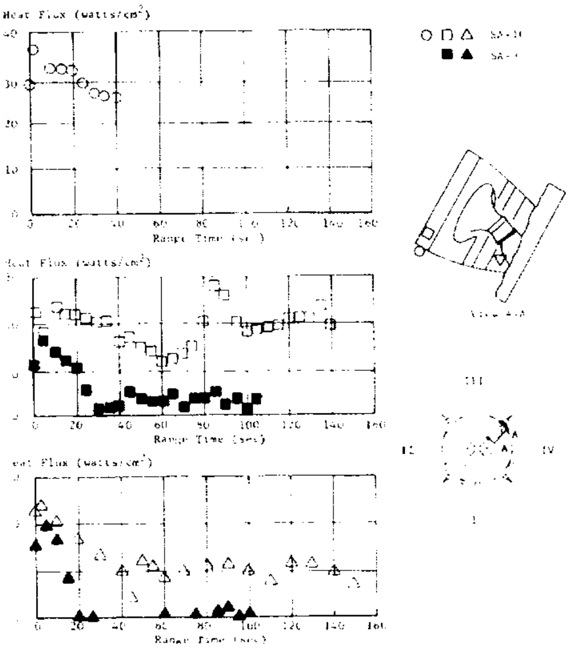

FIGURE 10-4. TOTAL HEAT FLUXES TO ENGINE BELL AND ASPIRATOR

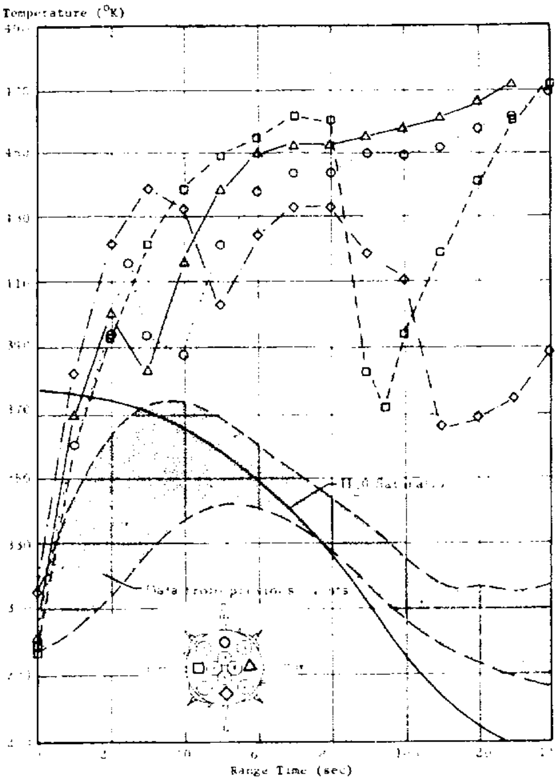

FIGURE 10-5. HEAT SHIELD FORWARD FACE STRUCTURAL TEMPERATURES

Structural temperatures measured on the forward side of the heat shield were very different on S-I-10 than on previous Block II flights (Fig. 10-5). For vehicles SA-5 through SA-9, temperatures in this area followed the pressure dependent curve of the saturation temperature of water which decays with increasing altitude, thereby indicating that water and ice are present in this area. Temperatures for SA-10 did not follow this trend but, instead, exceeded the boiling temperature of water at about 20 seconds and remained above maximum water temperature during the remainder of the flight. Maximum structural temperatures of approximately 450°K were measured. Sudden drops in temperature were observed and are probably the result of ice falling on the heat shield from the LOX lines feeding the engines. Investigations to date disclose that there was no significant difference in the atmospheric conditions or in the countdown procedures for SA-10 that would account for the apparent absence of water.

10.2.5 S-I/S-IV INTERSTAGE ENVIRONMENT

10.2.5.1 S-I/S-IV INTERSTAGE TEMPERATURES AND PRESSURES

Special pressure and temperature measurements were flown for the second time in the S-I/S-IV interstage area on SA-10 as part of an investigation to determine the cause of the interstage panel debonding phenomenon observed during S-IV separation on SA-5 and SA-7. Data from these measurements, flown on both the SA-8 and SA-10 vehicles, failed to reveal either the cause of the panel failure or that this phenomenon occurred during these flights.

Structural temperatures were measured by sensors located on the external and internal surface of the interstage at station 28.5 m (1122 in). The temperature rise recorded by the external sensor, subsequent to ullage and retro rocket ignition command, was less than half that experienced on SA-8. A maximum temperature of 326°K was recorded by this external sensor at 156 seconds, which is not considered detrimental to the structure (Fig. 10-6).

Pressure instrumentation in the S-IV-10 interstage area was similar to that of S-IV-8, consisting of one external static pressure measurement, two internal (compartment) pressure measurements, and a differential gauge to measure the pressure difference between the sealed honeycomb cell and the interstage compartment. One of the internal pressure measurements (0 to 13.8 N/cm^2 range) is a total pressure sensor; the pressure orifice inside the compartment faces forward and can detect any total head pressure that might arise from the main engine exhaust striking the interstage during separation. Pressure time histories of data from these sensors are shown in Figure 10-6. Also shown are the internal and external pressures in the form of pressure coefficients, referenced to ambient conditions.

As on SA-8 reduced data from the SA-10 total pressure sensor inside the aft interstage compartment indicated that no pressure rise resulted from engine exhaust gas impingement. Absolute honeycomb cell pressures, calculated by summing differential and compartment pressure data values, did not show any response to the expected constant volume heating resulting from retro and ullage rocket exhaust gases.

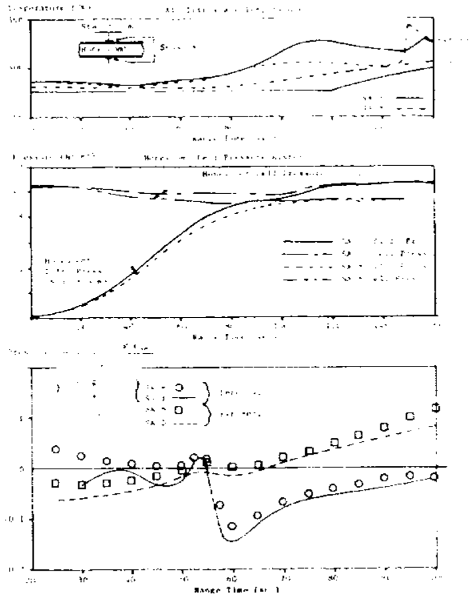

FIGURE 10-6. S-IV AFT INTERSTAGE

Reduced data from all interstage measurements are in good agreement with SA-8 results, giving no direct clues as to the possible cause of the interstage panel failure observed by onboard camera coverage of S-IV separation on the SA-5 and SA-7 flight vehicles. However, it can be concluded that the steady state environment, as measured on SA-8 and SA-10, during the separation process should not be severe enough to cause any problems.

10.2.5.2 DETONATION PRESSURES

Detonation pressure switches located near the separation plane indicated that there was no detonation or overpressurization of the boattail area during separation.

10.3 S-IV STAGE ENVIRONMENT

10.3.1 ENVIRONMENTAL PRESSURES

10.3.1.1 COMMON BULKHEAD PRESSURE

The common bulkhead absolute pressure remained less than 0.7 N/cm^2 (1.0 psi) throughout flight, as expected.

10.3.1.2 BASE HEAT SHIELD PRESSURE

Four base pressure sensors (0 to 0.7 N/cm^2 measuring range) located on the S-IV base heat shield failed to give useful data; they appear to have been plugged during most of the S-IV flight.

10.3.2 SURFACE TEMPERATURES AND HEAT FLUXES

10.3.2.1 HYDROGEN TANK TEMPERATURES

Hydrogen tank temperatures measured at stations 33.4 m and 32.4 m were considerably higher on S-IV-10 than on S-IV-8. This difference in measured temperatures between the two flights was approximately 90°K at liftoff and decreased to about 40°K during the time that peak temperatures were recorded (Fig. 10-7). The absence of tank surface ice and frost is believed to be the cause of the higher S-IV-10 tank surface temperatures at liftoff. Data from a sensor located at station 30.8 m indicated no appreciable temperature gradient between this location and station 33.4 m. The latter measurement did not operate properly on S-IV-8.

10.3.2.2 AFT SKIRT TEMPERATURES

Aft skirt external and internal temperatures measured at station 29.4 m were nominal and agreed well with those observed on S-IV-9 and S-IV-8 (Fig. 10-7). The external surface temperatures did not exhibit the anomaly observed on S-IV-8; a sudden temperature level-off occurred during the maximum aerodynamic heating portion of the SA-8 flight.

10.3.2.3 HYDROGEN VENT LINE TEMPERATURE

A temperature sensor was located on the underside of the hydrogen chilldown duct at station 27.6 m to determine the effects of aerodynamic heating on the duct temperature (Fig. 10-7). This temperature measurement behavior was consistent with the aerodynamic heating rates obtained from the aft interstage calorimeter for the significant aerodynamic heating portion of flight.

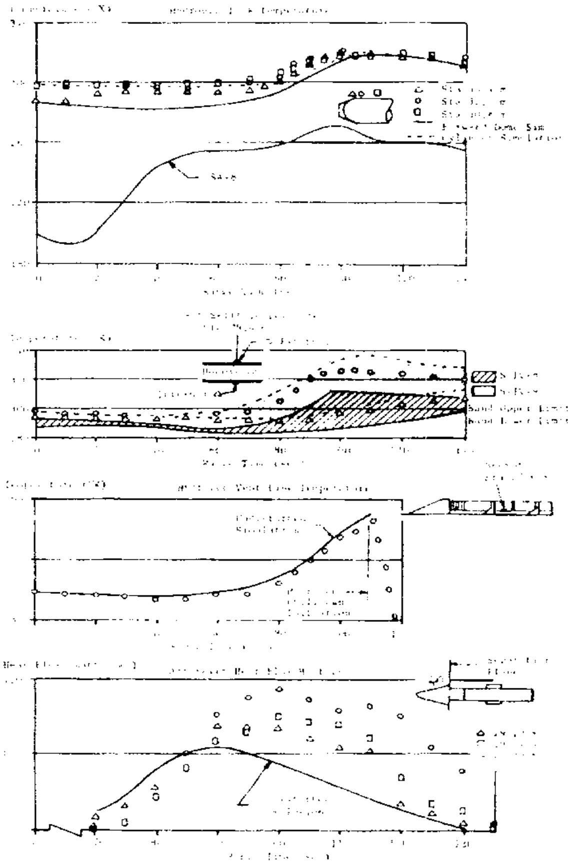

FIGURE 10-7. S-IV STAGE SURFACE TEMPERATURE ENVIRONMENT

The abrupt decrease in chilldown vent line temperature at 112.0 seconds indicates the presence of hydrogen in the vent line. This presence of hydrogen is a result of the initiation of hydrogen prestart at 111.1 seconds range time.

10.3.2.4 AFT SKIRT HEAT FLUX

The aft skirt surface total heat flux in the vicinity of the LH$_2$ chilldown vent fairing was measured by three calorimeters located between stations 29.2 and 29.4 m (Fig. 10-7). The maximum disturbed to undisturbed heat flux ratio measured was approximately 1.7, measured by the calorimeter at station 29.39 m. The disturbed to undisturbed heat flux ratios measured at all three calorimeter locations were within expected levels, based upon data from recent wind tunnel tests of protuberance effects on aerodynamic heating rates to flat plate surfaces. The wind tunnel ratios varied from 1.6 to 1.8 at this location for Mach numbers between 2.5 and 4.5.

10.3.2.5 AFT INTERSTAGE HEAT FLUX

A calorimeter was located on the aft interstage beneath the LH_2 chilldown duct at station 27.6 m to measure the protuberance effects of the duct on the aerodynamic heating rate to the interstage. The flight data are in close agreement with the predicted undisturbed heating rate during the period of maximum aerodynamic heating (Fig. 10-7), which indicates that the protuberance effect of the duct on heating rates to the interstage is minimal.

10.3.3 BASE TEMPERATURES AND HEAT FLUXES

10.3.3.1 BASE THRUST STRUCTURE TEMPERATURE

Thrust structure temperatures measured on stiffener 26 were in general agreement with the temperature trends observed on the previous Block II flights (Fig. 10-8).

10.3.3.2 BASE HEAT SHIELD TEMPERATURES

Three temperature sensors were flown for the second time on the S-IV-10 heat shield, between engines 3 and 6, to measure the heat shield hot-face temperature. Temperatures recorded at heat shield radii of 51.0 cm and 86.2 cm were slightly higher than the corresponding temperatures on S-IV-8 (Fig. 10-8). This observation is compatible with the higher heat fluxes measured on S-IV-10 as compared to those on S-IV-8 at these locations. Much lower temperatures were recorded farther away from the center, at radii location 152.2 cm, which is in agreement with the heat flux distribution obtained on wind tunnel model tests.

Forward face temperatures, measured by a sensor located at a radius of 40.6 cm, are in good agreement with the temperature trend observed on S-IV-8 (Fig. 10-8). The slightly higher temperature level observed on S-IV-10, when compared to S-IV-8, is consistent with the higher thermal environment measured on the aft face.

10.3.3.3 BASE HEAT FLUX

The base heat shield calorimeter-absorbed total heat flux history and the transient response of the base heat flux to stage events were similar to those of SA-6 and SA-8. The average level of absorbed heat flux for each of the calorimeters was slightly higher on S-IV-10 than it was on S-IV-8 (Fig. 10-8).

The rapid rise in heat flux measured by the inboard calorimeter beginning at 350 seconds is due to the helium heater cycling to single coil operation, which results in a higher helium heater exhaust temperature. The decrease in heat flux of the inboard calorimeter at approximately 500 seconds is again due to a change in helium heater exhaust temperature, which decreased due to hydrogen tank step pressurization at 491 seconds.

The outboard calorimeter showed an unexpected decrease in heat flux beginning at approximately 450 seconds. This phenomenon did not occur on either SA-6 or SA-8 and the cause for this deviation is not presently known.

10.4 EQUIPMENT TEMPERATURE AND PRESSURE ENVIRONMENT

10.4.1 S-I STAGE INSTRUMENT COMPARTMENT ENVIRONMENT

Two instrument compartments are located above S-I stage fuel tanks F1 and F2. These compartments house power supply and telemetry equipment which must be maintained within specified temperature limits to insure optimum telemetry equipment operation. Preflight cooling of the compartments is accomplished by pressurizing with air and GN_2 from a ground source from approximately -550 minutes through countdown. No inflight cooling of the equipment is necessary since the temperatures created by operation of the equipment in flight are not excessive.

Preflight instrument compartment cooling on S-I-10 stage was satisfactory. The preflight cooling temperatures were within the operating limits and were similar to temperature values experienced on past Saturn flights. The preflight temperatures and operating limits are shown below.

S-I INSTRUMENT ENVIRONMENT
TEMPERATURES (°K)

Instrument Compartment	Operating Limits		Preflight		Liftoff
	Minimum	Maximum	Minimum	Maximum	
F2 (XC55-12)	293	313	295	299	296
F1 (XC55-13)	273	50	293	298	295

10.4.2 INSTRUMENT UNIT ENVIRONMENT

The Instrument Unit houses various electrical and electro-mechanical devices which perform guidance, control, telemetering, and measuring operations during flight.

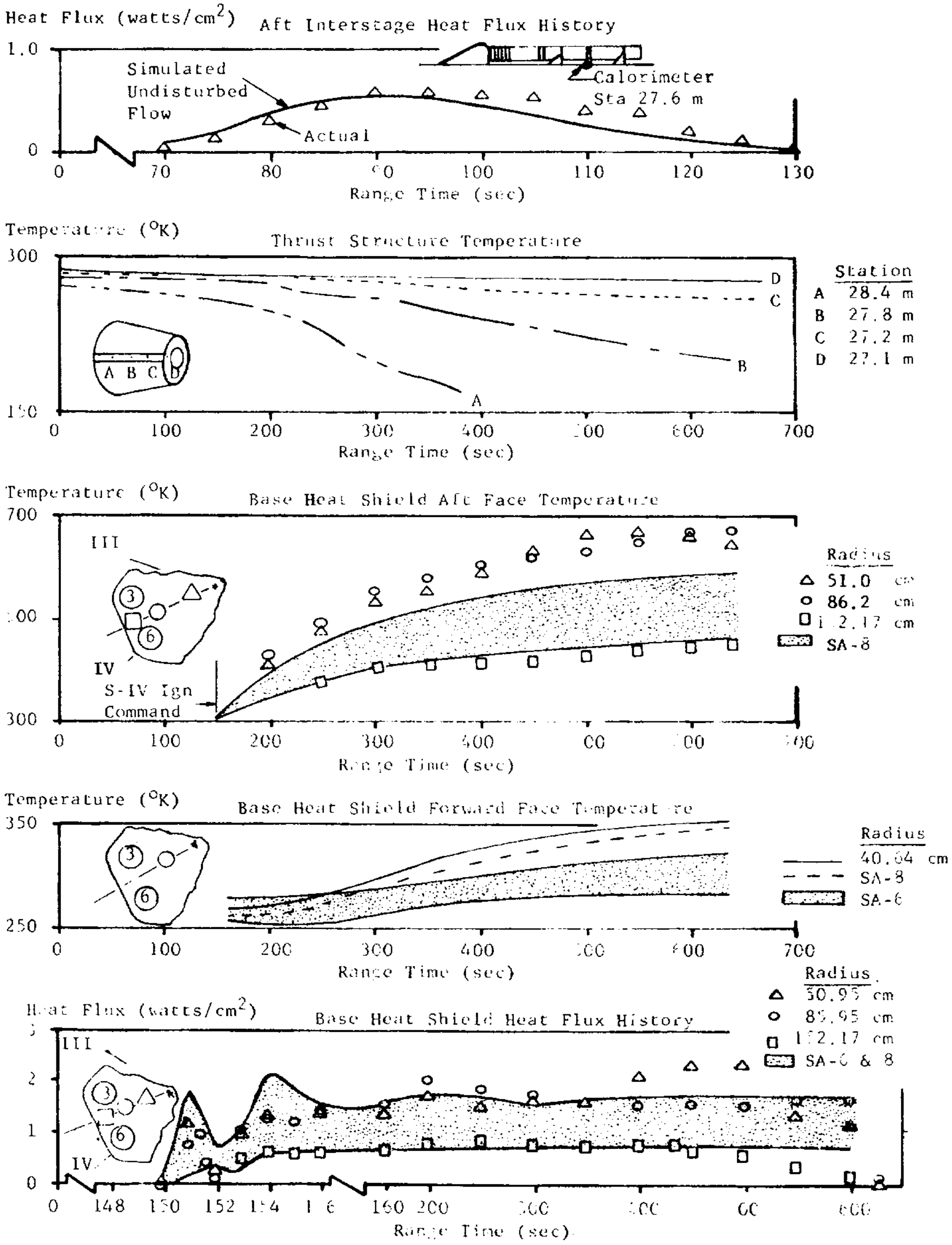

FIGURE 10-8. S-IV STAGE BASE TEMPERATURE ENVIRONMENT

Saturn SA-10 was the third of the Block II series vehicles to fly a prototype model of the production Instrument Unit to be used on Saturn IB and V vehicles. Components were mounted on panels attached to the interior wall. The Instrument Unit contained four vent ports to allow escape of cooling gases and purge flow during preflight conditioning and to obtain ambient pressure and temperature within the unit during flight.

A ground based environmental control system was provided to maintain an acceptable temperature within the Instrument Unit during preflight. During flight preparation and until umbilical separation, cooling or heating, as required, was provided by the ground support equipment. No inflight conditioning was required to accomplish the vehicle mission.

The ground based onboard cooling arrangement consisted of a manifold routed from the umbilical plate to various components of the IU. Precooled air was used until approximately 15 minutes prior to LH_2 tanking; then GN_2 was used until umbilical separation. The system also supplied cool GN_2 to purge various components. The purpose of the change from air to GN_2 cooling and purging was to prevent the possibility of air supporting combustion in the IU if electrical component sparking occurred.

IU environmental conditions were similar to those of the SA-8 and SA-9 flight. Minor temperature variations outside desired values were noted; however, they were not considered excessive or detrimental to normal equipment operation.

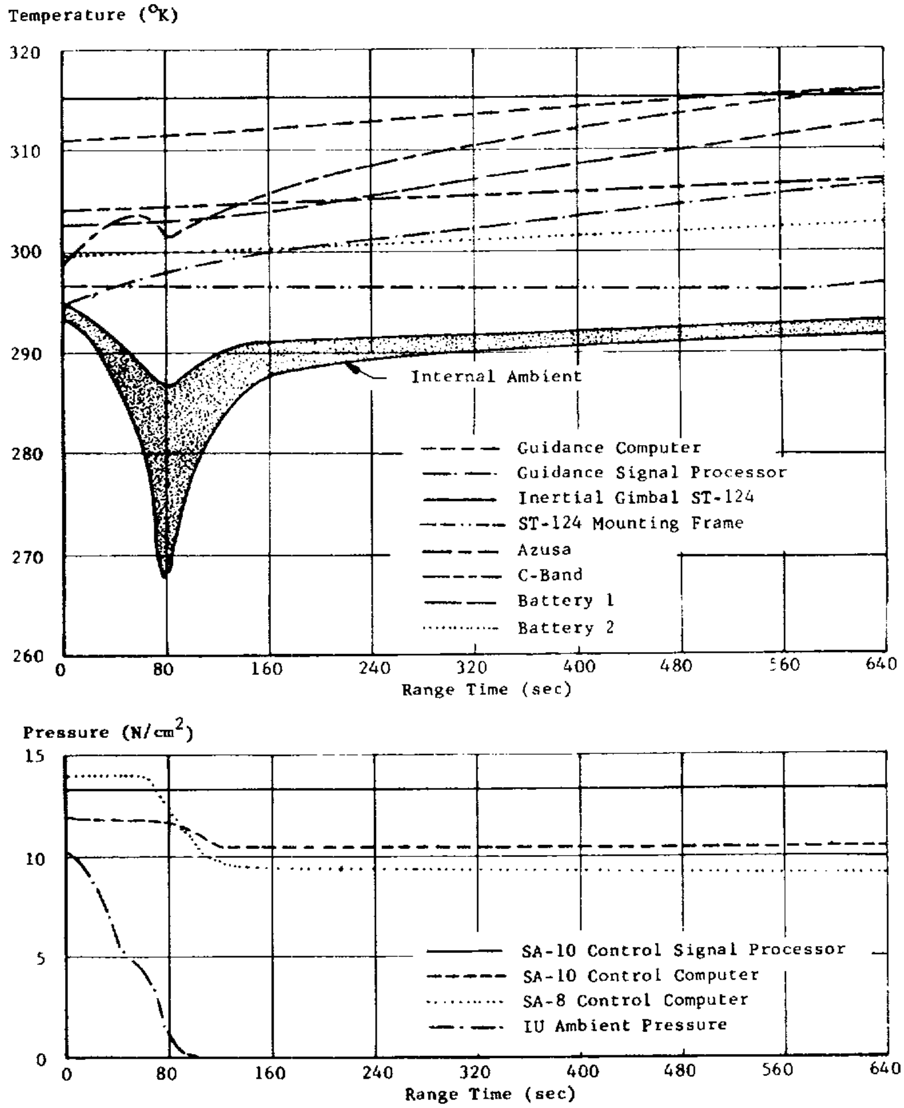

FIGURE 10-9. IU AMBIENT AND COMPONENT TEMPERATURES AND PRESSURES DURING POWERED FLIGHT

IU component surface temperatures were similar to those recorded during the SA-8 flight (Fig. 10-9). The PCM/RF assembly surface temperature reached 316°K which was the highest surface temperature recorded in the IU during the SA-10 flight.

IU ambient temperatures prior to and during flight were as expected. The band in Figure 10-9 shows the IU ambient temperatures during flight.

Control computer compartment seal leakage occurred again on SA-10 but was less severe than indicated for SA-8 and SA-9. Evidence to this effect is given by control computer pressure drop which occurred on all three flights between 32 and 80 seconds. A possible explanation for the seal leakage is compartment warpage introduced during mounting into the IU. A hermetic solder and seal will be used on S-IB compartments, which should prevent this leakage from reoccurring.

The IU environment in orbit was nominal. The results of the IU environmental evaluation during orbit are presented in Figure 10-10.

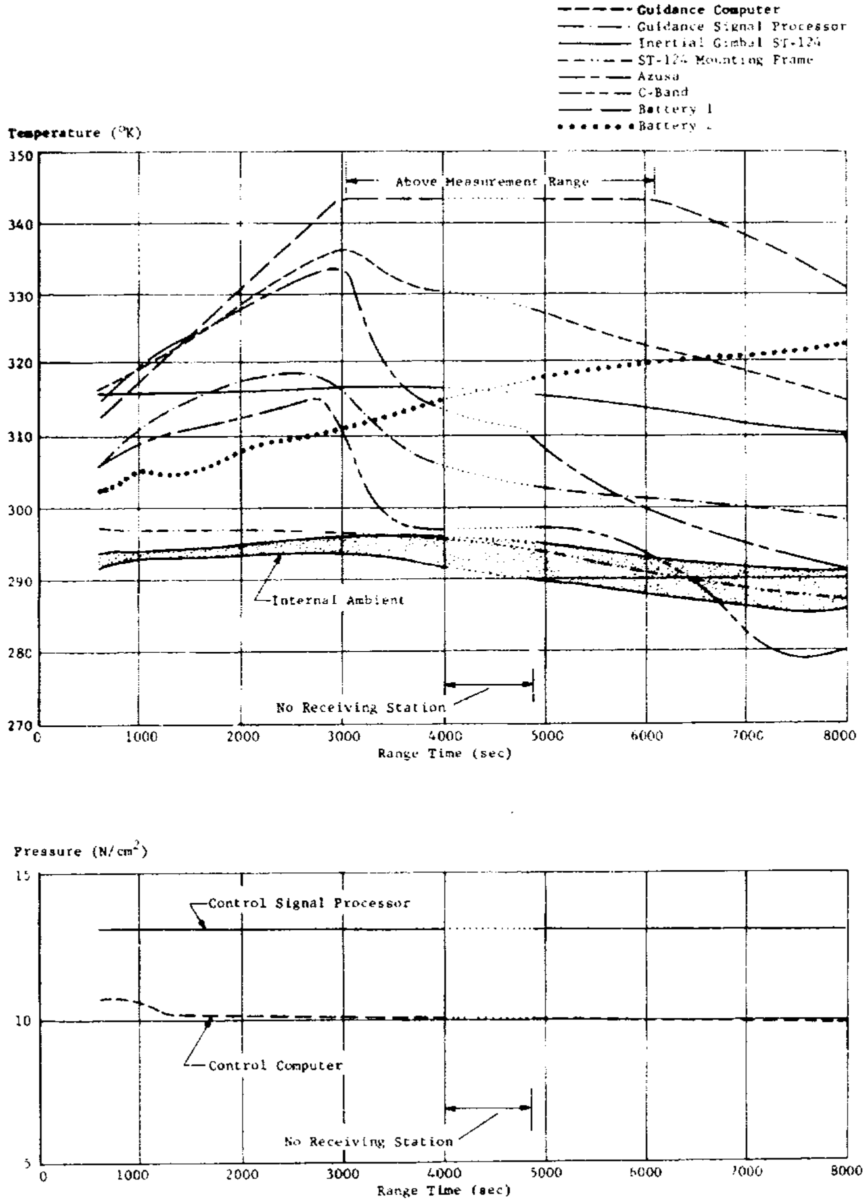

FIGURE 10-10. IU AMBIENT AND COMPONENT TEMPERATURES AND PRESSURES DURING ORBIT

SECTION XI. VEHICLE ELECTRICAL SYSTEMS

11.1 SUMMARY

The electrical systems of the SA-10 vehicle operated satisfactorily during the boost and orbital phases of flight and all mission requirements were met. The long life battery in the IU provided power to the P1 and F6 telemetry links for 140 minutes, which well exceeds the one orbit requirement.

11.2 S-I STAGE ELECTRICAL SYSTEM

The electrical system for the SA-10 booster was essentially the same as SA-8.

The electrical power source for the booster consisted of two identical 28-volt zinc silver oxide batteries, designated as 1D10 and 1D20. The capacity of the batteries was 2650 ampere-minutes.

During the boost phase of flight, the booster electrical system operated satisfactorily. The 1D10 battery current varied from 47 to 67 amperes dc. The 1D11 bus voltage varied from 27.7 to 28.4 volts dc. The 1D20 battery current varied from 35 to 42 amperes dc and the 1D21 bus voltage varied from 28.5 to 28.7 volts dc. Figure 11-1 shows the current and voltage profiles for the 1D10 and 1D20 batteries.

The output of the two 5-volt dc measuring supplies, one located in each measuring distributor, delivered a nominal 5 volts dc. The master measuring supply was a nominal 5 volts dc.

11.3 S-IV STAGE ELECTRICAL SYSTEM

The S-IV stage electrical system performed as expected throughout the flight. The system consisted of five major subsystem components: battery 1 (control battery), battery 2 (engine battery), instrumentation battery 1, instrumentation battery 2, and the static inverter. The current and voltages for batteries 1 and 2 and the static inverter voltages are presented in Figure 11-2.

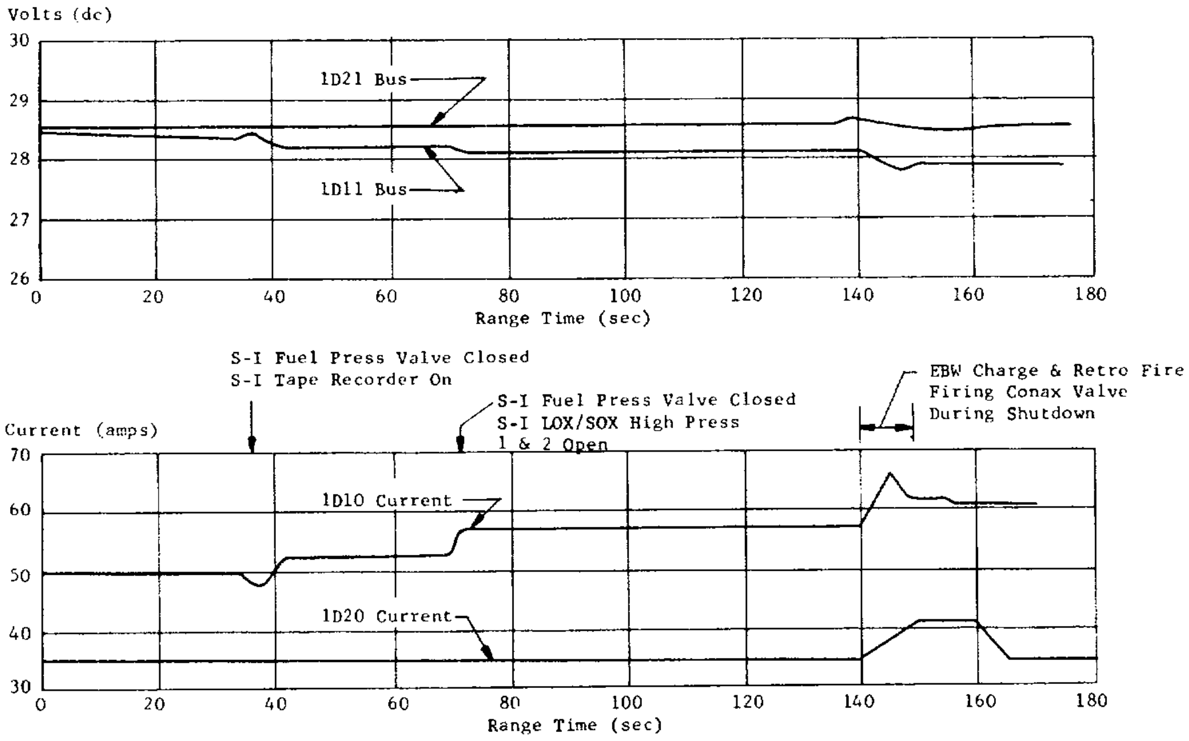

FIGURE 11-1. S-I STAGE CURRENT AND VOLTAGE

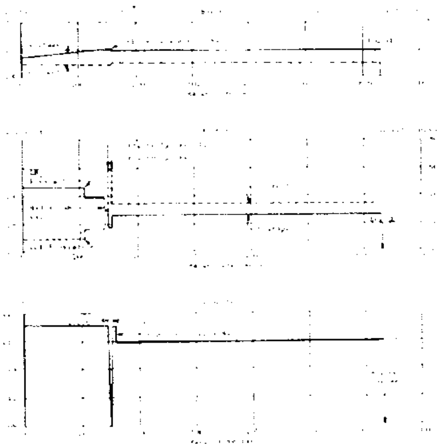

FIGURE 11-2. S-IV STAGE CURRENT AND VOLTAGE

Battery performance was satisfactory, with voltage and current remaining within predicted tolerances. The two instrumentation batteries were normal, with and output of 29.6 volts and a combined current of 16.2 amps. During S-IV powered flight, instrumentation battery 1 current was 9.5 amps, and the instrumentation battery 2 current was 6.7 amps.

Performance of the inverter was satisfactory. During separation, indicated output voltage dropped momentarily to the lower band edge, indicating 119 volts. This apparent drop was a false indication caused by ionization produced by retro rocket exhaust products on the umbilical recepticle. At PU activate, the voltage dropped to a nominal 114.9 volts, where it remained until S-IV engine cutoff.

All EBW firing units functioned properly in response to their respective commands. The range safety flight termination system performed properly and responded to the turn-off (safe) command satisfactorily. However, at 80 seconds, command destruct receiver (CDR) 1 indicated a 20 percent decrease in signal strength level lasting for about 2 seconds. This decrease is attributed to a bad look angle. Blackout of CDR signal strength data from 148 to 150 seconds coincided with the blackout of the T/M signal and therefore does not indicate a loss of signal to the CDR during this time period. At approximately 200 seconds, signal dropout occurred on both CDR signal strength measurements. This dropout was expected and is attributed to the switchover of the Sterling antenna on Grand Bahama Island.

11.4 IU STAGE ELECTRICAL SYSTEM

The Instrument Unit electrical system for SA-10 was similar to that of SA-8. During the boost and orbital phase of flight, the IU stage electrical system operated satisfactorily. One of the two IU batteries (8D10) had a current load of approximately 62 amperes except during cycling of the platform air bearing heater. The air bearing heater cycle period averaged 142 seconds. The "ON" part of the period averaged 15 seconds. The 8D10 battery load during the "ON" cycle of the heater was 69 amperes. The 8D11 bus voltage dropped about 0.24 volt when the heater was on. During the "OFF" cycle of the heater, the average 8D11 bus voltage was 28.8 volts. The other IU battery (8D20) had a current load of 30 amperes with an average terminal voltage of 28.4 volts. The 8D20 battery lifetime was approximately 140 minutes. Battery 8D20 was intentionally light loaded in order to power telemeters P1 and F6 during a complete orbit. The 5-volt dc measuring supply and 56-volt dc supply operated at their nominal values. All timing devices and logic and mode switching devices operated satisfactorily. The battery temperature, voltages and currents are shown in Figure 11-3 along with inverter 1 phase voltages.

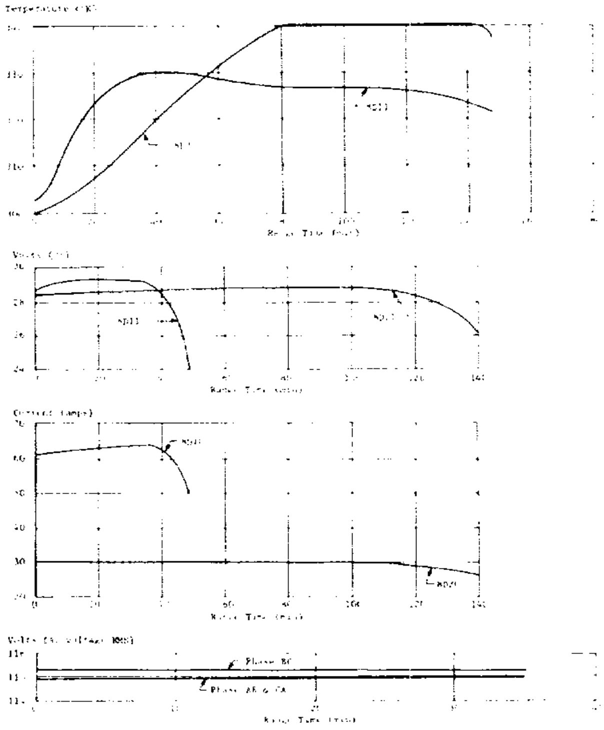

FIGURE 11-3. IU STAGE BATTERY TEMPERATURE, VOLTAGE, CURRENT AND INVERTER VOLTAGE

SECTION XII. AERODYNAMICS

12.1 SUMMARY

The axial (drag) force coefficient was higher than predicted during the subsonic regime of flight and lower than predicted during the supersonic portion of flight. A peak base drag of approximately 218,000 N (48,800 lbf) was measured at approximately 58 seconds by measurements on the heat shield and the flame shield.

12.2 DRAG

The axial force coefficient, obtained as an output of the propulsion system performance evaluation, is in excellent agreement with SA-8 flight results (Fig. 12-1). The axial force coefficient was higher than predicted during the subsonic regime and lower than predicted at supersonic Mach numbers.

Base drag contribution of the axial force, calculated from pressure measurements on the heat shield and flame shield of the S-I stage, is compared to results from the SA-8 and SA-9 flight vehicles in Figure 12-1. A peak base drag of approximately 218,000 N (48,800 lbf) was measured at approximately 58 seconds. A positive pressure thrust was observed beginning at approximately 70 seconds because of recirculation of engine exhaust gases. Base drag for SA-10 was generally slightly lower than measured on SA-8 and SA-9 flights. A maximum positive pressure thrust of approximately 7600 N (1702 lbf) was observed at 83 seconds of flight (Fig. 12-1).

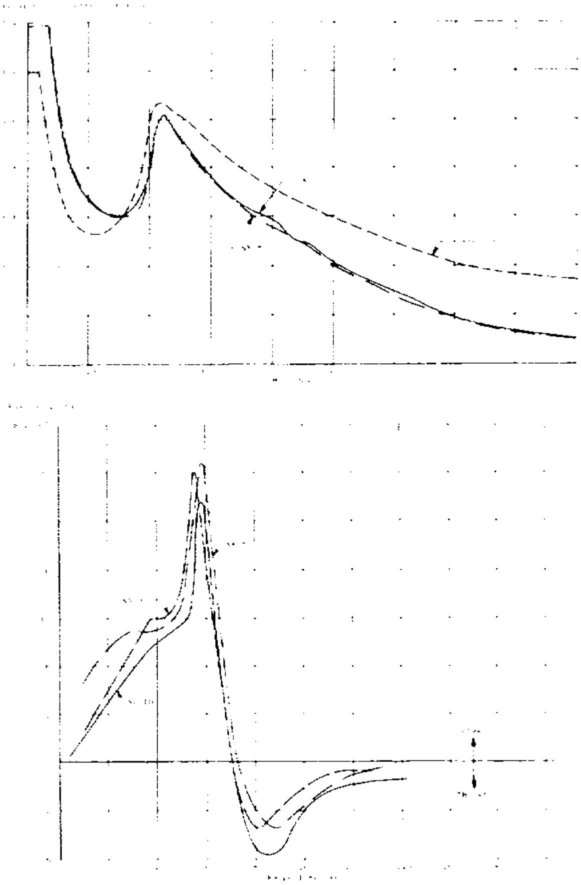

FIGURE 12-1. AXIAL FORCE COEFFICIENT AND BASE DRAG

SECTION XIII. INSTRUMENTATION

13.1 SUMMARY

There were 1018 telemetered measurements active at liftoff on SA-10. Twelve of the 1018 measurements failed in flight, resulting in an overall measuring system reliability of 98.8 percent. Three measurements were scrubbed prior to launch.

All preflight and inflight calibrations were normal and satisfactory.

Battery life was sufficient to give the planned orbital telemetry coverage. The last telemetry signal was received 2 hours and 28 minutes after liftoff.

Airborne tape recorders in the S-I, IU, and S-IV stages operated satisfactorily, and produced data free of attenuation effects caused by retro and ullage rocket firing.

The onboard TV system was cancelled prior to flight.

The altimeter system and associated return-pulse-shape experiment failed to operate.

RF performance of the 11 telemetry links was satisfactory.

Tracking commitments were met by the C-Band radar, ODOP, and Azusa/GLOTRAC systems; the MISTRAM transponder failed at 63 seconds. Excellent coverage was provided.

Overall quality of the film obtained during launch was good. However, downrange cloud conditions prevented all of the 10.2 m (400 in) and 12.7 m (500 in) focal length cameras from recording usable data.

13.2 S-I STAGE MEASURING ANALYSIS

13.2.1 S-I MEASUREMENT MALFUNCTIONS

A total of 376 inflight measurements were scheduled for the S-I stage. No measurements were scrubbed prior to launch. One of the 376 measurements active at launch failed completely; 17 measurements were only partially successful. The number of inflight measurements were reduced by 145 from S-I-8. Table 13-I lists the S-I stage measurement malfunctions. Eleven of the S-I measurement malfunctions listed in Table 13-I were in the group of aspirator and engine bell calorimeters on engines 3 and 7. These malfunctions are attributed to the extremely severe environment.

13.2.2 S-I MEASURING RELIABILITY

Reliability of the S-I measuring system was 99.7 percent, considering only those measurements active at liftoff compared to complete failures.

The combustion chamber dome vibration measurements (E-11 and E-33 series) had a significantly higher than predicted output level. Test stand data on these measurements indicated that there is a significantly higher input level at frequencies above 3000 Hz than originally anticipated. This coupled with a peak in the transducer response, apparently results in overloading the ac amplifier in such a manner that it puts out increased amplitudes in the normal frequency range (50 to 3000 Hz).

13.3 S-IV MEASURING ANALYSIS

13.3.1 S-IV MEASUREMENT MALFUNCTION

A total of 404 inflight measurements were scheduled for the S-IV stage. Two of the 404 measurements were scrubbed prior to launch. Eleven of the 402 measurements active at launch failed completely; 10 measurements were only partially successful. Table 13-1 lists the S-IV stage measurement malfunctions.

13.3.2 S-IV MEASURING RELIABILITY

Reliability of the S-IV stage measuring system was 97.3 percent, considering only those measurements active at liftoff compared to complete failures.

13.4 IU STAGE MEASURING ANALYSIS

13.4.1 IU MEASUREMENT MALFUNCTIONS

A total of 241 flight measurements were scheduled for the IU. One measurement was scrubbed prior to launch. There were no failures during flight. Table 13-I lists the single measurement malfunction.

13.4.2 IU MEASURING RELIABILITY

Reliability of the IU measuring system was 100 percent, considering only those measurements active at liftoff compared with complete failures.

TABLE 13-I. MEASUREMENT MALFUNCTIONS

Stage	Meas. No.	Meas. Title	Remarks
		Scrubbed Prior to Launch	
S-IV	C625-403	Thrust Chamber Outer Skin Temp E-3	Deleted by NASA
	D644-402	Actuator B Diff Press, E-2	Transducer not installed due to launch schedule
IU	M69-802	Input PRF, C-Band	Bad component in the transponder
		Failures	
S-I	C299-7	Temp. Eng. Nozzle Surface T. Cal.	Erratic After ignition. No valid data.
S-IV	D647-416	Acoustic, Fwd I/S External	Data invalid, dc bias level shifts.
	D648-416	Acoustic, Fwd I/S Internal	Data invalid, dc bias level shifts.
	D655-416	Pressure-Base Heat Shield	No response
	D656-416	Pressure-Base Heat Shield	No response
	D657-416	Pressure-Base Heat Shield	Data invalid, slow response
	D658-416	Pressure-Base Heat Shield	Data invalid, slow response
	E628-407	Vib-PU Sys Computer, Th Axis	No response
	E612-407	Vib-Inverter - Thrust Axis	Zero level offset 4%, levels low
	E641-401	Vib-LH$_2$ Feedline - Thrust	Data invalid, bandedge-to-bandedge response
	E642-415	Vib-LH$_2$ Tank at He1 Sphere-Th	No response
	E666-416	Vib-Heat Shield Support-Thrust	No response
		Partially Successful	
S-I	A12-2	Turbine RPM	Frequency divider intermittently divides by a higher number than specified.
	A14-C2	LOX Level Discrete	Pulse 10 missing
	A20-F2	Fuel Level Discrete	Pulse 1 missing
	C5-2	Temp Hi Speed Pinion Brg No. 6	Temperature drop instead of rise after 80 seconds.
	C286-3	Temp Eng Nozzle Surface T. Cal.	Dropped out at 127 seconds.
	C290-3	Temp Aspirator Surface T. Cal.	Dropped out at 65 seconds.
	C291-3	Same as C290-3	Erratic from 112 to 148 seconds.
	C292-3	Same as C290-3	Erratic from 45 to 150 seconds.
	C293-3	Same as C290-3	Out from 110 to 150 seconds.
	C295-7	Temp Eng Nozzle Surface T. Cal	Dropped out at 53 seconds.
	C296-7	Temp Eng Nozzle Surface T. Cal.	Erratic between 90 and 150 seconds.
	C297-7	Temp Eng Nozzle Surface T. Cal.	Dropped out at 28 seconds.
	C298-7	Temp Eng Nozzle Surface T. Cal.	Erratic after 10 seconds. Trend valid to 50 seconds.
	C300-7	Temp Eng Nozzle Surface T. Cal.	Erratic from 78 to 148 seconds.
	D1-6	Combustion Chamber Press	Failed at engine cutoff.
	D14-3	Turbine Inlet Press	Pressure decreases instead of increases throughout flight.
	D14-5	Turbine Inlet Press	Abrupt pressure drop at 100 sec, 20% low for rest of flight.
S-IV	C603-406	LH$_2$ Pump Housing Temp, E-6	Failed at 116 seconds.
	C625-401	Thrust Chamber Outer Skin Temp, E-1	Slow response
	D604-401	LOX Injector Diff Press, E-1	Noisy after 564 seconds.
	D604-402	LOX Injector Diff Press, E-2	Failed at 260 seconds.
	D604-403	LOX Injector Diff Press, E-3	Noisy after 185 seconds, failed at 380 seconds.
	D604-404	LOX Injector Diff Press, E-4	Noisy after 173 sec, failed at 210 seconds
	D604-406	LOX Injector Diff Press, E-6	Failed at 218 seconds.
	E600-408	Axial Acceleration	Failed at S-IV engine cutoff.
	E655-408	Vibration-LOX Tank Valve Par to Flow	Data invalid after 304 seconds.
	E663-407	Vibration-EBW Unit - Thrust Axis	Failed at 100 seconds.

13.5 AIRBORNE TELEMETRY SYSTEMS

13.5.1 TELEMETRY LINKS

Data transmission for flight testing Saturn vehicle SA-10 was effected by eleven radio telemetry system links on the combined S-I, S-IV, and IU stages. (Spacecraft instrumentation is presented in Section XIV.) The following systems were utilized on SA-10:

S-I STAGE			
Link	Modulation	Link	Modulation
F1	PAM-FM-FM; FM-FM	S1	SS-FM
F2	PAM-FM-FM; FM-FM	S2	PCM-FM
S-IV STAGE			
Link	Modulation		
D1	PDM-FM-FM		
D2	PDM-FM-FM		
D3	PDM-FM-FM		
INSTRUMENT UNIT			
Link	Modulation	Link	Modulation
F5	FM-FM; FM-FM-FM	S3	SS-FM
F6	FM-FM; FM-FM-FM PAM-FM-FM	P1	PCM-FM

Links P1 and P2, PCM system, also functioned as digital data acquisition system (DDAS) for their respective stages. The DDAS function of link P1 was to encode digitally and transmit simultaneously the output from the model 270 commutator in link F6 with the output from the multiplexer in link P1. The DDAS function of link P2 was to encode digitally and transmit the output from the model 270 commutator in links F1 and F2 at reduced sampling rates. The primary purpose of the DDAS in links P1 and P2 was preflight checkout of the IU and S-I-10 stage, respectively. DDAS information was also available from links P1 and P2 during flight. Insertion of digital data into the PCM output format worked very satisfactorily.

13.5.2 DATA ACQUISITION

Transmitted radio frequency power on all IU and S-I stage telemetry links was sufficient to produce the desired data coverage of all planned flight periods. IU orbital telemetry links P1 and F6 transmitted data for at least 2 hours and 28 minutes. No inflight telemetry calibrations were executed during orbital flight.

Transmission of all three S-IV telemetry links was good throughout the flight. The data indicate that links D1 and D3 were operational for at least 124 minutes after liftoff, and link D2 for 119 minutes after liftoff.

13.5.3 CALIBRATION

Preflight and inflight calibration of all telemetry channels was satisfactory, and as planned. Telemeter S1 was not scheduled to receive inflight calibration.

13.6 AIRBORNE TAPE RECORDERS

The airborne tape recorders used for the SA-10 flight were dual-track recorders capable of recording the mixer-amplifier outputs of two FM/FM telemeters. During the playback mode the transmitter was switched from the mixer amplifier to the recorder. The purpose of the recorder is to record data during the periods when RF dropout is anticipated due to flame attenuation, retro and ullage firing, critical look angle, etc.

13.6.1 S-I RECORDER

The S-I-10 stage contained one recorder which recorded the output of telemetry links F1 and F2. This recorder was in the record mode from 40.2 seconds to 175.2 seconds. Recorder transfer to playback mode was initiated at 172.2 seconds. An elapsed time of 1.4 seconds was required for the transfer from record mode to playback mode. The recorder began playback of good data at 176.6 seconds and completed data playback at 310.2 seconds. The playback contained 133.6 seconds (40.2 to 173.8 seconds) of good data. At completion of recorder playback, modulation was removed from telemeters F1 and F2. Operation of this airborne recorder was satisfactory, and data contained in the playback record are free from the effects of retro and flame attenuation.

13.6.2 S-IV RECORDER

The single tape recorder onboard the S-IV stage was in the record mode from 142.3 seconds to 168.4 seconds (26.1 seconds), and included the whole S-IV-10 separation sequence. The recorder was in the playback mode from 731.0 seconds to 761.0 seconds (30 seconds).

The S-IV tape recorder went into an unscheduled playback mode similar to that on SA-8 between 59 minutes, 0.4 second and 88 minutes, 50.5 seconds. It was concluded, as on SA-8, that this playback command was initiated by the IU and resulted in telemeter 1 and 2 transmitters being switched to the tape recorder playback amplifier. Telemeters 1 and 2 were returned to their preflight configuration as the IU voltage dropped below the relay dropout voltage. This malfunction is explained in more detail in Reference 6.

13.6.3 IU RECORDER

The S-IU-10 contained one onboard tape recorder that recorded the outputs of telemeters F5 (Mod B) and F6 (Mod A). This recorder was in the record mode from 141.2 seconds to 169.5 seconds. Recorder transfer to playback mode was initiated at 730.9 seconds. An elapsed time of 0.9 second was required for the transfer to the playback mode. The recorder began playback of good data at 731.8 seconds and completed data playback at 759.2 seconds. The playback contained 27.4 seconds (141.2 to 168.6 seconds) of good data. Real time modulation was reapplied to links F5 and F6 at 761.0 seconds. Operation of this airborne recorder was good, and data contained in the playback record are free from the effects of retro and flame attenuation.

13.7 RF SYSTEMS ANALYSIS

The RF systems on SA-10 experienced several problems. The altimeter system and the associated return-pulse-shape experiment both failed to operate. The MISTRAM system was operating at liftoff, but was intermittent after 63 seconds. The RF performance of the telemetry system was satisfactory throughout powered and orbital flight with the exception of a short dropout at retro rocket ignition. Tracking commitments were met by the C-band radar, ODOP, and Azusa/GLOTRAC systems, which provided excellent coverage.

13.7.1 TELEMETRY

The RF performance of the telemetry system was satisfactory throughout powered and orbital flight. The performance was degraded slightly by main engine flame attenuation, retro rocket attenuation, ionospheric effects, and ground station antenna scanning. Lower than predicted signal levels during certain periods of flight, and an unexplained change in signal level between 134 and 140 seconds also were evident. However, no data were lost except during retro rocket ignition, and these losses were not as extensive as on SA-5, SA-6, or SA-7.

Main engine flame attenuation during this flight was very similar to past Saturn flights with typical peak attenuation values of 20 to 25 db occurring at the Cape stations. The major attenuation effects ceased at 126 seconds at an altitude of approximately 57 km (within the region of 54 to 60 km where attenuation has ended on all previous Saturn flights). The reason for the decrease in attenuation at this altitude can probably be attributed to the cessation of afterburning due to a lack of oxygen. No data were lost as a result of main engine flame attenuation.

Retro rocket attenuation was very similar to that experienced on SA-8 and SA-9. Ignition occurred at an altitude of 92.7 km and the effects were very different from SA-5, 6, and 7 in which the retro rockets were fired in the 60- to 75-km altitude region. Data dropouts in SA-10 occurred on some of the links for short periods of time. However, the effects varied, depending on aspect angle to the ground station and vehicle antenna locations. The main effect on the S-I stage links, with antennas located aft of the retro rockets, was rapid fluctuations in signal strength with very little average attenuation. The IU and S-IV stage links, with antennas located forward of the retro rockets, experienced a 0.75-second dropout beginning approximately 0.75 second after retro rocket ignition and ending approximately 0.2 second prior to thrust termination. Had separation taken place in the 60- to 75-km altitude region, complete dropout would have occurred on all links simultaneously with retro rocket ignition, as on SA-5, 6, and 7.

Since this was an early morning firing, the E-layer had not reached the peak of its activity. The effects of the F1 and F2 layers are partially obscured by vehicle antenna nulls caused by low aspect angles and by antenna scanning at some of the ground stations.

Cape Tel 2 had a definite problem with scanning on this flight, similar to that experienced on SA-8 and SA-9. This antenna has not operated satisfactorily on any Saturn vehicle since SA-5. It was being modified during the flights of SA-6 and SA-7 and was not used. The original work was not satisfactory and the rework is behind schedule. At times, this scanning produced peak-to-peak variations in signal strength of 11 db (5 to 8 db more than it should be). This problem, combined with the low aspect angle and possible ionospheric disturbances, caused lower than normal signal levels at the uprange stations on all S-IV and IU links during S-IV powered flight. However, the use of diversity polarization and redundant station coverage prevented any loss of data.

The S-I stage and IU telemetry systems experienced some rather abrupt changes in signal level between 134 and 140 seconds. This effect was not present on the S-IV stage links. Similar anomalies were experienced on SA-5 and SA-7 at very nearly the same altitudes. A completely acceptable reason has not been found for any of these occurrences. However, the possibility of voltage breakdown at some point in the system is not being overlooked, especially since it happened in an altitude region where breakdowns are most likely to occur. Forward and reflected power measurements were made on the IU telemetry links. The measurements showed no change in forward power, but the reflected power increased by 3 to 6 db during this time. Another possibility is that the anomaly was caused by some type venting not apparent from the telemetered measurements. This is still under investigation.

13.7.2 TRACKING

The tracking systems, with the exception of MISTRAM and the altimeter provided excellent data throughout this flight. The ODOP system performed exceptionally well and provided data to 720 seconds. The C-band radar and Azusa/GLOTRAC systems exceeded their respective tracking commitments. The C-band radar system, composed mostly of the FPQ-6 radars, experienced no difficulties. The Azusa real time digital range data for range safety were invalid from 508 to 660 seconds because of a problem in the ground station. However, this discrepancy will not affect the metric data. The Azusa/GLOTRAC system provided Azusa and/or three station GLOTRAC coverage from liftoff to 883 seconds, with the exception of short interruptions at separation and at handover.

ODOP

The prime tracking requirement for the ODOP system was from liftoff to 150 seconds. As usual, all sites fulfilled this requirement. The signal strength was sufficient for good data beyond the point where the geometry would permit a trajectory solution. Retro rocket firing caused all stations to drop to a marginal level and break phase lock for periods varying from 2 to 4 seconds.

MISTRAM

The two MISTRAM sites received sporadic intervals of good data, but the overall performance of the system did not meet requirements. The system experienced a transponder failure at 63 seconds after liftoff. The reason for this problem has not been determined, but it is believed to be a power loss which may have originated in the calibrate channel. This system is not scheduled for any future Saturn flights, so the problem is not considered serious for the Saturn program. On most of the previous flights, the MISTRAM transponder failed during preflight checkout, but a change of transponders usually resulted in an acceptable flight performance. This poor reliability finally resulted in an inflight failure.

The MISTRAM I station received good data from 8 to 63 seconds, 70 to 80 seconds, 84 to 110 seconds, and 203 to 214 seconds. Except for these short periods, the signal levels were below threshold from 63 to 568 seconds. At 568 seconds the system apparently recovered. The signal level was low from 568 to 720 seconds, but sufficient to provide reducible data.

The MISTRAM II station experienced good signal levels from 308 to 328 seconds, 356 to 370 seconds, and from 568 to 700 seconds. The signal was below threshold at all other times.

The onboard measurements show that the loss of phase lock at each station is a direct result of a drop in the transmitted power output of the range calibrate channels.

C-Band Radar

The C-band radar system provided good data from liftoff to 720 seconds. No two receiving sites experienced simultaneous low or marginal power levels. The MILA and GBI (3.16) radars were turned off at 294 and 323 seconds, respectively, as instructed by the operations directive. The signal level at the time of cutoff at both stations was good. However, the range personnel believe that it is best not to have more than five radars interrogating the transponder simultaneously. If this is the case, the requirements should be reviewed to determine if the most advantageous use of the stations is being made.

The MILA station was again preprogrammed to skin track for the first 54 seconds. After this, it switched to beacon track. This was done to prevent any possible tracking problems due to the tilt of the polarization ellipse.

This system was not affected by main engine flame attenuation, and retro rocket attenuation was generally about 8 db, except at the PAFB site where a 17.5-db peak attenuation was experienced at approximately 150.5 seconds.

The C-band beacon expired over Carnarvon at about 13:59:10 U.T., approximately one hour after liftoff.

Azusa/GLOTRAC

The Azusa/GLOTRAC system provided excellent data from liftoff to 883 seconds except for a 2- to 4-second loss at handover and a short dropout at separation. The complete coverage illustrates the advantages gained by repositioning the Azusa antenna prior to SA-7 to provide higher gains for the GLOTRAC stations.

Azusa Mark II was the only station in the GLOTRAC network with an elevation angle above the radio horizon until 82 seconds. At this time, the Eleuthera station began tracking and good two-station coverage was continued until 190 seconds. A momentary decrease in signal strength occurred at 186 seconds while the ground antenna was looking into an undefined portion of the onboard antenna pattern. After this time, at least three-station coverage was maintained to 883 seconds. The Antigua station tracked the orbiting vehicle to 960 seconds. At times during this period, the system provided complete six-station coverage. Handover at 660 seconds caused a 2- to 4-second loss of data, but all stations except Azusa Mark II recovered.

No major problems were encountered by this system. Main engine flame attenuation caused modulation of the signal, but no loss of data occurred.

Altimeter

The altimeter system failed to operate on this flight. Although the exact reason is not known, it is thought to have been caused by a lack of receiver sensitivity. This problem could have been caused by a bad RF cable connection, interface problems between the altimeter and the pulse-return-shape experiment, or a malfunction in the front end of the receiver. It was known ten minutes prior to liftoff that the pulse-return-shape experiment had failed.

13.7.3 TELEVISION

Problems external to the onboard TV system caused its cancellation prior to flight. Analyses showed that the mounting brackets would not withstand the vibration loads during flight.

13.8 OPTICAL INSTRUMENTATION

An engineering photo/optical instrumentation system of 85 cameras (65 fixed and 20 tracking) was installed throughout the Saturn launch-tracking complex to provide a detailed recording of the ground support equipment (GSE) and of vehicle release, operation, and performance of SA-10 during its launch and flight. The overall quality of the film obtained during the launch was good; however, downrange cloud conditions at liftoff were such that none of the 12.7-m or 10.2-m (500 or 400 in) focal length cameras recorded usable data. Of the 85 cameras programmed to record the launch, two cameras malfunctioned, nine had no timing, and three had timing problems, i.e. erratic or overlapping time pulses. All other cameras had usable timing and a majority of the 16-mm Milliken cameras were time indexed for the first time since the beginning of the Saturn program (time displacement between an exposed frame of data and its related timing mark). All of the film from the tracking instruments was time indexed.

13.8.1 ENGINEERING SEQUENTIAL CAMERAS

Seventeen cameras were located on the launch pedestal to record the GSE release events and vehicle first motion. The GSE release events include the eight holddown arms, two short cable masts, the LOX and fuel fill and drain masts and the ignition of the eight H-1 engines (first frame of data showing the hypergolic flash). The GSE on the launch pedestal appeared to operate normally. Two of the cameras recording holddown arm release did not operate, two cameras had unusable timing, and the release of one arm was obscured by smoke and ice. The three arm releases that were timed were well within the release tolerance of 50 milliseconds.

All eight of the H-1 engine ignitions were recorded and timeable. The engines and heat shield appeared to function normally during ignition and liftoff. The four Milliken cameras recording these ignitions were time indexed for the first time in the Saturn program.

Release and retraction of the two short cable masts were recorded and timed. One of the cameras was not time indexed. No malfunctions were recorded.

The release of the LOX and fuel fill and drain masts was not visible due to frost and ice at the release time; however, both masts appeared to retract normally and no malfunctions were observed in these areas.

Vehicle first motion data were reduced from a camera specifically oriented on a holddown arm to record these data. Excellent results were obtained from this camera.

In addition to the 17 launch pedestal items, 11 cameras were located on the umbilical tower where they recorded the release of the four swing arms, exhaust and blast on the launch pedestal, and the forward section of the vehicle during ignition and liftoff. All cameras on the umbilical tower operated satisfactorily except for one camera. This camera was designated to record vertical motion for 5 to 7 meters but did not have range timing on the film. The camera field of view did not include all of the targets on the vehicle. No usable data were reduced from this film.

Nine cameras on the umbilical tower were oriented to record the release and retraction of the four swing arms. All of the arms appeared to release and retract normally. Ice formation on the S-IV and S-I stages of Saturn SA-10 was less than on Saturn SA-8.

13.8.2 TRACKING CAMERAS

Fifteen ground based long focal-length tracking cameras and two cameras from C-54 aircraft recorded the operation of the vehicle from liftoff through the ignition of the launch escape tower. Cameras in this system also recorded the vehicle exhaust flame shift, exhaust flame pattern growth (plume), ullage, and retro ignition.

Inboard and outboard engine cutoff signals were observed. The normal flareup (LOX and fuel residuals from the inboard engines), after inboard engine cutoff, was observed and lasted 0.49 second.

Ignitions of retro rockets number one, three, and four were observed. These rockets appeared to ignite simultaneously. No malfunctions were observed by the tracking cameras.

13.9 ORBITAL TRACKING AND TELEMETRY SUMMARY

13.9.1 TRACKING SUMMARY

Due to the long lifetime of the SA-10 orbiting vehicle, radar tracking coverage was requested for the first five revolutions only. This tracking summary covers all tracking over these five revolutions beginning at insertion (13:10:40.252 U.T.).

Orbital tracking of the SA-10 vehicle was conducted by the NASA Space Tracking and Data Acquisition Network (STADAN). STADAN is composed of the global network of Minitrack receiving stations and Minitrack optical tracking stations (MOTS), and of the Manned Space Flight Network (MSFN) which is a global network of radar tracking stations. MSFN is supported by elements of DOD. Additional tracking support was provided by the optical tracking network of the Smithsonian Astrophysical Observatory (SAO).

The last C-band beacon signal recorded was reported by Carnarvon, Australia, at approximately 14:00 U.T. (one hour after liftoff). All subsequent radar tracking was skin track.

One photo contact was made by the Johannesburg, South Africa, MOTS station at 16:54 U.T., and one visual sighting was reported by the SAO at Pretoria, South Africa, at 17:00 U.T. No additional optical sightings over the first five revolutions have been received.

Minitrack observations will continue to be made on the orbiting vehicle during the vehicle's lifetime or until termination of the Pegasus C experiment.

13.9.2 TELEMETRY SUMMARY

The last links to be recorded were links F6 and P1 at Tananarive, Madagascar, at 15:28:38, approximately two and one-half hours after liftoff.

SECTION XIV. PEGASUS C

14.1 SUMMARY

At 640.252 seconds, the S-IV-10 stage, Instrument Unit, Apollo shroud and Pegasus were inserted into orbit with no appreciable pitch, yaw, or roll rate. During orbital flight, the configuration experienced the following: high capacity blowdown of the LH_2 NPV tank, separation of the Apollo shroud, extension of Pegasus wings, and continuous nonpropulsive venting (NPV) until residual propellants were depleted. The Pegasus wing deployment and all spacecraft systems worked properly and all measurements were initially within their predicted limits.

The estimated total vented impulse was 167,208 N-s (37,590 lbf-s) from the hydrogen tank and 200,116 N-s (44,988 lbf-s) from the oxygen tank. The maximum roll rate of S-IV-10 was 6.3 deg/s. The tumble rate of the vehicle at T + 360 hours (15 days) was determined to be approximately 1 deg/s with a half-cone angle of approximately 20 degrees.

The Pegasus C is the first Pegasus spacecraft to have removable meteorite detector panels which can be recovered from orbit for purposes of analysis.

14.2 PEGASUS C PERFORMANCE

Pegasus/Service Module separation was accomplished as planned at 811.95 seconds, 2.32 seconds earlier than predicted. Wing deployment was initiated at 871.95 seconds and was completed by 912.0 seconds. A description of the Pegasus C is presented in the Appendix. Initially, all systems on the spacecraft worked properly and all measurements were within their predicted limits.

14.3 ORBITAL ATTITUDE

14.3.1 NONPROPULSIVE VENT SYSTEM PERFORMANCE

The SA-10 nonpropulsive venting (NPV) system was identical to that flown on SA-8. This system was utilized to prevent the occurrence of excessive angular rates caused by the venting of residual propellants after S-IV engine cutoff. An auxiliary LH_2 NPV system was also installed on SA-9, SA-8, and SA-10, which operates from cutoff to cutoff plus 180 seconds. This system vents the high boiloff rates immediately after engine cutoff which are caused by the latent heat in the LH_2 tank insulation.

Operation of the components of the S-IV NPV system was as expected. The hydrogen and oxygen nonpropulsive vent valves opened at S-IV engine cutoff and remained open, as designed. In addition, the auxiliary hydrogen nonpropulsive vent valve opened at cutoff and closed three minutes later, as designed.

At S-IV engine cutoff, the LH_2 tank ullage pressure began to decay, from 26.5 N/cm^2 (38.4 psi) at cutoff to 8.9 N/cm^2 (12.9 psi) at cutoff plus 181 seconds, due to the venting from the auxiliary hydrogen NPV. One second after the auxiliary nonpropulsive vent valve was closed, the Apollo shroud was separated, exerting a negative thrust on the S-IV stage. As a result, the LH_2 residual was forced toward the forward dome, causing an LH_2 boiloff rate that was greater than the capacity of the LH_2 NPV system. As anticipated, the LH_2 ullage pressure rose rapidly after Apollo payload separation, but did not reach the main LH_2 vent valve relief pressure. The peak pressure of 17.7 N/cm^2 (25.7 psi) was reached at approximately 2000 seconds. After one orbit, Tel 2 telemetry recorded an LH_2 tank ullage pressure of 8.9 N/cm^2 (13 psi), and at this time the ullage pressure was slowly decreasing. The LH_2 tank temperature probes indicated that the residuals at this time were entirely gaseous.

At S-IV engine cutoff, the LOX tank ullage pressure switch was transferred to the control of the cold helium shutoff valve. The LOX tank pressure was maintained within the 31 to 33 N/cm^2 (45 to 58 psi) design band by cycling the cold helium shutoff valve for as long as the cold helium pressurant was available. As a result, the LOX tank pressure remained stable for about 800 seconds after S-IV engine cutoff, in spite of the venting by the LOX NPV system. At the end of the first orbit, the Tel 2 telemetry recorded a LOX tank pressure of approximately 17.2 N/cm^2 (25 psi). An estimate was made of the mass and impulse vented during three periods:

1. S-IV engine cutoff to S-IV engine cutoff plus 180 seconds

2. S-IV engine cutoff plus 180 seconds to end of first orbit

3. End of first orbit to tank depletion.

The masses were based upon the following residual propellants and gases at S-IV engine cutoff:

1. 87 kg (191 lbm) of LH_2, plus 48.1 kg (106 lbm) of ullage gas

2. 454 kg (1001 lbm) of LOX, plus 53.5 kg (118 lbm) of GOX, plus 60.3 kg (133 lbm) of helium.

Masses presented in Table 14-I are based upon the ullage gas within the tank and vented impulse. There is excellent agreement between the residual and gas mass in the tank and those calculated from tank blowdown.

TABLE 14-I. NONPROPULSIVE VENT PERFORMANCE

Time	LH$_2$ Tank		LOX Tank	
	Mass Vented	Total Impulse	Mass Vented	Total Impulse
1) Cutoff to Cutoff + 180 sec	44 kg (96 lbm)	56,488 N-s (12,690 lbf-s)	GOX & He 107.5 kg (237 lbm)	55,727 N-s (12,528 lbf-s)
2) Cutoff + 180 sec to end of first orbit	75 kg (165 lbm)	85,272 N-s (19,170 lbf-s)		
3) End of first orbit to depletion	16 kg (36 lbm)	25,488 N-s (5,730 lbf-s)	* GOX & He 88.9 kg (196 lbm) ** GOX 371.3 kg (818.6 lbm)	39,967 N-s (8,985 lb-s) 104,422 N-s (23,475 lbf-s)
Totals	135 kg (297 lbm)	167,208 N-s (37,590 lbf-s)	567.7 kg (1,251.6 lbm)	200,116 N-s (44,988 lbf-s)

* Ullage Gas ** Residual

The results presented in Table 14-I show that after one orbit, 84.8 percent of the LH$_2$ tank total impulse were vented. The estimated time required to vent the LH$_2$ and LOX tanks to 0.6 N/cm^2 (1 psi) was about 4 to 6 hours for LH$_2$ and about 24 to 36 hours for LOX. This estimate correlates well with the recorded data.

14.3.2 VEHICLE ATTITUDE IN ORBIT

The regular LOX and LH$_2$ NPV systems were activated at the time of S-IV engine cutoff command (630.252 seconds). The auxiliary LH$_2$ NPV system, which was also activated at S-IV cutoff, was in operation for 180 seconds and then closed. The regular LOX and LH$_2$ NPV system remained open to complete the depletion of gaseous residuals. At 811.95 seconds, the Apollo shroud was jettisoned and 60 seconds later the Pegasus wing extension began. The deployment was completed by approximately 912.0 seconds.

On SA-9 GOX was vented to impinge upon the deployed Pegasus wing. However, on SA-10 and SA-8 the LOX and LH$_2$ regular flow NPV systems were interchanged so that GH$_2$, instead of GOX, impinged upon the Pegasus wing. Since GH$_2$ imparts less total impulse than GOX, it was predicted that a 30-percent reduction in roll acceleration (CW from the rear), from that observed on SA-9, could be achieved on SA-10. (See Reference 6 for a more detailed description of the SA-10 and SA-8 NPV configuration.)

In determining the roll rate history of the SA-10 Pegasus C vehicle, the data sources utilized were: AGC records from the Minitrack beacon and telemetry signals, rate gyro information, and solar sensor data. The results of the analysis are shown in Figure 14-1. Approximately 80 station passes of Minitrack data were examined, yielding some 60 to 65 "readable" passes in which a period could be determined. Approximately one-half of these passes were from the Green Mountain station, with the remaining passes from the other Minitrack stations. Telemetry AGC was available through T + 2½ hours; 8 records yielded valid data. Rate gyro information was secured until T + 2 hours providing 10 periods of data from various tracking stations. The average rate for each period is shown in Figure 14-2. The solar panel voltage data were obtained from a time history graph and represent an average of a series of points taken over short periods of time (10 to 15 minutes).

The predicted maximum roll rate for Pegasus C, considering possible vent system misalignments and predicted wing impingement effects, was 7.7 deg/s for the actual onboard fuel and oxidizer residuals.

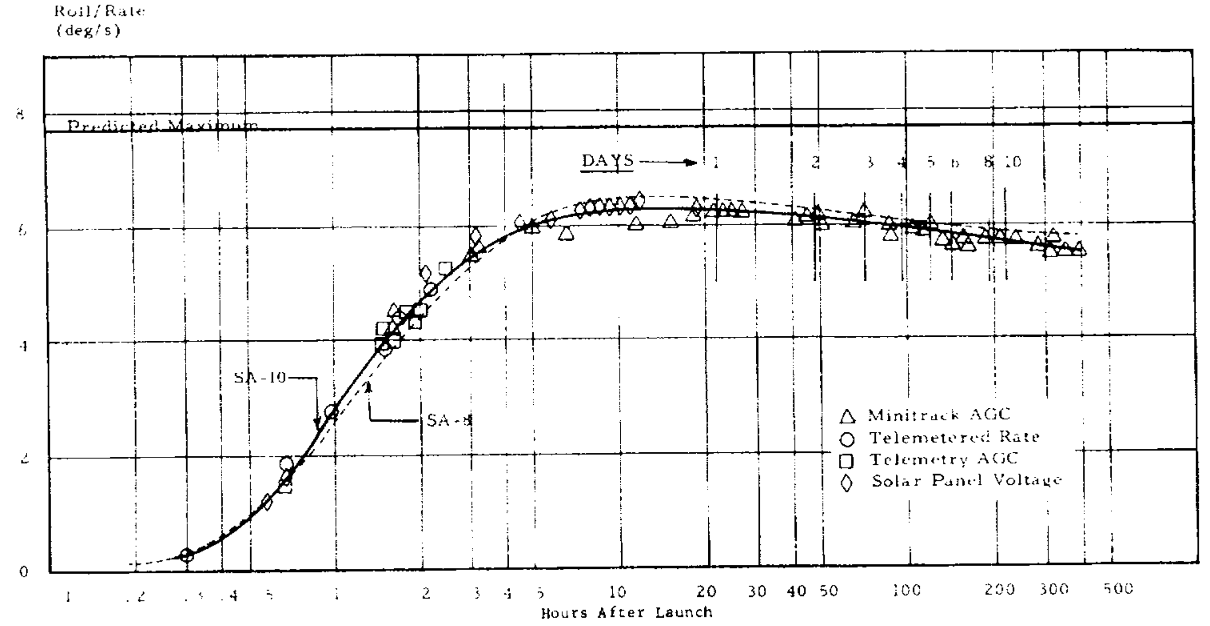

FIGURE 14-1. SA-10 ROLL RATE ANALYSIS

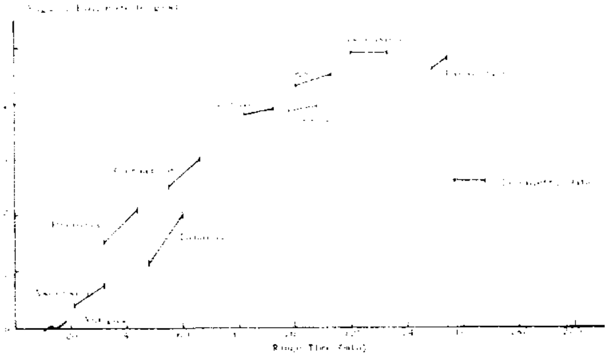

FIGURE 14-2. SA-10 ORBITAL ROLL RATES

As can be seen, the actual maximum rate was only 6.3 deg/s. This possibly indicates either a better thrust vector alignment, a smaller thrust imbalance, or a smaller jet impingement effect than was assumed in making the "maximum" prediction.

The Pegasus C roll rate history is very similar to that of Pegasus B (SA-8). The initial rate increase was slightly higher for Pegasus C, but the maximum rate attained was only approximately 0.2 deg/s less than the Pegasus B rate. After T + 12 hours, the Pegasus C roll rate began to decrease and was approximately 5.6 deg/s at T+360 hours (15 days). On August 20 a rapid readout was obtained and the information from the solar sensors indicated that the half-cone angle was approximately 20 degrees. All solar sensors were operating properly except for sensor 3, which is yielding bad data periodically. At the present there are indications that the SA-10 cone angle will continue to open up and cause the Pegasus C to tumble similar to Pegasus A (SA-9). The Pegasus B (SA-8) cone angle did not open up enough to cause it to tumble.

14.4 PEGASUS OPERATION

The Pegasus C spacecraft systems are operating properly and all system temperatures are within the permissible tolerance. On August 25 at 01:54:40 U. T., the temperature of the detector panels ranged from 228°K to 318°K. The maximum temperature differential on opposite sides of a detector panel was 15°K.

As of August 23, 6.517 m^2 of the 0.0381 mm (1.5 mil) detector panel area was active. No panels had been disconnected.

On the 0.2032 mm (8 mil) detector panels 13.982 m^2 of the detector panel area was active. Only 0.468 m^2 of the panel area was inactive.

On the 0.4064 mm (16 mil) detector panels 150.282 m^2 of detector panel area was active. The amount of detector panel area considered inactive was 12.584 m^2. Hits are being recorded continually on all three detector panel sizes.

The only significant change in the Pegasus C from Pegasus B is the removable meteorite detector panels, which can be recovered from orbit for purposes of analysis.

SECTION XV. SUMMARY OF MALFUNCTIONS AND DEVIATIONS

The flight test of Saturn SA-10 did not reveal any malfunctions or deviations which could be considered a serious system failure or design deficiency. However, a number of deviations did occur and are summarized below:

Launch Operations

1. A leak developed in the flex connection between the fixed LOX overland link from the storage facility and the S-I fill mast (Para. 3.4).

2. The ECS duct to the Pegasus came apart at the umbilical tower prior to launch (Para. 3.4).

3. Considerably more damage was done to the swing arms than has occurred during previous liftoffs, particularly to the flex hoses, electrical cables, and ECS ducts (Para. 3.7.1).

4. The S-IV stage LOX fill valve was closed manually when it was noted that the fill valve had not been commanded to close automatically at the 100 percent LOX level (Para's. 3.5.2.1 and 6.9).

Propulsion

1. The S-IV stage LH_2 pressurization control solenoid valve did not open when required during a portion of S-IV powered flight (Para. 6.8.1).

Instrumentation

1. Three measurements were scrubbed prior to launch. Twelve measurements failed during flight. Twenty-seven measurements were only partially successful during flight (Table 13-I).

2. The MISTRAM system did not meet performance requirements. The system transponder failed after 63 seconds of flight time (Para. 13.7.2).

3. The altimeter radar system and associated return-pulse-experiment failed to operate (Para. 13.7.2).

4. Of the 85 cameras programmed to record the launch, 2 cameras malfunctioned, 9 had no timing, and 3 had timing problems (Para. 13.8).

5. The Edcliff meters did not function properly during any portion of the flight (Para. 7.4.1.2).

APPENDIX

VEHICLE DESCRIPTION

A.1 SUMMARY

The flight of Saturn SA-10 was the sixth flight test of the Block II, Saturn I vehicles. This was considered the third flight of the Saturn I operational vehicles and the third to orbit a Pegasus meteoroid satellite (Pegasus C). This was the sixth consecutive Saturn I success in orbiting satellites. The vehicle, which measured approximately 57 m (188 ft) in length, consisted of four distinct units: the S-I stage, S-IV stage, operational Instrument Unit (third flight) and boilerplate Apollo spacecraft (BP-9). A pictorial description of the vehicle is presented in Figure A-1. The only appreciable change between SA-10 and SA-8 was the Pegasus C. Pegasus C has removable meteorite detector panels which can be recovered in orbit by astronauts, while Pegasus B does not.

A.2 S-I STAGE

A cluster of eight uprated H-1 engines powered the S-I stage (Fig. A-2) producing a total sea level thrust of 6.67 million N (1.5 million lbf). Each of the four outboard engines gimbal in a ± 8-degree square pattern to provide pitch, yaw, and roll control. Inboard and outboard engines were canted 3 degrees and 6 degrees outwards, respectively, from the vehicle longitudinal axis to minimize the disturbing moments that would be induced by an engine failure at critical dynamic pressure. Propellants were supplied to the engines through suction lines from the clustered arrangement of nine propellant tanks. These tanks consisted of four 1.78 m (70 in) diameter fuel tanks, four 1.78 m (70 in) diameter LOX tanks, and a 2.67 m (105 in) diameter center LOX tank. Each outboard tank (LOX and fuel) supplied propellants to one inboard and one outboard engine. The center LOX tank supplied the outboard tanks through the LOX interchange system. Thrust and longitudinal loads were carried by the pressurized LOX tanks. The propellant tanks were retained at the forward end by a structural member called a spider beam. Four 164,576 N (37,000 lbf) thrust solid propellant retro rockets mounted on the spider beam decelerated the S-I stage for inflight separation from the S-IV stage.

Four large fins and four stub fins were attached to the base of the S-I stage to provide flight stability plus support and holddown points at launch. Each large fin projected an area of approximately 11.24 m^2 (121 ft^2) and extended radially about 2.74 m (9 ft) from the outer surface of the thrust structure. Four stub fins were attached midway between the main fins. Stub fins II, III, and IV also provided enclosure and attachment for the three 0.3048 m (12 in) diameter ducts used to exit chilldown hydrogen from the S-IV stage. Four fairings between the larger fins and stub fins enclosed the inboard engine turbine exhaust ducts.

A.3 S-IV STAGE

Six gimbal mounted RL10A-3 engines, providing 400,340 N (90,000 lbf) total thrust at an altitude of 60,960 m (200,000 ft), powered the vehicle during the S-IV stage portion of powered flight. The engines were mounted on the thrust structure with a six-degree outward cant angle from the vehicle longitudinal axis. Each engine had a gimbal capability of a plus or minus four-degree square pattern for pitch, yaw, and roll control. The S-IV stage (Fig. A-3) carried approximately 45,359 kg (100,000 lbm) of usable liquid hydrogen and liquid oxygen.

The thrust structure provided engine thrust transfer to the LH_2 and LOX container. The tanks, LH_2 forward and LOX aft, were separated by a common bulkhead.

The LH_2 fuel system consisted of a 120.4 m^3 (4256 ft^3) cylindrical container with a bulkhead at each end. LH_2 flowed from the container through six suction lines, each of which connected to one RL10A-3 engine.

The LOX system consisted of a 35.8 m^3 (2164 ft^3) container. Vacuum jacketed suction lines transferred the LOX from the container through the antivortex screen, filter assembly and sump cone. The lower suction line flange ends were connected to the LOX inlet flange on each engine.

A nonpropulsive vent (NPV) system was installed on SA-7, in addition to the main pressure relief LOX and LH_2 vent systems, to obviate the excessive angular rates due to the venting of residual propellant after S-IV cutoff. An auxiliary NPV system was installed in SA-9 to provide a large initial pressure decay in the LH_2 tank to assure that the main LH_2 vent system is not activated. The system flown on SA-8 was identical to that of SA-9 with the exception of interchanging the use of the LOX vent for LH_2 and vice versa. The NPV system on SA-10 was identical to SA-8.

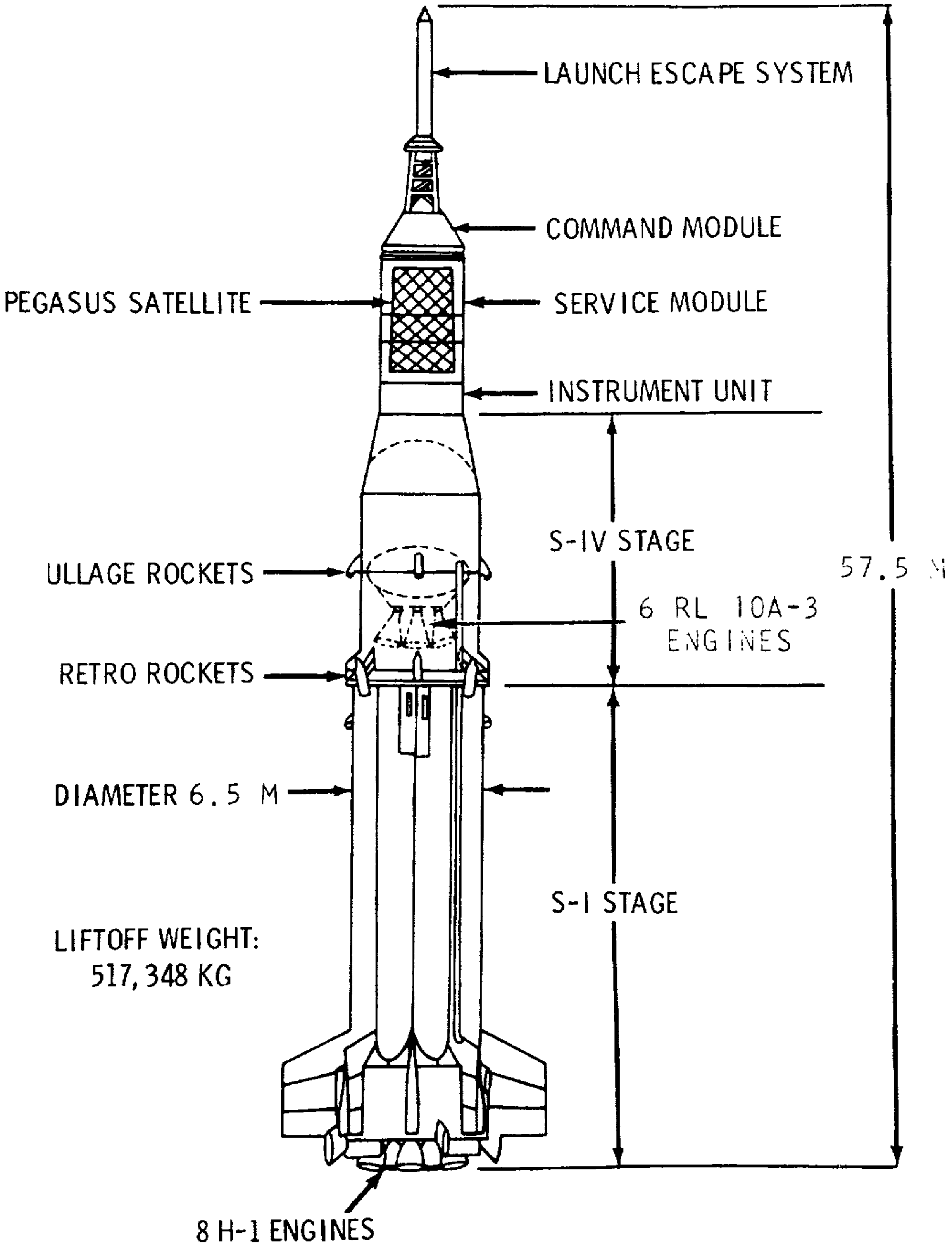
LAUNCH ESCAPE SYSTEM
COMMAND MODULE
PEGASUS SATELLITE
SERVICE MODULE
INSTRUMENT UNIT
S-IV STAGE
57.5 M
ULLAGE ROCKETS
6 RL 10A-3 ENGINES
RETRO ROCKETS
DIAMETER 6.5 M
S-I STAGE
LIFTOFF WEIGHT: 517,348 KG
8 H-1 ENGINES

FIGURE A-1. SA-10 VEHICLE CONFIGURATION

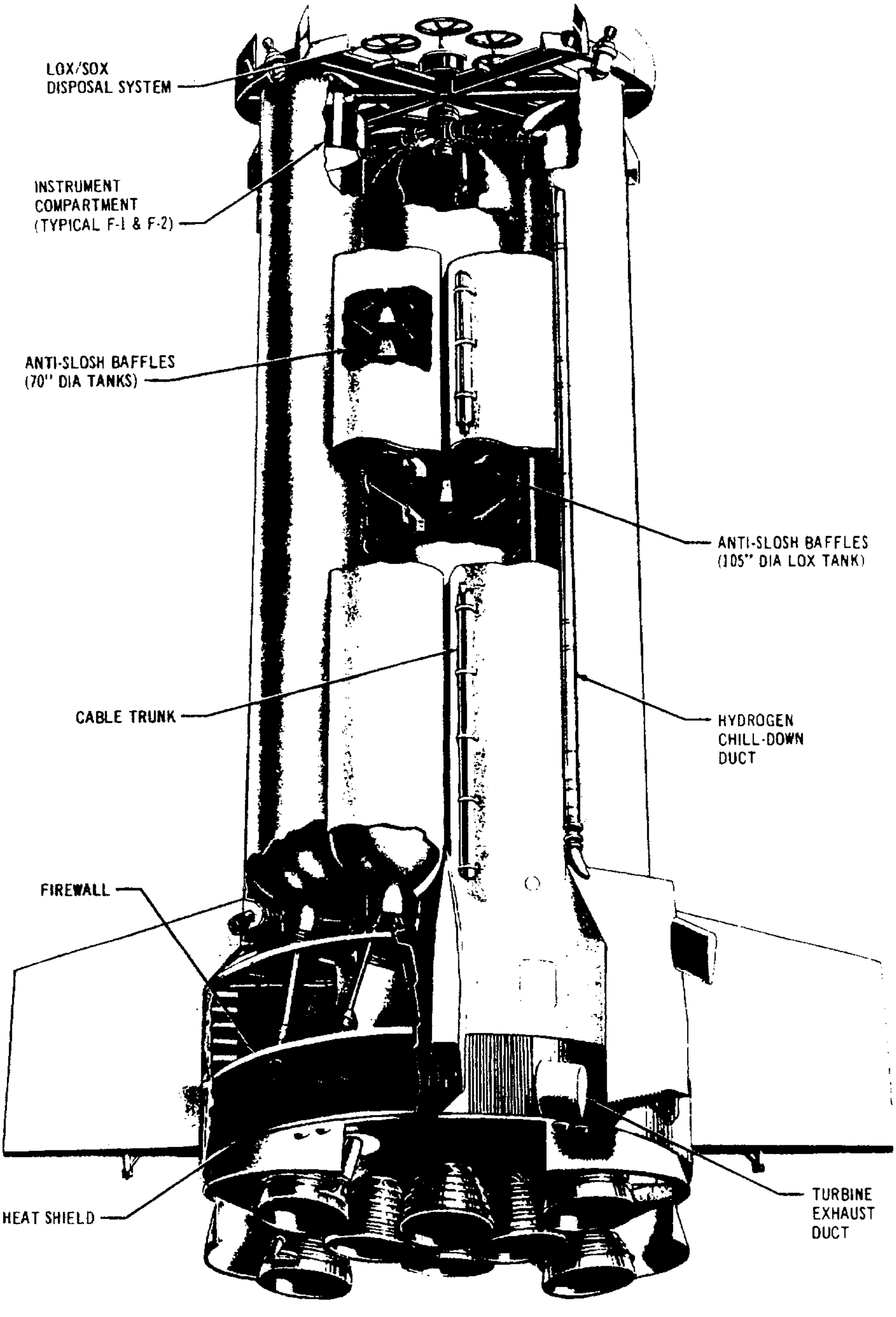
LOX/SOX DISPOSAL SYSTEM
INSTRUMENT COMPARTMENT (TYPICAL F-1 & F-2)
ANTI-SLOSH BAFFLES (70" DIA TANKS)
ANTI-SLOSH BAFFLES (105" DIA LOX TANK)
CABLE TRUNK
HYDROGEN CHILL-DOWN DUCT
FIREWALL
HEAT SHIELD
TURBINE EXHAUST DUCT

FIGURE A-2. S-I STAGE

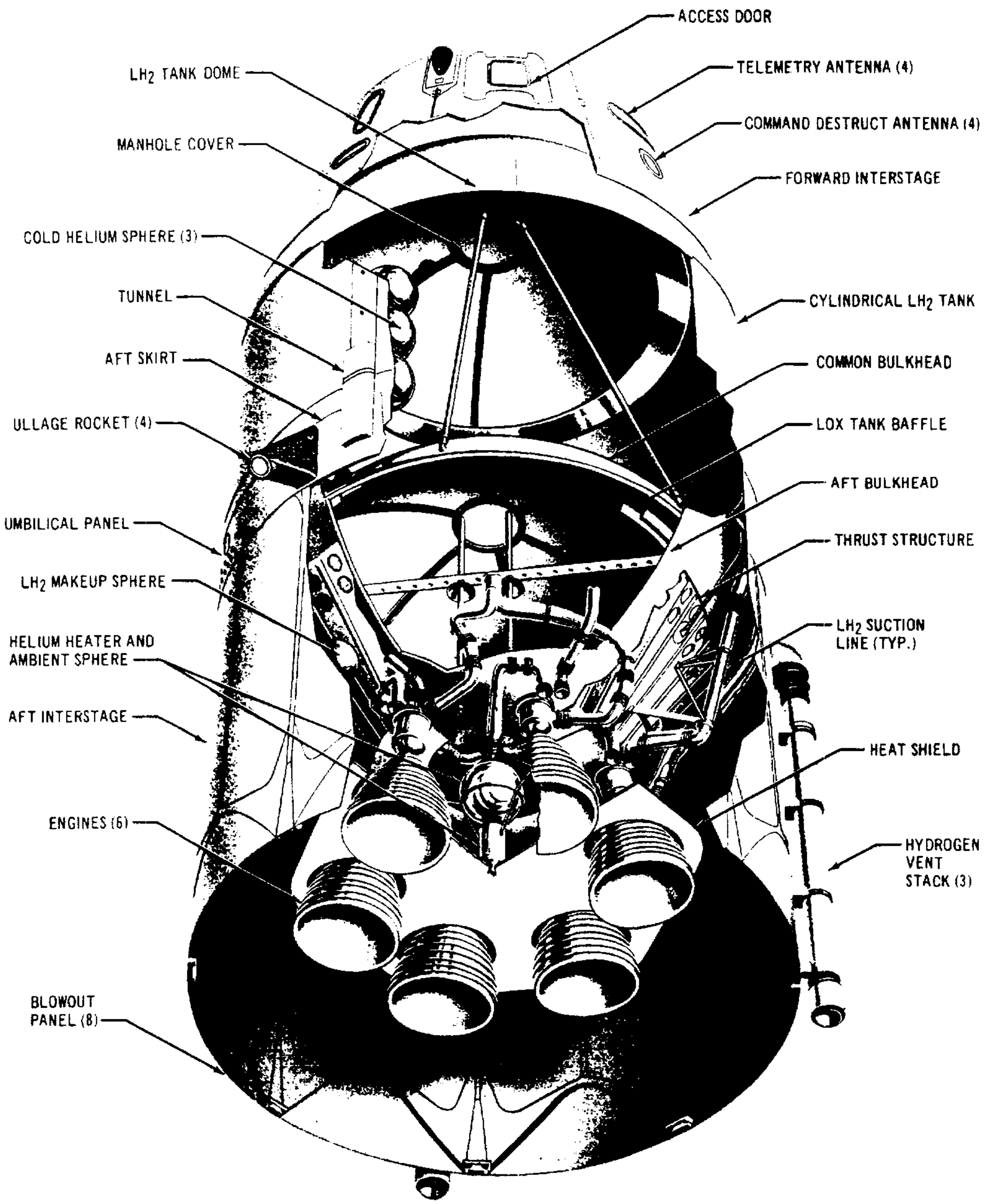
ACCESS DOOR
TELEMETRY ANTENNA (4)
COMMAND DESTRUCT ANTENNA (4)
FORWARD INTERSTAGE
CYLINDRICAL LH_2 TANK
COMMON BULKHEAD
LOX TANK BAFFLE
AFT BULKHEAD
THRUST STRUCTURE
LH_2 SUCTION LINE (TYP.)
HEAT SHIELD
HYDROGEN VENT STACK (3)
LH_2 TANK DOME
MANHOLE COVER
COLD HELIUM SPHERE (3)
TUNNEL
AFT SKIRT
ULLAGE ROCKET (4)
UMBILICAL PANEL
LH_2 MAKEUP SPHERE
HELIUM HEATER AND AMBIENT SPHERE
AFT INTERSTAGE
ENGINES (6)
BLOWOUT PANEL (8)

FIGURE A-3. S-IV STAGE

Four 15,390 N (3460 lbf) thrust solid propellant ullage rockets provided proper positioning of the propellants prior to the S-IV stage ignition.

A.4 INSTRUMENT UNIT

The Instrument Unit (Fig. A-4) located between the S-IV stage and the payload, housed the guidance and control equipment plus telemetry and the main electronic tracking equipment. This is the third flight of the prototype model of the production Instrument Unit to be used on future Saturn vehicles. This Instrument Unit is identical to that flown on SA-9 and SA-8. No environmental protection is provided for the instrumentation during flight. The overall diameter, height, and weight of the IU are 3.9 m (154 in), 0.9 m (34 in), and 1350 kg (2980 lbm), respectively.

A.5 PAYLOAD

The boilerplate Apollo (BP-9), shown in Figure A-5, consisted of a Command Module, Service Module, spacecraft adapter, and launch escape system. BP-9 served to simulate the characteristics of an Apollo spacecraft whose ultimate mission is a manned lunar soft landing and return to earth.

The Pegasus C meteoroid technology satellite was housed within the Service Module. The Service Module was attached to the payload adapter by six explosive nut assemblies and mounted on two guide rails (4.47 m or 176 in long, spaced 180 degrees apart) by three roller sleeve assemblies per rail. An additional explosive nut is located at the forward end of the Pegasus C satellite. After insertion into orbit, the Command and Service Modules were ejected, exposing the Pegasus C satellite. The ejection and separation mechanism consisted of 4 negator springs, each exerting a constant force of 178 N (40 lbf) through a distance of 3.96 m (156 in), and 12 compression springs each having a spring constant of 840 N/cm (480 lbf/in) and a stroke of 4.3 cm (1.7 in).

A.6 PEGASUS C SATELLITE

The objective of the Pegasus C satellite is to provide continued engineering data about the near-earth meteoroid environment in which future manned space vehicles will operate. In the stored position with panels folded inside the Apollo Service Module the approximate overall dimensions of the satellite are 4.5 m (177 in) high, 2.2 m (85 in) wide, and 2.4 m (95 in) deep. The X-axis of the satellite is along the longitudinal axis of the vehicle, the Y-axis extends in a plane parallel with the deployed wings, and the Z-axis is perpendicular to the deployed wings. The total capsule weight is approximately 1400 kg (3080 lbm). When deployed, the satellite has an overall wing span of 29 m (96 ft).

The Pegasus is divided into two major parts: the center section and the wing assemblies (Fig. A-5). The satellite's framework is made of riveted aluminum alloy extrusions. The center section is attached to the launch vehicle's second stage. It provides a mounting for the deployment mechanism, electronics cannister, solar power panels, and sensors.

Each wing consists of seven hinged frames which provide mountings for 208 panels (104 per wing). The hinges are spring loaded so that when released, the wings unfold in accordion fashion. A detector panel is composed of two flat plate capacitors of aluminum, Mylar, and copper bonded to each side of a one-inch thick foam core. The dimensions of the detector panels are approximately 101.6 by 50.8 by 2.54 cm (40 by 20 by 1 in). The capacitors have a target sheet thickness of 0.0381 mm (0.0015 in), 0.2032 mm (0.008 in), and 0.4064 mm (0.016 in), and both capacitors in a given panel are of the same thickness. The total exposed detector area is approximately 200 m^2; 8 m^2 of the 0.0381 mm material, 16 m^2 of the 0.2032 mm material, and 176 m^2 of the 0.4064 mm material. The Pegasus C has removable meteorite detector panels which can be recovered from orbit for purposes of analysis.

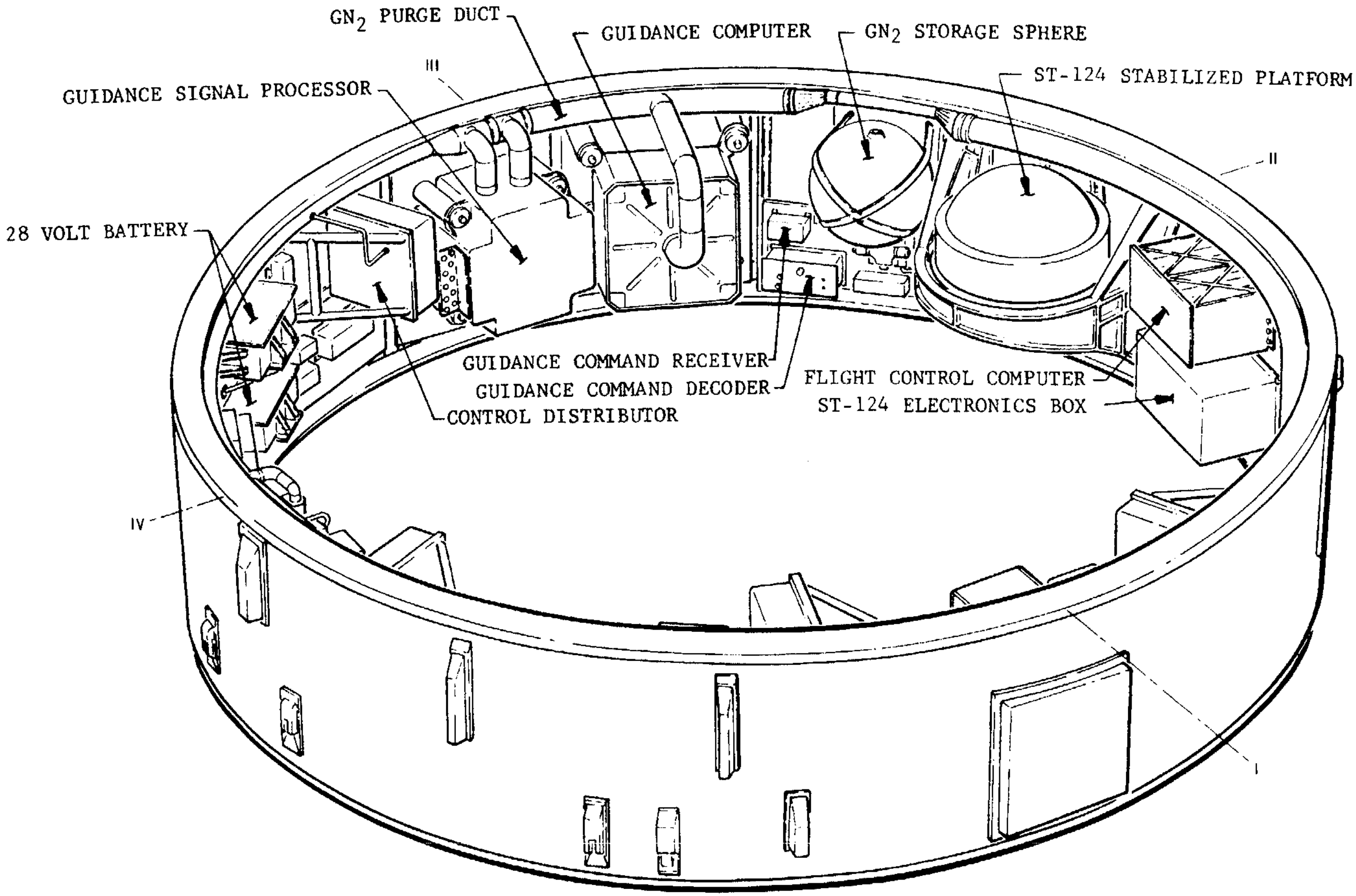
GN$_2$ PURGE DUCT
GUIDANCE COMPUTER
GN$_2$ STORAGE SPHERE
ST-124 STABILIZED PLATFORM
III
GUIDANCE SIGNAL PROCESSOR
II
28 VOLT BATTERY
GUIDANCE COMMAND RECEIVER
GUIDANCE COMMAND DECODER
CONTROL DISTRIBUTOR
FLIGHT CONTROL COMPUTER
ST-124 ELECTRONICS BOX
IV
I

FIGURE A-4. INSTRUMENT UNIT

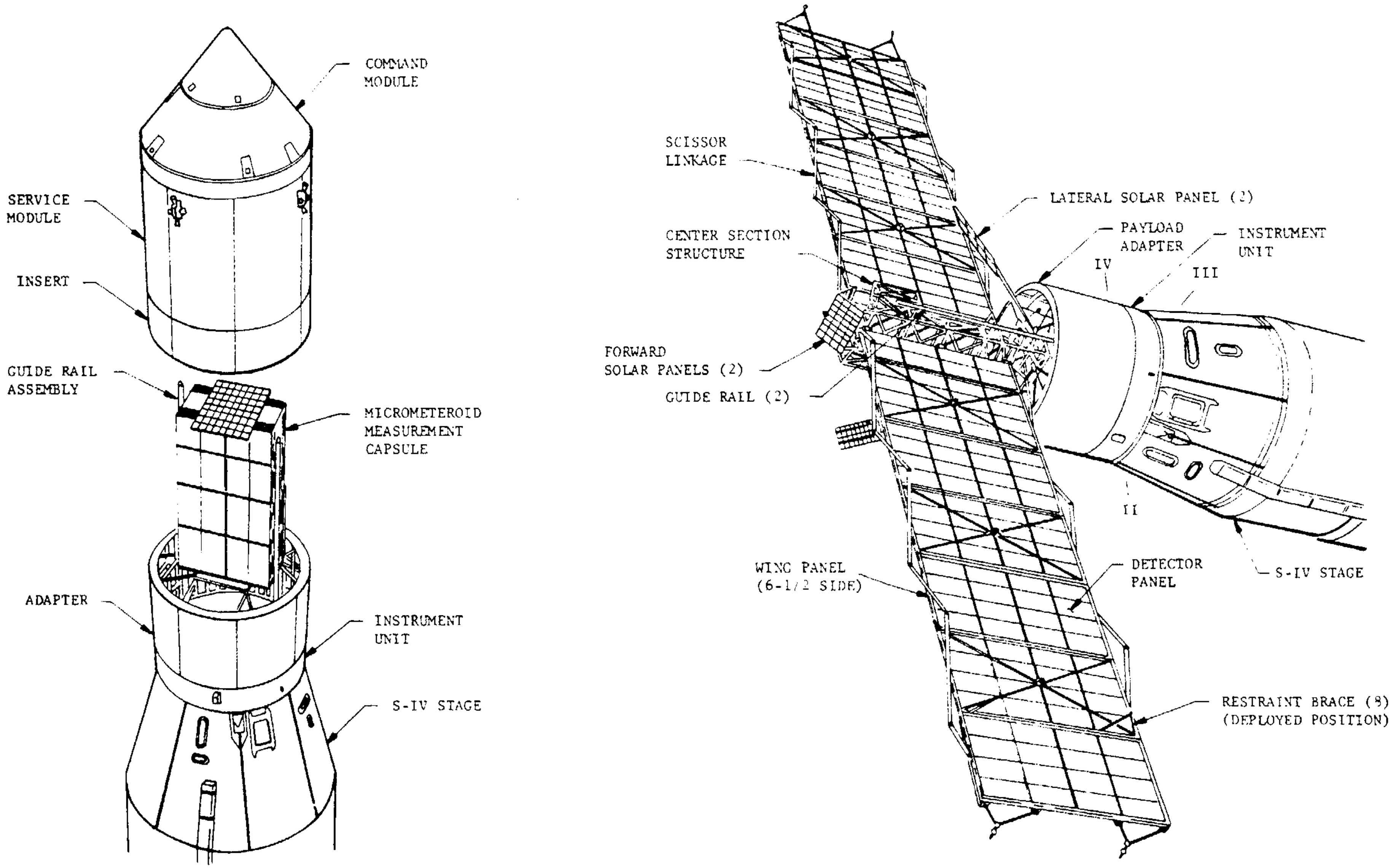
COMMAND MODULE
SERVICE MODULE
INSERT
GUIDE RAIL ASSEMBLY
MICROMETEROID MEASUREMENT CAPSULE
ADAPTER
INSTRUMENT UNIT
S-IV STAGE
SCISSOR LINKAGE
LATERAL SOLAR PANEL (2)
PAYLOAD ADAPTER
INSTRUMENT UNIT
IV
III
CENTER SECTION STRUCTURE
FORWARD SOLAR PANELS (2)
GUIDE RAIL (2)
II
WING PANEL (6-1/2 SIDE)
DETECTOR PANEL
S-IV STAGE
RESTRAINT BRACE (8) (DEPLOYED POSITION)

FIGURE A-5. PAYLOAD

INDEX

A

Acceleration
  control 36, 42, 43
  inertial 15
  lateral 36
  longitudinal 15, 25
  roll 86
  rotational 56
  space fixed 43
  structural 56
Accelerometer
  Apollo 61, 62
  body bending 57, 58, 63
  body fixed 36
  component 58, 60
  control 36, 42
  guidance 45, 47, 55
  H-1 engine 58, 60
  instrument unit 58, 61
  interstage 63
  Pegasus 61, 62
  S-I stage 58, 59, 60
  S-IV stage 60, 61, 64
Acoustics
  Apollo 62
  effects upon vibrations 58, 59
  instrument unit 58, 59, 62
  S-I stage 58, 59
  S-IV stage 62
Acquisition
  AGC 86
  data 80, 81, 82, 83, 84, 86
  DDAS 80
  PCM 80
  systems 80, 81, 82, 83, 84
Actuator
  deflection 38, 39, 40, 43
  gimbal, hydraulic 24
  position 38, 39, 40
Aerodynamic
  axial force coefficient 77
  forces, effects 36
  heating 66, 70, 71
  loading 66
Altimeter 2, 78, 81, 82, 83, 88
Altitude
  apex 15, 16
  apogee 1, 14, 15
  orbital 1, 14
  perigee 1, 14, 15
  S-IV cutoff 1, 14, 15
Angle of attack
  pitch 42
  Q-ball 38, 39, 42
  sensor 38, 39, 40, 42
  vehicle 38
  wind 38, 40
  yaw 40, 42
Angular
  motion 53
  velocity 54
Angular rate 36, 38, 39, 40, 42, 53, 85
  pitch 38, 42, 53
  roll 40, 42
  S-I stage 53
  S-IV stage 53
  yaw 2, 42, 53
Apogee
  altitude 1, 14, 15
Apollo 89, 93
  jettison 86
  orbital insertion 2, 85
  separation 2, 10, 55, 85
ASC-15 computer 36, 37, 38, 41, 43, 45, 48, 50
Atmospheric
  conditions at launch 1, 5
  U. S. Standard Reference 15
Attenuation
  effects, playback records 78, 80, 81, 83
  main engine flame 81, 82, 83
  retro rocket flame 78, 80, 81, 82
  ullage rocket flame 78, 80
Attitude
  angle 38
  orbital 85, 86, 87
Attitude error
  pitch and yaw 38, 39, 41, 42, 43, 44
  roll 36, 40, 41, 42
  signal 36
  S-IV stage 53, 54
Axial
  force coefficient 21, 77
  strain gauge 63
Azimuth
  alignment error 36, 45, 50

B

Battery
  instrument unit 2, 75
  instrumentation 75, 76
  1D10 75
  1D20 75

    1D11 75
    8D10 76
    8D11 76
    8D20 76
    5-volt measuring supply 75, 76
    voltage 75, 76
Beam
    spider 25, 66, 89
Bending
    body 57, 58, 63, 64
    oscillation 57
    pitch plane 2, 56, 57
    pitch and yaw 57, 58
Blockhouse
    redline values 9
Burn time
    retro rocket 25
    S-I stage 15, 24
    S-IV stage 15, 26, 33, 36
    ullage rocket 35

C

Calibrations
    inflight 80
    preflight 80
Calorimeter 2, 66, 67
    aft interstage 71
    aft skirt 70
    base heat shield 71
    heat flux 67
    purge 22
    radiation 67
    total 67
Camera
    coverage, GSE release 83
    coverage, H-1 engine ignition 83
    coverage, launch 1, 78, 83
    engineering sequential 83
    onboard TV 2, 78, 83
    tracking 83, 84
    umbilical tower 83
Center of gravity
    longitudinal and radial 10
    offset 48
    vehicle 42, 48
Chilldown
    duct impulse 29
    GH_2 duct 63
    LH_2 28, 70, 71, 89
    S-IV stage, LOX 23, 28
    vent thrust 25, 26
Cluster
    effects 20, 21, 25, 26
    performance 20
Coefficient
    axial force 21, 77
    tumbling, drag 16
Combustion
    chamber dome vibration 78
    chamber pressure 20, 23, 25, 26, 56
    stability monitor 9
    temperature 32
Control
    accelerometer 36, 42, 43
    GOX flow, valve 22
    helium shutoff valve 85
    LH_2 pressurization solenoid valve 29
    LOX replenish valve 22
    pneumatic, pressure system 22
    rate gyro 36, 43
    system, S-I 38, 39, 40, 41
    system, S-IV 41, 42
Cooldown
    engine, LH_2 8, 28, 30
    engine, LOX 7, 28, 33
Cutoff
    altitude 14
    conditions 14, 15
    events 15, 16
    impulse 29
    IECO 1, 18, 19, 20, 23, 24, 63, 84
    LOX starvation 23, 24
    OECO 1, 14, 15, 16, 18, 19, 20, 21, 23, 24, 36, 63, 84
    probe, LOX level 24
    S-I stage 15, 28, 58
    S-IV stage 1, 14, 15, 16, 27, 28, 29, 30, 31, 32, 33, 38, 42, 43, 47, 48, 50, 52, 76, 85
    S-IV weight 27, 28
    transients 29

D

Deflection
    actuator 38, 39, 40, 43
Deviations
    summary 88
Drag
    axial force coefficient 21, 77
    correction 20
    tumbling, coefficient 16

Duct
  boattail 69
  childown 29, 63, 70, 71
  ECS 88
  hydrogen vent purge 23
  turbine exhaust 36, 89

E

Electrical
  bridgewire 23, 25, 60, 76
  instrument unit system 76
  S-I stage system 75
  S-IV stage system 75, 76
  Support equipment 9
  system performance 2, 75
Engine
  actuator deflection 38, 39, 43, 44
  attenuation, flame 78, 80, 81, 82, 83
  chamber pressure 18, 20, 23, 25, 26, 56
  cluster 20, 21, 25, 26, 27
  cooldown 7, 8, 28, 30, 33
  cutoff transients 29
  exhaust 77, 89
  H-1 18, 24, 83, 89
  ignition 18, 32, 57
  individual performance 18, 21, 25, 26, 28, 89
  mixture ratio 18, 19, 24, 28, 34
  propellant mass flowrate 27
  RL10A-3 18, 28, 89
  shutdown, S-IV 36
  specific impulse 1, 18, 19, 21, 25, 26, 27, 28
  start transient 28
  thrust 18, 20, 21, 25, 26, 28, 57, 89
  turbopump gear box pressurization 22
  vibrations 58, 59, 60, 61, 64, 65
Events
  cutoff 14, 15
  significant 15, 16
  times of 2, 3
Exhaust
  flame (plume) 84
  main engine 69
  retro rocket 69
  turbine 21, 36, 77, 89
  ullage rocket 69

F

Fin 42
  plane 63
  pressure 66
  stub 23, 89
  trailing edge 67
First motion time 53, 83
Flame shield 67, 77
Flowrate
  helium 25, 26, 31
  LH_2 28
  LOX 28, 33
  propellant 18, 19, 21, 25, 26, 27
  S-I GOX 22
  S-I stage 18, 19, 20
  S-IV stage 25, 26, 27
Fuel
  bias 24
  density 7, 8
  level cutoff probe 23
  LH_2 boiloff rate 85
  LH_2 childown duct 70, 71
  LH_2 consumption 26
  LH_2 cooldown 8, 28, 30
  LH_2 feedline 60, 64
  LH_2 fill and drain mast 83
  LH_2 flowrate 28
  LH_2 fuel system 8, 89
  LH_2 load 8, 33
  LH_2 loading 8, 52
  LH_2 main fill valve 8
  LH_2 mass level 9, 34
  LH_2 NPV system 85
  LH_2 pressurization 1, 29, 30, 88
  LH_2 pump inlet 29, 30, 33
  LH_2 replenish 8
  LH_2 residual 26, 33, 34, 84, 85
  LH_2 slosh 44
  LH_2 tank dome 60, 61, 65
  LH_2 tank step pressurization 29, 30, 32, 34, 35, 71
  LH_2 tank temperature 70
  LH_2 tank ullage pressure 8, 29, 30, 31, 32, 85
  LH_2 tanking 73
  LH_2 transfer line 8
  LH_2 vent 8, 70, 89
  LH_2 vent duct purge 2, 23
  LH_2 vent valve 61, 65, 85
  LH_2 vented impulse 85, 86
  load 8, 24
  pressurization 18, 21, 22, 23, 25, 29, 30
  pump inlet pressure 21
  residual 84
  weight 7, 8

G

GLOTRAC 78, 81, 82, 83
GH_2 9, 30, 63, 86
GN_2
  gas bearing supply 51, 52
  pressure 35, 52
  pressure supply 22, 23
  purge 73
  temperature 52
GOX
  flow control valve 22
  flowrate 22
  venting 85, 86
Ground support equipment
  fill and drain mast 83
  holddown arm 9, 83
  LOX overland link 5, 88
  swing arm 9, 88
  umbilical tower 9, 83, 88
Gravity
  center of 10, 42, 48
  longitudinal and radial 10
Guidance
  accelerometer 47, 51, 55
  iterative 1, 2, 38, 48
  path 36, 38, 48
  pitch and yaw 41, 48, 50
  signal processor (GSP) 36, 37, 38
  S-IV cutoff 48
  ST-124 system 1, 36, 43, 45, 47, 50, 51, 52
  system hardware 50
Gyro
  error signal 50
  rate 45, 46, 47, 86

H

Heat
  flux 67, 68, 70, 71
Heat shield 60, 65, 77
  base 70, 71
  calorimeter 71
  heating rate 67
  inner region 67, 68
  outer region 67
  pressure 66, 70
  temperature 66, 67, 68, 69, 71
Heating
  aerodynamic 66, 70, 71
  rate 2, 66, 67
Helium
  cold, bubbling 22, 33
  cold, consumption 33
  cold, regulator 31, 60
  cold, residual 33
  cold, shutoff valve 85
  cold, supply 31, 33
  control system 33
  heater 18, 31, 60, 65
  heater combustion temperature 31
  heater exhaust temperature 71
  heater flowrate 25, 26, 31
  heater ignition 32
  heater performance 32
  heater single coil 31
  heater thrust 25, 26, 27
  inlet pressure 31
  solenoid valve 31
  triplex sphere 8, 9, 23, 33, 60, 61
Hydraulic
  actuator 24
  oil pressure and temperature 24, 25
  system, S-I 18, 24
  system, S-IV 18, 35

I

IECO (see cutoff)
Ignition
  command 8, 18, 23, 24
  helium heater 32
  propellant weight 7, 8
  S-I stage 24
  S-IV stage 93
  S-IV weight 27, 28
Impact
  booster 14, 15, 16, 17
Impulse
  chilldown duct 29
  LH_2 vented 85, 86
  LOX vented 85, 86
  specific, S-I 18, 19, 21
  specific, S-IV 18, 25, 26, 27, 28
  specific, vehicle 1, 18, 19, 20, 27
  S-IV cutoff 29
  ullage rocket 35
Insertion
  orbital 1, 2, 14, 48, 49, 50, 85
Instrument Unit 2, 36, 42, 89, 94
  battery 2, 75
  description 93, 94
  electrical system 76

  - orbital insertion 2, 85
  - telemetry 80, 82
  - temperature and pressure 71, 73, 74
  - umbilical separation 36, 73
  - vent ports 73
- Instrumentation
  - batteries 75, 76, 78
  - malfunctions 78, 79, 83, 84
  - photo/optical 2, 83, 84
- Interstage
  - aft 63, 69
  - heat flux 71
  - panel debonding 62, 63, 64, 69
  - pressure 63, 69
  - purge 22, 23
  - S-I/S-IV 22, 23, 62, 63
  - temperature 23, 63, 69
  - vent port 23
  - vibration 64
- Inverter
  - voltage 51, 76
- Iterative guidance mode (IGM) 1, 2, 38, 48

J

- Jettison
  - Apollo 86
  - launch escape system (LES) 58
  - ullage rocket 35

L

- Lateral
  - acceleration control 36
- Launch
  - anomaly 1, 5
  - camera coverage 1, 78, 83
  - complex 37B 1, 9
  - conditions 1, 5
  - damage 9
  - holds 1, 5, 9
- Launch escape system 42, 58, 93, 94
- LH_2 (see fuel)
- Load
  - factor 56
  - LH_2 8, 33
  - LOX 5, 7, 8, 19, 24, 33
  - longitudinal 56
  - propellant 24, 33
- LOX
  - boiloff 5
  - consumption 26
  - cooldown 7, 28, 33
  - density 7, 18, 21
  - feedline 60, 61, 64, 69
  - fill valve 33, 88
  - flowrate 28, 33
  - level 5, 8, 19, 88
  - level cutoff probe 23, 24
  - load 5, 7, 8, 19, 24, 33
  - loading system 7
  - main fill 7
  - mass 34, 35
  - NPV system 85
  - outboard suction line 23
  - overland line 5, 88
  - pressure relief valve 22
  - propellant utilization (PU) probe 61
  - pump inlet conditions 32, 33
  - pump inlet density 21
  - pump inlet pressure 21, 31, 56
  - pump inlet temperature 21, 32, 33
  - pump seal purge 22
  - replenish 7, 22, 31
  - residual 24, 26, 33, 34, 85
  - slosh 44
  - starvation cutoff 23, 24
  - suction line 24, 89
  - tank dome 60, 61, 65
  - tank pressure 22, 31, 85
  - tank pressurization 7, 31, 32, 33
  - tank pressurization system 18, 22, 32
  - vent valve 7, 8, 22, 31, 61, 85
  - vented impulse 85, 86
  - weight 5, 7
- LOX-SOX
  - disposal system 22, 23

M

- Mach number 15, 16, 38, 77
- Malfunctions
  - summary 88
- Mass (see weight)
  - characteristics 13
  - flowrate 26, 27
  - history 21, 27, 34
  - loss rate 27
  - moment of inertia 10
  - propellant 10, 11, 34
  - S-IV stage 10, 11, 26, 27
  - vehicle 10, 11, 12, 26, 27
- Mast
  - fill and drain 83

- Measurements, performance
  - IU malfunctions 78, 79
  - IU reliability 78
  - S-I system, malfunctions 78, 79
  - S-I system, reliability 78
  - S-IV system, malfunctions 78, 79
  - S-IV system, reliability 78
- Milestones 5, 6
- Minitrack 84, 86
- MISTRAM 78, 81, 82, 88
- MOTS 84

N

- Nominal
  - trajectory 14, 17
- Net positive suction pressure (NPSP) 30, 31
- Nonpropulsive vent (NPV) system 2, 18, 30, 85, 86, 89
  - LH_2 85, 86, 89
  - LOX 85, 86, 89
  - performance 85, 86

O

- ODOP 78, 81, 82
- OECO (see cutoff)
- Orbital
  - attitude 85, 86, 87
  - decay and reentry 16, 17
  - insertion 1, 48, 49, 50
  - insertion conditions 17
  - insertion, Apollo 2, 85
  - insertion, IU 2, 85
  - insertion, Pegasus 2, 85
  - insertion, S-IV stage 2, 14, 85
  - lifetime 1, 14
  - roll rate, Pegasus 86, 87
  - telemetry coverage 78

P

- Path guidance
  - initiation 1, 38, 41
  - pitch and yaw 1, 38
  - termination 8, 36
- Payload 93, 95
- Pegasus 1, 84, 89
  - description 93, 95
  - meteorite detector panels 85, 86, 87
  - mission 2, 93
  - operation 87
  - orbital insertion 2, 85
  - performance 2, 85
  - roll rate history 86, 87
  - separation 85
  - tumble rate 87
  - wing deployment 2, 85, 86, 93
  - wing impingement 86, 87
- Perigee
  - altitude 1, 14
- Pitch
  - angular rate 38, 39, 42
  - attitude error 38, 39
  - axis resolver chain error 43, 44
  - bending 2, 56, 57
  - path guidance 1, 38
  - program 38, 41
  - rate 2, 85
  - steering command 43
  - steering misalignment 38, 42
- Pogo
  - effects 2, 56, 57
- Pressure
  - base 66, 70
  - chamber buildup 25
  - chamber decay 20, 25
  - combustion chamber 18, 20, 23, 25, 26, 56
  - control system 22
  - detonation 69
  - fin 66
  - fuel pump 21, 56
  - fuel tank 21, 22
  - GN_2 22, 23, 35, 51, 52
  - heat shield 66, 70
  - helium heater inlet 31
  - helium sphere, decay 23
  - history 22, 69
  - instrument compartment 71
  - instrument unit 73, 74
  - interstage 63, 69
  - LH_2 tank ullage pressure 8, 29, 30, 31, 32, 85
  - LOX main fill line 7
  - LOX pump inlet 21, 31, 56
  - LOX tank 22, 31, 85
  - plenum chamber 23
  - S-I stage 66
  - S-IV stage 66, 69, 70
  - ullage 5, 22, 31
  - ullage rocket chamber 35
- Pressurization
  - control solenoid valve 18, 29, 30, 88
  - engine turbopump gear box 22
  - fuel 18, 21, 22, 25, 30

  - helium, flowrate 31
  - LH_2 1, 29, 30, 88
  - LH_2 tank step pressurization 29, 30, 32, 34, 35, 71
  - LOX tank 7, 18, 31, 32, 33
- Pressurization systems
  - fuel tank 18, 21, 22, 23, 25, 29, 30
  - LH_2 tank 29, 30
  - LOX tank 18, 22, 32
  - pneumatic control 33
  - S-I stage 21, 22, 23
  - S-IV stage 1, 29, 30
- Probe
  - continuous level 24, 44
  - discrete level 24
  - propellant level 24
  - PU 61
- Propellant
  - consumption 23, 26
  - depletion 25, 26
  - flowrate 18, 19, 21, 25, 26, 27
  - level sensor 36
  - load 24, 33
  - loading system 5, 7, 8, 23
  - mass 10, 11, 27, 33, 34
  - mixture ratio 18, 19
  - residual 24, 33, 34
  - slosh 38, 42, 44
  - system pressurization 7, 8
  - utilization (PU) system 8, 10, 18, 23, 24, 30, 33, 34, 44
  - weight, ignition 7, 8
- Propellant utilization (PU) system 8, 10, 18, 23, 24, 30, 33, 34, 44
  - computer 65
  - probe 61
  - valve 28, 60
- Propulsion system
  - S-I stage 1, 18, 19
  - S-IV stage 1, 18, 25, 26, 27, 28, 29
- Pump
  - engine turbopump gear box 22, 58, 60
  - inlet conditions 29, 30, 32, 33
  - inlet density 21
  - inlet pressure 21, 31, 56
  - inlet temperature 21, 32, 33
  - seal purge 22
- Purge
  - calorimeter 22
  - helium 23
  - interstage 22, 23
  - LH_2 vent duct 2, 23
  - LOX-SOX disposal 22, 23
  - system, performance 18

Q

- Q-ball
  - angle of attack 38, 39, 42
  - sensor 38, 39, 40, 42
  - transducer 42

R

- Radar
  - altimeter 2, 78, 81, 82, 83, 88
  - C-band 78, 81, 82, 84
- Radiation
  - calorimeter 67
  - heat shield 67, 68
- Rate
  - angular 36, 38, 39, 40, 42, 53, 85
  - control gyro 43
  - gyro drift 45, 46, 47
  - heating 66
  - pitch 2, 42, 38, 85
  - roll 2, 40, 42, 54, 85
  - roll, Pegasus 86, 87
  - vehicle, tumble 55
  - yaw 2, 42, 85
- Rawinsonde
  - winds 38, 39, 40
- Recorder
  - airborne tape 2, 78, 80
  - attenuation flame, effect 78, 80
  - instrument unit 81
  - playback mode 80
  - S-I stage 80
  - S-IV stage 80, 81
- Regulator
  - control pressure 22
- Resolver
  - "C" readings 50
  - chain error 38, 43, 44
  - command 36, 38
  - gimbal signal 36
- Retro rocket
  - attenuation, flame 81, 82
  - burn time 25
  - combustion chamber pressure 25
  - exhaust 69
  - ignition 25, 69, 81, 84
  - performance 25
- Roll
  - acceleration 86
  - actuator position 40
  - angular rate 40, 42
  - attitude error 36, 40, 41
  - rate 2, 54, 85
  - rate, Pegasus 86, 87

S

- Sensor
  - angle of attack 38, 39, 40, 42
  - data 25
  - point level 27
  - propellant level 36
- Separation
  - Apollo 2, 10, 55, 85
  - command 54
  - first motion time 53
  - instrument unit, umbilical 36, 73
  - Pegasus/SM 85
  - S-I/S-IV 1, 2, 23, 25, 36, 41, 53, 54, 56, 58, 63, 69, 82
  - transients 1, 41, 53
- Signal
  - loss of telemetry 15, 16
  - RF dropout 50, 80
  - RF performance 78, 81
  - telemetry 81
- Simulation
  - cluster performance 20, 21
  - drag 20, 21
  - flight 18, 20, 21
  - propulsion performance flight analysis 20, 21
  - thrust shape 20, 21
  - trajectory 20, 21, 25, 26, 27
- Slosh
  - LH_2 44
  - LOX 44
  - propellant 38, 42, 44
- Spacecraft (see Apollo)
  - adapter 2, 93, 94
  - BP-9 89, 93, 94
  - command module 2, 93, 94
  - launch escape system (LES) 93, 94
  - service module 2, 93, 94
- ST-124 system
  - accelerometer 45, 47, 55
  - azimuth alignment error 36, 45, 50
  - error source 45
  - gas bearing supply 51, 52
  - guidance intelligence error 44, 45, 46
  - guidance system 1, 36, 43, 45, 47, 50, 51, 52
  - leveling error 45, 50
  - stabilized platform 36, 37, 41
- Stability
  - combustion monitor 9
- Static inverter 60, 75, 76
- Steering
  - command 36, 42, 43, 48
  - correction 41
  - misalignment, pitch 38, 42
  - vehicle 38, 42
- Strain gauge 63
- System
  - airborne telemetry 81, 82
  - altimeter 2, 81, 82, 83
  - control pressure 22
  - electrical 2, 75, 76
  - emergency detection (EDS) 42, 43
  - fuel 8
  - guidance and control 1, 36, 50
  - helium, pneumatic control 33
  - hydraulic 18, 24, 35
  - LH_2 8, 85, 86, 89
  - LOX 85, 86, 89
  - LOX/SOX disposal 22, 23
  - NPV 2, 18, 30, 85, 86, 89
  - photo/optical 2, 83, 84
  - pressurization, fuel 18, 21, 22, 23, 25, 29, 30
  - pressurization, LH_2 29, 30
  - pressurization, LOX 18, 22, 32
  - pressurization, S-I 21, 22, 23
  - pressurization, S-IV 1, 29, 30
  - propellant loading 8, 23, 57
  - propellant utilization 8, 10, 18, 23, 24, 30, 33, 34, 44
  - propulsion 1, 26, 27
  - purge 18
  - RF 81
  - television, onboard 2, 78, 83
  - tracking 82, 83

T

- Telemetry
  - AGC 86
  - airborne system 80, 81, 82
  - links 2, 80, 81, 82, 84
  - loss 15, 16
  - orbital coverage 78
  - RF blackout 50, 80
  - RF performance 78, 81
- Television 2, 78, 83
- Temperature
  - access chute 67, 68
  - aft skirt 70
  - base 66, 67, 71, 72
  - combustion 32
  - engine compartment 67
  - engine shroud 66, 67
  - fin trailing edge 67
  - flame shield 67, 69
  - fuel 7

  - GN_2 52
  - heat shield 66, 67, 68, 69, 71
  - helium heater combustion 31
  - helium heater exhaust 71
  - helium triplex sphere 33
  - instrument unit 73, 74
  - interstage 69
  - LH_2 tank 70
  - LH_2 vent line 70
  - LOX pump inlet 21, 32, 33
  - tail shroud 66
- Test objectives 2
- Thrust
  - chamber dome 58
  - engine 21
  - engine buildup 18
  - engine decay 20
  - helium heater 25, 26, 27
  - level 18, 21
  - OK pressure switch 23, 36
  - S-I stage 18, 19, 20, 21
  - S-I buildup 18, 57
  - S-I longitudinal 1, 18, 19, 20, 21
  - S-IV stage 15, 25, 26, 28
  - S-IV buildup 28
  - S-IV chamber 23
  - S-IV decay 36, 38, 42
  - S-IV longitudinal 1, 18, 25, 26, 27
  - ullage rocket 27, 93
  - vector misalignment 42, 48, 87
- Time
  - first motion 53, 83
- Tracking
  - altimeter, radar 82, 83, 88
  - Azusa 81, 82, 83
  - C-band radar 78, 81, 82, 84
  - camera 84, 88
  - Minitrack 84, 86
  - MISTRAM 78, 81, 82, 88
  - MOTS 84
  - MSFN 84
  - ODOP 78, 81, 82
  - STADAN 84
  - S-I stage 16
- Trajectory
  - at orbital insertion 48, 49
  - deviation 21
  - free flight 14, 16, 17
  - ground track 17
  - observed 20, 26
  - precalculated 48
  - simulated 20, 21, 25, 26, 27
  - S-I stage 14
  - S-IV stage 14
  - tracked 20, 21
- Turbine
  - exhaust duct 36
  - gear box 22, 58, 60

U

- Ullage pressure 5, 8, 22
  - decay 31
  - LH_2 tank 29, 30, 32
  - LOX tank 31
  - S-IV stage 29, 30
- Ullage rocket
  - burn time 35
  - chamber pressure 35
  - exhaust 69
  - ignition 69, 84
  - impulse 35
  - jettison 35
  - misalignment 36, 54
  - performance 35
  - thrust 27, 93

V

- Valve
  - cold helium shutoff 85
  - GOX flow control 22
  - LH_2 main fill 8
  - LH_2 vent 61, 65, 85
  - LOX pressure relief 22
  - LOX prevalve control 22
  - LOX replenish control 22
  - LOX vent 7, 8, 22, 31, 61, 85
  - LOX/SOX 23
  - pressurization, control solenoid 18, 29, 30
  - pressurization, fuel tank 21
  - propellant 15, 28, 34
- Vehicle
  - description 89, 90, 91, 92, 93
  - weight 19, 21
- Velocity
  - angular 54
  - at orbital insertion 50
  - cross range 1, 14, 36, 38, 42, 48
  - earth fixed 14, 15
  - inertial, error 45, 46, 47, 50
  - measured and predicted 36
  - OECO 1, 14
  - S-IV cutoff 1, 14
  - space fixed 1, 15, 36, 38, 41, 47, 48, 50
  - vector 38
  - wind 40

Vent
    chilldown thrust 25, 26
    cooldown 27
    LH_2 duct purge 2, 23
    LH_2 line 70
    LH_2 tank 8
    LH_2 valve 61, 65, 85
    LOX valve 7, 8, 22, 31, 61, 85
Venting
    NPV propellant 85
Vibration
    Apollo 61, 62, 65
    combustion chamber dome 78
    component 60, 61, 64, 65
    instrument unit 58, 59, 60, 61, 62, 65
    interstage 64
    levels 2, 56, 58, 59, 60, 61, 64, 65
    Pegasus 61, 62, 65
    S-I stage 58, 59, 60
    S-IV stage 60, 64

W

Weight
    liftoff 19, 21
    loss rate 20
    propellant 7, 8
    S-IV cutoff 25, 27, 28
    S-IV ignition 27, 28
    vehicle 19, 21
Wind
    angle of attack 38, 39, 40
    effect, LOX load 5, 7
    rawinsonde 38, 39, 40
    velocity 40

DISTRIBUTION

INTERNAL

DIR
Dr. von Braun

DEP-T
Dr. Rees

DEP-A
Mr. Gorman

E-DIR
Mr. Maus

I-DIR
Gen. O'Connor } (1)
Dr. Mrazek

I-I/IB-MGR
Col. James

I-I/IB-T
Mr. Fikes (13)

I-MO-MGR
Dr. Speer (4)

I-V-MGR
Dr. Rudolph

R-DIR
Mr. Weidner

R-AS-DIR
Mr. Williams

R-AERO-DIR
Dr. Geissler
Mr. Jean

R-AERO-A
Mr. Dahm

R-AERO-AT
Mr. Wilson

R-AERO-D
Mr. Horn

R-AERO-F
Mr. Lindberg (35)

R-AERO-G
Mr. Baker

R-AERO-P
Mr. McNair

R-AERO-Y
Mr. Vaughan

R-AERO-YT
Mr. O. E. Smith

R-ASTR-DIR
Dr. Haeussermann

R-ASTR-E
Mr. Fichtner

R-ASTR-F
Mr. Hosenthien

R-ASTR-I
Mr. Hoberg
Mr. Powell

R-ASTR-IE
Mr. Price

R-ASTR-IMD
Mr. Avery

R-ASTR-N
Mr. Moore

R-ASTR-NGI
Mr. Nicaise

R-ASTR-S
Mr. Noel

R-COMP-DIR
Dr. Hoelzer

R-COMP-R
Mr. Prince

R-COMP-RR
Mr. Cochran

R-ME-DIR
Mr. Kuers

DISTRIBUTION (Cont'd)

INTERNAL (Concluded)

R-ME-M
Mr. Orr

R-ME-T
Mr. Franklin

R-ME-X
Mr. Wuenscher

R-P&VE-DIR
Dr. Lucas
Mr. Palaoro

R-P&VE-A
Mr. Goerner

R-P&VE-M
Mr. Kingsbury

R-P&VE-P
Mr. Paul (2)

R-P&VE-PPE
Mr. McKay (2)

R-P&VE-S
Mr. Kroll
Mr. Hunt

R-P&VE-SVM
Mr. Gassaway

R-QUAL-DIR
Mr. Grau

R-QUAL-A
Mr. Henritze

R-QUAL-DIE
Mr. Corder

R-QUAL-P
Mr. Brooks

R-QUAL-QVS
Mr. Peck

R-QUAL-R
Mr. Brien
Mr. Smith

R-RP-DIR
Dr. Stuhlinger

R-TEST-DIR
Mr. Heimburg (1)
Mr. Tessmann

R-TEST-C
Mr. Grafton

R-TEST-I
Dr. Sieber

R-TEST-S
Mr. Driscoll

R-TEST-M
Mr. Edwards

MS-H
Mr. Akens

MS-IP
Mr. Remer (2)

MS-IL
Miss Robertson (8)

LVO-JA
Mr. Rigell

LVO-JF
Mr. Pickett

LVO-JA
Dr. Gruene

EXTERNAL

Headquarters
National Aeronautics & Space Administration
Washington, D. C. 20546
Attn: Mr. Hilburn, AAD
Mr. Shapley, ADA
Mr. Kerr, E
Mr. Condon, KR
Dr. Mueller, M
Gen. Phillips, MA
Capt. Freitag, MC
Dr. Adams, R

EXTERNAL (Cont'd)

Mr. Tischler, RP
Dr. Newell, S
Mr. Garbarini, SE
Mr. Johnson, SV (10 copies)
Mr. Kerr, U
Mr. Day, MAT (8 copies)

Director, Ames Research Center: Dr. H. Julian Allen
National Aeronautics & Space Administration
Moffett Field, California 94035

Director, Flight Research Center: Paul F. Bikle
National Aeronautics & Space Administration
P. O. Box 273
Edwards, California 93523

Goddard Space Flight Center
National Aeronautics & Space Administration
Greenbelt, Maryland 20771
Attn: Herman LaGow, Code 300

John F. Kennedy Space Center
National Aeronautics & Space Administration
Kennedy Space Center, Florida 32899
Attn: Technical Library, Code ASO 3B
Mrs. L. B. Russell

INS-1
Dr. Burns
INS-13
Mr. Jelen
INS-4
Mr. Collins

Director, Langley Research Center: Floyd L. Thompson
National Aeronautics & Space Administration
Langley Station
Hampton, Virginia 23365

Director, Lewis Research Center: Dr. Abe Silverstein
National Aeronautics & Space Administration
21000 Brookpark Road
Cleveland, Ohio 44135

Manned Spacecraft Center
National Aeronautics & Space Administration
Houston, Texas 77058
Attn: Director: Dr. Robert R. Gilruth
Robert E. McKann, Code PM4 (3copies)
Charles M. Grant, Code BM1 (2 copies)
William E. Davidson, R-L
MSFC Liaison Office
Bldg. 2, Rm. 167 (1)

Director, Wallops Station: R. L. Krieger
National Aeronautics & Space Administration
Wallops Island, Virginia 23337

Director, Western Operations Office: Robert W. Kam
National Aeronautics & Space Administration
150 Pico Blvd.
Santa Monica, California 90406

Scientific and Technical Information Facility
P. O. Box 5700
Bethesda, Maryland 20014
Attn: NASA Representative (S-AK/RKT) (25 copies)

Jet Propulsion Laboratory
4800 Oak Grove Drive
Pasadena, California 91103
Attn: Irl Newlan, Reports Group, (Mail 111-122)
H. Levy, (Mail 179-203) CCMTA (4 copies)

Office of the Asst. Sec. of Defense for Research & Engineering
Room 3E1065
The Pentagon
Washington, D. C. 20301
Attn: Tech Library

Director of Guided Missiles
Office of the Secretary of Defense
Room 3E131
The Pentagon
Washington, D. C. 20301

Central Intelligence Agency
Washington, D. C. 20505
Attn: OCR/DD/Publications (5 copies)

Director, National Security Agency
Ft. George Mead, Maryland 20755
Attn: C3/TDL

U. S. Atomic Energy Commission, Sandia Corp.
University of California Radiation Lab.
Technical Information Division
P. O. Box 808
Livermore, California 94551
Attn: Clovis Craig

U. S. Atomic Energy Commission, Sandia Corp.
Livermore Br, P. O. Box 969
Livermore, California 94551
Attn: Tech Library

EXTERNAL (Cont'd)

Commander, Armed Services Technical
Information Agency
Arlington Hall Station
Arlington, Virginia 22212
Attn: TIPCR (Transmittal per Cognizant Act
Security Instruction) (5 copies)

Commanding General
White Sands Proving Ground
New Mexico 88002
Attn: ORD BS-OMTIO-TL (3 copies)

Chief of Staff, U. S. Air Force
The Pentagon
Washington, D. C. 20330
1 Cpy marked for DCS/D AFDRD
1 Cpy marked for DCS/D AFDRD-EX

Commander-in-Chief
Strategic Air Command
Offutt AFB, Nebraska 68113
Attn: Director of Operations, Missile Division

Commander
Arnold Engineering Development Center
Arnold Air Force Station, Tennessee 37389
Attn: Tech Library (2 copies)

Commander
Air Force Flight Test Center
Edwards AFB, California 93523
Attn: FTOTL

Commander
Air Force Missile Development Center
Holloman Air Force Base
New Mexico 88330
Attn: Tech Library (SRLT)

Commander, AF Missile Test Center
Patrick AFB, Florida 32925
Attn: Technical Information Intelligence Office,
MTGRY (3 copies)

Headquarters
6570th Aerospace Medical Division (AFSC)
U. S. Air Force
Wright Patterson Air Force Base, Ohio 45433
Attn: H. E. Vongierke

Systems Engineering Group (RTD)
Attn: SEPIR
Wright-Patterson AFB, Ohio 45433

Director
U. S. Naval Research Laboratory
Washington, D. C. 20390
Attn: Code 2027

Chief of Naval Research
Department of Navy
Washington, D. C. 20390
Attn: Code 463

Chief, Bureau of Weapons
Department of Navy
Washington, D. C. 20390
1 Cpy to RESI, 1 Cpy to SP, 1 Cpy to AD3,
1 Cpy to REW3

Commander
U. S. Naval Air Missile Test Center
Point Mugu, California 93041

AMSMI-RBLD; RSIC (3 copies)
Bldg. 4484
Redstone Arsenal, Alabama 35809

Aerospace Corporation
2400 East El Segundo
El Segundo, California 90245
Attn: D. C. Bakeman

Aerospace Corporation
Reliability Dept.
P. O. Box 95085
Los Angeles, California 90045
Attn: Don Herzstein

Bellcomm, Inc.
1100 Seventeenth St. N. W.
Washington, D. C. 20036
Attn: Miss Scott, Librarian

The Boeing Company
P. O. Box 29100
New Orleans, Louisiana 70129
Attn: R. H. Nelson (3 copies)

Chrysler Corporation Space Division
Michoud Operations
Dept. 2712, Bldg. 350
P. O. Box 29200
New Orleans, Louisiana 70129
Attn: Mr. Leroy Smith (5 copies)

EXTERNAL (Concluded)

Chrysler Corporation Space Division
Huntsville Operations
Dept. 4800
1312 N. Meridian Street
Huntsville, Alabama 35807
Attn: H. Bader, Jr. (3 copies)

Douglas Aircraft Company, Inc.
Marshall Space Flight Center
Bldg. 4481, Room 41
Huntsville, Alabama 35812
Attn: J. A. Tobias (15 copies)

NASA Resident Office
Grumman Aircraft Engineering Corp.
Bethpage, Long Island, N. Y. 11714
Attn: John Johansen

International Business Machine
System Design, Dept. 229
150 Sparkman Dr. NW
Huntsville, Alabama 35808
Attn: R. E. Poupard (2 copies)

Martin Company
Space Systems Division
Baltimore, Maryland 21203
Attn: W. P. Sommers

Foreign Technology Division
FTD (TDBDP)
Wright Patterson Air Force Base, Ohio 45433

Commander
Det. 11, 4th Weather Group
Code; ETQFW
Patrick AFB, Florida 32925

FFETR (ETLLG-1)
Patrick AFB, Florida 32925

P. O. Box 2691
West Palm Beach, Fla. 33402
Attn: T. C. Mayes & F. W. McAbee

Rocketdyne
6633 Canoga Avenue
Canoga Park, California 91303
Attn: T. L. Johnson (3 copies)

North American Aviation
Space & Information Division Systems
12214 S. Lakewood Blvd.
Downey, California 90241
Attn: W. T. Scleich (2 copies)
W. F. Parker (1 copy)

Pratt & Whitney Aircraft
P. O. Box 2691
West Palm Beach, Fla. 33402
Attn: T. C. Mayes & F. W. McAbee

Radio Corporation of America
Defense Electronic Products
Data Systems Division
8500 Balboa Blvd.
Van Nuys, California 91406

RCA Service Company
2611 Leeman Ferry Road
Huntsville, Alabama
Attn: D. E. Wise